Department of Chemical Engineering

Particulate Matter Emission during the Combustion of Bio-oil Based Biofuels under Conditions Pertinent to Stationary Applications

Chao Feng

This thesis is presented for the Degree of

Doctor of Philosophy

of

Curtin University

April 2018

Declaration

To the best of my knowledge and belief this thesis contains no material previously published by any other person except where due acknowledgment has been made.

This thesis contains no material which has been accepted for the award of any other degree or diploma in any university.

Signature: .....

Date: April, 2018

To my beloved family
and friends

Abstract

Coal as a fossil fuel dominates the world electricity generation as it supplies cheap electricity to power the world economy. Therefore, it is envisaged that coal-fired stationary power plants will continue to play an important role in the global electricity supply in the foreseeable future. However, coal combustion results in adverse environmental impacts due to emissions of greenhouse gas and other pollutants. It is therefore highly desired to substitute coal with renewable fuels in conventional coal-fired power stations.

Biomass based fuels are renewable fuels that have various advantages over coal. These advantages include their renewable and sustainable features, low net carbon dioxide (CO_2) emission during the full life cycle of utilization process, typically of low ash content, and good adaptability to the existing power generation systems. Among many biomass based fuels, an important category is fuels based on bio-oil and/or biochar from biomass fast pyrolysis. These fuels include fast pyrolysis bio-oil and its fractions (e.g. water-soluble fraction of bio-oil, referred to as "WSF"), bio-oil/biochar slurry (BB), WSF/biochar fuel slurry (WSFB) and their mixtures with crude glycerol (CG), i.e. bio-oil/methanol/CG fuel blend (BMCG), WSF/CG fuel blend (WSFCG), bio-oil/methanol/CG/biochar slurry (BMCGB), and WSF/CG/biochar slurry (WSFCGB). All these bio-oil based biofuels are known to meet specifications for stationary combustion applications.

The focus of this thesis is on particulate matter (PM) emission during the combustion of these bio-oil based biofuels in stationary applications under both conventional air or oxyfuel conditions. It is well known that PM emission has adverse impacts on environment and human health. Particularly, this study emphasizes the emission of PM with aerodynamic diameter of less than 1 and 10 μm (i.e. PM_1 and PM_{10}), respectively, and trace element emission. PM_1 and PM_{10} are difficult to capture through current dust collection devices in stationary power stations. These fine particles are also responsible for various respiratory system diseases. While there have been extensive studies on PM emission during the combustion of solid fuels such as coal, biomass and biochar, little investigation has been conducted so far on PM emission during the combustion of biofuels. Therefore, the objectives of this

PhD research program are to investigate: 1) PM_{10} emission during the incomplete combustion of fast pyrolysis bio-oil; 2) PM_{10} emission during the combustion of bio-oil and its different fractions under both air and oxyfuel conditions; 3) PM_{10} emission during the combustion of formulated water-soluble fraction of bio-oil; 4) synergy on PM_{10} emission during bioslurry combustion; 5) PM_{10} emission from the combustion of CG containing biofuels and synergy between CG and other fuel components; and 6) trace elements in various biofuels and their release in PM_{10} during combustion. All experiments were carried out using a laboratory-scale drop-tube furnace (DTF) at 1400 °C, with the research outcomes are listed below.

Firstly, a raw bio-oil from biomass fast pyrolysis and a filtrated bio-oil, which was prepared from the raw bio-oil via syringe filtration to remove fine char particles, were combusted under both air and oxygen (O_2) atmospheres to study the PM_{10} emission. Regardless of experimental conditions, it was found that the particle size distributions (PSDs) of PM_{10} follow a bimodal distribution. Whereas the PSDs of Na, K, Cl and S (in form of SO_4^{2-}) exhibit a unimodal distribution, those of Mg and Ca in PM_{10} are dependent on combustion atmosphere, i.e. a unimodal distribution for air combustion and a bimodal distribution for O_2 combustion. The results show that the fine char particles in the raw bio-oil play significant roles in the emission of PM_{10} as well as Mg and Ca in PM_{10}. The removal of the fine char particles in the raw bio-oil leads to considerable reductions in the mass of PM with aerodynamic diameters of 0.1−10 μm as well as that of Mg and Ca in the PM with a size range of 0.372−10 μm from the filtrated bio-oil combustion, compared to those from the raw bio-oil combustion. Combustion atmospheres also have significant effects on the emission and chemical composition of PM_{10}. Switching combustion atmosphere from air to O_2 increases the PM_1 yield by ~74.2% due to the increased yields of Na, K, Mg, Ca, SO_4^{2-} and PO_4^{3-} in PM_1, but decreases the $PM_{1\text{-}10}$ yield by ~27.2% most likely as a result of improved burnout and thereby decreased amounts of unburned carbonaceous material in $PM_{1\text{-}10}$.

Secondly, PM_{10} emission during the complete combustion of bio-oil under air and two oxyfuel conditions (i.e., 21%O_2/79%CO_2 and 30%O_2/70%CO_2, by volume) were studied. Three bio-oil samples were considered, i.e., a raw bio-oil, a filtrated bio-oil (prepared from the raw bio-oil after fine char particles were removed via filtration), and the water-insoluble fraction (WIF) of the filtrated bio-oil (blended with ethanol).

It was found that the total inorganic species of the raw bio-oil is distributed dominantly (74.7%) in the WSF but minorly in the WIF (10.4%) and suspended fine char particles (14.9%). The results from the combustion experiments show that the PSDs of PM_{10} from the complete combustion of bio-oil have a bimodal distribution, with a fine mode at ~0.03 μm and a coarse mode at ~2.0 μm. The WIF and the fine char particles suspended in the raw bio-oil have insignificant contributions to PM_{10} emission during the combustion of the raw bio-oil. The results suggest that the WSF plays a key role in the emission of PM_{10} during bio-oil combustion. PM_{10} emission during the complete combustion of bio-oil is also found to be insensitive to combustion atmosphere (air or oxyfuel) because complete bio-oil combustion is dominated by gaseous-phase reactions and the contribution of solid combustion is minimal. However, the excessive CO_2 under oxyfuel conditions leads to more Fe being partitioned into $PM_{0.1\text{-}1}$.

Thirdly, because the WSF separated from cold-water precipitation of biomass contains excessive water, it is not possible to investigate PM_{10} emission from its direct combustion. To address this issue, two formulated water-soluble fractions (FWSFs) of bio-oil were prepared. FWSF-1 was an organic-free calcium chloride solution with a calcium concentration similar to that in the bio-oil. FWSF-2 was formulated from the compositions of major organics in bio-oil WSF, doped with calcium chloride at the same concentration. A systematic set of experiments were then carried out to study PM_{10} emission from the combustion of the FWSFs under air or oxyfuel ($30\%O_2/70\%CO_2$) conditions. The results suggest that similar to bio-oil combustion, the FWSF combustion produces mainly particulate matter with diameter of between 0.1 and 10 μm (i.e. $PM_{0.1\text{-}10}$). Since there are no combustibles in the organic-free FWSF-1, the PM is produced via droplet evaporation followed by crystallization, fusion and further reactions to form CaO (in air or argon) or partially $CaCO_3$ (under oxyfuel condition). With the addition of organics, FWSF-2 combustion produces PM_{10} shifting to smaller sizes due to extensive break up of droplets via microexplosion. Sprays with larger droplet size produce PM_{10} with increased sizes. The results show that upon cooling CaO produced during combustion in air can react with HCl gas to form $CaCl_2$ in $PM_{0.1}$. The predicted PSDs of PM_{10} based on the assumption that one droplet produces one PM particle is considerably larger than experimentally-measured PSDs of PM_{10} during the

combustion of FWSFs, confirming that breakup of spray droplets takes place and such breakup is extensive for FWSF-2 when organics are present in the fuel.

Fourthly, a systematic study was also conducted to investigate PM_{10} emission from the combustion of bio-oil/biochar slurry (i.e. bioslurry) under air, 20% O_2/ 80% CO_2 and 30% O_2/ 70% CO_2 conditions. Similar to biomass combustion, the PSD of PM_{10} during bioslurry combustion also follows a bimodal distribution. Increasing char loading level in bioslurry leads to an increase in the emission of PM_{10}, especially $PM_{1\text{-}10}$, due to high content of inorganic species in biochar. Emissions of PM_1 and $PM_{1\text{-}10}$ during bioslurry combustion under 20% O_2/ 80% CO_2 conditions are lower than that under air conditions, apparently attributed to the lower char combustion temperature. However, under 30% O_2/ 70% CO_2 conditions, emission of the PM_{10} during bioslurry combustion are higher than that under air conditions. Such an increase in PM_{10} is mainly contributed by increasing PM_1, which appears to be a result of enhanced sulfation of alkali species at an increased oxygen concentration. The PM_{10} emission performance during the combustion of bioslurry was also benchmarked against those during the combustion of solid fuels such as coal, biomass or biochar under similar conditions. The results show that the combustion of bioslurry emits considerably lower PM_{10} than that of coal, biomass or biochar on the basis of the same energy input, which is normally the case when bioslurry is used to replace solid fuels. The results suggest that from PM emission point of view, bioslurry is a competitive candidate for substituting other solid fuels in stationary combustion applications.

Fifthly, a set of experiments were also carried out to demonstrate the significant synergy on PM_{10} emission during bioslurry combustion. The PM_{10} emission from the direct combustion of bioslurry (with 5 or 10 % biochar loading level) is higher than the sum of those from separate bio-oil and biochar combustion, clearly indicating the existence of synergy. It is evident that at least two mechanisms are responsible for such synergistic effects. One mechanism is the leaching of inorganic species from biochar by acidic bio-oil in the bioslurry system. This is demonstrated by the direct comparisons between PM_{10} emissions from the combustion of bio-oil or biochar before and after bioslurry preparation. The experimental results show that such a leaching effect leads to both an increase in PM_1 and a decrease in $PM_{1\text{-}10}$ during combustion, because of the redistribution of inorganic species between the bio-oil

and biochar fractions of bioslurry. The other mechanism is the synergy between the bio-oil and biochar fractions that takes place during bioslurry combustion. This is demonstrated by the comparison between PM_{10} emissions from the direct bioslurry combustion and the sum of PM_{10} from the separate combustion of bio-oil and biochar fractions separated from bioslurry. The interactions between the combustions of bio-oil and biochar fractions lead to an increase in PM_1 and a decrease in PM_{1-10} during bioslurry combustion. The results further show that the second mechanism (i.e. interactions between the combustions of bio-oil and biochar fractions) accounts for ~80% of the total increase in PM_1 and ~60% of the total decrease in PM_{1-10}.

Sixthly, a series of investigations were carried out to understand the effect of interactions among fuel components on PM_{10} emission during the combustion of for CG-containing biofuels. Four fuel components, i.e. bio-oil, water-soluble fraction of bio-oil (WSF), biochar and CG, two fuel blends, i.e. bio-oil/methanol/CG blend (BMCG) and WSF/CG blend (WSFCG), and four slurry fuels, i.e. bio-oil/biochar slurry (BB), WSF/biochar slurry (WSFB), BMCG/biochar slurry (BMCGB) and WSFCG/biochar slurry (WSFCGB), were considered. The results show that PM_{10} from the combustion of CG-containing fuel blends (i.e. BMCG and WSFCG) has unimodal distributions with a fine mode at ~0.043 μm. Therefore, the PM_{10} are dominantly PM_1, which contributes to ~88.2% and ~99.3% of the total PM_{10} during the combustion of BMCG and WSFCG, respectively. However, the combustion of CG-containing slurry fuels (i.e. BMCGB or WSFCGB) produce PM_{10} having bimodal distributions of PM_{10} with a fine mode at ~0.022 μm and a coarse mode at ~1.624−2.438 μm. The introduction of biochar increases the contribution of PM_{1-10} to the total PM_{10} from ~11.8% and ~0.7% for BMCG and WSFCG to ~53.1% and ~8.4% for BMCGB and WSFCGB, respectively. For CG-containing fuel blends, the interactions between CG and other fuel components result in enhanced chlorination of volatile inorganic species due to the abundant Cl originated from CG, leading to increasing emissions of these species in PM_1. For CG-containing slurry fuels, such enhanced chlorination also take place for both volatile and refractory inorganic species in biochar, leading to increasing emission of both volatile and refractory inorganic species in PM_1 and decreasing emission of refractory inorganic species in PM_{1-10}.

Lastly, a systematic set of experiments were also carried out to investigate the abundance of eleven trace elements (including Ti, V, Cr, Mn, Ni, Co, Cu, Zn, As, Cd, and Pb) in a wide range of biofuels and the emission of these trace elements in PM_{10} from the combustion of these biofuels. These biofuels include four individual biofuels, i.e., biochar, bio-oil, water-soluble fraction of bio-oil (WSF), and crude glycerol (CG), and six mixed fuels, i.e. bio-oil/methanol/CG blend, WSF/CG blend, bio-oil/biochar slurry, WSF/biochar slurry, bio-oil/methanol/CG/biochar slurry, and WSF/CG/biochar slurry. The results show that the main trace elements presented in all biofuels are Zn and Mn, and the concentrations of trace elements in biochar are much higher than those in the other biofuels. In the slurry systems, the presence of Ti, V, Cr, Mn, Ni and Co is mainly contributed by biochar fraction, while that of the other elements (Cu, Zn, As, Cd, and Pb) are mainly from the liquid fraction. During the combustion of all the biofuels, the elemental particle size distributions (PSDs) of both Group I elements (Ti, Mn, Ni, and Co, mainly in PM_{1-10}) and that of Group III element (Pb, mainly in PM_1) exhibits unimodal distributions. The elemental PSDs of Group II elements (V, Cr, As, Cu, Zn and Cd, predominantly in PM_1) from the combustion of liquid fuels also have unimodal distributions, while that from biochar shows bimodal distributions. During the combustion of slurry fuels, the elemental PSDs of V and Cr have bimodal distributions, while those of the rest of Group II (As, Cu, Zn and Cd) exhibit unimodal distributions in PM_1. On the basis of same energy input, biochar combustion produces highest total trace element emission in PM_{10} among these biofuels, followed by slurry fuels, and then liquid fuels. It produces highest emission of Ti, Mn, Ni, V, and Cr in PM_{10} than the other fuels on unit energy input basis while combustion of liquid and slurry fuels produces highest Pb emission and combustion of all ten biofuels produces similar Cu and Zn emission. Comparisons between the experimental and calculated results of trace element emission in PM_{10} from mixed biofuels combustion indicate that synergies takes place among individual fuel components during the combustion of the mixed biofuels, resulting in enhanced PM_1 emission.

Acknowledgement

I gratefully acknowledge the Chinese Scholarship Council (CSC) and Curtin University for providing scholarships to support my PhD study. I'm also grateful to partial financial support from Australian Research Council through its Discovery Project Program.

I would like to express my warmest thanks to my supervisor, Prof. Hongwei Wu, for his guidance, inspiration, training, patience and continuous supports during the course of my study. He is an excellent mentor and a role model from whom I have learnt so much and will learn for a long time in my future career. I also want to extend my gratitude to Dr. Xiangpeng Gao and my thesis committee chairperson, Prof. Shaobing Wang, for their kind assistance and advice during my PhD study.

Special thanks also go to all Chemical Engineering Department lab technical staffs, Mr Araya Abera, Mr Xiao Hua, Mr Andrew Chan, Dr. Roshanak Doroushi, Dr. Guanliang Zhou, Ms Ann Carroll and Ms Melina Miralles, for their assistance and technical support in the lab. I would also like to thank our group members: Dr. Yun Yu, Dr. Sui Boon Liaw, Dr. Mingming Zhang, Dr. Matthew Witham, Dr. Mohammad Usman Rahim, Mr Yu Long, Mr Bing Song, Ms Wenran Gao, Mr Xujun Chen, Ms Yee Wen Chua, Mr Changya Deng, and Ms Jinxiu Cao, for their assistances in various aspects.

My gratitude is also for all the dear friends I have met in Perth, for their kind help and warm-hearted accompany during the four-year life in Australia. All the friendships and the memories will be cherished in my mind.

A special person will also be acknowledged here is my lovely girlfriend, Ms Xiyu Zhang, who is the best gift I have received in this beautiful country.

Last and most importantly, I would like to thank my parents who are far away in my hometown but have been providing me with endless support, love and care whenever in need. I am really proud to be your son and my love for you is beyond any words that can possibly express.

List of Publications from My PhD Study

Papers published in refereed journals:

1. Feng, C.; Zhang, M.; Wu, H., Trace elements in various individual and mixed biofuels: abundance and release in particulate matter during combustion, Energy & Fuels, 2018, ***32***(5): p. 5978-5989.
2. Feng, C.; Wu, H., Mechanistic investigation into particulate matter formation during air and oxyfuel combustion of formulated water-soluble fractions of bio-oil, 37th International Symposium on Combustion, PROCI-D-17-00507, *accepted for oral presentation* on 26 March 2018
3. Feng, C.; Zhang, M.; Wu, H., Combustion of biofuel mixtures containing crude glycerol (CG): Effect of interactions between CG and fuel components on particulate matter emission. Industrial & Engineering Chemistry Research, 2018, ***57***, 4132-4138 (*selected to appear on the supplementary journal cover page*)
4. Feng, C.; Wu, H., Synergy on particulate matter emission during the combustion of bio-oil/biochar slurry (bioslurry). Fuel 2018, ***214***, 546-553.
5. Feng, C.; Wu, H., Bioslurry for stationary applications: Particulate matter emission during combustion under air and oxyfuel conditions. Energy & Fuels, 2017, ***31***, 7241−7246.
6. Feng, C.; Gao, X.; Wu, H., Emission of particulate matter during the combustion of bio-oil and its fractions under air and oxyfuel conditions. Proceedings of the Combustion Institute 2017, ***36***, 4061–4068.
7. Feng, C.; Gao, X.; Wu, H., Particulate matter emission from bio-oil incomplete combustion under conditions relevant to stationary applications. Fuel 2016, ***171***, 143-150.

Papers published in refereed conference proceedings:

1. Feng, C.; Gao, W.; Wu, H., Combustion of bioslurry and its fractions: different contributions to PM10 emission. The 11th Asia Pacific Conference on Combustion (ASPACC-11), 10-14th, December 2017, Sydney, Australia.

Table of Contents

List of Tables

List of Figures

Chapter 1 Introduction

1.1 Background and Motive

Stationary coal-fired power plants contributes to over 40% of the global electricity supply.[1] In Australia, coal plays even more important role because coal-based electricity contributes to over three quarters of the total electricity market.[2] However, coal-fired power stations are the major emitters of greenhouse gas (CO_2 being the most important one), contributing to a third of the nation's total greenhouse gas emission.[3] Therefore, it is of critical importance to develop new technologies to transform traditional power generation systems to be cleaner and more sustainable.

Biomass is widely regarded as a key sustainable energy source.[4-6] Depending on the production process, biomass has the advantage of nearly zero net CO_2 emission in its whole life cycle of uitlization.[7] Direct combustion of biomass or co-firing with coal in boilers is a mature technology and practiced worldwide successfully.[8-10] However, such direct uses are limited by expensive fuel transport and poor biomass grindability.[11]

Several technologies have been developed to address these issues in order to improve techno-economic performance of biomass-based energy supply chains, mainly via drastically increasing fuel energy densities.[5,7,12-16] Fast pyrolysis is one promising option that has gained extensive attention.[17-25] This process converts biomass into high-energy-density biochar and bio-oil that are therefore suitable for storage, transport and adaptive to various applications in vast existing infrastructures.[11,12,19,26] Besides further upgrading and refining into liquid transport fuels,[12,20,27,28] bio-oil is also proved to be a good candidate for substituting coal in large-scale stationary combustion applications.[20,28,29] Biochar is also an excellent fuel for co-firing in coal-fired power stations.[11,26] Considering that biochar is dusty and prone to

spontaneous combustion, recent studies showed that suspending biochar into bio-oil is an excellent technical option to produce a new class of fuel (i.e. the so-called bioslurry) that is suitable for stationary applications.[30] In Australia, life cycle analysis demonstrated that bioslurry fuels from the fast pyrolysis of mallee biomass have low energy and carbon footprints[31] and are cheap to produce.[32] It was also shown that mixing crude glycerol (CG), which is a waste byproduct of biodiesel production, with bio-oil (and/or biochar) is a good option to prepare CG-containing blend (or slurry) biofuels that are suitable for stationary combustion applications.[33-38]

Emission of particulate matter (PM) is a notorious issue concerned with stationary power stations because of its adverse impacts on environment and human health,[39-41] especially for those containing toxic heavy metals or trace elements.[40,42] The existing cleaning devices equipped for PM capturing, such as electrostatic precipitators are also inefficient in capturing these fine particulates, especially PM with aerodynamic diameter of less than 1 μm (PM_1).[39,40,43]

In the open literature, extensive reports are dedicated to investigations into formation/emission of PM during the combustion of various solid fuels such as coal,[44-57] biomass,[58-66] biochar,[67] and solid wastes.[68,69] There are also scattered studies on PM emission from the combustion of liquid fuels including heavy fuel oil[70-73] and crude glycerol (CG).[74,75] However, for bio-oil based biofuels, such as bioslurry and those containing CG, there have been no reports on PM emission during combustion under conditions pertinent to stationary applications. In addition, bio-oil is an essential component in these biofuels so that it is of critical importance to understand PM emission during bio-oil combustion. It is also known that bio-oil combustion will often face the challenge of incomplete combustion due to the fuel's high water content and multicomponent nature.[20,76,77] The effect of such combustion conditions on PM emission is largely unknown. Bio-oil also contains various fractions (i.e. fine char particles, water-soluble fraction and water-insoluble fraction) and the contributions of different bio-oil compositions to PM emission during

combustion are also unknown. Recently, oxyfuel combustion has also been considered a step-change technology for retrofitting existing stationary coal-fired powerstations to enable CO_2 capture.[78] Therefore, combustion of biofuels under oxyfuel conditions becomes very attractive because it potentially enables power generation with negative carbon emission. While extensive research were carried out PM emission during the oxyfuel combustion of coal[55,56] and biomass,[8] little is known on PM emission during the combustion of bio-oil and bio-oil based biofuels under such conditions. Lastly, while extensive previous studies were also conducted on transformation and release of trace elements in PM during the combustion of solid fuels (coal,[42,51,79-86] biomass,[87-90] and biosolid[68,91,92]) and liquid fuels (heavy fuel oil[70,71,93,94]), there is not report on the trace element emission in PM during the combustion of biofuels.

1.2 Scope and Objectives

Therefore, this PhD thesis reports a systematic study on emission of PM with aerodynamic diameter < 10 μm (i.e, PM_{10}) during the combustion of various biofuels. The biofuels include bio-oil, bio-oil fractions, bioslurry and CG-containing mixtures. The detailed objectives are to:

- investigate PM_{10} emission during the incomplete combustion of bio-oil;
- carry out a systematic study into PM_{10} emission during the complete combustion of bio-oil and its fractions under air and oxyfuel conditions;
- conduct investigation into PM_{10} emission during biolsurry combustion and the potential synergy taking place on PM_{10} emission among different fuel components in bioslurry during combustion;
- reveal the roles of potential interactions between CG and other fuel components in CG-containing biofuels during combustion in PM_{10} emission;

- study trace elements in biofuels and their emission in PM_{10} during the combustion of individual and mixed biofuels from bio-oil, biochar, and/or CG.

1.3 Thesis Outline

This thesis consists of 11 chapters (including this chapter) listed below, with the thesis map illustrated in Figure 1-1.

- Chapter 1 Introduction
- Chapter 2 Literature review
- Chapter 3 Research methodology and analytical techniques
- Chapter 4 Particulate matter emission from bio-oil incomplete combustion under conditions relevant to stationary applications
- Chapter 5 Emission of Particulate matter during the combustion of bio-oil and its fractions under air and oxyfuel conditions
- Chapter 6 Mechanistic investigation into particulate matter formation during air and oxyfuel combustion of formulated water-soluble fractions of bio-oil
- Chapter 7 Bioslurry for stationary applications: particulate matter emission during combustion under air and oxyfuel conditions
- Chapter 8 Synergy on particulate matter emission during the combustion of bio-oil/biochar slurry (bioslurry)
- Chapter 9 Combustion of biofuel mixtures containing crude glycerol (CG): effect of interactions between CG and fuel components on particulate matter emission
- Chapter 10 Trace elements in various individual and mixed biofuels: abundance and release in particulate matter during combustion
- Chapter 11 Conclusions and recommendations

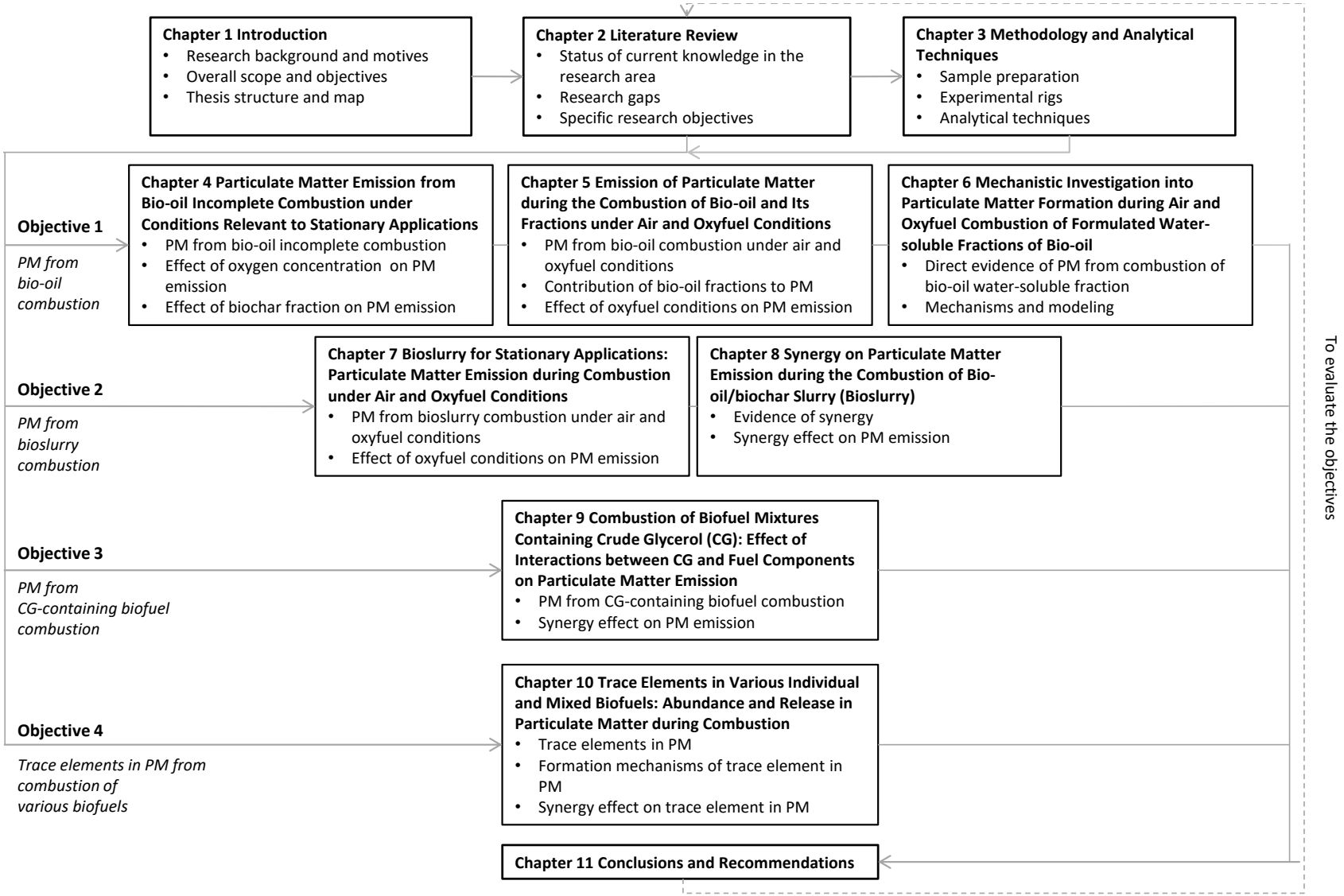

Figure 1-1 Thesis map

Chapter 2 Literature Review

2.1 Introduction

Coal is envisaged to continue to play a vital role as a cheap and secure fuel for power stations in world energy mix in the foreseeable future.[1] However, renewable energy sources have the potential to gradually penetrate into the energy mix.[95] Extensive efforts have been made worldwide to develop new technologies for efficient utilisation of renewable and green energy sources, such as biomass,[5,7] for reducing greenhouse gas emissions. Recent efforts have been focused on converting biomass into biofuels that are easy for storage and transportation. For example, fast pyrolysis of biomass has been widely recognised to be an attractive technology to produce bio-oil and biochar, which are both of high-energy density and favourable for transport.[15,17,19,21,28,96,97] In Western Australia (WA), a series of systematic studies have been conducted investigating the production, characterisation, and applications of various bio-oil based biofuels in stationary applications. Such biofuels include bio-oil, bio-oil fractions, bioslurry (a mixture from bio-oil and biochar) fuel,[30-32,98-101] and the mixed biofuels of crude glycerol (CG), which is a waste by-product of biodiesel industry.[33-36,38,102,103]

Particulate matter (PM) emission is a concern for stationary combustors[39,40] due to its adverse impacts on environment and human health. These impacts are especially prevalent for PM_1 (PMx refers to PM with aerodynamic diameter of $< x$ μm) and trace toxic element species. In past decades, extensive studies had been carried out to investigate the formation/emission of PM from the combustion of various solid fuels such as coal,[44-57] biomass,[58-66] biochar,[67] and solid waste,[68,69] and scattered studies for that of liquid fuels such as heavy fuel oil[70-73] and CG.[74,75] However, little reports have been given for PM emission from the combustion of the bio-oil based biofuels.

This chapter will review the open literature identifying the research gaps related to bio-oil and the bio-oil based biofuels and outline the objectives of this thesis. This chapter is organised as follows. It firstly presents an introduction into the properties and combustion performance of bio-oil. The chapter then reviews the properties and advantages of bio-oil based biofuels for power stations. Following an introduction of the PM emission issues and the current cleaning technologies in practice, a detailed literature review on PM_{10} emission from the combustion of solid fuels (i.e. coal, biomass, and biochar) and liquid fuels (i.e. residual oil and CG) is presented. In addition to concluding PM_{10} transformation mechanisms and emission performance from different types of fuels, the effect of combustion conditions (i.e. incomplete combustion, air and oxyfuel combustion) on PM emission are summarised. Due to the significant effects of trace elements in PM on human health, a section is also dedicated to trace element in PM_{10} emission during fuel combustion. Finally, this chapter is concluded with key research gaps identified via literature review, along with the proposed research program in this PhD study to fill in at least some of these key research gaps.

2.2 Strategy of Bio-oil Based Biofuels for Stationary Applications

Bio-oil based biofuels include bio-oil/biochar slurry fuel (bioslurry) and bio-oil/CG/biochar blend and/or slurry fuels (CG-containing biofuels). These bio-oil based biofuels are known to be good candidates for stationary applications.[29,30,36,104] This section reviews the properties and combustion performance of these biofuels.

2.2.1 Bio-oil

Bio-oil, which is produced from biomass fast pyrolysis oil, initially gained attention due to its potential as a substitute for crude oil during the oil crisis in mid 1970s.[12,20,21] However, in recent years, its ecological advantages as a biomass fuel have increased its notoriety.[20] Comprehensive reviews [12,20,28,29,105] have been

published on the utilization of bio-oil for both heat and power generation as well as the production of transport fuels. There are still challenges in the commercialization of bio-oil due to its unique fuel properties.[25,27,76,77,105,106]

2.2.1.1 Overall properties

Table 2-1 features a review of the overall physical and chemical properties of various fuels, including bio-oil, heavy fuel oil, crude glycerol, and solid fuels such as coal, biomass, and biochar, and biosolids. It is noticeable from this comparison that bio-oil has comparably higher water content than fossil fuels. This would lower its heating value and worsen fuel combustion performance but improve its flow performance due to the reduction of viscosity.[107] Bio-oil has considerably higher oxygen content, which is due to the components of highly reactive oxygenated organic compounds.[20] This also leads to the reduction of the energy value of bio-oil when compared to the fossil fuels due to there being lower energy contained in carbon-oxygen than in carbon-carbon bonds.[7]

Viscosity of bio-oil was reported in Table 2-1 with a wide range of values depending on the feedstocks and pyrolysis conditions.[20] Viscoisty is a key issue for transportation and atomization of liquid biofuels. However, it could be reduced by moderately elevation of temperature,[108] hence made pumpable and sprayable.[20] Spraying bio-oil for combustion was reported successfully reaching a mean droplet diameter of ~40 μm (measured via a conventional microscope).[108] The relationship between droplet size and bio-oil properties was also reported recently along with development of a new method for precise measurement of the spray droplets.[100]

Table 2-1 Overviews of the physical and chemical properties of common fuels (including liquids of bio-oil, fossil oil, and crude glycerol, and solids of coal, biomass, biochar, and biosolid) for stationary applications

	bio-oil (400-500 °C pyrolysis)	heavy fuel oil	crude glycerol	coal	biomass	biochar (400-500 °C pyrolysis)	biosolid
Proximate analysis (wt %)							
Moisture/water content[a]	10-30[20,107,109,110]	0.1,[20] 0.32-0.5[70,71]	0-1.47[74]	1.44-14.0[82,111]	5.6-13.1,[10,67,112] 16-30,[7] 45[6]	1.56-3.17,[99,113] 4.6-5.1[67]	5.5,[68] 23-43[91]
Ash content[b]	0-1.4[20,107,109,110]	0.02-0.1[70,71]	2.2-3.1[74]	5.0-19.3[7,111]	0.5-19.2[6,7,10]	2.3-16.1[67,99,113]	13-25[68,91]
Volatile[c]	65.9-69.7[114]			25.7-40.9[7,111]	46-82[6,7,112]	31.9-39.6[67], 16.1-23.2[99,113]	68-77[68,91]
Fixed carbon (Carbon residue)[c]	1.21,[109] 14-23[110,115]	12.2[70]		38.2-61.0[7,111]	17-21[6,7,112]	50.1-54.4,[67] 63.1-80.9[99,113]	12.8[68]
Elemental composition (wt %[c])							
C	38.8-46.9,[107] 54-58[20]	85.5-88.1[71,109]	39.1-67.3[74]	63.5-81.5[10,78,111]	38.1-51.6[6,7,112]	69.8-85.8[99,113]	46-50,[91] 53.7[68]
H	1.5-8.5[20,107]	10.5-11.3[71,109]	8.7-11.4[74]	2.8-6.8[10,78,111]	5.0-6.5[6,7,112]	2.6-3.1[99,113]	6.3-6.9,[91] 7.8[68]
O	35-40,[20] 45.6-52.7[107]	0.03,[116] 0.3-1.2[71]	17.0-52.2[74]	3.3-17.5[10,111113]	35.5-56.1[6,10,112]	8.3-22.67[99,113]	28.62[68]
N	0-0.4[20]	0.2-0.4[71,116]	0[74]	0.7-1.9[10]	0.26-0.57[7,112]	0.1-0.5[99,113]	0.6-1.1,[91] 8.66[68]
S	0.006-0.05,[110] 0.13[109]	0.46-3.3[70,71,109,116]	<0.27[74,75]	0.2-0.9,[111] 3.0[10]	<0.1,[7] 0.08,[6] 0.52,[112] 50-500[87]	0.02-0.04[113]	0.14-0.44,[91] 1.11[68]
Cl	<0.001,[110] 0.008-0.033[110]	0.006-0.04,[70] 20[75]	153-314[75]	0.3[10]	10-400[87]		0.39-1.5[91]
Major inorganic element concentration (ppm[c])							
Al	41-55[107,115]			108900[78]	17[67], 50-400[87]	59-132[67]	6811.6[68]
Ca	14-179,[99,107] 540[115]	53[75]	0-119,[74] 108-115,[75] 140[117]	15800[78]	65-600,[87] 13937[67]	3504,[99] 39313-55712[67]	20434.3[68]
Fe	47-86[107,115]			50500[78]	16,[67] 80-300,[87]	41-103[67]	3296.5[68]
K	10-55[99,107], 440[115]	0.1,[116] 22[75]	0-628,[74] 536-580,[75] 27300-31250[117]	17800[78]	400-1700[67,87]	3472-4236[67,99]	2181.5[68]

	bio-oil (400-500 °C pyrolysis)	heavy fuel oil	crude glycerol	coal	biomass	biochar (400-500 °C pyrolysis)	biosolid
Mg	<55,[99,107] 71[115]	17[75]	0-29[74,75]	13900[78]	160-620,[87] 869[67]	1364,[99] 2179-3187[67]	4857.3[68]
Na	<2,[107] 1-10,[99] 21[115]	3.4,[116] 70[75]	214-17500[74,75,117]	5900[78]	180-360,[87] 2550[67]	101,[99] 7082-9677[67]	1366.8[68]
Si	93-112,[107] 330[115]		17.3-62[117]	267300[78]	21,[67] 300-2000[87]	71-108[67]	19021.4[68]
Trace element (ppm[c])							
As		<0.1,[70] 0.1-2[71]		0.5-80[84]			1.7-20[68,91]
Cd		<0.01,[70] 0.1-0.6[71]		0.1-3[84]	0.05-1.3[87]		0.34-4.1[68,91]
Co	0.04[115]			0.5-30[84]			3.3-19[68,91]
Cr	2[115], <17[107]	0.9-14[70], 0.5-1.1[71]		0.5-60[84]			21-600[68,91]
Cu	2.8[115]	<1,[70] 0.5-4[71]		0.5-50[84]	7-25[87]		67-12000[68,91]
Hg		0-0.1[70,71]		0.02-1[84]			
Mn		0.54-2.1[70]		5-300[84]			130-350[91]
Ni	1.6,[115] <22[107]	11,[116] 22-25[70]		0.5-50[84]			18-340[68,91]
Pb	0.5[115]	<0.1,[70] 0.4,[116] 0.6-4.5[70,71]		2-80[84]	0.1-7[87]		13,[68] 120-470[91]
Sb		<0.1,[70] 1.6[70]		0.05-10[84]			9.8-57[91]
Se		0-2[71]		0.2-4[84]			
Sn		0.81-1[70]					
Ti	5-17[107]			5300,[78] 10-2000[84]			
V	0.06[115]	18,[116] 29-220[70,71]		2-100[84]			6.7-12[68,91]
Zn	14-28[107,115]	<0.1,[70,116] 3.7-74[71]	<2.5,[117]	5-300[84]	100-150[87]		
HHV (MJ/kg[a])	16-19,[20] 22.5[114]	42.4-43.7[71,109]	16.0-26.0[74,75]	15.4-30.0[7,10,111,112]	18.7-22.0[10,67]	25.9[67]	
Viscosity							
(at 20 °C, mPa s)	175-666[114]		1200[102]				
(at 40 °C, mPa s)	28.8-54.3,[99,114] 141[114]	77.7-826.4[71,116]	10.6-32.7[118]				
(at 50 °C, mPa s)	13-100[20,110]	124.2-193.7[20,70,109]					
pH	2.5-3.7[20,109,110]						

	bio-oil (400-500 °C pyrolysis)	**heavy fuel oil**	**crude glycerol**	**coal**	**biomass**	**biochar (400-500 °C pyrolysis)**	**biosolid**
Gravity (g/mL, g/cm^3)	1.18-1.26[20,109,110]	0.95-0.99[70,71,109,116]	1.26[119]	1.3[10]	0.5		
Solids (wt %)	0.18-1[20,110]	1[20]					
Flash point (°C)	56,[110] 64,[115] 72,[109] >106[110]	110[109]	177,[120] 190[103]				
Fire point/ignition temperature (°C)			204,[120] 400[103]	217-322[10]	145-153[10]		
Pour point (°C)	-36[115]	15[115]					

[a] as received basis; [b] as received basis for liquid fuels, and dry basis for solid fuels; [c] as received basis for liquid fuels, and dry and ash free basis for solid fuels.

Table 2-1 also shows that bio-oil has low ash content when compared to coal, biomass, and biochar. This is reasonable as the concentrations of the major inorganic elements (i.e. Al, Ca, Fe, K, Mg, Na, and Si) in bio-oil are low (seen in Table 2-1). However, in practice, this does not mean that there is no need to worry about the ash related issue according to bio-oil combustion. The amount of alkali and alkaline earth metals (Na, K, Mg, and Ca) in bio-oil are known to contribute to fly ash emission (PM) during biomass combustion and lead to subsequent issues such as system corrosion and pollution.[58,63] Three paths were reported as responsible for the transfer of inorganic species to bio-oil during biomass pyrolysis;[121] 1) direct release via vaporization of these species or alone with volatilization of light organics; 2) release from char particle via reaction between volatiles and char; 3) transfer with fine biochar particle and condense in bio-oil fraction after pyrolysis. As a consequence of the last pathway, solid content can be found in bio-oil, which is carried over fine biochar particles.[107,121]

Bio-oil is also corrosive, with a pH value of ~2−4 (seen in Table 2-1) due to its inherent acidic organic constituents like acetic and/or formic acids.[76,115,122,123] The acidic property of bio-oil leads to the corrosion of common construction materials such as carbon steel and aluminum.[20] Apart from the organic acids, bio-oil is also a complex mixture with various organic components including polysaccharide derivatives, some low-molecular-mass volatile compounds, degradation of lignin, and alcohols.[12,110,124] The complex components, especially those with high reactive function groups lead to the instability of bio-oil. Long term storage leads to the formation of larger molecules and the increase of both water content and viscosity due to polymerization of the reactive organics.[125,126] Phase separation occurs due to its high water content, the aging effect and the different solubility of the components.[76,77]

Precipitation in cold water is the most common method used for bio-oil fractionation and further characterization.[127,128] By this method, bio-oil could be divided into

water-soluble fraction (WSF) and water-insoluble fraction (WIF, also known as pyrolytic lignin). Significant research[127,129-134] has been done to find the different chemical composition groups of WSF and WIF for purpose of bio-oil characterization, upgrading and chemical recovery. However, further investigations are still needed for a deeper understanding of WSF and WIF compositions and quantifications.[132]

2.2.1.2 Combustion performance and adaption to burners

The combustion of bio-oil has been extensively studied in both lab scale and industry burner. Research on bio-oil combustion fundamentals was carried out through the combustion of single droplets.[105,114,135] The studies demonstrated that bio-oil combustion is a process comprised of a multitude of steps, including: (i) water evaporation followed by ignition and quiescent burning of light volatiles, (ii) droplet swelling and distortion, followed by microexplosion, (iii) sooty burning and formation of cenospheres, and (iv) subsequent combustion of cenospheres particles. This is different from that of petroleum distillate oil, which only includes quiescent and sooty burning throughout the whole process. The burning time of bio-oil was reported as comparable to fossil fuel oil under the same conditions.[114] Bio-oil ignition requires high energy support due to evaporation of water, however once ignited, a stable self-sustaining flame was observed.[20,105] The evaporation and combustion rates of bio-oil droplet are slower than that of a mineral oil droplet because of its high density and high heat requirement for water evaporation.[105] No residual ash was reported as it has low inorganic contents.[105]

Studies of industrial scale combustion of bio-oil reported that the thermal efficiency of bio-oil combustion can achieve 32.4−44.9%, which is comparable to that of diesel.[29] Its combustion flame can be divided into two different stages due to the combustion of light and heavier compounds, which is a challenge for a stable combustion.[105] Sparks were found generated and escaped from the bio-oil flame front,

which leads to the increase of its PM emission and even deposits formation on the furnace walls. The ignition delay of bio-oil combustion was found not only to depend on its water content, but also due to the severity of thermal cracking during its production process.[29] Long term running of burners with bio-oil was limited due to the damage of the nozzle and injection systems since the corrosiveness and solid content of bio-oil. This is followed by the subsequent build-up of carbon deposits in the combustion chamber and exhaust valve due to inefficient combustion.[29]

Detailed suggestions were given for bio-oil utilization in burner systems like boilers, diesel engines, gas turbine, and co-firing with coal and/or biomass in large-scale power stations.[29,105,136] Firstly, the materials of all the parts in contact with bio-oil should be replaced with resistant materials such as stainless steel or better, to adapt for the acidity of bio-oil. Secondly, the solid contents must be reduced, and a homogenous liquid with water content lower than 30 wt% was suggested. Thirdly, preheating or mixing with additives such as alcohol was recommended to reduce viscosity. Finally, modification and a well-designed feeding system and burner is suggested to adapt to the high density and low heating value of bio-oil, and optimize the combustion condition for achieving uniform, symmetrical, and stable combustion of bio-oil.

2.2.1.3 Summary

Bio-oil as a fuel shares the advantage of bioenergy with low greenhouse gas emission. As a liquid fuel, it is the closest green energy technology that can be used as a substitute for fossil oil in the near future. It is easier to transport and store than biomass and cleaner (lower ash content and no dusty issue) than biochar. Bio-oil has been proven to be adaptable to most of the current combustion devices or coal/biomass co-firing facilities. However, obviously, the unique properties of bio-oil, such as high viscosity, coking, aging, and corrosiveness are still the obstacles for bio-oil to be a commercial fuel product. Both upgrading of bio-oil and modification

of applications were required for its further utilization and commercialization. In addition, due to the various compositions and properties of bio-oil from different feedstock, pyrolysis conditions and devices, the development of standards specific for different grades of bio-oil, different applications, and the respective national legislations are needed.[136]

2.2.2 Bioslurry

Bioslurry is a method to suspend biochar into bio-oil to produce a slurry mixture. It is a concept developed by commercial developers.[32,104,137] Extensive studies have been completed to research the feasibility of the strategy of bioslurry as a fuel.

2.2.2.1 Advantages of bioslurry as a fuel

Utilization of bioslurry as a fuel has several advantages. Firstly, after pyrolysis, biochar contains about ~20−40 % the initial bioenergy.[104] Utilization of bio-oil together with biochar can achieve almost fully uptake (~90%) of the bioenergy in biomass. Secondly, bioslurry-based energy chain can save costs from production, handling, storage, and transport. Bioslurry has higher volumetric energy density[30] (~23.2 GJ/m^3, which is much higher than that of biomass of ~5 GJ/m^3), which can achieve lower cost and higher efficiency of transport compared to that of biomass.[32] Production of bioslurry as a single product can also make the bioenergy utilization chain simplified and save cost compared to separate processing and storage of bio-oil and biochar. Thirdly, as a bioenergy fuel, bioslurry also shares the advantages of low life-cycle energy and carbon footprints.[31] Fourthly, even the low quality of bio-oil, that prone to phase separation or contaminated with biochar or ash species, is still suitable for bioslurry energy chain.[104] Lastly, there is no more concerning with the issues of self-ignition and dusty handling and/or transport.

2.2.2.2 Feasibility and properties of bioslurry as a fuel

The feasibility of using bioslurry as a fuel is evaluated from two aspects: the economic feasibility and the acceptable properties for power plants or devices.

The research on bioslurry-based energy chain from Mallee wood in WA showed that overall economy of bioslurry energy chain consists of biomass transport cost, the cost for the introduction of the distributed pyrolyser, and subsequent bioslurry transport cost. When the bioenergy plant situated within the biomass production area and the whole scale of the energy plant is large enough (> 1500 dry tonnes per day), the bioslurry-based energy chain would be competitive. Thus, dedicated biofuel plants near biomass production area and application to large scale power plants were recommended for the economy of bioslurry-based energy chain. Utilization of bioslurry as a feedstock to produce syngas via gasification was also investigated and proved to have the feasibility of scaled-up production and cost efficiency.[104]

Following this is the study of fuel property of bioslurry for the target of utilization in power station burners. The result shows that bioslurry as a fuel can achieve substantial volumetric energy densification and can be suitable for combustion and gasification applications.[30,104,138] Research indicates that the slurry samples would transform from liquid to a pseudo-phase at a biochar loading level of 15−20 wt% and become totally solid phase at 25 wt% which is not fit for pumping anymore.[138] The viscosity of bioslurry is low (< 453 mPa s), at a biochar loading level in range of 10−20 wt%, and shows non-Newtonian characteristics with pseudo-plastic behaviour indicating a good pumpability.[30,138] Increased viscosity is observed when the temperature is decreased from 60 to 25 °C or biochar loading rate increases up to 20 wt%.[138] The pump tests were successful for bioslurry with biochar loading of 10−20 wt% at 25 °C and indicate that the flow rates of the slurry samples were not influenced by the char loading rates in the range of 0−20 wt%. The larger size of biochar in bioslurry leads to blocking of the pumping line due to the accumulation of char on the tube wall. Thus, smaller particle size of biochar (such as d_{80} of 118 μm) was recommended for bioslurry preparation for capabilities of both pumping and

subsequent atomization. The atomization of bioslurry with biochar loading levels up to 20 wt% via both impact atomizer and twin-fluid atomizer was successfully conducted with the results indicating that: for both the two spray nozzles, the spray droplet size would be increased along with the increase of viscosity and biochar loading level; and the twin-fluid atomizer is more applicable at lower fuel flow rate, and increasing of gas/fuel ratio would lead to reduction of droplet sizes.[100]

Further research on the stability of bioslurry during storage shows that ageing of bioslurry leads to reduction in acidity and viscosity, and increase in water content.[99] Increase of biochar loading level strengthens the aging effect. Furthermore, redistribution of inorganic species between biochar and bio-oil phase of bioslurry was found due to the leaching effect between the two phases. Such effect was proven to be mostly attributed to bio-oil WSF, especially for the organic acids and water in bio-oil.[101] This redistribution process was verified to be almost finished in approximately one week.

2.2.2.3 Summary

Bioslurry as a fuel shares the advantages of low greenhouse gas emission with other biomass fuels. As a single product with high energy density, utilization of bioslurry would save cost resulting from handling, storage, and transport. The bioslurry-based energy chain would benefit from the efficient transportation of bioslurry fuel. It was also verified to have suitable rheological properties for pumping and spray. As a result, bioslurry as a fuel is competent for substitution of fossil fuels in stationary applications, especially for large-scale power plants. However, despite the research on the advantages and feasibility of bioslurry as a fuel, there is no research on the evaluation of its combustion performance in both lab and industry combustors which should be considered as further work carried out in the future.

2.2.3 Crude glycerol (CG) containing biofuels

Biodiesel is also been considered as an alternative liquid transport fuel in recent years.[139] However, the rapid growth of the biodiesel industry also leads to extensive production and accumulation of waste crude glycerol (CG),[118] which arises the interest in its recycled utilisation. Direct combustion of CG had been proven to be difficult due to its poor fuel properties like high viscosity and low heating values[102,139-141] (seen Table 2-1). Mixing CG with bio-oil (and/or biochar) to produce CG containing biofuels is proved to be a good option which can solve the above problems and also share the advantages as a biofuel.[33,120] Several kinds of CG containing biofuels were prepared and tested.

2.2.3.1 Various CG containing biofuels

Research was firstly focused on the preparation of a blend fuel from bio-oil and glycerol. Methanol was also used in as an additive since it is found that methanol can help with the homogeneity of the blend[33] and methanol is also a typical component of crude glycerol from industry.[118] The study suggested a potential feasible composition of the bio-oil/glycerol/methanol blend (BGM) as bio-oil ≥70 wt %, glycerol ≤ 20 wt %, and methanol ≤ 10 wt % with considerations with safety of transportation and storage, and economic benefits based on the normal ratio of glycerol to methanol in industry produced crude glycerol.[33] Such research was further extended to prepare slurry fuels from the BGM blend and biochar, and verify the feasibility of BGM/biochar (BGMB) slurry as a fuel (with char loading levels of 5, 10, 15, 20 wt%).[35] As bio-oil could be divided into WSF and WIF fractions, research found that by mixing WSF with CG and/or biochar to produce WSF/CG blend (WSFCG) or WSF/CG/biochar slurry (WSFCGB), the up-taking of glycerol level could be obviously elevated (the blending ratio of CG could reach as ~50−70 %).[36] As a result, four CG containing biofuels (i.e., BGM, BGMB, WSFCG, and WSFCGB) were proposed and verified feasible for further consideration as a fuel.

2.2.3.2 Feasibility and properties of the CG containing mixture as fuels

Research on BGM[33] shows that the blend consisting of only bio-oil and glycerol cannot form a homogeneous solution, while, the addition of suitable amounts of methanol could improve the solubility of glycerol in bio-oil and vice vasa. The BGM has improved fuel properties such as higher heating value, lower viscosity, lower surface tension, and comparable density compared to that of bio-oil and glycerol individually. The density, viscosity, and surface tension are key factors related to atomization. Further calculation based on the three factors shows that BGM has lower Ohnesorge number value (0.5−2.9) compared to bio-oil (4.0) and glycerol (11.1) indicating an improved atomization ability.

An increase in biochar loading level of GMBB slurry was reported to lead to an increase of heating value, density, viscosity, surface tension, and decrease of water content and acidity, however, compared to bio-oil/biochar slurry (bioslurry) at the same biochar loading level, the GMBB has much lower viscosity, water content, and acidity.[35] The GMBB slurry fuel also exhibits non-Newtonian and thixotropic behaviour, which indicates its good pumpability.

When it comes to the WSF prepared CG containing blend or slurry fuels (CG is prepared as a formulated crude glycerol[36]), the study shows that the WSFCG blend has considerably lower acidity and water content, and higher density and heating values than WSF only. With a comparable energy density with bio-oil, the WSFCGB slurry exhibits favourably better viscosity, Ohnesorge number, and acidity than the bio-oil/biochar or GMBB slurries.

Similarly with bio-oil and bioslurry, the CG containing biofuels also suffer with aging after long term storage.[33,35,36] Ageing would lead to the decrease of acidities and viscosities and increase of water contents of these fuels. The decrease in acidity is due to esterification reactions between acidic compounds in bio-oil and glycerol or biochar, while, the increase of water content is the results of esterification,

acetalization, and/or polycondensation reactions.[35] The leaching effect on inorganic species was also observed similar with the case of bioslurry. The presence of methanol and glycerol was found slowing down the ageing and reducing the leaching capability of water and/or acidic compounds in the mixture.

Recent research[37] on ignition temperatures of these CG containing biofuels was also carried out with thermogravimetric analysis and method according to ASTM standard with results showing that the ignition temperatures of these CG containing biofuels (445−510 °C) are equal or slightly lower than that of bio-oil (506 °C) and WSF (511°C), higher than that of biochar (375 °C).

2.2.3.3 Summary

Preparing CG containing biofuels, i.e., BGM, BGMB, WSFCG, and WSFCGB, is a good option to address the key issue associated with waste glycerol combustion and also take advantage of biofuels as a sustainable green energy sources. Especially, WSFCGB is proved to achieve a high up-taking proportion of industry CG and to be a feasible fuel for stationary burners with a comparable energy density with bio-oil and good pumpability. However, further tests on the combustion performance of these CG containing biofuels in both lab and industry burners is still a requirement for its further utilization.

2.2.4 Summary of the bio-oil based biofuels

To deal with greenhouse gas emission and achieve economic and ecological bioenergy utilization, bio-oil based biofuels, including bioslurry and four CG containing biofuels, were studied and proved to be good options as substitution fuels for coal-fired power stations. Particularly, the CG containing biofuels not only share the advantages of low greenhouse gas emission as a bioenergy, but also benefit from recycle utilization of waste glycerol from biodiesel industry.

However, study of the combustion performances of these bio-oil based biofuels, such as ignition, combustion fundamentals, flame characteristics, combustion efficiency, and ash deposition or fly ash emissions, are still not sufficient in both lab and industry scales, which needs to be paid further attention in the future.

2.3 Issue of Particulate Matter Emission from Stationary Applications

PM emission from stationary combustion is a significant source of primary particles with size smaller than 2.5 μm ($PM_{2.5}$) in urban areas.[40,41] It is an issue of concern for both power plant operation and environment protection. Extensive efforts have been made to study PM formation mechanisms during combustion (detailed in following sections), pathological mechanism, and capturing methods.

2.3.1 Introduction of PM emission and related issues

Combustion of coal, biomass, and fossil oils would generate PM with sizes ranging from nanometre to millimetre, including cenospheres, soot aggregates, and fly ash particles.[41] Some larger particles are removed in the combustion zone as bottom ash or wall deposits, or collected by the gas cleaning devices, while, the smaller, especially PM_1 travel with the exhaust gas and contribute to ambient air pollution. The U.S. Environmental Protection Agency have regulated PM particles into two size categories[142] for establishment of air pollution standards: (i) fine particles of $PM_{2.5}$, and (ii) PM_{10} for concerning coarse particles in the size range of 2.5−10 μm. Once emitted into the atmosphere, the PM suspends over long time (days to weeks for $PM_{2.5}$) and travel over long distances (100 to 1000 kilometres for $PM_{2.5}$) in the air[143] and finally lead to a wide range of diseases and become a threat to human health.

PM is a key indicator of air pollution since as it has adverse impacts on human health. Both the fine and coarse PM particles were reported with penetration capacity into trachea, bronchi, and deep lungs.[142] Figure 2-1 shows the deposition potential for

particles with various sizes.[143] Exposure to PM has been identified as the reason for numerous health effects including respiratory symptoms,[144,145] exacerbation of chronic respiratory and cardiovascular disease,[146,147] decreased lung function,[145] and premature mortality.[143] Under insufficient combustion, PM may include organic constituents such as soot, formed from benzene-based polycyclic aromatic hydrocarbons (PAH), which is toxic and can lead to respiratory disease and even lung cancer.[148-150] The inorganic constituents of PM also consist of trace element species.[84] The so-called trace elements are defined due to their low concentrations (<100 ppmw) in fuels (initially in coal), however, they cannot be ignored. Some of them had been regulated as high toxic chemicals such as arsenic (As), beryllium (Be), cadmium (Cd), chromium (Cr), copper (Cu), mercury (Hg), lead (Pb), and nickel (Ni), and some as radionuclides, such as polonium (Po), radon (Rn), radium (Ra), thorium (Th), and uranium (U).[151] Some of them such as As, Be, Cd, and Cr have been classified as carcinogenic metals[42] as they can lead to a wide range of cases of carcinoma.[40] Trace elements in PM emission had attracted more and more attention from scientists due to their toxicological effects to human health.[39,40] The pathological mechanisms relating to PM and trace element resulting diseases are still under investigation for the help of subsequent therapy and establishment of emission regulation or policy.[40,143,146,147]

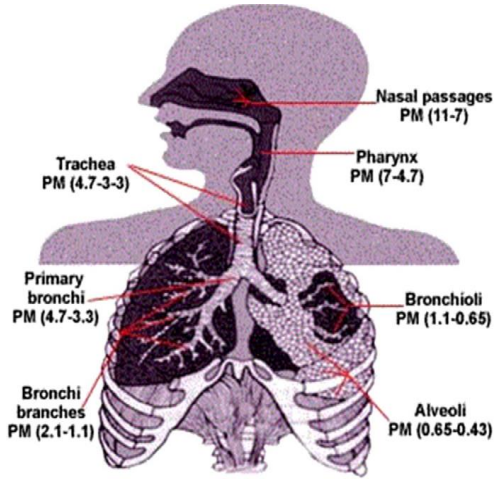

Figure 2-1 Deposition potential for particles of various sizes.[143]

Apart from concerns with air pollution and human health, the generated PM in stationary applications can also lead to ash related issues in furnaces. The ash deposition of these PM particles on furnace walls and/or bottom would lead to slagging and/or fouling, and then subsequent reduction of running efficiency.[58,152,153] Corrosion of the furnace also occur due to the chemical attack of the ash species on the surface of the furnace, especially in the area of the heat exchanger section, and then shorten the life of the facility.[63,153,154]

2.3.2 Methods and status of PM capture

To deal with the PM emission issue, many studies had been carried out on the PM particle size distribution (PSD), morphology, chemical composition, and capturing. The collection efficiency of cleaning devices directly determines the amount of PM emitted from power plants to the environment. Current PM control technology can be divided into two groups: dry and wet.[155] Examples of dry devices include cyclones, fabric filters, ceramic filters, electret filters, and electrostatic precipitators (ESPs). The wet devices include inertial, centrifugal, Venturi, or electrostatic scrubbers, foam precipitators, and irrigated ESPs. The mechanisms of the cleaning devices include applying mechanical (inertial and gravitational) forces to precipitate the particles from gas, or molecular forces to capture particles on a solid or liquid collector, or the dense obstacles in the form of fibrous or porous media for filtration.

ESP is a technology using electrical energy to remove the PM from the gas stream and is most widely applied in power plants.[86] Compared to conventional cleaning methods, the utilizing of ESP can achieve a higher collection efficiency with an average value of >99%, and has better performance for small particles in the range of 0.1-1 μm (compared to <90% of conventional method for such particles).[43,86] However, the efficiency of ESP is affected by several factors including particle size,[156] boiler load,[157] ESP voltage, flue gas composition,[158] and particle composition.[159,160] Research reported that improvement of ESP was carried out with

adding a low temperature economizer to enhance the capture of PM_1 and trace elements in PM_1.[86] More improvement work for ESPs is needed and currently under development to deal with issues such as insufficient collection efficiency for particles in submicron range and trace elements,[86] the back corona which may lead to lack of discharge current, then low cohesiveness of the dust and particle re-entrainment from the collection electrode, and contamination of the discharge electrode leading to corona failure, ozone generation, and dust re-entrainment.[43] Large-scale ESPs are also relatively costly and are not economically viable without government subsidies.[161] They also face problems with safety due to high voltage equipment and high maintenance requirements.[161]

Methods of mixing additives (such as calcium hydroxide or limestone[162-164]) into feedstocks or change the atmosphere conditions[165] during combustion was also conducted to relieve the fly ash caused boiler corrosion[61] and PM_1 emission. However, these methods were reported with limited reduction in PM emission and in some cases even increase the emission of ultrafine particles.[161] Co-firing of biomass and coal was reported leading a shift in the PM_1 formation ash species to coarse ash particles due to interaction of alkali metals with refractory element species thus enhance the capture efficiency of PM_1.[166]

2.3.3 Importance of study on PM emission from fuel combustion

From the above discussion it could be concluded that PM_{10} is a big concern for stationary applications due to its adverse impacts on the environment and human health. Especially, PAHs during incomplete combustion and trace elements in PM_{10} are significant due to their toxic nature. Collection of PM_{10} via current technology, especially ESPs, can achieve a relatively high efficiency, however, further improvement is still needed and under development for a better performance and low cost of utilization. Therefore, considering the application of new fuels and combustion technologies in recent years, the study of PM emission is still an

important subject, including further understanding of formation mechanisms, size distributions, and physical and chemical characteristics, development of new or improved capturing methods, and exploring related pathological mechanisms.

2.4 PM_{10} Emission from Solid Fuel Combustion

Combustion of coal and biomass is a well-known producer of significant PM emissions in stationary applications. Extensive studies have been carried out on the formation and emission of PM from the combustion of these solid fuels. Recently, such studies were also extended to biochar combustion. This section will give a brief review on the transformation mechanisms and characteristics of PM emission from previous study on combustion of coal, biomass and biochar. It should be noted that all the discussions in this section are based on complete combustion therefore only the inorganic PM will be concerned, and as the complexity and comparably lower amount of trace element retention and emission compared to major elements, the review of trace element emission in PM_{10} will be given in of Section 2.7.

2.4.1 PM_{10} emission from coal combustion

The bottom ash and PM is transformed from the mineral matter in coal during combustion which consists of a variety of inorganic elements (seen in Table 2-1). The mineral matter includes inherent mineral matters (chemical bond with carbonaceous matrix) and excludes minerals that show different performance of inorganic transformation during combustion. The characteristics, such as PSD and elemental PSD of PM_{10} will be introduced, followed by the discussion of the associated formation mechanisms.

2.4.1.1 Characteristics of PM_{10} from coal combustion

It has long been well known that coal fly ash has a bimodal distribution with a fine mode centred at ~0.1 μm and a coarse mode usually larger than 1 μm.[41,167,168] The two modes are correlating to two different formation mechanisms (detailed in next

subsection). However, some recent reports also present results that coal fly ash PSD might also be trimodal with an additional mode between the fine and coarse modes.[169-172] In details, the fine mode was in the range of <~0.5 μm, with peak usually at ~0.1 μm, the coarse mode in the range of >~1 μm, with peak located in the range of ~1−10 μm,[171] and a central mode in range between ~0.5−5 μm with peak at an ubiquitous location in the range.[52] Less attentions of the central mode in the past work were attributed to the low resolution of the previous particle sizing instruments,[173] as the central mode is usually overlapping with either the fine mode in PM_1 range [172] or the coarse one in PM_{1-10}.[174] Thus, normally, in the range of PM_{10}, bimodal distribution could be applied and discussed according to the two distinct formation mechanisms corresponding to PM_1 and PM_{1-10}.

To further understand the particle formation mechanisms, information of detailed elemental PSD is important. In fact, the physical PSD of PM should be consistent and verified by the elemental PSD.[175] Research has reported three kinds of elemental distributions in PM_{10} during coal combustion.[176] First is the unimodal distribution of SiO_2, Al_2O_3, CaO, SO_3 and P_2O_5. The former three element species are predominantly in PM_{1-10} with mode peak at ~2.5 μm, while, the later are prevalent in PM_1 with mode peak at ~0.06 μm. Then is the bimodal distribution of Fe_2O_3, Na_2O, K_2O and MgO with both fine and coarse modes at ~0.06 and ~2.5 μm, respectively. The third is Cl due to its unimodal distribution with peak in the range of ~0.2−0.5 μm. The elemental PSDs are correlating well with the aforementioned PSD of PM_{10}. However, another report on coal combustion[172] presented different elemental distributions in PM_{10} for Na, S, and Cl. In details, Na and Cl were unimodal distributions with only fine mode at ~0.03 μm and S was bimodal with fine and coarse modes at ~0.03 and ~1.6 μm, respectively. Though they reported these elemental PSD in different chemical forms, i.e. oxides and elements, this is not the reason for the different PSD results. The exact reason can be attributed to the

different transformation mechanisms during combustion due to their different coal types and mineral retention forms.

2.4.1.2 PM_{10} formation mechanisms during coal combustion

Coal combustion aerosols (PM) can be divided into two groups based on their formation mechanisms, i.e. the vaporized and the residual ash particles.[52] The 1.0 μm just acts as the boundary line between these two groups,[176] i.e. PM_1 and PM_{1-10}. It is well-known and verified extensively via both experiments and modelling that the PM_1 is formed by solid−vapour−particle processes including vaporization, gas-phase reaction, followed by homogeneous nucleation, heterogeneous condensation on the existing particles, and coagulation and/or agglomeration,[44,45,47,49,170,177] while, the PM_{1-10} is generated via solid−to−particle processes with mineral coalescence and particle fragmentation.[49,50,152,169,170,178-181] Figure 2-2 gives the diagram of the major process governing the PM formation during coal combustion.[52] The detailed formation mechanisms for PM_1 and PM_{1-10} from coal combustion are briefly discussed as follows.

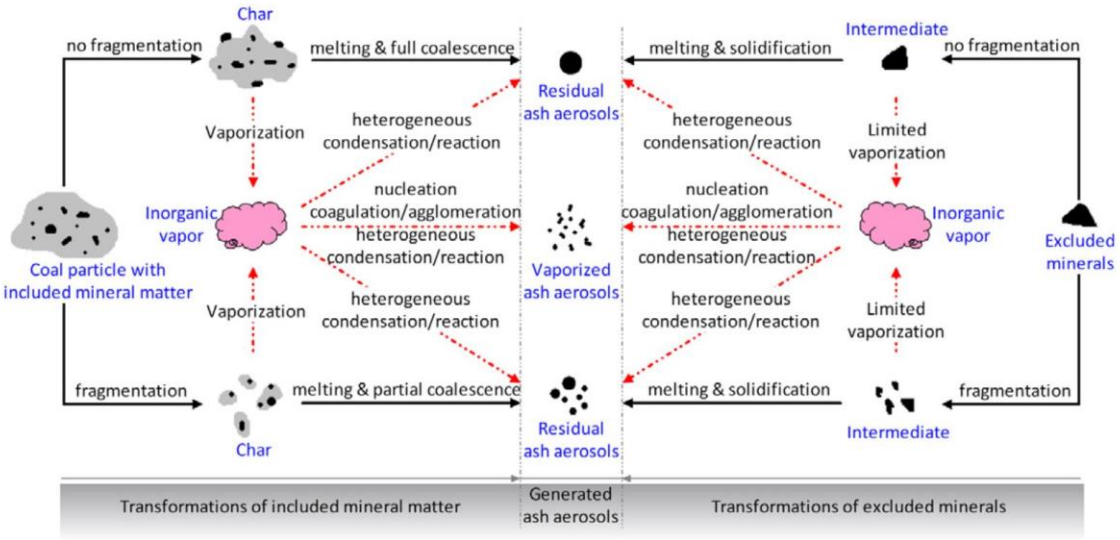

Figure 2-2 Major ash aerosol formation mechanisms during coal combustion (solid arrows indicate solid-to-particle processes while dotted arrows indicate solid-vapour-particle process)[52]

Formation of PM_1. The mechanism of PM_1 formation during coal combustion was believed mainly due to vaporization and condensation (dotted arrows in Figure 2-2).[47,49] The vaporization of mineral matters depends on their inherent volatilities and occurrence forms in coal, and the combustion conditions such as particle temperature and atmospheres. In details, the inherent volatilities of the major elements follow a decreasing order of Na > K > Fe > Mg > Ca > Si > Al.[176] As a result, the vaporization degree of Na was reported in the range of ~30−65%, higher than the rest elements, such as K/Fe (~3−20%), and then Mg (≤ 5%).[176] Actually, based on their volatility, Na and K are grouped as volatile elements, while, Fe, Mg, Ca, Si, and Al are refractory elements.[182] Those organic-bound minerals could be easier vaporized as their volatilization process is at the very start, while, the evaporation of those associated with silicates would be quite hard.[49,172,183] The vaporization can also be enhanced by higher particle temperature and reducing environments, especially for refractory elements such as Si, Al, Fe, Ca, and Mg, which can contribute to PM_1 due to the gas-phase release of their sub-oxides (SiO and AlO) and/or metal forms (Al, Fe, Ca, and Mg) under reduction atmosphere.[49,176] Fuel properties such as coal rank and fuel particle size can also influence the vaporization and then the final PM particle sizes. Both the volatile components and char fraction of coal were reported to have significant contribution to PM_1 emission during combustion.[184,185]

Once these metal species are released into the gas phase, followed by further reaction with oxygen, steam,[172] HCl (g),[186] SO_3 (g),[172,176] or other metallic vapors,[176] homogeneous nucleation occurs to form large numbers of small particles (precursor of PM_1), followed by coagulation, agglomeration, and/or heterogeneous condensation on the pre-existing particles, leading to the subsequent particle growth and then distributed in PM_1.[39] As a result, the morphology of PM_1 particles is spherical and/or aggregate-like. To be concluded, the distribution of the major

inorganic species (both metals of Na, K, Fe, Mg, Ca, Si, Al, and Cl and S) in PM_1 can be well explained by the mechanism of vaporization and condensation.

Apart from the classic "vaporization and condensation" mechanism, some other mechanisms were also reported as possibly responsible for PM_1 emission during coal combustion, including surface ash shedding,[46,50,187] cenospheres bubble bursting,[177] directly carryover by submicron coal particles or minerals,[175] and convective transport of minerals during devolatilization.[188] However, all the four possibilities are still in the hypothesis phase without direct experimental evidences.

Formation of PM_{1-10}. PM_{1-10} formation during coal combustion was reported to be driven by three mechanisms, i.e. included mineral coalescence, coal fragmentation, and excluded mineral fragmentation (seen the solid arrows in Figure 2-2). Included mineral coalescence is a process that during coal particle combustion, more than one piece of minerals in one coal particle would have the chance to coagulate together on the size-reducing burning surface under a temperature higher than their melting points, followed by formation of one molten or semi-melting droplet, and finally cool down and condense as one new larger (spherical or irregular shaped) particle that finally distributes as PM_{1-10}.[169,178,189,190] This mechanism was reported not to happen between the excluded minerals or those inherent minerals in separate coal particles due to the few opportunities for them to reach each other.[52] As a result, this mechanism is highly in relevant with the combustion temperature and occurrences of mineral matters, such as particle size distribution and chemical compositions.[191] It is reported that under typical coal combustion temperature of 1200−1600 °C,[192] minerals like kaolinite and iron oxides will melt and coalesce together completely.[193] Modelling work via calculation based on thermodynamic equilibrium[176] further proved that during coal combustion, Al and Si species inside one coal particle would form together as mullite ($Al_6Si_2O_{13}$), and Ca, Mg, Na, and K would all have the possibility to be absorbed by aluminosilicate to form various compounds such as $CaAl_2Si_2O_8$ ($Ca_2Al_2SiO_7$ or $CaAl_4O_7$), $Mg_2Al_4Si_5O_{18}$, NaAlSi3O8 and KAlSi2O6,

while, only small amount of Ca would be released as vapor. The gas phase release of Mg, Na, and K is enhanced under higher particle temperature conditions. The modelling results are consistent with the experiments which observed various aluminosilicate salts including Na, K, Mg, Ca, and/or Fe in PM particles at the coarse mode (~2.5 μm) and indicated the significance of chemical reactions between different mineral species during the transformation of the inherent minerals.[176] As a result, the coarse mode distribution of these elements in PM_{10} could be explained by that during coal combustion, the inherent mineral species would transform and contribute to PM_{1-10} via coagulation and formation of aluminosilicates on the surface of burning char particles.

However, the coalescence of inherent minerals can also be influenced by coal particle fragmentation. Coal fragmentation is a process to break one coal particles into numbers of smaller pieces during the processes of devolatilization, pyrolysis and further combustion.[179,180,194] Contrary to coalescence, which leads to formation of larger ash particles from numbers of small minerals, fragmentation would lead to reduction of coal particle size, thus decrease of the quantity of inherent minerals in one new-born coal particle fragment, and subsequently formation of a relatively smaller ash particle via coalescence of the minerals.[187] The intensity of coal fragmentation depends on several factors including coal rank, particle size, combustion conditions, and the structure of formed char.[181,190,193,195]

Excluded minerals would also contribute to PM_{1-10} via direct transport of tiny minerals, or larger size mineral fragmentation. Studies on the fragmentation of excluded minerals in coal during combustion have been conducted previously.[196] Fragmentation of excluded pyrite (FeS_2) was found with process of decomposition to form pyrrhotite (FeS) and sulphur, followed by further fragmentation and then oxidation.[196,197] Excluded carbonates such as siderite, ankerite, and calcite, would undergo fragmentation combined with releasing of CO_2.[196,197] However, no

observation of fragmentation was found for silicate minerals, like quartz, illite, and muscovite.[196]

2.4.1.3 Summary of PM_{10} emission from coal combustion

PM emission from coal combustion would follow mainly bimodal distribution in PM_{10} with a fine and a coarse mode in PM_1 and PM_{1-10}, respectively. The PM_1 is mainly formed by the evaporation of inorganic species (of both volatile elements and refractory elements), followed by gas-phase reaction, nucleation, agglomeration and/or coagulation, or heterogeneous condensation on the existing particles; while, the PM_{1-10} is mainly formed by coal particle fragmentation followed by coalescence of included minerals and fragmentation of excluded minerals. The coalescence of included minerals would lead to the formation of aluminoslicate salts including elements of Na, K, Mg, Ca, and/or Fe in PM_{1-10}.

2.4.2 PM_{10} emission from biomass combustion

PM emission from biomass combustion was also extensively studied in recent years due to the prevailing utilization of bioenergy for power generation. The occurrence of inorganics in biomass is quite different with that of coal, such as the dominant contents of nutrient elements like K, Na, Cl, S, Mg, Ca, P, and little Si, and considerably lower contents of Al and Fe (seen in Table 2-1), as well as the excluded minerals.[198] As a result, the ash compositions of the two fuels are different (seen in Table 2-2[198]). The combustion characteristics of biomass are also different with that of coal due to their different fuel properties.[10] Therefore, the PM emission from biomass combustion would have different characteristics compared to that of coal.

2.4.2.1 Characteristics of PM_{10} emission from biomass combustion

Similar with PM emission from coal combustion, biomass combustion was also commonly reported to produce PM_{10} with PSD of bimodal distribution,[58,66,199-201]

Table 2-2 Average ash composition of wood, husk/shells, grass/plant, peat and coal[198]

composition (wt% of ash, daf[a])	coal	peat	wood	husk/shells	grass/plant	straw
Al_2O_3	16.4	22.2	2.9	2.3	2.92	0.5
Fe_2O_3	12.4	30.5	1.5	1.6	0.33	0.5
SiO_2	53.5	24.8	19.9	16.8	34.24	19.4
CaO	4.6	9.5	77.0	7.53	11.34	13.7
MgO	0.7	2.9	5.5	12.01	3.6	2.8
K_2O	1.2	0.3	2.1	0.6	1.15	1.1
Na_2O	2.8	0.6	10.9	35.1	20.1	20.9
P_2O_5	n.a.[b]	3.0	4.8	14.9	4.5	4.7

[a] dry and ash free; [b] not applicable.

including a fine mode in the range of PM_1 (peak at ~0.02[66,200,201] or ~0.3[58,199] μm) and a coarse mode in the range of PM_{1-10} (peak at ~2.0,[199] ~4.0,[66,200,201] or ~6.0[58] μm). There is also one case reporting trimodal distribution[202] of PM_{10} with a fine mode in the range of ~0.01−0.1 μm, a central mode at ~1.6 μm, and a coarse mode at ~8.3 μm. The different modes and peak positions of these reports on PM_{10} emission from biomass combustion are all reasonable since that several factors may influence the results of PM_{10} emission such as biomass types, inorganic occurrence forms, ash compositions, combustion conditions, and sampling methods.[65,153,183] However, it can still tell the story of the distinction of PM_1 and PM_{1-10}, consistant with the case of coal combustion that the formations of PM_1 and PM_{1-10} are dominated by two different mechanisms.[203]

When it comes to the elemental compositions of PM_{10}, biomass shows an obvious difference with that of coal, which is that most of the research on biomass combustion reported lower proportion of aluminosilicates in PM_{10} than that of coal. In details, the fine modes of PM_1 from biomass combustion were reported composed of mainly (volatile elements of) K, Na, Cl, and S, [58,61,66,202] in forms of chlorides, sulphate, hydroxide,[202] and/or carbonate,[58] and also low amounts of refractory elements such as Ca, Mg, Si, Al, Fe, and P,[202] while, the coarse modes of PM_{1-10} are all refractory elements, dominated by Ca-species (rather than Si and Al in coal), followed by Mg, and low amounts of Si, Al, Fe, and P, in forms of mainly Ca/Mg

oxides and/or carbonates,[165,200,201,204] and less aluminosilicates[58,202] and phosphates.[153,201] Alkali metals like K and Na may also have the chance to distribute in PM_{1-10} during the combustion of biomass with retentively high silicate or calcium contents.[60,63] As a result, the elemental PSDs of both volatile elements (Na, K, Cl, and S) and refractory elements (Ca, Mg, Si, Al, and Fe) in PM_{10} from biomass combustion all show mainly unimodal distribution, with a fine mode at ~0.02[66,200,201] or ~0.3[58,199] μm for the former, and a coarse mode at ~4.0,[66,200,201] or ~6.0[58] μm for the latter, which can combine together to the bimodal PSD of PM_{10} during biomass combustion.

2.4.2.2 PM_{10} formation mechanisms during biomass combustion

The formations of PM_1 and PM_{1-10} during biomass combustion also follow the classic mechanisms found in coal combustion, i.e., the vaporization and condensation for PM_1, and fragmentation and coalescence for PM_{1-10}. Whereas, there are some unique features during biomass combustion due to the different inorganic species compositions.

Formation of PM_1. Similar to coal combustion, the formation of PM_1 during biomass combustion is also driven by the mechanism of vaporization of volatile species, followed by gas-phase reaction, nucleation, coagulation/agglomeration, and/or condensation on the existing particles. The difference is that PM_1 especially $PM_{0.1}$ from biomass combustion is mainly consisting of alkali (Na and K) species with negligible refractory element species.[199] Figure 2-3 is a summary of possible reaction pathways and release mechanisms of K and Na during biomass pyrolysis and subsequent combustion.[205] It could be found from Figure 2-3 that there are several pathways for K and Na to release in gas phase during biomass combustion: 1) direct release from K/Na bonded organic volatiles during devolatilization and/or from salts via vaporization, 2) release from char via volatile-char interaction[69] and/or during char combustion. Release of only alkali species and PM_1 from the volatile

constituents of biomass was verified by direct combustion of the situ produced volatiles from biomass fast pyrolysis.[206] As the key alkali elements in PM_1, there are several findings from previous research for the release and nucleation of the K (Na) species during biomass combustion: 1) when Cl is sufficient, the aerosol would be KCl, while, when absence of Cl, the sulphates and hydroxides would appear instead;[58,202] 2) when S is sufficient, the significant amount of SO_2 would lead to sulfation of the alkali chloride and form of sulphate with releasing of HCl in gas phase;[165] 3) Cl is the main factor that dominants the release of K via sublimation of KCl at a reaction temperature of ~700−800 °C, and dechlorination of the biomass can effectively reduce the emission of K;[154,201] 4) the K_2SO_4 would nucleate earlier than that of KCl when the gas cools to ~900 °C, followed by the condensation of KCl on the K_2SO_4 nuclei at ~560 °C and to a great amount at ~360 °C;[199] 5) the existence of Si species would lower the release of K as the retention of K in solid form of K_2SiO_3;[60,207,208] 6) equilibrium calculation was also indicating the possibility of formation of K_2CO_3 at 700 °C from reaction of KOH and CO_2 when there is not enough S and Cl to bind all the K, and subsequently condensation on the K_2SO_4 particles when temperature lower than 650 °C,[58] however, when quenched at higher temperature, KOH would be condensed rather than K_2CO_3;[165] (7) lower ash content and dilution would lead to the delay of the nucleation/condensation process during the cooling process.[165,199]

Research also reported that during combustion of biomass, ~25−70 % of Cl would be released when heated to 500 °C, followed by release of KCl at 700−800 °C, and depleted when higher than 800 °C.[60] The release of S is complicated: ~30−50 % of S would release firstly before 500 °C, and further release of S from K/Ca-sulphates would be difficult due to the stability of sulphates up to 1000 °C; while, the thermodynamic equilibrium calculation suggests that in the presence of silicate, this temperature would reduce to 800−900 °C due to the formation of Ca-K-silicates and

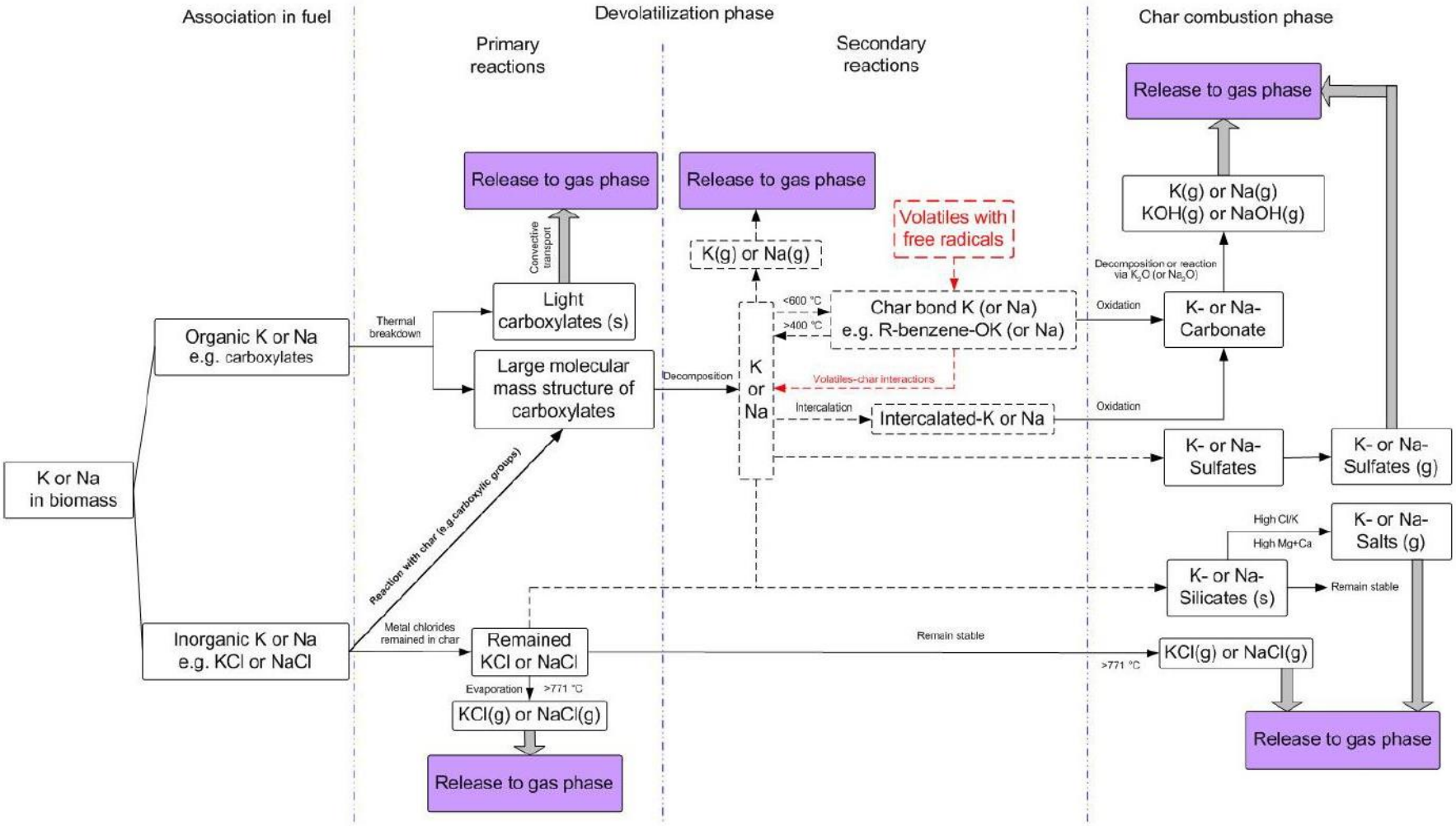

Figure 2-3 Possible reaction pathways and release mechanisms of K and Na during biomass pyrolysis and combustion[205]

low solubility of SO_2 in the silicates.[60] Due to the release of acidic gases HCl and SO_2, sampling temperature for PM_{10} collection was also verified to be set as 115 °C, which is the dew point of SO_3.[65]

The refractory elements are also partially vaporised during biomass combustion forming fine particles by nucleation, but this contribution is insignificant in $PM_{0.1}$.[58,202] The particles of $PM_{0.1\text{-}1}$ were also reported to have similar composition with $PM_{1\text{-}10}$ i.e., predominately Ca, followed by Si, Al, and Fe, indicating their similar sources during combustion, while, the Na and K was also observed in $PM_{0.1\text{-}1}$ which is a result of alkali aerosol condensation and bonding with other minerals.[202]

Formation of $PM_{1\text{-}10}$. The mechanism of $PM_{1\text{-}10}$ formation during biomass combustion also has similarities with that of coal, such as fragmentation[204] and the formation of aluminosilicates via coalescence of inorganic species on the burning char particles.[58,183,200-202] However, there is a major difference in $PM_{1\text{-}10}$ formation from biomass compared to coal. As the dominant composition of $PM_{1\text{-}10}$ is Ca species during biomass combustion, followed by Mg, apart from formation as aluminosilicates, there is another pathway for the transformation of Ca species into $PM_{1\text{-}10}$, which is called catalysed sintering.[200,202] The CaO particles during combustion would sinter under CO_2 atmosphere at temperature higher than 897 °C with the process of repeated formation and decomposition of $CaCO_3$, thus leading to the formation of larger Ca-rich particles[209,210] during char burning. This process can be verified by the observations of porous Ca-rich skeletal particles with size of ~8.3 μm which are unfused ash particles with only surface sintering.[202] Observation of $PM_{1\text{-}10}$ via water-leaching of the PM sample followed by analysis of the leachate also indicated the formation of not only the carbonates, but also Mg/Ca-phosphates during char combustion.[200,201]

Further discussion. Research on PM_{10} emission from biomass combustion was further extended to upgraded biomass such as spent biomass,[200] torrefied biomass,[201]

and biomass that has undergone light pyrolysis under 300 °C.[211] It was found that the leaf component of biomass after steam distillation (spent biomass) would produce similar yields of PM_1 and Na, K, and Cl in PM_1 compared to the raw leaf, however, produce lower amount of PM_{1-10} and Mg and Ca in PM_{1-10} which is due to the remove of essential oil (mainly 1,8-cineole) and the discrepancy of the structure of the produced char from distillation (analysed as reduced char particle surface area),[200] as both of the absence of the essential oil and change of char structure would lead to less intense fragmentation and then less PM_{1-10} formation during combustion. However, when it comes to torrefied biomass, research found the propensity of decrease of PM_1 and increased PM_{1-10} during combustion compared to raw biomass due to the loss of Cl and intensified char fragmentation after torrefication.[201] The biomass upgrading via heating under inert atmosphere and temperature of lower than 300 °C was also carried out followed by combustion and indicates that such pre-treatment would lead to increase of PM_1 emission during combustion due to the absolute increase of K and Cl quantities in biomass after upgrading.[211]

Research on separate combustion of the major fractions of Mallee biomass, i.e., bark, leaf, and wood, indicates that PM_{10} emission from the combustion of the three components all shows bimodal distributions similar to that of the whole biomass, however, with the PM_{10} yields following a decreasing order of bark > leaf > wood, consisting with the comparison of their ash contents.[66] Further comparison of calculated PM_{10} from the separate combustion of the three components with direct combustion of the whole biomass shows that there is no synergy between the three components during combustion, and thus the PM_{10} from the whole biomass combustion could be roughly estimated by the composition of its three components. Efforts on PM emission prediction were also made to find the linear correlation between the inorganic occurrences and their release in PM during biomass combustion and finally concluded that prediction of PM emission based on such

correlation would be particularly effective for biomass with similar characteristics, such as woody biomass.[183]

2.4.2.3 Summary of PM_{10} emission from biomass combustion

It could be finally concluded that PM_{10} emission from biomass combustion shares some similar characteristics with that of coal combustion, such as bimodal distribution with a fine and a coarse mode in PM_1 and $PM_{1\text{-}10}$, respectively. In addition, PM_1 from biomass combustion is mainly consisted of volatile element species, particularly alkali species, while, $PM_{1\text{-}10}$ is dominated by refractory element species major as Ca, followed by Mg, and small amount of Si, Al, Fe, and P. The inorganics transformation to PM during biomass combustion also follows the two classic mechanisms, i.e., vaporization and condensation for PM_1, and fragmentation and coalescence for $PM_{1\text{-}10}$. The distinct differences compared to that of coal are that for biomass combustion, the PM_1 is mainly driven by complicated gas-phase reaction of alkali species, while, for $PM_{1\text{-}10}$, the dominant process is catalysed sintering of Ca species to form CaO and $CaCO_3$.

2.4.3 PM_{10} emission from biochar combustion

Fast pyrolysis biochar from biomass is also considered as a potential fuel for substitution of coal for stationary application as it has good grindability and comparably higher energy density than biomass.[11,26] Therefore, the PM emission from biochar combustion was also paid attention to.[67,211,212] Since it is well known that during biomass fast pyrolysis, the volatile inorganic elements, especially alkali, Cl, and S are released to gas phase and most of the inorganic species would be left in the biochar fraction,[60,154,206] the transformation of PM_{10} during biochar combustion is quite simple compared to that of coal and biomass.

Research was carried out to prepare biochar produced from both slow and fast pyrolysis of Mallee bark under various temperatures in the range of 400−500 °C and

subsequently burn the biochar and raw biomass at 1300 °C for PM_{10} collection and analysis.[67] The result shows that compared to bimodal distribution of PM_{10} from biomass combustion, biochar combustion has mainly unimodal distribution of PM_{10} with only a coarse mode at ~6.0 μm, except the case for fast pyrolysis biochar under 500 °C, which shows bimodal distribution with an addition of a fine mode at ~0.01 μm. As a result, the rest of the slow and fast pyrolysis biochar samples all have only unimodal distributions of Mg and Ca in $PM_{1\text{-}10}$ with coarse modes at ~6.0 μm, except for the case of 500 °C−fast pyrolysis biochar, which shows not only the coarse-mode-unimodal distribution of Mg and Ca in $PM_{1\text{-}10}$, but also unimodal distributions (fine mode at ~0.01 μm) of Na and K in PM_1. The production of $PM_{1\text{-}10}$ and the refractory elements of Mg and Ca in $PM_{1\text{-}10}$ could easily be understood by the retention of these refractory elements in biochar and their subsequent transformation via fragmentation followed by catalysed sintering or coalescence during combustion. The exception of PM_1 emission from 500 °C−fast pyrolysis biochar combustion could be explained by the comparably high retention of Na, K, and Cl in biochar and the subsequent vaporization and condensation of these elements during combustion. Similar retention of Na, K, and Cl in biochar and their further contributions to PM_1 during combustion were also reported and further verified recently,[211] with results demonstrating that with the increase of pyrolysis temperatures for biochar preparation from 250−1000 °C, the PM_1 emission from the subsequent combustion would increase first and reach a maximum at 500 °C (pyrolysis temperature), due to the comparable increase of absolute K and Cl quantities in the biochar, and then decrease due to the extensive release of these volatile elements during pyrolysis.

Two further findings were also found for PM_{10} emission from biochar combustion when compared to that of biomass:[67] 1) though most of the inorganic species would retain in biochar including volatile elements like Na and K, the PM_1 emission from biochar combustion is extensively lower than that of biomass, which points out the

significance effects of volatile organics on PM_1 emission during biomass combustion; 2) the PM_{1-10} emission from biochar combustion is higher than that of biomass which is contributed by the enhanced fragmentation during biochar combustion.

2.4.4 Further discussion on PM_{10} emission from co-firing of biomass and coal

Extensive efforts were made for the co-firing of biomass with coal since biomass as a solid fuel can be easily adapted to existing coal-firing power stations.[213,214] The PM_{10} emission from co-combustion still shows bimodal distribution with both a fine and a coarse mode,[215] which is similar with that of separate combustion of coal and biomass. When burned together, the PM_{10} emission cannot be simply estimated by adding the related PM from separate combustion due to occurrence of synergy effect between coal and biomass.[62,215-221] Research reported that significant interaction would happen when the blending ratio of cedar chips with coal is higher than ~20%, which leads to the shift of 90% of PM_1 to coarse particles during combustion with temperature of 1200 °C.[166] Similar observations were also reported by other researches.[216,218,219] Two reasons are proposed to be possibly responsible: 1) enhanced homogeneous coagulation of the alkali species from both coal and biomass, and 2) the capture of alkali by refractory species such as aluminosilicates,[166] as alkali chloride is known to react with aluminosilicates to form alkali-aluminoslicates and release Cl as HCl.[222] Study on co-firing of S-rich coal with biomass also reported synergy of sulfation of chloride during combustion which leads to the change of composition of PM_1 from KCl to K_2SO_4.[62] Such phenomenon is due to the presence of extra S from coal which accelerates the formation of SO_3, and then K_2SO_4, with releasing of HCl gas. Since PM_1 is the major concern (due to its low capturing efficiency via conventional cleaning devices), and chlorides in PM_1 is the main reason leading to the ash related corrosion issues, co-firing of biomass with coal would be benefited from its synergy on decrease of PM_1 emission and chloride contents in PM_1 during combustion.

2.4.5 Summary of PM_{10} emission from solid fuel combustion

PM_{10} emission from the combustion of solid fuels like coal, biomass, and biochar, is briefly reviewed in this section. Due to the differences of fuel properties and inorganic occurrences and compositions, their PM_{10} emission shows distinct characteristics. However, they also share some similarities in the inorganic transformation process during combustion. It could be concluded that: 1) the PSD of PM_{10} from solid fuel combustion usually shows bimodal distribution with a fine mode in range of PM_1 and a coarse mode in range of PM_{1-10}, except for biochar which exhibits mainly a coarse mode; 2) PM_{10} emission from the solid fuel combustion commonly can be divided into two distinct parts, i.e. PM_1 and PM_{1-10} due to their different formation mechanisms during combustion, briefly, for the former one via vaporization and condensation, and for the latter one via catalysed sintering and/or fragmentation and coalescence; 3) PM_1 is commonly dominated by volatile elements like Na, K, Cl, and S due to the high volatility, while, the refractory elements also have the chance to distribute in PM_1 via direct contribution from fine mineral particles or fragmented mineral particles, and vaporization of sub-oxides or metals under reduction conditions followed by further gas-phase reaction, nucleation and condensation; 4) PM_{1-10} is dominated by the coalescence of refractory element (Mg, Ca, Al, Si, and Fe) species like aluminosilicates and catalysed sintering of Ca/Mg species.

2.5 PM_{10} Emission from Liquid Fuel Combustion

Liquid fuels such as fossil oil, crude glycerol, and bio-oil usually have considerably lower ash contents compared to that of solid fuels such as coal and biomass (seen in Table 2-1). However, these liquid fuels are dominated by volatile organics, and as in the aforementioned discussion, volatile species have strong effect on PM_1 emission, therefore, their PM_{10} emission during combustion cannot be ignored. The study on PM_{10} emission from liquid fuel combustion is not as abundant as that of solid fuels,

while, a brief review of the PM_{10} emission/formation from the combustion of liquid fuels like residual oil and crude glycerol will be given in this section, and followed by the differences compared to that of solid fuels.

2.5.1 PM_{10} emission from residual oil combustion

The research on PM emission from fossil oil combustion is rare compared to that of coal and biomass, possibly due to its low emission, as report indicating that most oil-fired plants operating without particulate control system.[223] Almost all the studies were carried out based on PM emitted from commercial size boilers and reported PM containing high content of carbon materials due to poor burning of carbon residue.[70-73,223-227] However, there is significant research on complete combustion of residual oil (residual part of fossil oil after distillation) in a laboratory-scale refractory-lined combustor for PM study.[72,73] The studies report that during complete combustion of residual oil, the PM_{10} is dominated by PM_1 emission with only a fine mode at ~0.1 μm which contains mainly inorganic element of Cu, Fe, Ni, V, Zn, and S.

Figure 2-4 shows the simplified schematics of particle formation mechanisms during fossil oil combustion.[70] It could be found that the combustion of fossil oil shares common mechanisms of volatilization and gas-phase burning, soot and char formation, and further burnout of char with solid fuels like coal and biomass, however, it has unique features due to its liquid phase nature. In detail, when a fuel droplet starts to be heated, the light organics vaporize and diffuse away firstly followed by gas-phase combustion with diffusion flame surrounding the droplet. The heavy organics left further crack to send volatiles to the flame front and lead to the significant swelling of the remaining heavy tar droplet followed by carbonization. Along with the depletion of volatile vapours, the remaining heavy tar collapses to form carbonaceous residues or cenospheres and when the flame front recedes to cenospheres, followed by further heterogeneous combustion until carbon

burnout.[71,226] Solid fuel combustion is mainly driven by char combustion, while, for liquid fuels, the dominant process is volatile gas-phase combustion. The metal components would vaporize throughout the whole combustion process, and when the gas cools down, followed by nucleation or condensation on the existing particles to form PM_1. Especially, during the fragmentation and combustion of cenospheres, the metal species bond with organic matrix release to the gas phase more likely followed by condensation on existing submicron particles and contribute to PM_1, which explains the unimodal distribution (with only fine mode) during complete combustion of residual oil.[71]

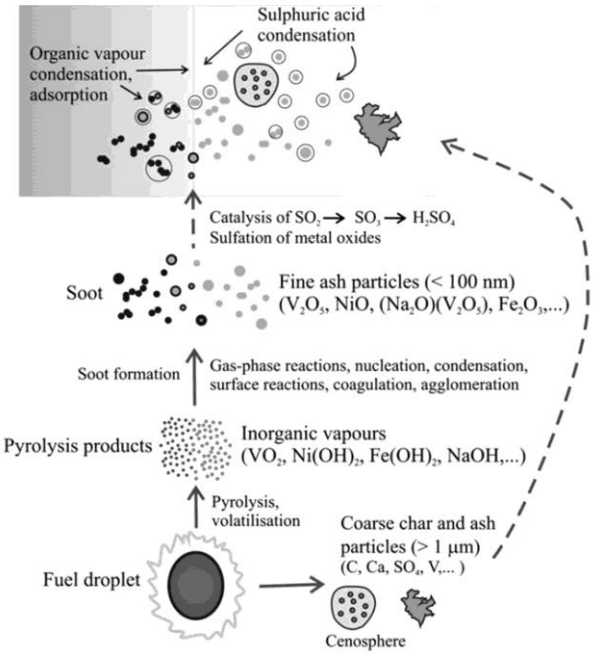

Figure 2-4 Simplified schematics of particle formation mechanisms in fossil oil fired boilers.[70]

2.5.2 PM_{10} emission from crude glycerol combustion

A number of combustion tests for crude glycerol had been carried out in recent years.[74,75,102,119,140] However, only two cases mentioned its PM emission.[74,75] As a result, unimodal distribution of PM_{10} was reported from crude glycerol combustion with a distinct accumulated fine mode observed at ~0.1 μm, and no observation for coarse mode or particle growth beyond 1 μm. Complete combustion was almost

achieved as the hydrocarbon concentration in the fly ash was low (~1 wt%). The PM_{10} (mainly PM_1) is dominated by Na (40−50 %) species, followed by P (4−6 %), Cl (1−2 %), K (1−2 %), which is consistent with the very high alkali metal contents. Mg, Ca, Fe, Zn, and other trace elements were reported only sharing less than 1% of the total PM.

Similar with fossil oil, whose combustion is dominated by vaporization and gas-phase combustion, the combustion of crude glycerol is also driven by gas-phase combustion in the whole process. When the crude glycerol droplet is heated, its impurities like methanol, water,[102] and inorganic species,[140] would reach the boiling points firstly and evaporate before glycerol, leading to the formation of bubbles, followed up by bubble growing, collapse and even explosion, and then glycerol evaporation and burning.[102] As glycerol is known to decompose to generate acrolein at 280 °C, acrolein is formed and burned during this process.[119] The combustion time of crude glycerol was reported comparably short due to a longer ignition delay time and a fast combustion rate compared to that of biodiesel and diesel.[102] The significant contribution of PM_1 emission from crude glycerol combustion is easy to be understood as its high alkali species and volatile contents are known to lead to PM_1 emission via vaporization of these alkali species followed by gas-phase reaction, nucleation, coagulation and/or condensation.

2.5.3 Summary of PM_{10} emission from liquid fuel combustion

It could be concluded from the studies on residual oil and crude glycerol combustion that as complete combustion is achieved, only PM_1 would be produced from liquid fuel combustion, which is dominated by vaporization of alkali species, followed by nucleation, coagulation, and/or condensation. Compared to solid fuel combustion, the distinct difference is that no PM_{1-10} emission from liquid fuel combustion is observed, which is possibly due to the low refractory element concentrations, lack of char base

for ash particle coalescence, short burning time, and the enhanced vaporization of inorganic species during volatilization of the organic compounds of liquid fuels.

2.6 PM_{10} Emission under Different Combustion Conditions

Liquid fuels were reported as facing issues of incomplete combustion in industry scale boilers, which may lead to change of PSD, and physical and chemical properties of PM_{10}, compared to that of complete combustion. Similar situations were also studied for coal and biomass combustion. Moreover, recently, new combustion technologies were developed for capturing the CO_2 to reduce its emission from power stations, such as oxyfuel combustion, which recycles the flue gas back into the burner to achieve a high concentration of CO_2 in the final flue gas for its subsequent capture. An atmosphere of high CO_2 content would have influence on the PM_{10} emission. This section will review the PM_{10} emission from the two combustion conditions, i.e. incomplete combustion and oxyfuel combustion, based on previous study on combustion of coal, biomass, and fossil oil.

2.6.1 Influence of incomplete combustion condition on PM_{10} emission

Insufficient combustion occurs due to various reasons such as lack of oxygen, low temperature, bulky feedstock, poor fuel properties, deactivation of char, and/or short residence time of fuel particle/droplet inside the furnace chamber.[228-231] Under incomplete combustion condition, the PM would be generated consisting of mainly organic carbon matters, such as soot, condensed vapour (tar), or char cenospheres,[41,231] resulting in different emission quantities and PSDs.

Very few studies had been carried out focusing on organic aerosol formation during coal combustion. Study on carbon residues in fly ash from coal combustion in pulverized-fuel combustors had reported that the high content of carbon in fly ash would lead to high emission of coarse particles and high proportion of carbon in these coarse particles due to the retention of unburned fine char particles in these

coarse fly ash fractions.[228,229,232,233] The large coal particle size was deemed mainly responsible for the failure of coal particle burnout.[228] The difficulty of coal-char burnout was also reported related to the char deactivation in boiler environment.[229] A recent study on organic aerosol emission from coal combustion concluded that the organic materials in PM produced from combustion share similar components with pyrolysis products consisting of non-aromatic hydrocarbons, carboxylic acids/oxygenated organic compounds, and aromatic compounds.[234] Two types of formation mechanisms of organic carbon materials in ultrafine ash were reported: 1) formation of soot from PAH, followed by nucleation, coagulation, anneal, and agglomeration into chain-like structures; 2) homogeneous nucleation of gas-phase hydrocarbons or heterogeneous condensation on existing soot or inorganic particles as temperatures cool.[235]

The insufficient combustion of biomass was mainly found in cases of domestic furnaces or small boilers due to their usually low load running, low excess air ratio or low-quality of fuel as feedstock.[231,236] Under such conditions, increase of PM particle size was observed, and actually, both the number/mass concentrations and sizes of PM particles would be increased due to formation of soot, condensation of heavy organic compounds, and/or unburned char particles.[231,236-238] In addition, insufficient combustion usually related to lower gas flow and longer residence time which favours particle growth via coagulation or condensation.[231] Attention was paid to insufficient combustion of biomass due to the emission of toxic PAH (precursor of soot) into atmosphere. During incomplete combustion of biomass, soot would be formed via formation of aromatic rings and colliding of hydrocarbon fragments (rather than oxidation to form CO_2 and/or H_2O), followed by further growth to PAH (fine as 1−2 nm) due to hydrogen abstraction and/or acetylene addition, or polymerization of the aromatic moieties,[41] and then agglomeration to form solid carbon spherules (~30−50 nm) as PM_1.[237] Furthermore, PM_1 from biomass incomplete combustion could also be formed via condensation of both inorganic and

organic vapours on the pre-existing particles such as metal oxides (<13 nm),[238] as the ultrafine mode was reported with high ash contents.[236,238] There is no report that mentioned PM_{1-10} or larger coarse particle emission from incomplete combustion of biomass, however, the situation should be similar with that of coal, as the retention of unburned char residue particles would contribute to both increased sizes and yields of coarse particles.

For liquid fuels, the total carbon contents in PM from heavy fuel oil combustion were reported as 80−90 wt% even though the combustion efficiencies were greater than 99.7% in boilers.[71,223-225] Different to unimodal distribution of PM from complete combustion of fossil oil (seen in Section 2.5), bimodal distribution was reported from the incomplete combustion in fire-tube boiler, with a fine mode at ~0.1 μm and a coarse mode at ~3−5 μm[70] or ~50 μm.[71,226] PM formation during fossil oil incomplete combustion would also follow the mechanisms of organic vaporization, nucleation, coagulation, condensation, and formation of residual char cenospheres due to low rate of carbon burnout.[71] In detail, the PM_1 accounts for only ~0.2 wt% of the total PM and consists of mainly trace elements and Na, sulphuric acid, soot, and other organic materials, such as fragments of cenospheres, while, PM_{1-10} accounts for ~99.8 wt% of the total PM and contains mainly cenospheres and inorganic species.[70,72,73] Apart from the difference of coarse mode in PSD, it was found that PM_1 emission from incomplete combustion of residual oil is lower than that of complete combustion, which is due to the growth of particles via condensation of organic matters and carryover of ash species inside the cenospheres in the coarse mode during incomplete combustion.[71]

As a result, it could be concluded from above discussion that, incomplete combustion condition would generally lead to increase of both quantities and particle sizes of PM_{10} (both PM_1 and PM_{1-10}) emission compared to complete combustion condition due to the extensive generation of organic carbon materials such as soot, organic condensing matters, and char cenospheres in PM_{10}. PM_1 from incomplete

combustion would be mainly generated from three mechanisms: soot agglomeration, ash nucleus followed by condensation of both inorganic and organic species, and fine fragments of cenospheres, while, PM_{1-10} are dominated by fragmentation of char cenospheres including ash species.

2.6.2 Influence of oxyfuel combustion condition on PM_{10} emission

Oxyfuel combustion is a combustion condition that replaces N_2 in air with flue gas with high CO_2 concentration and small amount of water and aerosols.[78] The major difference is caused from the distinct radiative and thermos-physical properties of CO_2 and N_2. The higher heat capacity of CO_2 and lower diffusion rate of O_2 in CO_2 compared to N_2 are blamed responsible for the decrease of combustion temperature of coal, biomass, or char particles, reported up to ~300 °C, during combustion at a same O_2 concentration level.[78] Therefore, to achieve the same flame and temperature profile to the conventional combustion in air, oxyfuel condition usually considers increasing the oxygen concentration to a higher level such as 30−35 % depending on fuel types.[78]

There are mainly two kinds of experimental study on PM emission from oxyfuel combustion. One is simulated oxyfuel condition via mixing O_2 with pure CO_2. Research found that compared to air combustion, oxyfuel combustion has no influence on the components of ash species as no new minerals were identified while changing the relative mineral amounts since the different fuel particle combustion temperature it may achieve. To be more precise, oxyfuel combustion has few influences on excluded minerals that exposed to bulk gas as little change happed to gas phase temperature, while, leads to strong effects of the evolution of included minerals in char matrix due to the change of its burning temperature.[239]

Directly replacing N_2 with CO_2 during combustion would lead to the shift of PM_1 toward smaller sizes and decrease of PM_1 emission[55,56,78,240,241] due to two possible reasons: 1) the hindered reduction reaction of refractory metal oxides due to the

higher partial pressure of CO_2 which leads to the decrease of subsequent formation of volatile sub-oxides and then the absence of refractory species in PM_1; 2) the lower combustion temperature and then weakened vaporization, devolatilization, and fragmentation.[55] When O_2 content increases in oxyfuel condition and the combustion temperature matches a similar level with that of air condition combustion, the emission of PM_1 is enhanced and the fine mode peak position shifts to larger sizes compared to that of oxyfuel in same O_2 level with air, and similar with that of air condition combustion, which can be explained by the enhanced combustion temperature, vaporization of metal species and char fragmentation and burnout.[55,78,240] Such influence on PM_1 emission due to increased O_2 concentration is also reported to be more significant in N_2 environment than in CO_2.[55]

When it comes to $PM_{1\text{-}10}$ emission, research reported that there are no clear trends found when the background gas changes regardless the O_2 concentration,[241] as numbers of factors could influence on $PM_{1\text{-}10}$, such as fuel type, residence time and combustion temperature, and particularly, the competence of two formation mechanisms, i.e. fragmentation and coalescence. Under oxyfuel condition of same O_2 level with air, since the lower combustion temperature, the fragmentation of char particles is mitigated, which may lead to larger PM particle sizes due to that more minerals would have the chance to coagulate together on the surface of one char particle, however, simultaneously, the low combustion temperature would also mitigate the extent of mineral coalescence and then the formation of larger particles.[239] When the O_2 content is raised, the situation is changed to the opposite.[57] Even so, when the O_2 content is increasing, it is proved that the coarse mode of PM_{10} is generally shifting to the left due to the more violent char fragmentation.[57,241] Studies also reported an enhanced reaction of aluminosilicates with alkali species during combustion under higher O_2 level of oxyfuel condition due to the increased combustion temperature.[241] Under high O_2 concentration oxyfuel condition, Fe is

also reported favouring presented in glass phase in coarse particles rather than in ultrafine vaporization mode.[242]

It is known that CO_2 background atmosphere can lead to char-CO_2 gasification during thermal treatment of solid fuels.[78,243] The CO_2 gasified char is reported with higher surface area and pole size compared to that from N_2, and therefore, would undergo enhanced fragmentation during oxyfuel condition combustion.[184,185] However, such differences due to CO_2 gasification are believed to be minor compared to the significance of combustion temperature.[78]

Different to the above study using simulated oxyfuel conditions via mixing pure O_2 with CO_2, research was also carried out via a self-sustained oxyfuel combustor in which the actual flue gas stream was recycled instead of the once through CO_2 and mixed with O_2 as oxyfuel conditions.[242,244,245] Furthermore, three kinds of cleaning devices were also applied to remove ash, moisture, and sulphur from the recycled flue gas, respectively, to study the possible influence of these matters in recycled flue gas on PM emission. The results show that the recycled flue gas with different clean-up options under oxyfuel condition with 27% O_2 inlet (same radiant heat flux with air condition) have little effect on the ash aerosol formation compared to air condition.[244,245] However, when the O_2 fraction increases to 50%, the vaporization mode shifts from 0.06 to 0.17 μm due to the enhanced ash vaporization and then PM_1 formation from the higher temperature combustion. Both Si and Ca in PM_1 are found to increase under such conditions. While, the mass fraction of Na in PM_1 is found to be slightly higher in 27% O_2 case compared to the 50% case due to the enhanced reaction between Na and silicate or aluminosilicate under higher combustion temperature in 50% O_2 condition.[245]

Therefore, at last it could be concluded that the major difference between air and oxyfuel condition during solid fuel combustion is the lower particle combustion temperature under oxyfuel condition with O_2 level equal to air, which leads to lower

emission of PM_1 whose formation is driven by the combustion temperature and then ash evaporation. Increasing of O_2 concentration to ~30% can achieve similar combustion profile with that of air condition and thus similar PM_1 emission. Further increase of O_2 fraction in oxyfuel condition would lead to increase of PM_1 emission and particle size of evaporation mode due to the enhanced vaporization under higher combustion temperature. Higher combustion temperature would also lead to capturing of alkali species by coarse particle species to form alkali including silicates or aluminosilicates.

2.7 Trace Elements in PM_{10}

Trace elements are of significance due to their toxic and hazardous nature to human health and substantial emission from fossil fuel combustion in power plants. Various studies had been carried out for its transformation and emission during combustion of coal, biomass, biosolid, and fossil oil. This section will start with a brief introduction of trace elements, followed by the review of trace element emission in PM_{10} during combustion, and then develop a summary of the characteristics and transformation of trace elements in PM_{10}.

2.7.1 Definition and classification

Trace elements are distinguished from major elements such as Si, Al, Fe, Mg, Ca, Na, K, and P. The latter is the common rock forming mineral elements and has higher retention in fossil fuels (usually > 10,000 ppm), while, the former consists of incompatible, refractory, or rare elements that is usually present in low concentrations (< 1000 ppm, seen in Table 2-1).[80]

Similar with major elements, the occurrences of trace elements in fuel are also in forms of either bonded with organic matrix or discrete minerals,[80] and during combustion or gasification, their transformation would also be complex including processes like vaporization, condensation, agglomeration, and coagulation.[42,84]

According to their partitioning during combustion and boiling points of the elements and their compounds, the trace elements would be classified into three broad groups: Group I, non–vaporisation; Group II, vaporisation–condensation; and Group III, vaporization–non-condensation.[151] The Group I elements are usually concentrated in the coarse residue ash, or equally partitioned in both coarse residues and PM, the Group II elements are concentrated more in PM, and some fine particles which can escape from the PM control system, and lastly the Group III elements are always ready for volatilization and concentrated in vapour or gas phase. Table 2-3 gives the classification of trace elements based on their vaporization properties during combustion.[151] Table 2-4 gives the phase equilibrium temperatures and boiling points of trace elements and some typical compounds. It should be noted that such classifications from different reports could have minor differences for some intermediate elements due to the complexity of their occurrences in fuels and transformations during combustion under different conditions with different sampling methods.[80,151] However, they roughly follow the trends based on their volatilities. Table 2-3 and 2-4 could be used as references for study of trace element performance during fuel combustion.

2.7.2 Trace element emission in PM_{10} during combustion

Extensive studies on trace element emission in PM_{10} were carried out during the combustion of coal,[42,51,79,81,82,84,85,246] biomass,[87,88,90,247] biosolid,[68,91] and their co-combustion.[83,92,248] Several cases[71,225,226] of fossil oil combustion also reported trace element emission. Both experimental studies and modelling based on thermodynamic equilibrium calculation had been carried out.

It was found that the proportion of trace element species in PM_{10} is low in all the fuel combustion cases. Even for biosolid in which the concentrations of trace elements are much higher than the other fuels (seen in Table 2-1), the contribution of trace elements in PM_{10} accounts for less than 0.5 wt%.[68] The trace elements prefer to

release in fly ash rather than bottom ash,[79,84,246] as its amount in fly ash was reported accounting for ~90% of the total during coal combustion.[86] Almost all the trace elements could be vaporized (completely or partially) and distributed in PM_1 via the mechanism of volatilization and condensation.[84,247,248] Some trace elements would also distribute in coarse fly ash particles via condensation or interaction with coarse ash particle species such as major element species of Mg, Ca, Al, Si, and Fe.[83,247,248] The transformation of trace elements is highly dependent on their occurrences and mineral compositions in fuel, combustion temperature, and atmosphere condition during combustion. Those in inclusion minerals bound with organic matrix or under co-firing situation with high volatile contents were reported easily to be vaporized via the volatilization process of organics,[79,81-83,87,246] while, those close to minerals with Ca, Al, and Si species or under co-combustion with high mineral contents such as kaolin, bauxite, and/or alumina, prefer to form coarse particles due to the existence of interactions.[81,83,85,248] Similar to previous combustion, trace elements also favour vaporization and contribution to PM_1 under higher combustion temperatures. Additional HCl and SO_2 gases were reported having significant influence on trace element emission in PM_{10}.[83,92,247] Detailed discussion for each trace element (As, Cd, Hg, Se, Cr, Pb, Cu, Ni, V, Zn, Mn, Co, and Sb) was given below.

Table 2-3 Classification of trace elements based on their vaporization properties during combustion[151]

Group I, non–vaporisation
Ba, (Be), Ca, Ce, Co, (Cr), Eu, Fe, Hf, K, La, Mn, (Ni), Rb, Sc, Si, Sm, Sr, Ta, Th, Ti, (U), (Zr)
Group II, vaporisation–condensation
As, (B), (Ba), (Be), Cd, (Co), Cu, Ga, (Ge), Mo, (Ni), Pb, Sb, Se, (Sn), (Te), (Tl), (V), Zn
Group I/II, intermediate
(Ba), (Bi), (Co), Cr, Cs, (Cu), (I), (Mo), Ni, (Se), (Sr), (Ta), U, V, (W)
Group III, vaporization–non-condensation
B, Br, Cl, F, Hg

Arsenic (As) could be partially volatilized during combustion of coal.[83] The retention of As in PM_1 would account for ~86% of total in PM_{10}.[86] The equilibrium calculation suggests that it could be totally vaporized in gas phase as $AsO_{(g)}$ or $AsO_{2(g)}$,[247] while condenses as As_2O_5 under 500 °C,[248] which is unstable and further decomposes to $As_2O_{3(s)}$. Its retention in coarse ash particles could be a result of the interaction with Mg, Ca, and Fe, as suggested by thermodynamic equilibrium calculation to form related arsenates such as $Mg_3(AsO_4)_2$, $Ca_3(AsO_4)_2$, and $FeAsO_4$.[83,247,248] One case reported that when Si is considered, the predicted volatility of As was increased.[248] Additional HCl or SO_2 gas was reported leading to increase retention of As in sinter ash during wood-bark combustion,[83] however, this is not predicted by equilibrium calculation.[83,248] On the contrary, the gaseous species of $AsCl_3$ was predicted stable between 400−800 °C[248] and it has a low boiling point as 130 °C (seen in Table 2-4) indicating high propensity of gas phase releasing.

Cadmium (Cd) was reported to be partially volatilized during the combustion of various fuel samples and blends.[83] ~70% of Cd was reported distributed in PM_1 during coal combustion. The proportion can even increase to ~96% for $PM_{2.5}$ indicating the substantial amount of Cd in range of $PM_{1\text{-}2.5}$.[86] However, ~45−75 % of Cd in bottom ash was also reported during the combustion of wood-bark.[247] Equilibrium calculation[248] gives prediction of gas phase of $CdCl_{2(g)}$ between 600−1000 °C and $Cd_{(g)}$ at higher temperature such as > 1000 °C. Condensation of Cd in forms of $CdSO_4$ and CdO was also suggested. Interaction of Cd with aluminium and silica would form compounds of $CdO{\cdot}Al_2O_3$ and $CdO{\cdot}SiO_2$, which should be the main forms of Cd retention in $PM_{1\text{-}10}$.[248] Injecting HCl into the system would lead to the release of $CdCl_{2(g)}$ which is consistent with the equilibrium prediction.[247] However, injection of SO_2 would lead to reduction of Cd retention in bottom ash which is contrary to the prediction of recondensation of sulfates.[247]

Table 2-4 Phase equilibrium temperatures and boiling points (volatility °C) of trace elements and some typical compounds[80]

Group[a]	element	volatility °C	oxide	volatility °C	chloride	volatility °C
I	Co	2870	CoO	1800	$CoCl_2$	1049
	Cr	2670	Cr_2O_3	4000	$CrCl_2$	1302
	Mn	1960	MnO	3127	$MnCl_2$	1225
	Ni	2730	NiO			
	Ti	3287	TiO_2	2972	$TiCl_3$	960
II	As	77 [b], 613	As_2O_3	465	$AsCl_3$	130
	B	2550	B_2O_3	1800		
	Be	1016[b]	BeO	1927[b]		
	Cd	157[b]	CdO	604[b]	$CdCl_2$	964
	Cu	2570	CuO	2000	$CuCl_2$	993
	Mo	4660	MoO_3	795		
	Pb	488[b], 1749	PbO	1535	$PbCl_2$	950
	Sb	399[b]	Sb_2O_3	211[b], 1155		
	Se	217	SeO_2	317		
	V	1482[b], 3407	V_2O_5	1750	VCl_2	1506
	Zn	907	ZnO	1725	$ZnCl_2$	732
III	F	-188				
	Hg	357				

[a] Rough classification; [b] phase equilibrium temperature for solid phase change to gas phase, the others are boiling points.

Mercury (Hg) can be completely volatilized during combustion of almost all fuels[83,86] which is consistent with the equilibrium calculation results, indicating the strong release of gas phase Hg (> 98%) and HgO (< 2%).[83,247] However, report was also mentioned retention of Hg in sinter ash with a solid compound or compounds possibly containing sulfur[247] which is unknown, especially in the case of injection of SO_2 gas during wood-bark combustion.[83]

Selenium (Se) was reported almost completely volatilized during combustion of all the fuels, except cases of sewage sludge combustion or co-combustion, which reported almost complete retention of Se in ash fraction.[83] Wood-bark combustion also reported ~15−30 % of Se retention in bottom ash.[247] Equilibrium calculations

suggest release of gas phase Se in forms of SeO_2 (> 99%) and SeO (< 1%).[83,247] Se retention in coarse particles could be caused by the formation of $CaSeO_4$.[249]

Chromium (Cr) was also partially volatilized during combustion. The retentions of Cr in PM_1 and $PM_{2.5}$ during coal combustion account for ~60% and ~95% of its total in PM_{10}, respectively.[86] Even though the equilibrium calculation was reported that Cr would mainly retain in coarse ash as $Cr_2O_{3(s)}$,[83,248] it still exhibits strong volatility during combustion due to the fact that the formed $CrO_{3(g)}$ from Cr atoms released from fuel would has low chance to further transform to $Cr_2O_{3(s)}$ as the very low concentrations of Cr.[83] Cr was also reported to preferentially form oxides during combustion and HCl and SO_2 have unobvious influences on Cr emission.[83] However, equilibrium calculation predicts the formation and condensation of sulfates,[248] and its increased volatilization due to limited formation of $CrCl_2$ and CrO_2Cl_2.[247] Interaction of Cr and Mg was also suggested by predictions during co-firing study to retain Cr in coarse ash particles.[248]

Lead (Pb) was also partial volatilized during combustion, except with cases of complete retention in bottom ash during the combustion of Colombian coal and sewage sludge.[83] Another case of coal combustion reported ~51% and ~92% of Pb released in PM_1 and $PM_{2.5}$, respectively.[86] As equilibrium calculations suggest, Pb alone would be completely volatilized as gases of Pb, PbO, and $PbCl_2$.[83] The retention of Pb in bottom ash was resulted from interaction of Pb with silicate and/or aluminosilicate and recondensation of $PbSO_4$.[83,248] Equilibrium calculations also report the retention of $Pb_3(PO_4)_2$ when P is considered.[248]

Copper (Cu) was similar with Pb, which is also partially volatilized during combustion and shows complete retention in bottom from cases of Colombian coal and sewage sludge.[83] Thermodynamic equilibrium calculation would predict fully retention of Cu in bottom ash due to the formation of Al, Si, Fe, or P containing Cu compounds such as $CuO{\cdot}Al_2O_3$, $Cu_6Si_6O_{18}{\cdot}6H_2O$, $CuO{\cdot}Fe_2O_3$, $CuFeO_2$, and

$Cu_2P_2O_7$,[248] however, due to the low concentration of Cu, such interactions are limited. Substantial of Cu was released via the volatilized form rather than retention in ash.[83] Cu in the organic matrix would be readily released into gas phase. The volatilized Cu would further form CuO in oxidizing environment. HCl would enhance the release of Cu in gas phase of $CuCl_2$.[83] SO_2 gas would lead to the formation and condensation of $CuSO_4$.[248]

Nickel (Ni) was also reported to be partially volatilized during combustion.[83] 80% of Ni was reported retained in bottom ash during wood-bark combustion which is consistent with the equilibrium prediction that Ni would complete retained as NiO (s) and $NiSO_4$ (s) at 800 °C, only forming gaseous $Ni(OH)_2$ and $NiCl_2$ at higher temperatures (> 900 °C).[247] Interaction of Ni with Fe and Al was predicted to form $NiO{\cdot}Fe_2O_3$, Fe_2NiO_4, and $NiO{\cdot}Al_2O_3$ however in a very low amounts.[248] Increase of HCl concentration was predicted leading to higher volatilization of Ni in forms of $NiCl_2$ (g) and NiCl (g), while, additional SO_2 leads to the formation and condensation of sulfates.[248]

Vanadium (V) was partially volatilized during combustion. The thermodynamic equilibrium modelling suggested complete retention of V in bottom ash with formation of VO_2, V_2O_5, and compounds including Ca, Fe, and Mg in forms of $Ca_2V_2O_7$, $3CaO{\cdot}V_2O_5$, $CaO{\cdot}V_2O_5$, $Fe(VO_3)_2$, and $Mg_2V_2O_7$.[83,248] Gaseous phase of V was predicted in forms of V_4O_{10} (700−1000 °C) and VO_2 (> 1100 °C).[248] HCl gas has no influence on V transformation while SO_2 gas would lead to formation and condensation of $VOSO_4$.[248] Fly ash collected from heavy oil combustion had been reported with retention of V identified as V_2O_5 and $VOSO_4{\cdot}3H_2O$.[223]

Zinc (Zn) was also partially volatilized during combustion.[83] ~40 % of Zn from wood-bark was reported remained in bottom ash during combustion.[247] Zn that bound with organics or those in inorganic forms that ready for decomposition, would volatilize during combustion, followed by oxidation and condensation of ZnO (s). Zn

could also interact with Al and Si to form $ZnO \cdot Al_2O_3$ and $2ZnO \cdot SiO_2$ then remain in coarse ash particles.[247]

Manganese (Mn) is a low volatile element.[248] Equilibrium calculations would suggest complete retention of Mn in sintered ash, which correlates well with the result from wood-bark combustion reported with 70−100 % retention of Mn in bottom ash.[247] Four kinds of oxides were predicted to be formed between 700 and 1000 °C including MnO, Mn_3O_4,Mn_2O_3 and MnO_2.[248] Interactions of Mn with Na, Fe, Al, Si, and P were also reported via modelling to form compounds of $NaMnO_4$, Fe_2MnO_4, $MnO \cdot Fe_2O_3$, $MnO \cdot Al_2O_3$, $MnSiO_3$, and $Mn_3(PO_4)_2$.[248] Reaction with HCl to form $MnCl_{2(g)}$ could lead to the volatilization of Mn in gas phase. SO_2 would lead to the formation of solid Mn-sulfate.[248]

Cobalt (Co) would be partially volatilized during combustion.[83] Complete retention of Co in coarse ash was predicted by equilibrium calculation, while its volatilization is blamed due to incomplete recondensation.[83] Injection of HCl would lead to formation and emission of $CoCl_{2(g)}$ at temperature higher than 800 °C.[83] SO_2 would lead to the formation and condensation of $CoSO_{4(s)}$.[248] Co in coarse ash would be in forms of oxides (CoO), or compounds from interaction with Fe and Al such as $CoFe_2O_4$ and $CoO \cdot Al_2O_3$.[248]

Antimony (Sb) was partially volatilized during combustion[83] and predicted to be totally volatilized at temperature higher than 600 °C in form of $SbO_{(g)}$. HCl and SO_2 gases have no influence on Sb transformation. Interaction with other ash particles was also not observed.[248]

Apart from above discussion, research[68,69] on biosolid combustion and separate combustion of its volatile and char fractions were carried out and came up with interesting findings that: 1) during pyrolysis of biosolid, As, Cd, and Pb prefer to release and retain in volatiles, while, Cr, Ni, Co, Cu, and V are mostly retained in char; 2) volatile combustion generates As, Cd and Pb in PM_1, while, trace elements

during char combustion contributes to both PM_1 (As, Cd, Pb, Cr, and V) and PM_{1-10} (Ni, Co, V, and Cu); 3) comparison of biosolid combustion with calculated cases from separate combustion of volatile and char indicates that synergy between volatile and char would lead to increase of trace element emission in both PM_1 and PM_{1-10} and the shift of the fine mode to right side; 4) two synergies are responsible to the increase of PM_1 emission during biosolid combustion, i.e. enhanced releasing of Cu in PM_1 due to interaction of Cl and Cu, and "volatile-char interaction" which leads to the enhanced volatilization of volatile trace elements (Pb and Cr) in char during combustion of the whole biosolid; 5) the increased PM_{1-10} during combustion of whole biosolid is due to the more violent fragmentation.

2.7.3 Summary of Trace elements in PM_{10} emission

Trace elements can contribute to both PM_1 and PM_{1-10} emission during fuel combustion. Based on their volatility, they can be divided into three groups that would contribute to bottom ash, fly ash, and gas phase emission, respectively. However, such classification would be hard and arbitrary as the complexity of the transformation mechanisms during combustion. Roughly, all the trace elements studied could be totally volatilized or partially volatilized. Hg and Sb would be totally vaporized and prefer to release as gas phase during combustion. As, Cd, Se, Cr, Pb, Cu, Zn, and V would contribute to both PM_1 and PM_{1-10} due to their possibilities to be released both as volatiles followed by gas-phase reaction (oxidation, chlorination, or sulfation), nucleation, and/or condensation, and as coarse particles to form oxides or bond with major refractory element species such as Mg, Ca, Al, Si, and Fe. Lastly, Ni, Mn, and Co would prefer to be retained in PM_{1-10} or coarse ash particles due to their lower volatility as only limited volatilization of these elements in forms of chlorides was reported from equilibrium calculation modelling. Several factors during combustion would lead to increase volatilization of trace elements including organic bond occurrence in fuels, volatile-char interaction, and addition of HCl.

2.8 Conclusion and Research Gaps

Based on above literature reviews, it could be concluded that:

1) Bio-oil based biofuels such as bioslurry and CG containing biofuels are promising fuels to substitute or partially substitute coal as clean and sustainable energy sources for stationary applications due to their verified advantages of low life-cycle energy and carbon footprints, and fuel properties adaptable to existing combustors.
2) PM emission from power stations is a significant issue considering its adverse impacts on human health and the insufficient efficiency and high cost of capturing by existing cleaning technologies.
3) Extensive studies on PM_{10} emission from the combustion of solid fuels such as coal, biomass, and biochar, had been carried out, and came up with the understanding of characteristics and formation mechanisms of PM_{10} emission during the combustion of these solid fuels.
4) Limited studies reported PM_{10} emission from the combustion of liquid fuels, however, from the research on residual oil and crude glycerol, it could be found that PM_{10} formation during liquid fuel combustion shares some common mechanisms with that of solid fuels and also certainly has some discrepancies such as dominance of PM_1 emission.
5) Different combustion conditions such as incomplete combustion and oxyfuel combustion would have influences on PM_{10} formation/emission.
6) Studies on trace element in PM emission and transformation mechanisms during fuel combustion were carried out based on both experiments and thermodynamic equilibrium modelling.

Therefore, it could be concluded that, firstly, there is no study carried out focusing on the combustion performances of these bio-oil based biofuels in both lab scale and industrial scale combustors. Secondly, the knowledge on the PM emission from the

combustion of liquid fuels is still in shortage, especially for bio-oil, considering the different liquid fuel properties compared to that of solid fuels, such as the complex compositions of bio-oil. Thirdly, as a two-phase mixture fuel, the PM_{10} emission from the combustion of slurry fuel such as slurry of coal/water, coal/oil, and bio-oil/biochar in this study is absent and deserved to be studied. Fourthly, as a new type of fuel mixtures, the well understanding of the PM_{10} emission from the combustion of the CG containing biofuels should also be carried out considering the possibilities of synergy during combustion. Fifthly, considering the foreseeable situation of partially substitution of coal by these bio-oil based biofuels, there is no knowledge covering the PM_{10} emission and synergy during the co-combustion of coal with these bio-oil based biofuels, therefore, such study is also a requirement considering the advantages of utilization of these bio-oil based biofuels for stationary applications. Sixthly, it should also be noted that there is no sufficient existing knowledge on the trace element in PM emission during fuel combustion, especially for the biofuels focused in this thesis study which should be paid attention. Lastly, the influences of the different combustion atmosphere conditions such as incomplete combustion and oxyfuel combustion conditions on PM emission from these biofuels are unknown, as well.

Therefore, further research and development should be carried out in the above research area, including:

1) Test of combustion of the bio-oil based biofuels in both lab- and industry-scale burners to study its combustion performances and the correlating adjustment/modification for burners.
2) Understanding of formation/emission of PM_{10} and trace elements in PM_{10} during the combustion of bio-oil and its fractions under various combustion conditions.
3) Understanding of formation/emission of PM_{10} and trace elements in PM_{10} during the combustion of bioslurry under various combustion conditions with

considering of the different significances of fraction components and possible synergy between them.

4) Understanding of formation/emission of PM_{10} and trace elements in PM_{10} during the combustion of CG containing biofuels under various combustion conditions with considering of different significances of fraction components and possible synergy between them.
5) Understanding of formation/emission of PM_{10} and trace elements in PM_{10} during the co-combustion of coal with the bio-oil based biofuels with considering of different significances of fraction components and possible synergy between them.
6) Benchmarking of PM_{10} emission from the combustion of different fuels including coal, biomass, biochar, bio-oil, and these bio-oil based biofuels on different calculation bases such as fuel mass input, ash input, and energy input.

2.9 Study Objectives of the Present Study

As identified by the above literature review and discussion, there are various research gaps in the research field. However, it is impossible to fill all the research gaps within the limiting time of a PhD study. Therefore, this study will mainly focus on the below objectives:

1) To investigate the PM_{10} emission during the combustion of bio-oil with consideration of the different contributions of its fractions and under different atmosphere conditions.
2) To investigate the PM_{10} emission during the combustion of bioslurry with consideration to the different contributions of its fractions, influence of oxyfuel combustion conditions and possible synergy effect on PM_{10} emission.
3) To investigate the PM_{10} emission during the combustion of CG containing biofuels with consideration of the interactions between the fuel components.

4) To investigate the trace elements in PM_{10} during the combustion of the individual and mixed biofuels from bio-oil, biochar, and/or CG, with consideration of the interactions between the fuel components during fuel mixture combustion.

Chapter 3 Research Methodology and Analytical Techniques

3.1 Introduction

This chapter introduces the research methodologies, the experimental and analytical techniques applied for the investigation targeting at the objectives outlined in Chapter 2.

3.2 Methodology

Considering the objectives of this thesis, seven fuel samples are considered for study of PM_{10} ($PM\boldsymbol{x}$ refers to PM with aerodynamic diameter of < x μm) emission, including bio-oil and six bio-oil based biofuels, i.e., bio-oil/biochar fuel slurry, WSF/biochar fuel slurry, bio-oil/methanol/CG blend fuel, WSF/CG blend fuel, bio-oil/methanol/CG/biochar fuel slurry, and WSF/CG/biochar fuel slurry, hereafter referred to as "BB", "WSFB", "BMCG", "WSFCG", "BMCGB", and "WSFCGB", respectively (WSF refers to water-soluble fraction of bio-oil and CG refers to crude glycerol). A series of systematic experiments were thus conducted for the research of PM_{10} emission from the combustion of these biofuels, including three procedures:

1) Fuel sample preparation. Several methods were applied for sample preparation, such as fast pyrolysis, filtration separation, and cold-water precipitation.
2) Combustion and PM collection. The prepared fuel samples were sent into a high temperature drop-tube furnace (DTF) for combustion to produce a constant stream of flue gas containing PM_{10} for further sampling and analysis. Various combustion atmosphere conditions were considered. The PM particles would pass through the sampling system and be collected in different size ranges by a low-pressure impactor.

3) Fuel and PM analysis. The fuel samples were analysed to obtain rheological properties, Proximate and Ultimate analysis, and inorganic element concentrations, etc. The collected PM samples were analysed via series of techniques such as gravimetrical, chemical composition and morphology analysis, etc., to obtain characteristics such as particle size distribution, morphology, yields, and inorganic compositions.

All the experiments were repeated to ensure the reproducibility of the results. The overall research methodology could be found in Figure 3-1. The detailed demonstration of methodology for each research objective is given below.

3.2.1 PM_{10} emission from the combustion of bio-oil

Three aspects of study on PM_{10} emission from the combustion of bio-oil are to be considered, i.e., the influence of incomplete combustion, the influence of oxyfuel condition, and the different contributions from fractions of solid, WSF, and WIF (water-insoluble fraction of bio-oil). Detailed methodologies are listed below.

PM emission from bio-oil incomplete combustion under conditions relevant to stationary applications (see Chapter 4). In this part, two kinds of bio-oils, i.e., raw bio-oil and filtrated bio-oil, were considered. The raw bio-oil is a fast pyrolysis bio-oil produced from pine wood at 500 °C. The filtrated bio-oil was prepared via filtration to remove the suspended fine char particles in raw bio-oil. The two bio-oils were then injected into the DTF system for combustion at 1400 °C under both air and pure oxygen conditions, respectively, followed by PM sampling and analysis, to study the PM_{10} emission from bio-oil incomplete combustion, influence of atmosphere change on PM_{10} emission under incomplete combustion condition, and role of fine char particle fraction on PM_{10} emission during the incomplete combustion of bio-oil.

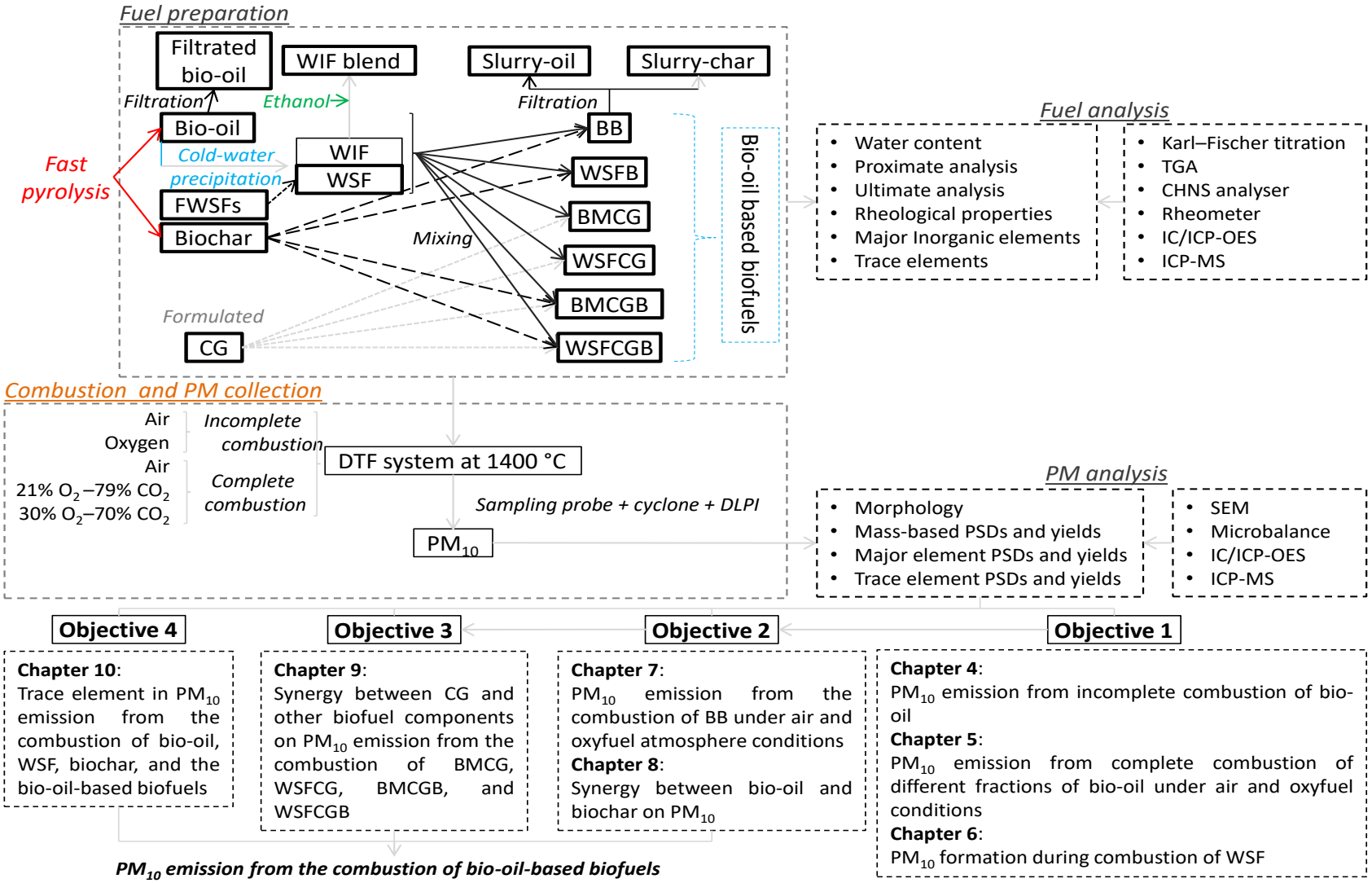

Figure 3-1 Research methodology

PM emission during the combustion of bio-oil and its fractions under air and oxyfuel conditions (see Chapter 5). Three combustion atmospheres were considered including air and two oxyfuel atmospheres, i.e., 21% O_2 –79% CO_2 and 30% O_2–70% CO_2. The contributions of three bio-oil fractions, i.e., solid fraction, WSF, and WIF, to PM_{10} emission were considered. For this purpose, three fuel samples were prepared, including raw bio-oil, filtrated bio-oil, and a blend of WIF of filtrated bio-oil with ethanol. The ethanol was added to improve the atomization ability of WIF. The three fuel samples were then injected into the DTF system for combustion at 1400 °C under three atmosphere conditions, respectively, followed by PM collection and analysis. Thus, the contributions of solid fraction and WSF fraction to PM_{10} emission could be obtained by the difference of PM_{10} emission between the combustion of raw bio-oil and filtrated bio-oil, and between filtrated bio-oil and the WIF-ethanol blend. The influence of oxyfuel combustion could also be studied by the comparisons of PM_{10} emission from combustion under the three atmosphere conditions.

Mechanistic investigation into PM formation during air and oxyfuel combustion of formulated water-soluble fractions of bio-oil (see Chapter 6). Due to the added water during the cold-water precipitation, direct study of WSF is impossible. Therefore, two formulated bio-oil WSF (FWSF) samples were prepared, including a calcium chloride solution and a mixture of calcium chloride solution with several typical organic components of bio-oil. The two samples were then injected into the DTF at 1400 °C under three atmosphere conditions, including air, argon, and oxyfuel (30% O_2–70% CO_2), to generate PM_{10} samples followed by analysis, to explore the formation of PM_{10} from WSF during the combustion of bio-oil.

3.2.2 PM_{10} emission from the combustion of bioslurry

The study of PM_{10} emission from the combustion of bioslurry will mainly focus on two aspects. One is PM_{10} emission from bioslurry (with different char loading levels)

during combustion under various atmosphere conditions including air and two oxyfuel atmospheres (i.e., 21% O_2 –79% CO_2 and 30% O_2–70% CO_2). The second is a synergy study during bioslurry combustion.

Bioslurry for stationary applications: particulate matter emission during combustion under air and oxyfuel conditions (see Chapter 7). Bio-oil and biochar were prepared and mixed together to produce bioslurry with two char loading levels (5 and10 wt%). With considering bio-oil as a bioslurry with zero char loading level, bio-oil and the two bioslurry samples were sent into DTF for combustion at 1400 °C for PM_{10} collection and analysis, respectively. Three atmosphere conditions were applied including air, 21% O_2 –79% CO_2 and 30% O_2–70% CO_2. The comparisons of the PM_{10} emission from the combustion of different bioslurry samples and different atmosphere conditions were then made, followed by benchmarking against biochar, biomass, and coal.

Synergy on particulate matter emission during the combustion of bioslurry (see Chapter 8). Bio-oil and biochar were prepared and mixed to produce bioslurry with 10 wt% biochar. To study the synergy between the liquid and solid phases of bioslurry during combustion, the produced bioslurry after 1 week storage was further separated into liquid and solid phases via filtration. Then, the bio-oil, biochar, bioslurry, and liquid and solid phases separated from bioslurry were sent into DTF for combustion at 1400 °C under air, for PM_{10} collection and analysis, respectively. Thus, the comparisons of PM_{10} emission from the combustion of both bio-oil and biochar fractions before and after mixed as bioslurry, and the comparisons between direct combustion of bioslurry and calculated values from addition of PM_{10} from bio-oil and biochar separate combustion, were made to study the synergy effects on PM_{10} emission during bioslurry combustion.

3.2.3 PM_{10} emission from the combustion of CG containing biofuels

The PM_{10} emission from the combustion of CG containing biofuels was mainly focused on their emission of PM_{10} and the synergy effects during combustion, especially interactions between CG and other fuel components, i.e., bio-oil/biochar based fractions (see Chapter 9). Bio-oil, WSF, and biochar were produced, respectively, and mixed with CG (formulated from chemicals based on previous research[36]) to produce four CG containing fuel mixtures, including BMCG, WSFCG, BMCGB, and WSFCGB; BB and WSFB were also prepared to support the synergy investigation. All the individual fuel components (i.e., bio-oil, WSF, biochar, and CG), and fuel mixtures, including BB, WSFB, BMCG, WSFCG, BMCGB, and WSFCGB were introduced into DTF for combustion at 1400 °C under air for PM_{10} collection and analysis, respectively. The synergy effects on PM_{10} emission during combustion of CG containing biofuels were then studied via comparisons between PM_{10} from direct combustion of the CG containing fuel mixtures and corresponding calculated values from separate combustion of the fuel components.

3.2.4 Trace elements in PM_{10} emission from the combustion of bio-oil based biofuels

To study the trace elements in PM_{10} emission from the combustion of bio-oil based biofuels, all the individual fuel components, i.e. bio-oil, WSF, biochar, and CG, and bio-oil based fuel mixtures, i.e. BB, WSFB, BMCG, WSFCG, BMCGB, and WSFCGB, were prepared and sent to the DTF for combustion at 1400 °C under air for PM_{10} collection and trace element analysis (see Chapter 10). The estimated values of trace elements in PM_{10} from the combustion of the bio-oil based biofuels were also made via calculations based on the corresponding values from separate combustion of each fuel components. Via the comparison of the estimated values and corresponding experimental results from direct combustion of each mixture, the synergy effects on trace element emission is be obtained. Benchmarking of trace element emission from the combustion of each biofuels was also obtained.

3.3 Experimental Section

3.3.1 Sample Preparation

Bio-oil (see Chapter 4–10). The bio-oil studied in this thesis was supplied by a company who chose to be anonymous, produced from pine wood at 500 °C via a fluidised bed reactor and stored in fridge at ~4 °C prior to the experiment.

Filtrated bio-oil (see Chapter 4 and 5). The filtrated bio-oil was prepared via filtration of raw bio-oil via a 0.45 μm polyvinylidene difluoride (PVDF) syringe filter to remove the inherent suspended fine char particles.

WSF and WIF (see Chapter 5, 9 and 10). The bio-oil WSF and WIF were obtained by adding water into bio-oil with water to bio-oil ratio of 0.5:1, known as cold-water precipitation, and after phase separation, the upper fraction is regarded as WSF (with additional water) and the bottom fraction is regarded as WIF. It should be noted that the cold-water precipitation was applied to filtrated bio-oil to produce WIF in the text of PM_{10} emission during bio-oil combustion to distinguish the different contributions of solid fraction and WIF fraction of bio-oil (see Chapter 5).

WIF blend with ethanol (see Chapter 5). For the purpose of spraying of WIF, ethanol was added and mixed with WIF to make a blend solution with WIF proportion same to that of the filtrated bio-oil.

FWSFs (see Chapter 6). Calcium is the most abundant refractory element in the bio-oil, which was used in our previous study.[99] Therefore, in this study, calcium was chosen as the representative inorganic element in the preparation of FWSFs. Based on the concentration of Ca in bio-oil,[99] calcium chloride was loaded into the FWSFs to make solutions with a Ca concentration of 0.02 wt%. Two types of FWSF were prepared. FWSF-1 is a calcium chloride solution that is free of organic matter. Since the bio-oil WSF contains various organic groups, including polysaccharide derivatives, volatile acids, some low-molecular-mass volatile compounds,

degradation of lignin, and alcohols,[12,110,124,250] FWSF-2 is prepared via blending a list of key light organics in bio-oil, doped with the same concentration of Ca. The detailed compositions of the two FWSFs could be found in Table 3-1.

Table 3-1 Compositions of the two formulated bio-oil water-soluble fractions (FWSF-1 and FWSF-2)

Composition (wt%)	FWSF-1	FWSF-2
Calcium chloride	0.05 [a]	0.05 [a]
Water	99.95	24.95
Formic acid		7
Acetic acid		8
Acetone		6
Ethanol		6
Formaldehyde		18
Cellobiose		10
Glucose		10
Furfural		6
Phenol		4

[a] equivalent to 0.02 wt% of Ca in the FWSFs

Biochar (see Chapter 7–10). The biochar was prepared from fast pyrolysis of a local pine wood sourced in Western Australia at 500 °C via a laboratory drop-tube/fixed-bed pyrolysis reactor (see the schematic diagram in Figure 3-2). Briefly, the quartz reactor was firstly heated to 500 °C with a stream of ultrahigh-purity argon flowing through the reactor at 1 L/min. Then, the biomass samples were fed into the reactor via a water-cooling feeding probe with feeding rate of ~1 g/min. After 10 min of pyrolysis at 500 °C, the reactor was lifted from the furnace for rapidly cooling (with the ultrahigh-purity argon continuously flowing) to room temperature and then ready for sample collection. The collected biochar was ground and sieved to the size fraction of < 75 μm prior further utilisation. Multiples of experiments were carried out for the production of adequate amounts of biochar required for the study. It should be noted that in this study, the bio-oil and biochar were produced from different pine woods; however, this should not have influence on the conclusions of PM_{10} emission.

Bioslurry (bio-oil/biochar) or BB (see Chapter 7−10). The bioslurry was produced via suspending biochar particles into bio-oil. Different biochar loading levels were applied in this thesis, such as 5% (see Chapter 7) and 10% (see Chapter 7−10). The bioslurry was stored for 1 week at room temperature to achieve the equilibrium distributions of inorganic species in the solid and liquid fractions of bioslurry.[99]

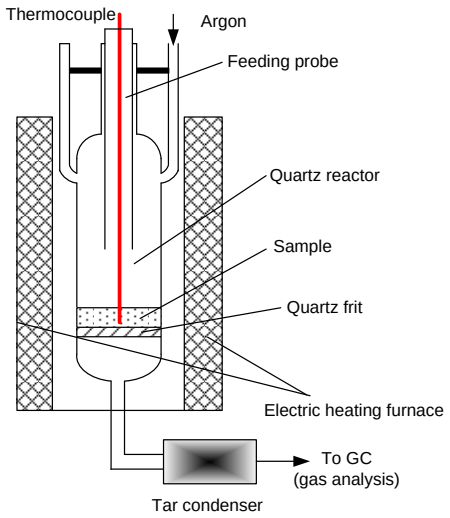

Figure 3-2 Schematic diagram of the pyrolysis system

Slurry-oil and slurry-char (see Chapter 8). Bio-oil and biochar fractions after mixing as bioslurry were also prepared via filtration separation from the bioslurry with 10% biochar via a 0.45 μm polyvinylidene difluoride syringe filter. Briefly, the bioslurry was firstly separated into the filtered-oil and the residue via filtration. The residue, i.e. biochar particles soaked with the residue fraction of bio-oil, was further washed using acetone followed by filtration. Acetone was chosen because as a solvent it leaches little inorganic species from biochar.[101] The solid residue after filtration was then collected and dried in an oven at 110 °C to evaporate residue solvent, yielding a new biochar sample that is hereafter referred to as “slurry-char”. The bio-oil fraction in the acetone solution was also collected after acetone evaporation in an oven at 45 °C and mixed with the filtered-oil to make as a new bio-oil sample hereafter referred to as “slurry-oil”. The mass balance of these samples is presented in Figure 3-3 for the bioslurry with 10% biochar.

WSF/biochar slurry or WSFB (see Chapter 9 and 10). Biochar was also suspended into WSF with loading ratio of 10 wt% to make slurry fuel, referred to as "WSFB".

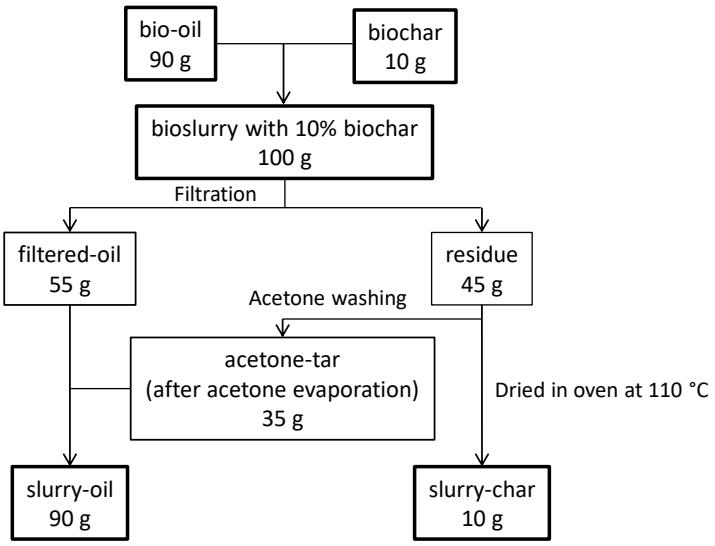

Figure 3-3 Flow chart of sample preparation of bioslurry and its different fractions, i.e., slurry-oil and slurry-char

CG (see Chapter 9 and 10). CG was formulated via mixing glycerol ($C_3H_8O_3$, analytical-grade, Sigma-Aldrich), sodium chloride (analytical grade, Chem-Supply) and deionized water with a mass ratio of 20:1:4.[35] The CG (formulated) composition could be found in Table 3-2.

CG containing biofuels (see Chapter 9 and 10). The CG containing biofuels include two fuel blends and two slurry fuels. The two fuel blends include a bio-oil/CG blend (hereafter referred to as "BMCG") prepared via mixing bio-oil and CG with methanol (analytical grade, Chem-Supply) with a mass ratio of 45:2:3, and a WSF/CG blend (hereafter referred to as "WSFCG") prepared via mixing WSF and CG with a mass ratio of 3:7.[36] All fuel components and blends were stored in fridge at ~4 °C. For slurry fuels, biochar particles were suspended into BMCG and WSFCG at a loading level of 10 wt% to prepare BMCG/biochar slurry and WSFCG/biochar slurry (hereafter referred to as "BMCGB" and "WSFCGB"), respectively. After preparation, these slurry samples were kept at room temperature for one week[35] before combustion for stabilising inorganic species redistribution between liquid and

solid phases. The detailed compositions of the CG containing biofuels could be found in Table 3-2.

Table 3-2 Formulas of crude glycerol (CG), CG-containing biofuels (BMCG, WSFCG, BMCFB, and WSFCGB)

sample	composition (%)						
	glycerol	water	NaCl	bio-oil	WSF[a]	methanol	biochar
CG	80.0	16.0	4.0				
BMCG[b]	3.2	0.6	0.2	90.0		6.0	
WSFCG[b]	56.0	11.2	2.8		30.0		
BMCGB[b]	2.9	0.6	0.1	81.0		5.4	10.0
WSFCGB[b]	50.4	10.1	2.5		27.0		10.0

[a] WSF stands for water-soluble fraction of bio-oil; [b] BMCG stands for bio-oil/methanol/CG blend; WSFCG stands for WSF/CG blend; BMCGB stands for bio-oil/methanol/CG/biochar slurry; WSFCGB stands for WSF/CG/biochar slurry.

3.3.2 Combustion and PM collection

The generation of PM_{10} sample was carried out through a lab-scale DTF system (see Figure 3-4) consisting of three sub-systems: feeding system (see Figure 3-4 a/b), combustion zone (see Figure 3-4 c), and sampling system (see Figure 3-4 d).

Feeding system. Two types of feeding systems were applied. One (see Figure 3-4 a) is nozzle-feeder system, designed for feeding of liquid fuels like bio-oil, filtrated bio-oil, WIF blend, WSF, FWSFs, CG, BMCG, and WSFCG, and slurry fuels like BB, WSFB, BMCGB, and WSFCGB. The other (see Figure 3-4 b) is entrained flow feeder system (detailed elsewhere[65]), which is specific for feeding of solid fuels such as biochar and slurry-char in this study. Briefly, the nozzle feeder system consists of a syringe pump (model: KDS LEGATO 210), a two-fluid nozzle set (model: VLA-3, VLT-3 and VLB, Paasche Airbrush), and a feeding probe equipped with a water-cooling jacket. The sample was injected into the furnace by the pump via a 20 mL stainless steel syringe and sprayed out via the air-assisted nozzle set (assisted by primary gas) at the exit of the feeding probe. Secondary air was also introduced to provide a laminar flow profile in the combustion zone. The feeding probe was protected by both the water-cooling jacket and the secondary gas to maintain the

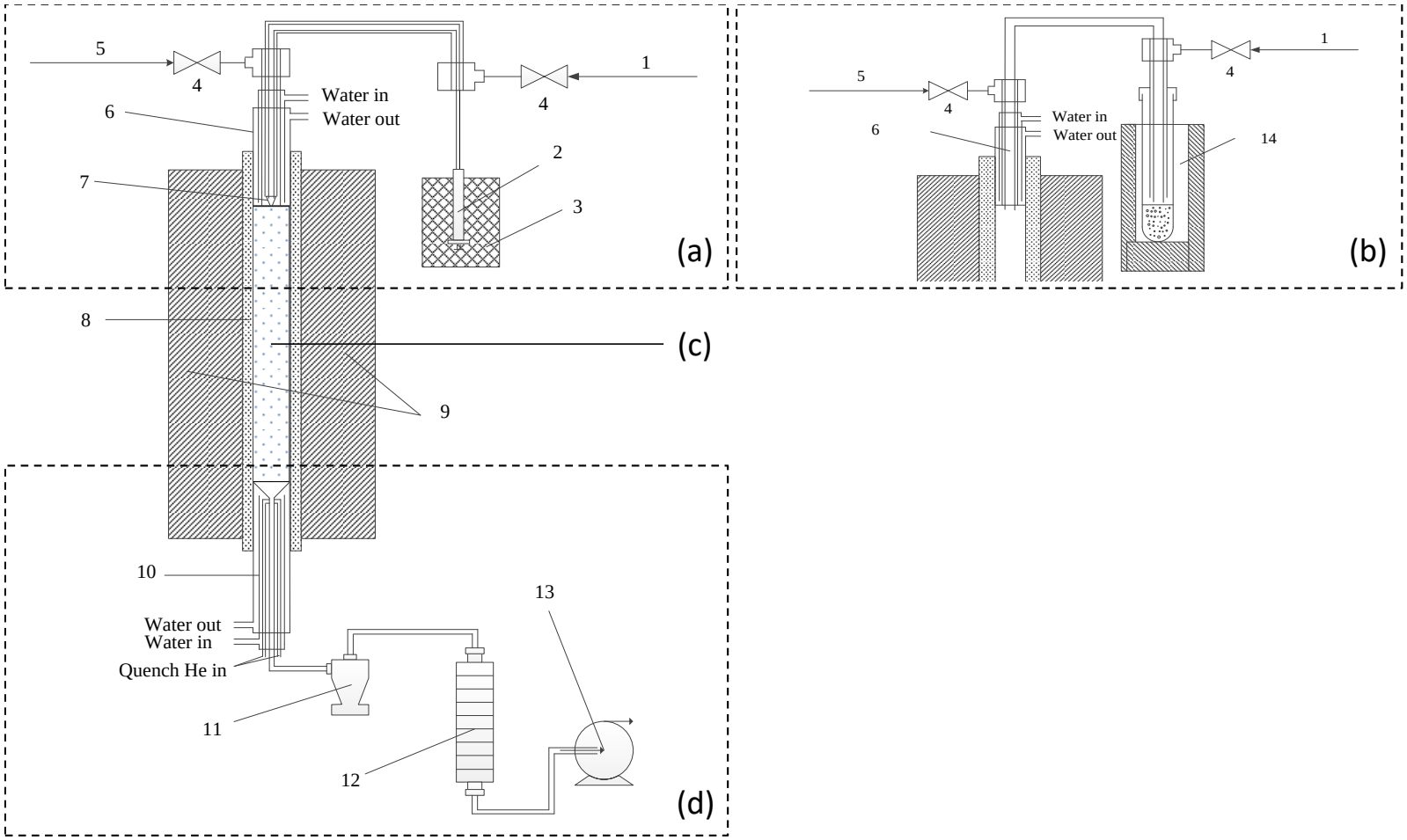

Figure 3-4 Schematic diagram of DTF system with two feeders: (a) feeding system for liquid and slurry fuels; (b) feeding system for solid fuels; (c) combustion zone; (d) sampling system. 1- Primary air; 2- Stainless steel syringe; 3- Syringe pump; 4- Mass flow controller; 5- Secondary air; 6- Feeding probe (equiped with water-cooling jecket); 7- Nozzle set; 8- Mullite tube; 9- Electrical heating furnace; 10- Quench sampling probe; 11- Cyclone; 12- Low pressure impactor; 13- Vacuum pump; 14- Entrained flow feeder.

temperature of the nozzle outlet < 70 °C to prevent bio-oil coking.[115] The spray conditions were adjusted to deliver similar mean droplet sizes (less than 60 μm) measured according to the method developed previously,[100] except for study of incomplete combustion in Chapter 4 where larger mean droplet sizes (~120 μm) were produced. In the study of incomplete combustion, the feeding rate was set as ~1.6 mL/min, while, in the case of complete combustion, the feeding rate was set as ~0.2 mL/min. The entrained flow feeder system is made-up of an entrained flow feeder and a water-cooling feeding probe. The solid fuel particles are then fed in at a rate of ~0.05 g/min with a stream of primary gas (~1.0 L/min) as carrier gas.

Combustion zone. The combustion zone (see Figure 3-4 c) is inside the main drop-tube reactor which is a vertical dense mullite tube with length of 1200 mm and inner diameter of 56 mm and heated via 6 electrical elements. In each combustion experiment the reactor was pre-heated to 1400 °C with an isothermal zone (~600 mm length) of gas temperature of 1400 °C achieved. As a result, when bio-oil was fed in the furnace, the droplet would undergo evaporation and gas-phase combustion at 1400 °C. Various combustion atmosphere conditions were considered, including incomplete combustion under air and pure oxygen (see Chapter 4), and complete combustion under air (see Chapter 5−10) and two oxyfuel atmospheres of 21% O_2–79% CO_2 (see Chapter 5 and 7) and 30% O_2–70% CO_2 (see Chapter 5−7). In study on FWSFs (Chapter 6), an atmosphere of pure argon was also applied. In the study of incomplete combustion in Chapter 4, the values of λ (i.e., the ratio of the actual air/fuel ratio to the stoichiometric air/fuel ratio) are calculated as ~1.8 and ~8.6 for atmospheres of air and oxygen, respectively, and the residence time of the fuel in the isothermal zone is estimated as ~0.9 s. In the cases of complete combustion in Chapter 5−10, the λ values are ~8−21 and the residence time is ~1.8 s. Complete combustion was achieved with evidences that the thermogravimetric analysis suggested no unburned carbon was detected in the PM samples and the total organic

carbon analysis showed no organic carbon was detected in the leachates from these samples washed by deionized water.

Sampling system. The sampling system is composed of a quench sampling probe, a Delkati cyclone (model: SAC-65), a Delkati low pressure impactor (DLPI) with backup filter, and a vacuum pump (model: Leybold Sogevac SV25). The quench sampling probe would achieve rapid quenching of flue gas particles by both water and helium (1 L/min). The helium also plays a role to dilute the particle stream to minimize the interaction among particles and force the nucleation of vaporized species during quenching. The cyclone works with a nominal particle cut-off size of ~10 μm. The DLPI is composed of 13 stages of impaction plates and a backup filter with the detailed cut-off particle size in each stage shown in Table 3-3 (calibrated by the manufacturer). Aluminium foils and polycarbonate filters were used as the PM collection substrates for each stage of impaction plates. The diluted Apiezon-H vacuum grease was applied to each polycarbonate filters (pre-treated at 115 °C for 12 h) to avoid the influence of particle bounce during collection.[65] The vacuum pump was used to maintain the work pressures of the inlet and outlet of the DLPI as ~1013.3 and ~100 mbar, respectively, and the gas flow rate at the outlet of the bottom stage as ~10 L/min. The temperature of the flue gas at the outlet of sampling probe and the PM sampling line (including cyclone and DLPI) was kept at 115 °C in order to avoid the condensation of acidic gases (e.g., SO_3 and HCl) in the flue gas.[65] As a result, when the flue gas generated from combustion zone was passing through the sampling system, the coarse ash particles (aerodynamic diameter > 10 μm) would be removed firstly and retained in the cyclone, the PM_{10} particles with sizes in range of ~0.0218−10 μm would be captured by the 13 stages of DLPI, and the ultrafine particles would be collected by the backup filter. In the whole thesis, the PM collected with aerodynamic diameters of <0.1, 0.1−1, 0.1-10, <1, 1-10, <2.5 and <10 μm hereafter referred to as $PM_{0.1}$, $PM_{0.1\text{-}1}$, $PM_{0.1\text{-}10}$, PM_1, $PM_{1\text{-}10}$, $PM_{2.5}$ and PM_{10}, respectively.

3.3.3 Fuel and PM analysis

Various instruments and analytical techniques were applied for analysis of both fuel samples and PM_{10} particles.

Table 3-3 Nominal cut-off size of each stage of the low-pressure impactor.

Stage	Cut-off size ($D_{50\%}$, μm)
13	10.1891
12	6.8628
11	4.0938
10	2.4421
9	1.6269
8	0.9573
7	0.6120
6	0.3730
5	0.2476
4	0.1385
3	0.0773
2	0.0429
1	0.0218
Backup filter	0.01

3.3.3.1 Fuel sample analysis

Analysis of proximate, ultimate, calorific values, inorganic element, trace element, and rheological properties were carried out for all the fuel mentioned in Section 3.3.1 with methods and procedures detailed below.

Proximate analysis. Proximate analysis reports water/moisture content, ash content, volatile content, and fixed carbon content of a fuel sample. The analysis for solid fuels like biochar and slurry-char was carried out by a thermogravimetric analyser (TGA, model: Mettler TGA/DSC 1 STAR) according to Australia Standards of AS 1038.4-2006 (R2016).[251] Briefly, ~5 mg of fuel sample was loaded into the crucible, and argon and firstly purged in for 15 min followed by heating to 110 °C and holding for 20 min. The weight loss in this stage was regarded as moisture content. Then, the temperature was increased to 950 °C at a heating rate of 50 °C/min and held for 20

min and then decrease to 600 °C with the weight loss in this process regarded as volatile content and the remaining as fixed carbon. Lastly, the atmosphere was then changed to air to burn the rest of the fuel samples for 30 min until no further weight loss observed and the weight of the residue is regarded as ash content. The temperature program of proximate analysis for solid fuels could be found in Figure 3-5.

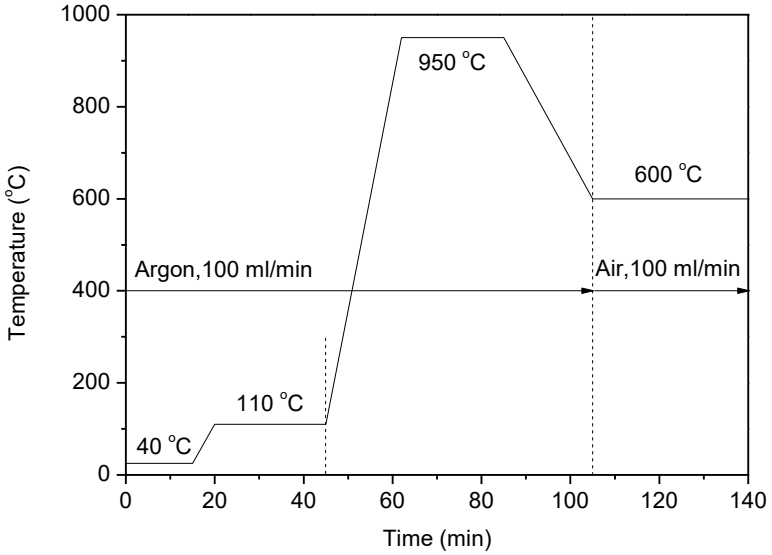

Figure 3-5 Temperature program of proximate analysis for solid fuels

Due to the higher water and volatile contents and low ash contents of liquid (i.e., bio-oil, filtrated bio-oil, WIF blend, slurry-oil, BMCG, and WSFCG) and slurry fuels (BB, WSFB, BMCGB, and WSFCGB) and low sample loading level, it is hard to distinguish their release of water and volatiles and measure their ash contents via TGA method. Therefore, different methods were applied for analysis of water and ash contents in liquid and slurry fuels, with exception for formulated samples like FWSFs and CG whose properties were reported based on composition calculation. The water contents of liquid and slurry fuels were carried out via method of Karl Fischer titration detailed elsewhere.[115] Briefly, ~0.25 g of fuel sample was injected and dissolved in a solution (mixture of Hydranal methanol and chloroform with mass ratio of 3:1) and titrated in a titrator (model: Mettler V30) with additive of Hydranal Composite 5K which works to prevent fading of the titration end point. The ash

contents of liquid and slurry fuels were carried out via ashing of the fuel samples in a Muffle furnace. Briefly, ~500 mg of fuel samples were added in a platinum crucible and burned (under air, 2 L/min) in the Muffle furnace with a temperature program developed recently[252] detailed shown in Figure 3-6.

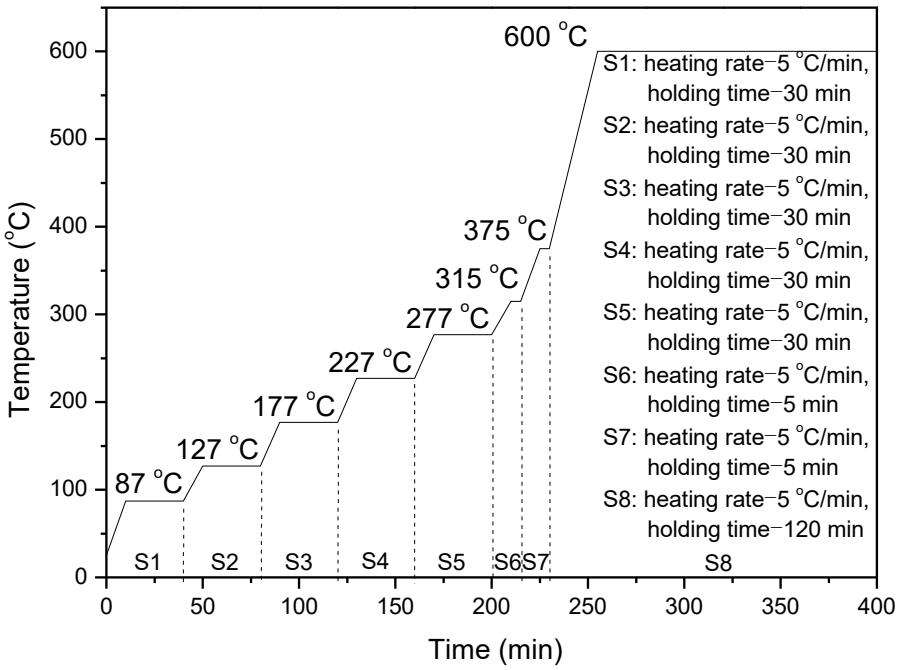

Figure 3-6 Temperature program for ashing of liquid and slurry fuel samples in Muffle furnace[252]

Ultimate analysis. The ultimate analysis was carried out via a CHN analyser (model: PerkinElmer 2400 Series II) according to AS 1038.6.1-1997 (R2013).[253] The oxygen (O) content was determined by calculation of the difference from the results of carbon (C), hydrogen (H), and nitrogen (N) contents.

Calorific values. The higher heating value (HHV) and lower heating value (LHV) were calculated based on the proximate and ultimate analysis via correlations[254] between heating values and contents (wt %) of water (M), C, H, N, and O, in details:

$$\text{HHV (MJ/kg)} = -1.3675 + 0.3137C + 0.7009H + 0.0318O \quad (3\text{-}1)$$

$$\text{LHV (MJ/kg)} = \text{HHV} - 0.0245M - 0.212H - 0.0008O^{201} \quad (3\text{-}2)$$

Rheological properties. The rheological properties of the liquid and slurry fuels were determined by a rheometer (model: Haake Mars II) fitted with a cone−plate (model:

C35/4) sensor system and a Haake Thermocontroller (model: TC501). Briefly, ~1 mL of fuel sample was applied for each time of steady shear test. The viscosity was averaged from the results in a shear rate range of 100−500 s^{-1} where the sample shows Newtonian behaviour.

Inorganic element contents. Different analysis methods were applied for the quantifications for the concentrations of the major inorganic elements including Na, K, Mg, Ca, Al, Si and Fe. The Na, K, Mg, and Ca were determined via a previous method[255] mainly consisting of ashing and digestion. Briefly, the fuel sample was put into a platinum crucible (~30 mg for solid fuels and ~500 mg for liquid and slurry fuels) and put into the Muffle furnace for ashing with a same temperature program seen in Figure 3-6. The crucible and the ash residue were then placed into a Teflon vial and added with a mixture of concentrated hydrofluoric acid (HF) and nitric acid (HNO_3) with mass ratio of 1:1 at 120 °C for 12 h for complete oxidation and ash digestion. After the excessive acid was evaporated, the residue sample was further dissolved in 0.02 M methanesulfonic acid (MSA) solution followed by quantification via an ion chromatography (IC, model: Nionex 3000) equipped with CS12 guard and analytical columns and a conductivity detector.

The quantification of Al, Si, and Fe was conducted via a different method[255] including ashing, fusion, and then quantification. Briefly, the fuel sample was burned in the Muffle furnace with a same ashing method described in the last paragraph. After cooling of the crucible, X-ray flux (35.3 % lithium tetraborate and 64.7 % lithium metraborate) was then added with mass ratio of flux to ash as 30:1 for the purpose of ash decomposition by fusion at 950 °C for 2 h in Muffle furnace. After cooling, the residue after fusion was dissolved into 2% Nitric acid solution and quantified via a inductively coupled plasma optical emission spectrometry (ICP−OES, model: PerkinElmer Optima 8300).

The contents of Cl and S were quantified via an improved Eschka method developed recently.[256] A novel two-stage reactor was applied, consisting of a volatile generation zone at the top, a volatile combustion zone at the bottom, and bubblers at the outlet of the bottom combustion zone with detailed schematic diagram shown in Figure 3-7. Briefly, ~150 mg of fuel sample was loaded into a platinum crucible and thoroughly mixed with ~300 mg of Eschka flux (sodium carbonate and magnesium oxide, Sigma Aldrich, 00166) followed by further covering of ~200 mg of Eschka mixture on the top surface of the fuel-flux mixture. The bottom combustion zone was firstly heated to 950 °C and then the sample-loaded crucible was placed in on the quartz frit in the top side reaction zone with total air flow rate of 2 L/min fed in simultaneously. The volatile generation zone was then started to heat to 675 °C (with heating rate of 10 °C/min) and hold for 2 h in accordance with the Eschka method for capture of Cl,[257] and then further heated to 800 °C (with heating rate of 10 °C/min) and hold for another 2 h for capture of S.[258] The Cl and S released via volatilization would be burned in the bottom combustion zone and captured by the bubblers in which 0.1 M NaOH solution was loaded followed by quantification by IC (model: Dionex ICS-1100) equipped with an IonPac AS22 fast analytical column (4×150 mm) and 2.25 mM Na_2CO_3/0.7 mM $NaHCO_3$ solution as eluent. The residue in crucible was also dissolved in ultra-pure water and quantified by the same IC.

The total P in each fuel was also quantified via ICP−OES however, after direct acid digestion of fuel sample using concentrated HNO_3/HF/H_2O_2 mixtures according to a method detailed elsewhere.[259] The nitric acid would oxidise most of the organic matter, however, hydrogen peroxide is needed for break down the fatty components. Briefly, ~500 mg of liquid or slurry fuel sample was loaded in a Teflon digestion vessel (overnight evaporation of the liquid or slurry fuel samples at room temperature was conducted to minimize the volatile contents prior digestion) or ~30 mg of solid fuel sample was loaded in, mixture of concentrated HNO_3 and HF acid with mass ratio of 3:1 was then added in followed by holding at 120 °C for 4 h with

vessel lid covered. After cooling, H_2O_2 was then added in with quantity same to HF, followed by heating at 120 °C for another 4 h. Then, after cooling again, the lid was opened, and heated back to 120 °C for acid evaporation until there is no liquid left in the vessel. The residue in the vessel was then dissolved into 2% nitric acid solution for further quantification.

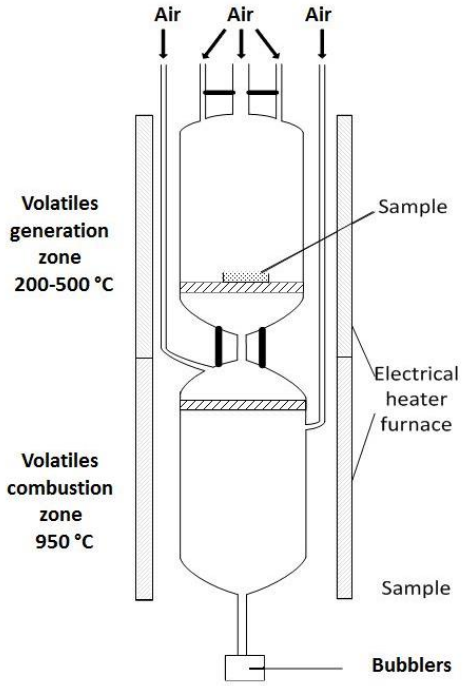

Figure 3-7 Schematic diagram of the two-stage reactor

The measurement of trace elements (including Ti, V, Cr, Mn, Ni, Co, Cu, Zn, As, Cd, and Pb) in fuel samples were carried out via same method with P via fuel sample digestion by concentrated HNO_3/HF/H_2O_2 mixtures followed by dissolving into 2% nitric acid solution for quantification, however, via a inductively coupled plasma mass spectrometry (ICP−MS, model: PerkinElmer NexION 350D). It should be noted that the determination of trace element concentration in CG is carried out via dilution with 2% nitric acid followed by direct analysis via ICP−MS.

3.3.3.2 PM sample analysis

PM samples were collected for analysis of mass based particle size distribution (PSD), organic carbon content (OC), morphology, inorganic element composition.

Mass based PSD. A microbalance (model: Mettler MX5, accuracy: 0.001 mg) was applied to measure the mass of PM collected from each DLPI stage.

OC. For determine the achievement of complete combustion, the PM samples were extracted in ultra-pure water for 24 h and the leachate was then sent to a TOC analyser (model: Shimadzu TOC-V_{CPH}) for total OC analysis.

Morphology. Selected PM samples (collected in stage 2 and 8 or 9 of DLPI) were sent for platinum coating and then image scanning via a dual-beam field emission scanning electron microscopy (FESEM, model: Zeiss Neon 40EsB). Chemical composition analysis could also be applied via an energy dispersive O-ray spectrometer (EDS) combined with the FESEM. It should be note that, in case of incomplete combustion, copper tape was applied as basement to determine the high content of C in PM sample, while, in complete combustion case, carbon tape base was usually applied.

Inorganic element composition. Four methods were applied for analysis of inorganic elements in PM samples (see Figure 3-8, which is a schematic diagram of quantification of inorganic elements in PM sample collected from DLPI). One is water leaching of polycarbonate filters in each stage of DLPI by ultra-pure water for 24 h followed by analysis of the leachate via IC for analysis of water-soluble Na, K, Mg, Ca, Al, Si, and Fe, and chloride (Cl^-), phosphate (PO_4^{3-}), sulfate (SO_4^{2-}). Second is the method of ashing of PM containing polycarbonate filters followed by digestion by mixture of concentrated HNO_3 and HF mixture and then dissolved into 0.02 M MSA solution for quantification of total contents of Na, K, Mg and Ca in PM via IC. Third is for the quantification of total Al, Si, and Fe with method similar with the aforementioned borate fusion method including steps of ashing, fusion, and quantification via ICP−OES. Last is the quantification of trace elements (Ti, V, Cr, Mn, Ni, Co, Cu, Zn, As, Cd, and Pb) via the same method of digestion by concentrated HNO_3/HF/H_2O_2 mixtures followed by quantification through ICP−MS.

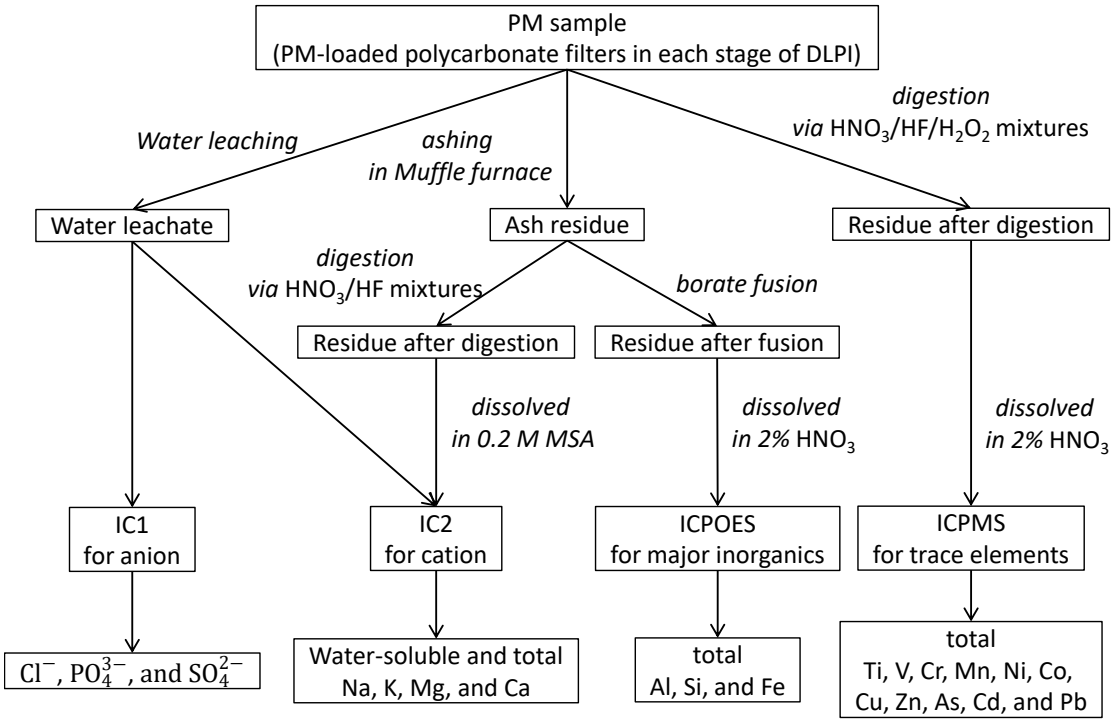

Figure 3-8 Schematic diagram of quantification of inorganic elements in PM sample collected from DLPI

3.4 Summary

To achieve the research objectives in this thesis, series experiments of combustion and PM collection were conducted via a DTF system at 1400 °C under various atmosphere conditions. Various fuel samples were considered including bio-oil, filtrated bio-oil, WIF blend, FWSFs, biochar, slurry-oil, slurry-char, BB (with two char loading levels), WSFB, CG, BMCG, WSFCG, BMCGB, and WSFCGB. The combustion atmospheres include air and pure oxygen for incomplete combustion study, and air, 21% O_2 –79% CO_2 and 30% O_2–70% CO_2 for complete combustion. The mass based PSDs, morphology, OC, and inorganic element contents (including major elements of Na, K, Mg, Ca, Al, Si, Fe, Cl, S, P, and trace elements of Ti, V, Cr, Mn, Ni, Co, Cu, Zn, As, Cd, and Pb) were analyzed for PM particles collected from each stage of DLPI.

Chapter 4 Particulate Matter Emission from Bio-oil Incomplete Combustion under Conditions Relevant to Stationary Applications

4.1 Introduction

While it can be upgraded/refined for producing liquid transport fuels, bio-oil produced from biomass fast pyrolysis is also a suitable fuel for stationary combustion applications.[20,21] Bio-oil combustion offers several advantages over direct biomass combustion. For instance, bio-oil has a high volumetric energy density suitable for transport [32] and after biomass pyrolysis the majority of key ash-forming inorganic species are retained in biochar.[67] Therefore, bio-oil combustion may potentially mitigate ash-related issues including ash deposition, corrosion, and fine particulate matter (PM) emission that are often encountered during biomass combustion.[153]

Extensive research has been conducted on its evaporation and combustion behaviour via thermogravimetric analysers,[260] fibre-suspended droplet tests,[135] and entrained flow reactors.[114,261] There are four major stages[114,261] during bio-oil combustion, including (i) quiescent combustion of light volatiles, (ii) droplet swelling and distortion, followed by microexplosion, which usually results in the breakup of droplet to various degrees, (iii) droplet coalescence, and (iv) its subsequent combustion. Recent studies on the combustion of bio-oil or bio-oil/ethanol blends [262-266] on pilot- or commercial-scale combustion systems led to better understanding on ash deposition and emissions of pollutant gases (e.g., NO_x, SO_2 and HCl). While scattered data were reported on the PM produced from the combustion of bio-oil/ethanol blends,[264-266] there is no systematic study on the emission of PM with aerodynamic diameter of <10 μm (PM_{10}) which is an important environmental concern for fuel utilisation.[267-270] Especially, bio-oil has some undesired fuel properties such as high viscosity, high water content and high coking

propensity[76,261,264,271-273] leading to achieving complete combustion being challenging. In addition, complete particle size distributions (PSDs) of key inorganic elements in PM_{10} are also seldom reported, which is of great importance in understanding the transformation of these inorganic species during bio-oil combustion. Most importantly, bio-oil generally contains substantial amounts of fine char particles of micron and, to a lesser extent, submicron size ranges,[107] which accelerate microexplosion during bio-oil combustion. [261] However, the contribution of these fine char particles in PM_{10} emission remains unclear due to the lack of comparison study on the combustion of both char-removed bio-oil and its corresponding raw bio-oil. Such knowledge is important in developing strategies for PM reduction during bio-oil combustion.

Therefore, this study aims to conduct a systematic research on the emission of PM_{10} from the combustion of both a raw bio-oil and its filtrated bio-oil at 1400 °C in air and oxygen atmospheres, using a laboratory-scale drop tube furnace (DTF). The properties of the raw bio-oil and the filtrated bio-oil could be found in Table 4-1. The produced PM_{10} samples were collected and characterised to understand its emission behaviour. The complete PSDs of PM_{10} and its key inorganic species were reported. The effects of fine char particles in bio-oil and combustion atmosphere on PM_{10} emission during bio-oil combustion were discussed.

4.2 Mass-based PSDs and Yields of PM_{10} and Key Inorganic Species in PM_{10}

Figure 4-1 depicts the mass-based PSDs and yields of PM_{10} produced from the combustion of the raw and filtrated bio-oil samples under air or oxygen atmosphere, normalized to unit mass (dry basis) of the respective bio-oil input into the furnace. Clearly, all the PSDs demonstrate a bimodal distribution: a fine mode at ~0.04-0.07 μm and a coarse mode at ~1.6 μm. Consequently, ~37-62% and ~38-63% of PM_{10} are distributed in PM_1 and PM_{1-10}, respectively, depending on combustion feedstock and atmosphere. The discrepancies in the PSDs and yields of PM_{10} produced from

the combustion of the raw bio-oil and the filtrated bio-oil in air demonstrate the significant contribution of the filtrated fine char particles in PM_{10} emission. Combustion atmosphere change also substantially affects the PSDs and yields of PM_{10} from the raw bio-oil combustion which will be discussed in the following sections. In addition, the yields of $PM_{2.5}$ and PM_{10}, which are of practical importance, are ~0.09-0.22 and ~0.13-0.25 mg/g bio-oil (dry basis), respectively, equivalent to ~5.08-12.43 and ~7.34-14.12 mg/MJ LHV input. Such energy-based yields of $PM_{2.5}$ and PM_{10} from the combustion of the two bio-oils are considerably lower than those from the combustion of a Mallee leaf and its torrefied biomass,[201] demonstrating an advantage of using bio-oil as a fuel for combustion.

Table 4-1 Properties of the raw bio-oil and the filtrated bio-oil

Properties	**Raw bio-oil**	**Filtrated bio-oil**
Water content (wt%, ar[a])	26.0	27.0
Solids (wt%, db[c], as acetone insoluble)	0.23	nd[b]
Ash (wt%, db[c])	0.07	0.07
Elemental Analysis (wt%)		
C[d]	55.6	54.1
H[d]	12.7	12.7
N[d]	0.1	0.1
O[e]	31.6	33.1
Inorganic element concentration (wt%)		
Na[c]	0.0021	0.0021
K[c]	0.0063	0.0063
Mg[c]	0.0051	0.005
Ca[c]	0.0245	0.0231
Cl[c]	0.0036	0.0035
S[c]	0.0048	0.0045
P[c]	0.0025	0.0017
Lower heating value (LHV)[f], MJ/kg, ar[a]	17.7	17.4

[a] As-received basis. [b] Not detected. [c] Dry basis. [d] Dry and ash-free basis. [e] By difference of C, H, N on dry and ash-free basis. [f] Lower heating value from calculation.

Figure 4-2 illustrates chemical compositions of PM with aerodynamic diameters of <0.1 μm ($PM_{0.1}$), 0.1-1 μm ($PM_{0.1-1}$) and 1-10 μm (PM_{1-10}), reported as oxides of inorganic species (excepting Cl), with two important findings observed. One is that

PM's chemical compositions are size dependent. Among the detected species, the oxides of Ca and Mg (to a lesser content) are mainly present in $PM_{0.1\text{-}1}$ and $PM_{1\text{-}10}$, whereas $PM_{0.1}$ also contains considerable amounts of Na, K, S and Cl. The other is that, apart from the quantified inorganic species, PM samples also contain ~40-49 wt% of species that are not quantified individually, denoted as "others" in Figure 4-2. These could include inorganic species Si, Al and Fe, and unburned carbon, the presence of which is demonstrated by the EDS spectra of PM with aerodynamic diameters of 2.438-4.087 μm from the raw bio-oil combustion under air and oxygen conditions (see Figure 4-3). It should be noted that copper (Cu) tape was used during the SEM-EDS analysis to avoid background carbon signal from commonly-used carbon tape. The presence of unburned carbon in the PM samples is further supported by the fact that the contents of "others" in the $PM_{0.1\text{-}1}$ and $PM_{1\text{-}10}$ from the raw bio-oil combustion in oxygen are substantially lower than those from their air combustion counterparts, as a result of improved burnout. Figure 4-3 also suggests that these PM samples mostly contain round particles with coarse surface. The coarse surface is deposited with some lighter spots that contain mainly inorganic species. This further confirms that bio-oil were not completely burned, otherwise these inorganic particles may either liberate from the coarse carbonaceous surface or coalesces to form large ash particles.

Although the PM_{10} from the combustion of the two bio-oils contains unburned carbonaceous materials, the carbon concentration in PM_{10} was not measured in this work with two reasons: measurement of the carbonaceous in PM_{10} under current technology was hard due to the very low yields of PM from bio-oil combustion, and this study focuses on the transformation of inorganic species and their contribution to PM_{10}. This is because that, from a practical point of view, complete combustion is the final goal, under which the emitted PM_{10} should dominantly contain inorganic species. In addition, comparison on PM_{10} emission from the combustion of the raw bio-oil in air and oxygen provides us an opportunity to qualitatively investigate the

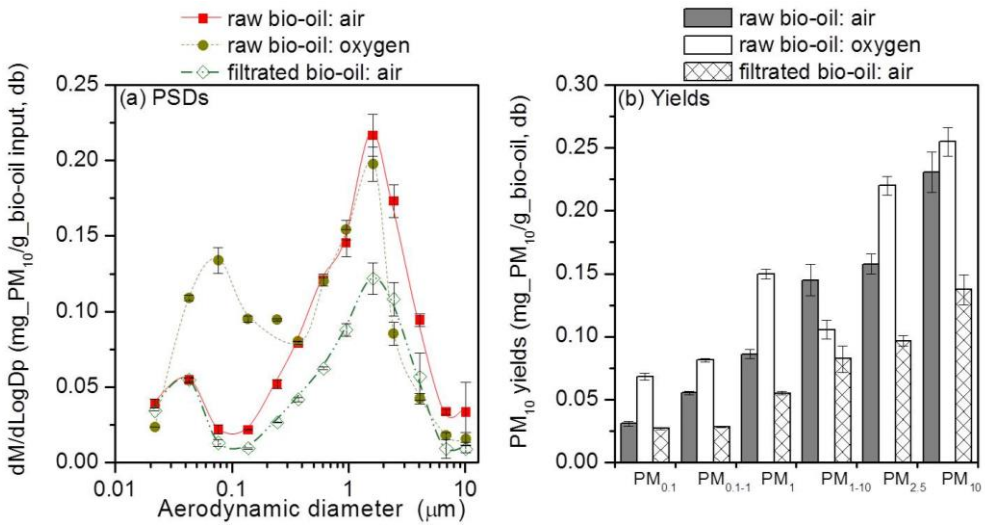

Figure 4-1 (a) Mass-based PSDs of PM_{10} and (b) yields of $PM_{0.1}$, $PM_{0.1\text{-}1}$, PM_{1}, $PM_{1\text{-}10}$, $PM_{2.5}$ and PM_{10} collected from the combustion of the raw bio-oil and the filtrated bio-oil under air and oxygen conditions.

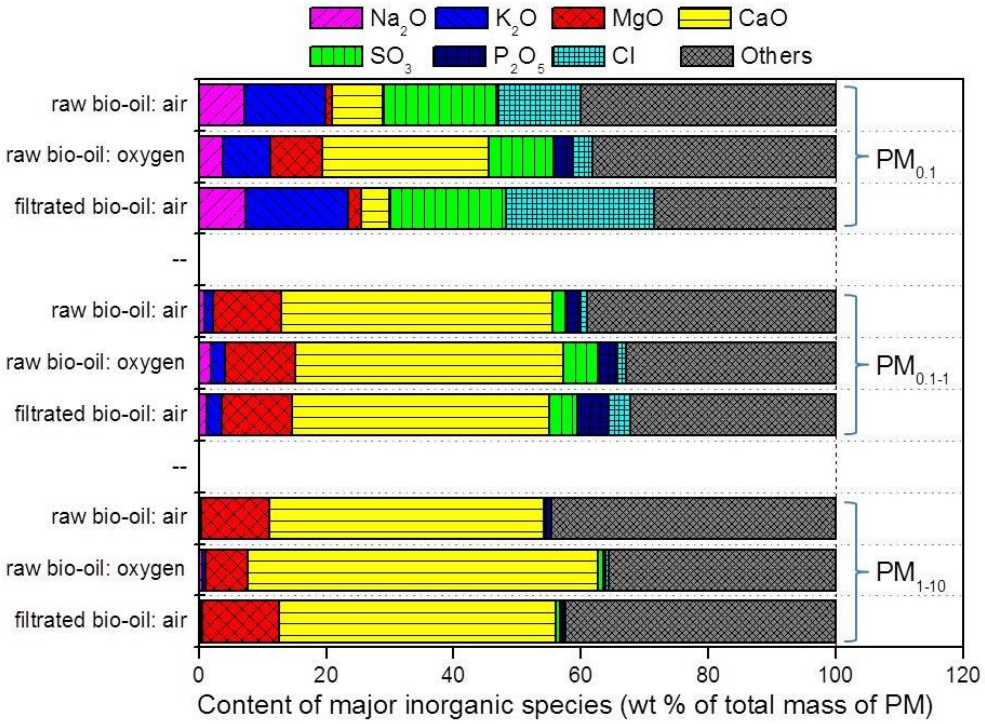

Figure 4-2 Chemical composition of (a) $PM_{0.1}$, (b) $PM_{0.1\text{-}1}$ and (c) $PM_{1\text{-}10}$ from the combustion of the raw bio-oil and the filtrated bio-oil. Data are reported as oxides. Others are calculated by difference, most likely dominated by unburned carbon

transformation of these key inorganic species (i.e., AAEM species, Cl, S and P) at different extent of burnout. This will pave a way for thoroughly understanding the emission of inorganic PM_{10} from the complete combustion of the bio-oils.

To better understand the transformation of AAEM species, Cl, S and P during the combustion of the two bio-oils, their PSDs and yields in PM_{10} are shown in Figure 4-4 and 4-5, respectively, with three important findings observed. First, the PSDs of volatile elements Na, K, Cl and S (in form of SO_4^{2-}) all follow a unimodal distribution, with mode diameters of ~0.043-0.077 μm. Consequently, ~87-93% of Na, ~92-96% of K, ~85-97% of Cl^-, and ~92-93% of SO_4^{2-} in PM_{10} are distributed in PM_1. Such observations are plausible and similar to those reported on biomass combustion.[65,201,206] During bio-oil combustion, Na, K, Cl and S are easily released into gas phase and effectively contribute to PM_1 emission via a series of gas-phase reactions, homogeneous nucleation, and/or heterogeneous condensation/reaction of the vapours on the surface of existing fine particles.

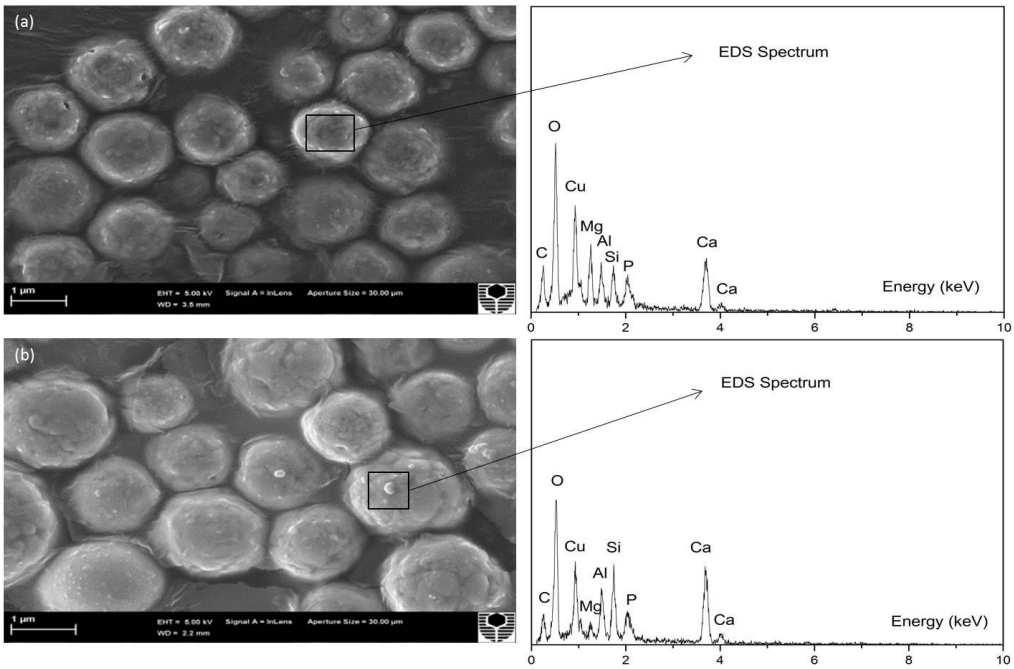

Figure 4-3 SEM images and EDS spectra (copper tape used as backgrounds) of PM with an aerodynamic diameter of 2.438−4.087 μm from the combustion of the raw bio-oil. Panels a and b are under air and oxygen combustion, respectively.

Second, Mg and Ca behave similarly and their PSDs in PM_{10} are dependent on combustion atmosphere. The PSDs of Mg and Ca in PM_{10} from the combustion of the two bio-oils in air show a unimodal distribution with a mode diameter of ~1.624 μm. As a result, ~32.5-73.0% of Mg and ~52.6-74.0% of Ca in PM_{10} are concentrated in PM_{1-10}. The concentration of Mg and Ca in PM_{1-10} can be explained by the so-called catalysed sintering of their oxides and/or their interactions with Si- and Al- containing minerals, similar to that reported previously on torrefied biomass combustion.[201] The later mechanism may lead to the formation of silicates and/or aluminosilicate that subsequently coalesce on the surface of burning char particles [201]. On the other hand, switching combustion atmosphere from air to oxygen results in the appearance of a fine mode with a peak diameter of 0.077 μm and thus the PSDs of Mg and Ca in PM_{10} from the raw bio-oil combustion in oxygen follow a bimodal distribution. The effects of combustion atmosphere on the PSDs of Mg and Ca will be discussed in Section 4.4.

Third and last, the PSDs of PO_4^{3-} in PM_{10} from the combustion of the two bio-oils under both air and oxygen conditions all follow a bimodal distribution, with fine mode and coarse mode being located in PM_1 and PM_{1-10}, respectively. Approximately ~51-94% and 6-49% of PO_4^{3-} in PM_{10} being distributed in PM_1 and PM_{1-10}, respectively. The presence of PO_4^{3-} in PM_1 suggests that some P in the raw and filtrated bio-oils has gone through gaseous phase reactions during combustion. The partition of water-soluble PO_4^{3-} in PM_{1-10} can be attributed to the formation of Mg and Ca phosphates which can be partial dissolved during water washing.

4.3 Contribution of Filtrated Char Particles in the Emissions of PM_{10} and Its Key Inorganic Species.

Considering the data presented in Figures 4-1, 4-4 and 4-5 together, the contribution of filtrated fine char particles in the raw bio-oil in the emission of PM_{10} and its key forming elements can be summarised as follows. First, whereas the shape of PSDs of

PM_{10} from the combustion of the two bio-oils remains unchanged, the mass of PM with aerodynamic diameters of 0.1−10 μm ($PM_{0.1\text{-}10}$) from the filtrated bio-oil combustion is considerably lower than that from the raw bio-oil combustion. This leads to ~49.1 and ~35.9% of reductions in the yields of $PM_{0.1\text{-}1}$ and $PM_{1\text{-}10}$, respectively (see Figure 4-1). On the other hand, among all the inorganic elements analysed, Mg and Ca demonstrate the most noticeable discrepancies on the PSDs and yields of these elements in PM_{10} produced from the combustion of the raw bio-oil and the filtrated bio-oil (see Figures 4-4 and 4-5). Specifically, the filtrated bio-oil combustion leads to considerable reductions in the mass of Mg and Ca in the PM with aerodynamic diameters of larger than 0.372 μm, in comparison with that from the raw bio-oil combustion. As a result, the yields of Mg and Ca in $PM_{0.1\text{-}1}$ from the filtrated bio-oil combustion decrease by ~47.1 and ~51.9%, respectively, compared to those from the raw bio-oil combustion. Similarly, the yields of Mg and Ca in $PM_{1\text{-}10}$ decrease by ~35.4 and ~42.8%, respectively, due to the removal of fine char particles in the raw bio-oil.

Since the reduction in the PM mass mainly takes place in the size range of 0.1-10 μm, the breakdown of the yields of $PM_{0.1\text{-}10}$ from the combustion of the raw and filtrated bio-oils is shown in Figure 4-6. It can be seen that the removal of fine char particles from the raw bio-oil leads to considerable reductions in the yields of Mg and Ca, and more substantially, unquantified species (denoted as "others" that include unburned carbonaceous material, see Section 4.2) in $PM_{0.1\text{-}10}$. In other words, the filtrated fine char particles contribute to both inorganic species (mainly Mg and Ca) and unburned carbonaceous materials in $PM_{0.1\text{-}10}$. Whereas exact mechanisms responsible for such contributions remain unclear, there may be at least two possible mechanisms. One is the possible alteration in the combustion behaviour of the filtrated bio-oil due to the removal of fine char particles. It is reported that the presence of fine char particles in bio-oil can facilitate the nucleation of the vapour bubbles inside a bio-oil droplet and thereby accelerates the occurrence of droplet microexplosion.[261] Such

microexplosion can lead to the breakup of bio-oil droplets and ejection of matter in the bio-oil [135]. Therefore, during the raw bio-oil combustion, the presence of fine char particles may intensify the breakup of the bio-oil droplets, which may in turn contribute to the emission of $PM_{0.1-10}$. The other possible mechanism is the direct carryover of fine char particles that are not completely burned. Indeed, our previous study shows that fine char particles can be a significant source of PM_{10} emission.[274] As bio-oil generally contains considerable amounts of fine char particles in micron sizes,[107] direct carryover of unburnt fine char particles into $PM_{0.1-10}$ is possible, which may contribute to both unburned carbonaceous material and inorganic species (embedded in char) in $PM_{0.1-10}$. Figure 4-7 shows that the filtrated char particles are rich in Ca and, to a lesser content, Mg. Direct carryover of the unburnt fine char particles is also indirectly supported by the solubility of Ca in the PM_{10} produced from the combustion of the raw and filtrated bio-oils. Figure 4-8 shows that ~100% of Ca in the PM_{10} from the filtrated bio-oil combustion (i.e., in the absence of fine char particles larger than 0.45 μm) is water-soluble. However, there is considerable amount of water-insoluble Ca in the PM_{10} from the raw bio-oil combustion (i.e., in the presence of fine char particles). This is consistent with the fact that Mg and Ca in the filtrated char particles must be water-insoluble because of the acidic nature of the raw bio-oil. It is also reasonable to conclude that the water-insoluble fraction of Ca in the PM_{10} from the raw bio-oil combustion is mainly originated from the fine char particles.

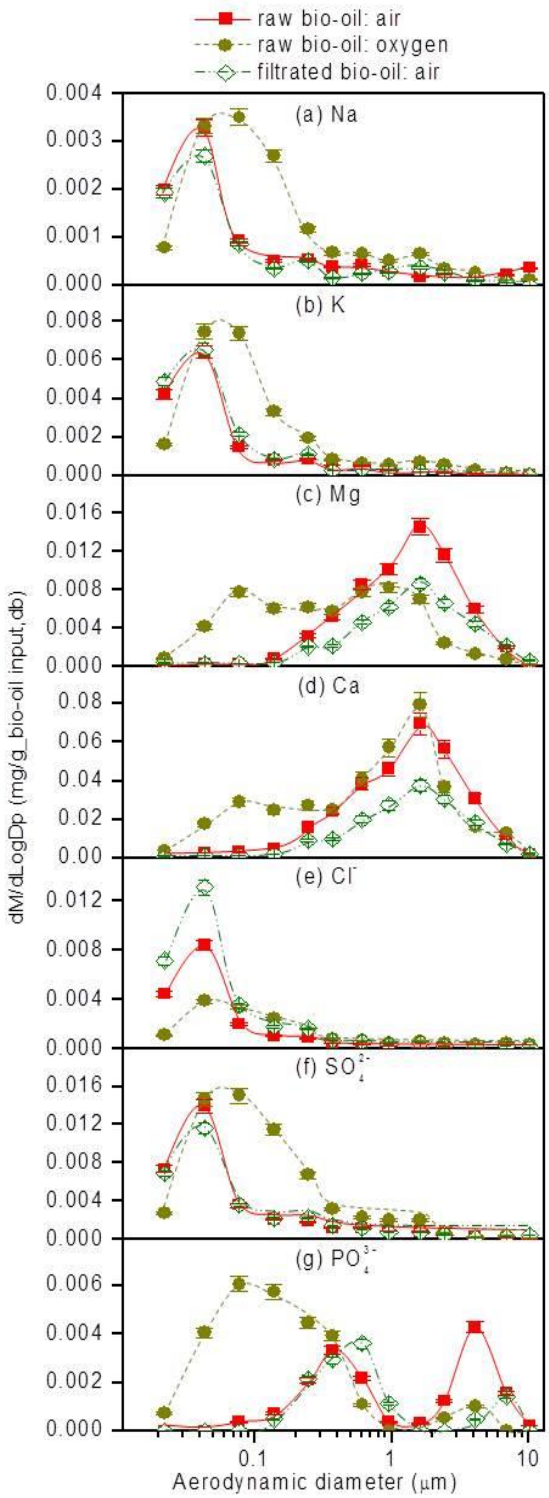

Figure 4-4 Elemental mass size distribution of (a) Na, (b) K, (c) Mg, (d) Ca, (e) Cl, (f) SO_4^{2-} and (g) PO_4^{3-} in PM_{10} from the combustion of the raw bio-oil and the filtrated bio-oil under air and oxygen conditions.

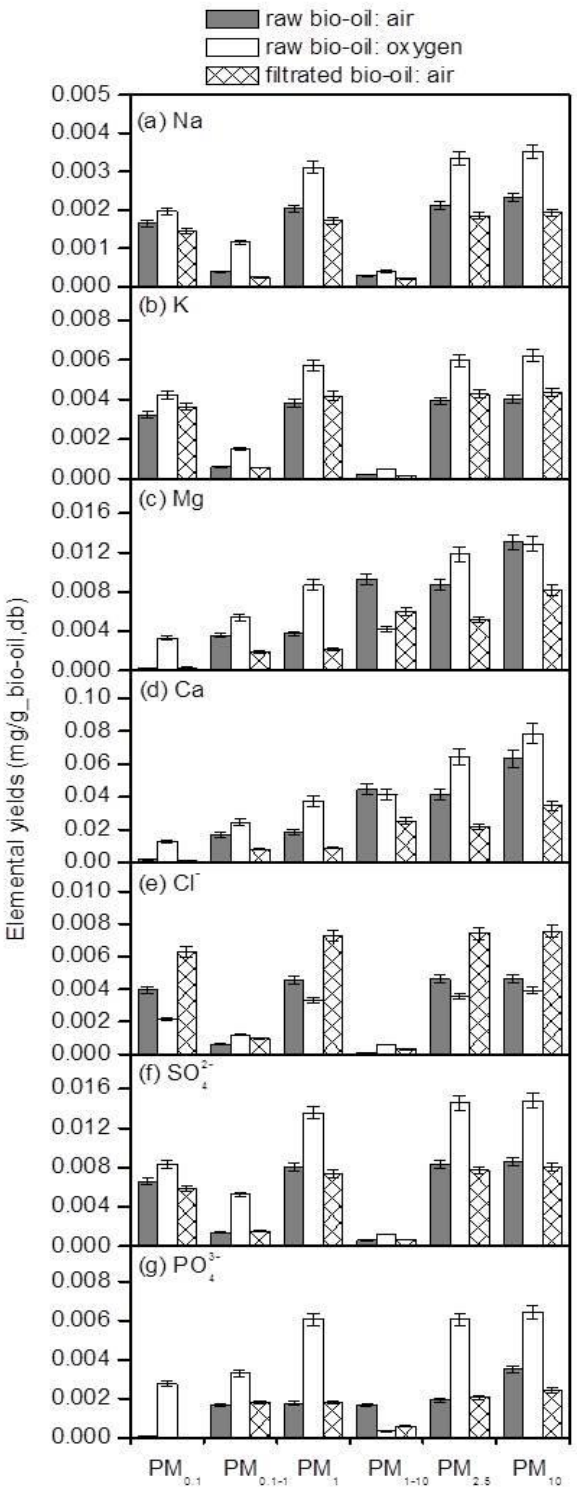

Figure 4-5 Yields of (a) Na, (b) K, (c) Mg, (d) Ca, (e) Cl, (f) SO_4^{2-} and (g) PO_4^{3-} in PM_{10} from the combustion of the raw bio-oil and the filtrated bio-oil under air and oxygen conditions.

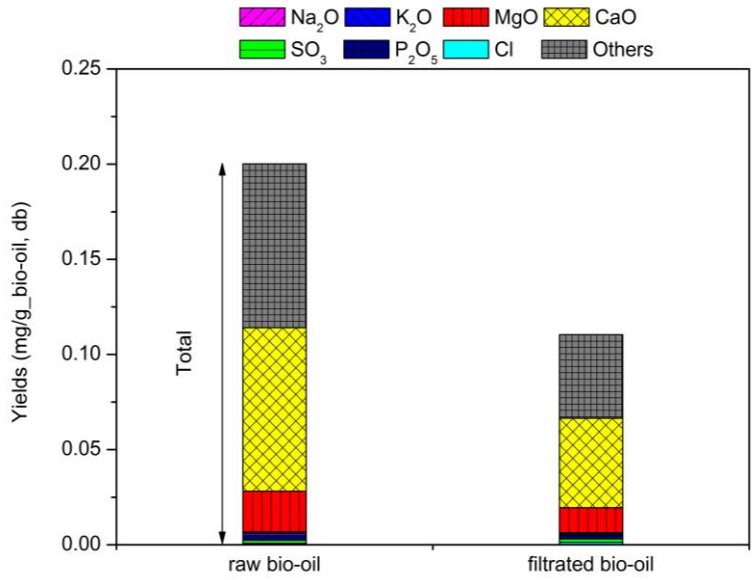

Figure 4-6 Yields of particulate matter with aerodynamic diameters of 0.1−10 μm ($PM_{0.1-10}$) from the combustion of the raw bio-oil and the filtrated bio-oil in air

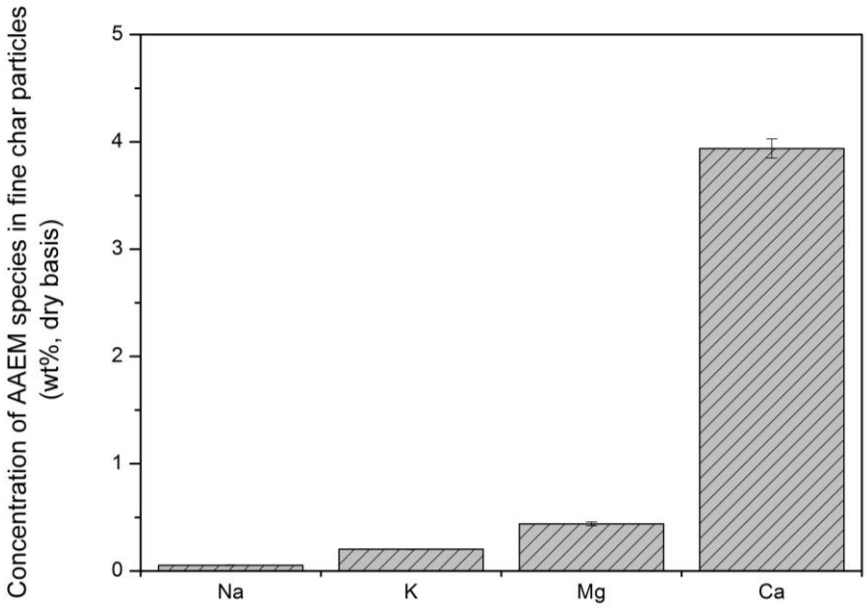

Figure 4-7 The contents of AAEM species in the filtrated char particles

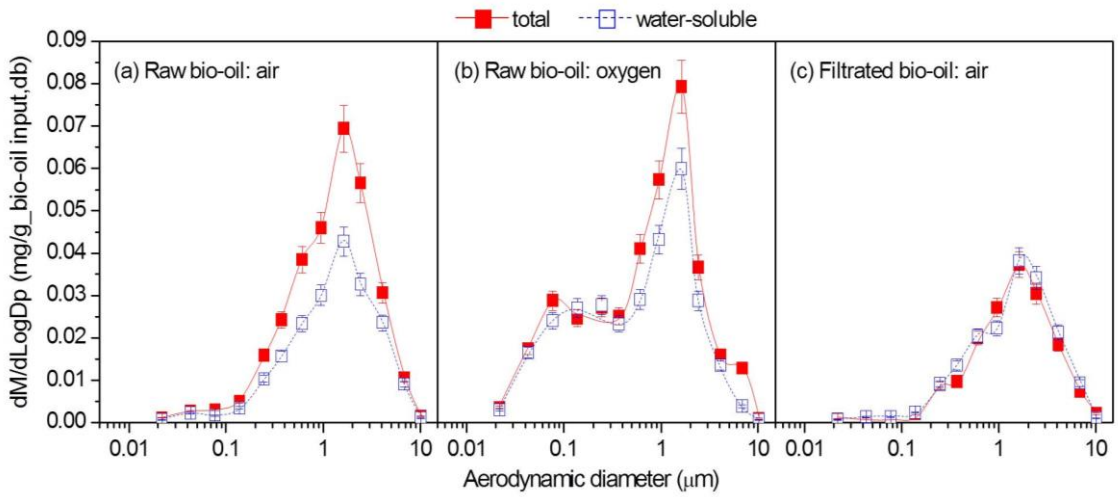

Figure 4-8 Comparison on the mass-based PSDs of total and water-soluble Ca in the PM_{10} produced from the combustion of the raw bio-oil in (a) air and (b) oxygen as well as (c) the filtrated bio-oil in air. PM_{10} means particulate matter (PM) with aerodynamic diameters of <10 μm.

4.4 Effects of Combustion Atmosphere on the Emissions of PM_{10} and its Key Inorganic Species.

The data in Figures 4-1, 4-4 and 4-5 also demonstrate the significant effect of combustion atmosphere (air and oxygen) on the PSDs and yields of both PM_{10} and its key inorganic species from the raw bio-oil combustion, leading to two observations. First, switching from air to oxygen shifts the fine mode diameter from ~0.043 to ~0.077 μm and leads to considerable increase in the mass of PM smaller than ~0.372 μm but decrease in that of PM larger than ~2.438 μm. As a result, the yields of PM_1 and $PM_{1\text{-}10}$ from the combustion of the raw bio-oil in oxygen are ~74.2% higher and ~27.2% lower, respectively, than those from its air combustion counterpart. The increase in the PM_1 yield is attributed to the increased yields of inorganic species, including Na, K, Mg, Ca, SO_4^{2-}, and PO_4^{3-}, in PM_1 (see Figure 4-5). The reduction in the $PM_{1\text{-}10}$ yield can be explained by the decrease in unburned carbonaceous material in $PM_{1\text{-}10}$ because of the improved burnout under oxygen conditions.

Compared to those in the PM_{10} from air combustion, the PSDs of Na, K and SO_4^{2-} in the PM_{10} from oxygen combustion shift to larger size. Consequently, the yields of Na, K and SO_4^{2-} in PM_{10} (mostly concentrated in PM_1) increase by ~53.2, 50.2 and 69.9%, respectively. For Mg and Ca, oxygen combustion leads to the appearance of a fine mode in the PSDs. The yields of Mg and Ca in PM_1 increase by ~131.2 and 100.4%, respectively, compared to those from air combustion. It appears that during air combustion, most of Mg and Ca may be associated with unburned carbonaceous structure, which lead to the absence of a fine mode in their PSDs. Switching the combustion atmosphere to oxygen may intensify direct liberation of fume Mg and Ca oxides particles due to the increased consumption of carbon structure on the burning char surface. Another possible reason for the increase of Mg and Ca in PM_1 is the enhanced evaporation of these elements into volatiles followed by subsequent oxidation and coagulation due to the higher combustion temperature under oxygen atmosphere. The liberated fume particles are known to effectively contribute to PM_1 emission, similar to that reported for coal combustion.[275,276] This is consistent with the data on possible occurrence form of Ca in PM_1. As can be seen in Figure 4-8b, nearly all the Ca in the PM_1 from the raw bio-oil combustion is water-soluble, indicating the possible existence of CaO, and to a lesser content, $Ca_3(PO_4)_2$. As expected, the yield of water-soluble PO_4^{3-} in the PM_1 from the combustion of the raw bio-oil in oxygen is also substantially higher than that in its air combustion counterpart, due to the increased availability of cations (e.g., Mg and Ca) in PM_1.

Surprisingly, the yield of Cl in PM_1 from the raw bio-oil combustion in oxygen is ~26.0% lower than that in the PM_1 from air combustion, which corresponds to the increase in the SO_4^{2-} yield in PM_1 (see Figure 4-5 e and f). This can be explained by the enhanced sulfation of alkali chlorides.[277-279] Briefly, the alkali chloride is able to react with SO_2 or SO_3 via homogeneous or heterogeneous reactions to form sulphate and to release Cl as gaseous HCl, which are promoted with increasing O_2 partial pressure. Under oxygen combustion condition, the partial pressure of O_2 is much

higher than that of air combustion, enhancing the chlorides sulfation reaction. The enhanced sulfation reaction leads to a reduction in the yield of Cl in the PM_1 from oxygen combustion, in comparison with that in the PM_1 from air combustion.

4.5 Conclusions

This study reports the complete PSDs of PM_{10} and its key inorganic elements from the incomplete combustion of a raw bio-oil and its filtrated bio-oil at 1400 °C under both air and O_2 atmospheres. The PSDs of the PM_{10} and water-soluble PO_4^{3-} in PM_{10} all exhibit a bimodal distribution. On the other hand, whereas the PSDs of volatile elements (i.e., Na, K, Cl, and S in form of water-solubleSO_4^{2-}) demonstrate a unimodal distribution, those of Mg and Ca are dependent on combustion atmosphere (i.e., unimodal distribution for air combustion and bimodal distribution for O_2 combustion). Fine char particles (>0.45 μm) in the raw bio-oil play significant roles in the emission of PM_{10} and its key forming elements (Mg and Ca). The combustion of the filtrated bio-oil in air results in considerable reductions in the mass of PM with aerodynamic diameters of 0.1−10 μm as well as that of Mg and Ca in the PM with a size range of 0.372−10 μm, in comparison with their raw bio-oil combustion counterparts. Combustion atmospheres also have significant effects on the emission of PM_{10} and its key inorganic elements. Switching combustion atmosphere from air to O_2 leads to an increase of ~74.2% in PM_1 yield but a decrease of ~27.2% in $PM_{1\text{-}10}$ yield. Whereas the increased PM_1 yield can be attributed to the increased yields of Na, K, Mg, Ca, SO_4^{2-} and PO_4^{3-} in PM_1, the reduction of $PM_{1\text{-}10}$ yield is most likely due to the decreased amount of unburned carbonaceous material in $PM_{1\text{-}10}$, as a result of the improved burnout under O_2.

Chapter 5 Emission of Particulate Matter during the Combustion of Bio-oil and Its Fractions under Air and Oxyfuel Conditions

5.1 Introduction

Bio-oil produced from biomass fast pyrolysis is considered as a potential fuel for stationary combustion applications.[28,29] Bio-oil addresses the key issue of high logistic cost associated with biomass and is suitable for transport due to its considerably higher volumetric energy density.[19,21] As a fuel, bio-oil has high acidity, poor stability, high water content and high viscosity.[21,115] During biomass fast pyrolysis, a small proportion of inorganic species in biomass can partition into bio-oil.[107] While the concentrations of such inorganic species are low in bio-oil, the ash-related issues during bio-oil combustion may not be overlooked. On the other hand, oxyfuel combustion technology replaces air combustion with O_2/CO_2 combustion and consequently produces a CO_2-dominant and sequestration-ready flue gas.[243] Therefore, bio-oil combustion under oxyfuel conditions becomes very attractive as it enables the renewable carbon in bio-oil to be readily captured for sequestration, potentially enabling power generation with negative carbon emission. However, there is little study on ash transformation during bio-oil combustion under oxyfuel conditions. Furthermore, it is known that bio-oil contains suspended fine char particles, water-soluble fraction and water-insoluble fraction.[107,127] Unfortunately, there has been little study on the emission of particulate matter with aerodynamic diameters of <10 μm (PM_{10}) during bio-oil combustion, particularly under oxyfuel conditions. The roles of different bio-oil fractions in PM_{10} emission during bio-oil combustion are also largely unknown.

Consequently, the objective of this study is to investigate the emission of PM_{10} from the combustion of fast pyrolysis bio-oil or bio-oil fractions using a laboratory-scale

drop-tube furnace (DTF) at 1400 °C under both air and oxyfuel conditions. Three bio-oil samples were then prepared with properties reported in Table 5-1.

Table 5-1 Properties of the raw bio-oil, the filtrated bio-oil and water-insoluble fraction

Samples	raw bio-oil	filtrated bio-oil	water-insoluble fraction blend with ethanol
water content (wt%, ar[a])	26.0	24.5	nd[b]
solids (wt% ar[a], as acetone insoluble)	0.16	nd[b]	nd[b]
ash (wt%, db[c])	0.07	0.06	0.003
Elemental Analysis (wt%)			
C[d]	41.51	41.33	49.61
H[d]	6.93	8.27	6.23
N[d]	0.11	0.09	0.03
O[e]	51.45	50.31	44.17
density (g/ml, ar[a])	1.18	1.18	0.81
viscosity (20 °C, mPa s)	102	128	6.5
LHV[f] (MJ/kg, db[c])	15.98	16.52	18.59

[a] As-received basis. [b] Not detected. [c] Dry basis. [d] Dry and ash-free basis. [e] By difference. [f] Lower heating value from calculation.

5.2 Yields and Mass-based Particle Size Distributions (PSDs) of PM_{10} from the Combustion of the Raw Bio-oil, the Filtrated Bio-oil and the Water-insoluble Fraction under Air and Oxyfuel Conditions

The concentrations of major inorganic elements (Na, K, Cl, S, Mg, Ca, Al, Si, and Fe) in the bio-oil samples and also the distribution of these inorganic elements in the water-soluble fraction, water-insoluble fraction and suspended fine char particles within the raw bio-oil could be found in Figure 5-1. It can be seen from Figure 5-1a that Ca is the most abundant element in both the raw and filtrated bio-oils, followed by Si, K, S, Mg, Fe, Cl, Al, and Na in a decreasing order. Figure 5-1a also indicates that filtration results in a slight decrease in the concentrations of these inorganic elements after the removal of fine char particles. As illustrated in Figure 5-1b, the inorganic elements of the raw-oil are distributed as ~47.2-88.7% in the water-soluble fraction, ~2.4-40.5% in the water-insoluble fraction and ~3.5-27.1% in the suspended fine char particles, respectively.

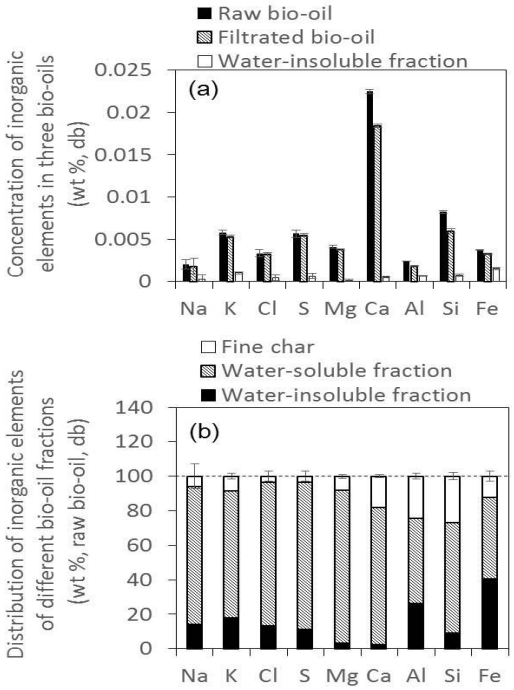

Figure 5-1 (a) Concentrations of major inorganic elements in the raw bio-oil, filtrated bio-oil and water-insoluble fraction; (b) Distribution of inorganic elements in water-soluble fraction, water-insoluble fraction, and suspended fine char particles within the raw bio-oil.

Figure 5-2 presents the mass-based PSDs and yields of PM_{10} produced from the combustion of the raw, filtrated and water-insoluble bio-oil samples in air, 21% O_2/79% CO_2, and 30% O_2/70% CO_2 atmospheres. The data are normalized to unit mass (dry basis) of equivalent raw bio-oil input into the furnace. The data demonstrate that substantial PM_{10} were produced from the combustion of the raw and filtrated bio-oils, with the PSDs of PM_{10} having a bimodal distribution (i.e., a fine mode at ~0.03 μm and a coarse mode at ~1.6 μm). In addition, the combustion of the raw and filtrated bio-oils produces dominantly PM_{1-10}, which accounts for ~65-75 wt% of the total PM_{10}. This is consistent with that the concentrations of refractory elements (Mg, Ca, Al, Si, Fe) are considerably higher than those of the volatile elements (Na, K, Cl, S) in both the raw bio-oil and the filtrated bio-oil (in Figure 5-1a). These refractory elements contribute more effectively to PM_{1-10} emission than the volatile elements.[231] However, the PSDs of PM_{10} from the water-insoluble fraction combustion exhibit a fine mode but no obvious coarse mode.

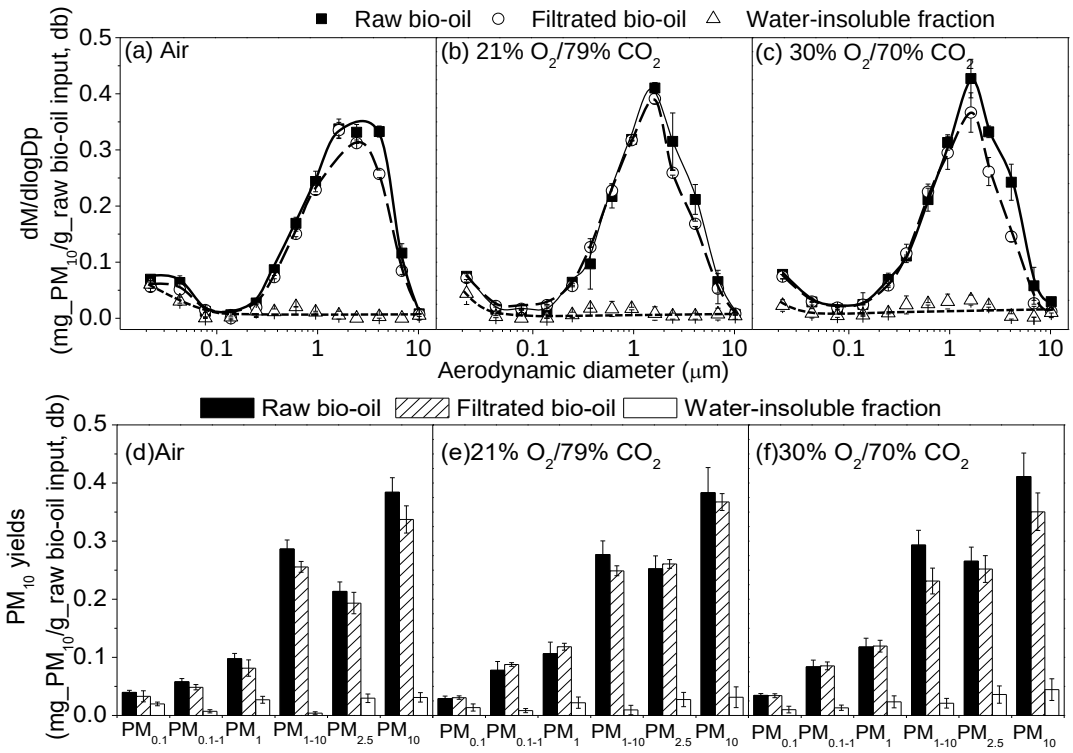

Figure 5-2 Mass-based PSDs (a-c) and yields (d-f) of PM_{10} produced from the combustion of the raw bio-oil, filtrated bio-oil and water-insoluble fraction in air, 21% O_2/79% CO_2, and 30% O_2/70% CO_2.

Figure 5-3 illustrates chemical compositions of $PM_{0.1}$, $PM_{0.1-1}$, and PM_{1-10}, reported as oxides of inorganic species (excepting Cl). It is important to note that the inorganic species are reported in the forms of oxides but it does not mean that the inorganic species are present in the PM as oxides. Clearly, the compositions of $PM_{0.1}$ are dominantly Na, K, Cl and S. Calculated in the form of oxides, S is the most dominant element in the $PM_{0.1}$ (~39-64 wt%), followed by K, Cl and Na, while Ca is the most dominant element in the $PM_{0.1-1}$ and PM_{1-10}, (~20-57 wt%), followed by Fe, Si, Mg, and Al. Therefore, the data clearly show that the $PM_{0.1}$ are mainly produced from the volatile elements including Na, K, Cl, and S, while the PM_{1-10} are produced mainly from refractory elements including Mg, Ca, Si, Al, and Fe. This observation is clearly supported by the elemental PSDs and yields of inorganic elements in PM_{10} from the combustion of the three bio-oils in air and the two oxy-fuel conditions, as

shown in Figures 5-4 and 5-5, respectively. The PSDs of Na+K and Cl+S (in form of SO_4^{2-}) in Figure 5-4 all follow a unimodal distribution that has a fine mode at ~0.022-0.043 μm, similar to the PSD data in Figure 5-1 a-c. Consequently, ~36-87 % of Na+K, ~54-82 % of Cl+S in PM_{10} are distributed in $PM_{0.1}$ (see Figure 5-5). This is understandable because Na, K, Cl and S are volatile and easily released to contribute to PM_1 emission.

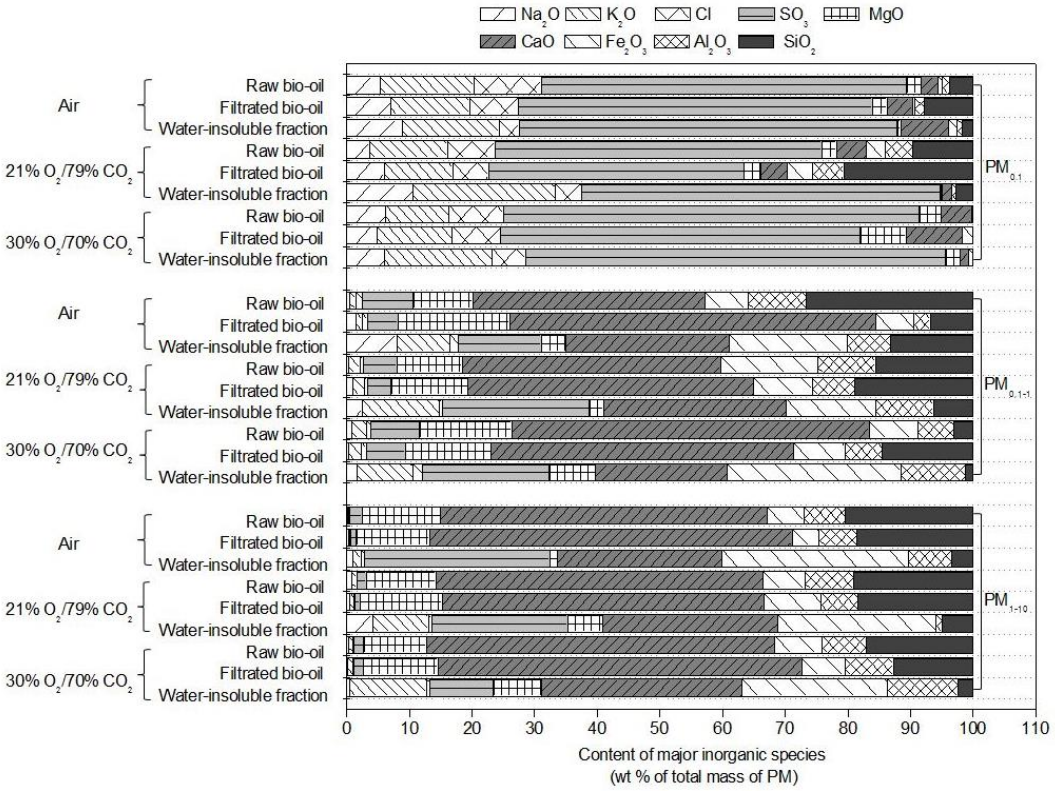

Figure 5-3 Compositions of $PM_{0.1}$, $PM_{0.1\text{-}1}$, $PM_{1\text{-}10}$ from the combustion of the raw bio-oil, the filtrated bio-oil and the water-insoluble fraction in air, 21% O_2/79% CO_2 and 30% O_2/70% CO_2, respectively. Data are reported as oxides.

In addition, the PSDs of Mg, Ca, Al+Si, Fe in Figure 5-4 also follow a unimodal distribution that has coarse mode diameters of ~1.6-6.8 μm. Consequently, $PM_{1\text{-}10}$ is dominantly contributed by Mg, Ca, Al+Si, and Fe, which account for the majorities (i.e. ~40-83, ~51-77, ~44-74, and ~33-80 wt%, respectively) of the corresponding PM_{10}. Figure 5-5 also shows that these refractory elements also contribute to $PM_{0.1\text{-}1}$, possibly because of the mechanisms including direct release of oxides of these

elements to form fume followed by subsequent agglomeration,[275] direct ejection of these elements into volatiles followed by subsequent oxidation and coagulation, and reduction of oxides to volatile sub-oxides in burning char particles followed by its release, subsequent oxidation, nucleation of formed oxides and possible further coagulation.[49]

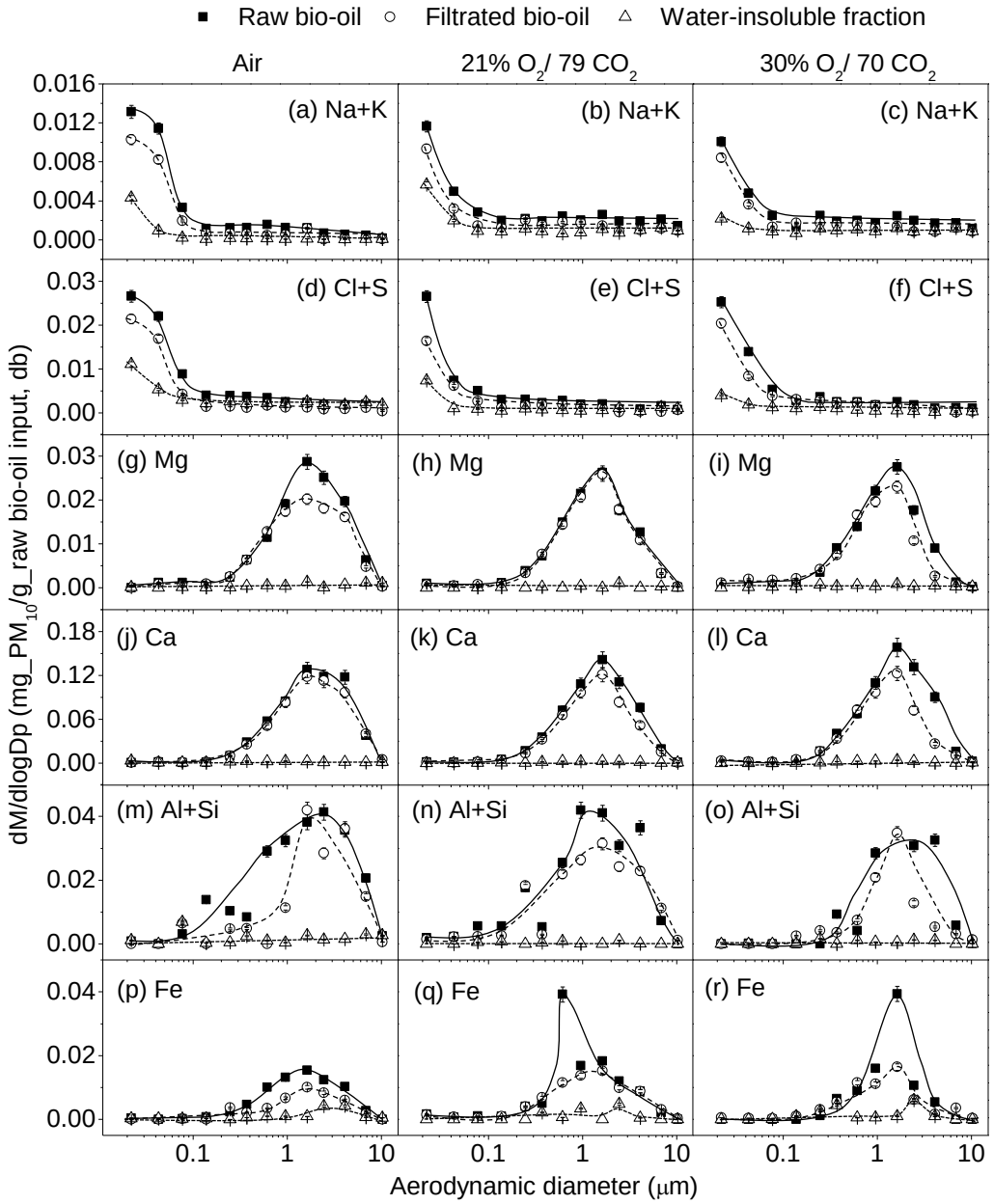

Figure 5-4 Elemental mass-based PSDs of PM_{10} collected from the combustion of the raw bio-oil, the filtrated bio-oil and the water-insoluble fraction in air, 21% O_2/79% CO_2 and 30% O_2/70% CO_2. Panels (a-c): Na+K; panels (d-f): Cl+S; panels (g-i): Mg; panels (j-l): Ca; panels (m-o): Al+Si; and panels (p-r): Fe.

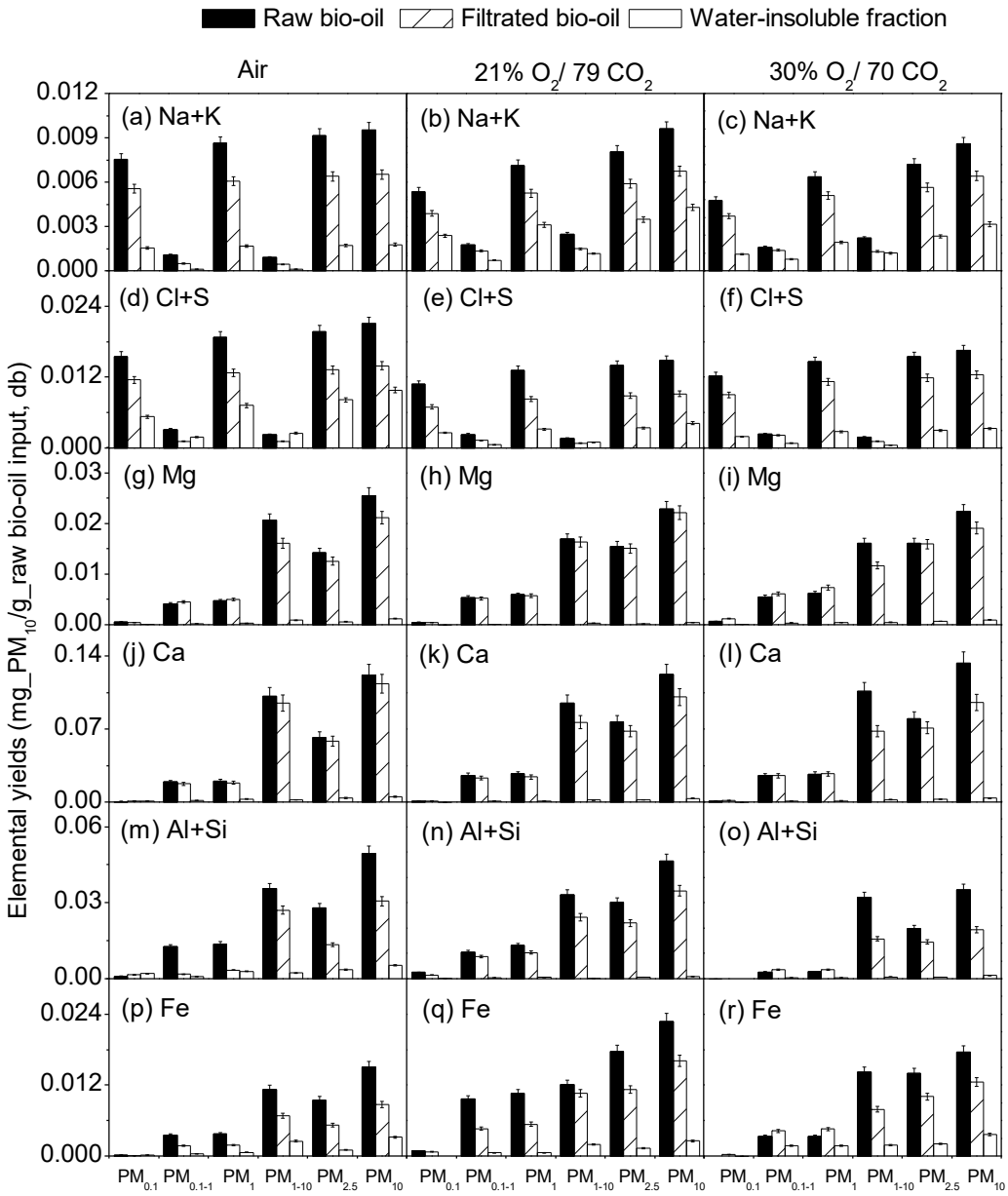

Figure 5-5 Elemental yields of PM_{10} collected from the combustion of the raw bio-oil, the filtrated bio-oil and the water-insoluble fraction in air, 21% O_2/79% CO_2 and 30% O_2/70% CO_2. Panels (a-c): Na+K; panels (d-f): Cl+S; panels (g-i): Mg; panels (j-l): Ca; panels (m-o): Al+Si; and panels (p-r): Fe.

5.3 Contributions of Inorganic Species from Different Fractions of Bio-oil to PM Formation

Figure 5-2 shows that the coarse modes in the PSDs of the PM_{10} collected from the combustion of the water-insoluble fraction are considerably lower than that from combustion of the raw and filtrated bio-oil. The yields of $PM_{0.1}$, $PM_{0.1\text{-}1}$, $PM_{2.5}$,

PM_{1-10} and PM_{10} from the combustion of the water-insoluble fraction are small. In addition, Figure 5-2 also shows that the combustion of the raw bio-oil and filtrated bio-oil leads to very similar PSDs and yields of PM_{10}, suggesting that the combustion of suspended fine char particles in the raw bio-oil also has an insignificant contribution to PM_{10} emission when the bio-oil is completely combusted. Therefore, the water-soluble fraction plays a key role in the emission of PM_{10} during the combustion of the raw bio-oil. This is consistent with the fact that the total inorganic species of the raw bio-oil is distributed dominantly (74.7%) in the water-soluble fraction but minorly in the water-insoluble fraction (10.4%) and suspended fine char particles (14.9%), as illustrated in Figure 5-1b.

Figure 5-2 shows that the coarse modes of PSDs curves from the combustion of the raw and filtrated bio-oils are similar but much higher than that of water-insoluble fraction. However, the fine modes of PM from water-insoluble fraction combustion are only slightly lower than those of the PM from the raw and filtrated bio-oil. These are reflected in the yields of PM_{10}, which show that the yields of $PM_{0.1-1}$ and PM_{1-10} from the combustion of the raw and filtrated bio-oils are similar but considerably higher than that of water-insoluble fraction by ~8-10 times. However, the yields of $PM_{0.1}$ show much less differences. Such observations in Figure 5-2 are reflected by the elemental PSDs and yields of these elements in PM_{10} presented in Figures 5-4 and 5-5. As shown in Figure 5-4, the coarse modes of Mg, Ca, Al, Si, and Fe from the combustion of raw and filtrated bio-oils are much higher than that from the combustion of the water-insoluble fraction. As a result, the yields of Mg, Ca, Al, Si, and Fe in PM_{1-10} from the combustion of the raw and filtrated bio-oils are considerably higher than that from the combustion of the water-insoluble fraction (see Figure 5-5). Therefore, the data suggest that the combustion of the water-insoluble fraction in the raw bio-oil has insignificant contributions to PM_{10} emission.

Furthermore, Figure 5-2 shows that the yield of PM_{10} from the combustion of the filtrated bio-oil is only slightly lower (by ~12 wt%) than that from the raw bio-oil. This is consistent with the fact that ~14.3% of the total inorganic species in the raw bio-oil is distributed in the suspended fine char particles. The elemental PSDs and yields of PM_{10} in Figures 5-4 and 5-5 show that the differences are mainly due to the contribution of the inorganic elements (especially the refractory elements) in the suspended fine char particles to the emission of $PM_{0.1\text{-}10}$. Nevertheless, the data also show that overall the combustion of fine char particles suspended in bio-oil makes a small contribution to PM_{10} emission.

In sum, it is the water-soluble fraction that plays a key role in the emission of PM_{10} during the combustion of the raw bio-oil. This is consistent with the fact that the total inorganic species of the raw bio-oil is distributed dominantly (74.7%) in the water-soluble fraction but marginally in the water-insoluble fraction (10.4%) and suspended fine char particles (14.9%), as seen in Figure 5-1b.

5.4 Difference in PM Emission during the Combustion of Bio-oils in Air and Oxyfuel Conditions

In Figure 5-2, the PSDs curves of PM_{10} from the combustion of both the raw bio-oil and the filtrated bio-oil in air and oxy-fuel conditions are similar. Similar observations can also be found in the elemental PSDs and yields presented in Figures 5-4 and 5-5, respectively. The data suggest that switching atmosphere from air to oxyfuel conditions leads to insignificant change on the PM emission during the combustion of the bio-oils. Such results appear to be very different to the substantial differences in PM_{10} emission during the combustion of solid fuels (e.g. coal and biomass as previously reported[55]) under air and oxyfuel conditions. For solid fuels (e.g. coal or biomass) combustion, it is widely accepted that the presence of CO_2 mainly leads to a lower O_2 diffusion rate in CO_2 than in air and a lower particle surface temperature hence less char fragmentation during combustion,[48] resulting in

significant differences in PM_{10} emissions.[280] However, the combustion of bio-oil is completely different to solid fuels combustion. Bio-oil contains little solid (i.e. merely 0.16% even in the raw bio-oil, as seen in Table 2-1) so that bio-oil combustion is dominated by gaseous-phase reactions. The contribution of solid combustion to bio-oil combustion is minimal. This explains that PM_{10} formation during bio-oil combustion is insensitive to atmosphere. There are insignificant differences in the PM_{10} emission from the combustion of bio-oils under air and oxyfuel conditions, as shown in Figures 5-2−5-4. The only exception is the emission of Fe which increases as the atmosphere being switched from air to oxyfuel conditions (see Figures 5-3 and 5-4), mainly in the form of $PM_{0.1\text{-}1}$. It is known that the high CO_2 concentration under oxyfuel conditions possibly interferes the reactions related to the formation of carbonates or oxides [281]. The data in Figures 5-3 and 5-4 suggest that the excessive CO_2 under oxyfuel conditions leads to more Fe being partitioned in $PM_{0.1\text{-}1}$.

5.5 Conclusions

The study focuses on PM_{10} emission during the combustion of the raw bio-oil, the filtrated bio-oil, as well as the mixture of the bio-oil water-insoluble fraction and ethanol in the DTF system at 1400 °C under air and oxyfuel conditions. It was found that the PSDs of PM_{10} from the combustion of bio-oil have a bimodal distribution (i.e. a fine mode at ~0.03μm and a coarse mode at ~1.6 μm). The water-insoluble fraction and the fine char particles in the raw bio-oil have insignificant contributions to PM_{10} emission during the combustion of the raw bio-oil. The results suggest that water-soluble fraction plays a key role in PM_{10} emission during the combustion of the raw bio-oil. As gaseous phase reactions play a dominant role during bio-oil combustion, switching combustion atmosphere from air to oxy-fuel conditions leads to insignificant differences in PM_{10} emission, expect that more Fe appears to be emitted as $PM_{0.1\text{-}1}$ as influenced by the excessive CO_2 under oxyfuel conditions.

Chapter 6 Mechanistic Investigation into Particulate Matter Formation during Air and Oxyfuel Combustion of Formulated Water-soluble Fractions of Bio-oil

6.1 Introduction

Biomass is regarded as one of the most important renewable energy sources in the future and its production is under development in many regions of the world.[5] However, biomass is typically widely dispersed and as a fuel is bulky, has high moisture content and low-energy-density.[32] For example, chipped green mallee biomass has a moisture content of 45% and a low volumetric energy density of ~5 GJ/m^3, which dictates long-distance transport of biomass is not feasible.[32] Therefore, efficient and economic utilisation of biomass requires the development of technologies for significant volumetric energy densification. Fast pyrolysis is such an attractive technology to convert biomass into high-energy-density bio-oil that can be cheaply transported for centralised stationary combustion applications,[20,32] while biochar can be either applied locally for soil amendment and carbon sequestration.[282]

Emission of particulate matter with aerodynamic diameter <10 μm (i.e. PM_{10}) is an important consideration for stationary combustion applications because it is difficult to capture these fine particles that have adverse impacts on human health.[41] In the open literature, most of previous studies concerned PM_{10} emission during solid fuels combustion.[52,283] For liquid fuels combustion in stationary applications, there were only scattered studies on PM_{10} emission during the combustion of residual fuel oil[72] and crude glycerol[75,284] and only one report on PM_{10} emission from the combustion of bio-oil.[285] PM_{10} emission during bio-oil combustion was dominantly contributed from its water-soluble fraction (WSF) because direct combustion of the water-insoluble fraction (WIF) of bio-oil has limited contribution to PM_{10} and there

is little difference in PM_{10} emission between the combustion of raw bio-oil and filtered bio-oil.[285] During the process of cold-water precipitation, bio-oil is separated into WIF and WSF. [36] In addition to inherent water in bio-oil, the WSF is also inevitably added with substantial extra water which is impossible to be removed. Therefore, investigation into PM_{10} emission during the direct combustion of WSF without the added water has not been possible. Therefore, the key objective of this study is to explore PM_{10} emission from the air and oxyfuel combustion of formulated bio-oil WSF samples (prepared based on the compositions of bio-oil WSF without additions of extra water) in a drop-tube furnace at 1400 °C.

6.2 PSDs and Yields of PM_{10} Emission from the Combustion/Pyrolysis of FWSFs

As discussion in Chapter 3, two samples of formulated water-soluble fraction of bio-oil were applied in the study of this chapter, i.e., calcium chloride solution (FWSF-1) and mixture of calcium chloride solution with typical chemical compositions of bio-oil (FWSF-2). Figure 6-1 presents the PSDs and yields of PM_{10} from the combustion of FWSF-1 and FWSF-2 with spray Sauter mean diameters (SMDs) of ~40 and ~60 μm under air or 30% O_2/70% CO_2 condition. It is noted that FWSFs are used for simulating bio-oil WSF (or its special case). Therefore, in this paper, the phrases "combustion" and/or "pyrolysis" are still used in describing the thermochemical processes of these FWSFs, even though there is no combustible in FWSF-1. Because FWSF-1 is free of organics and contains only water and $CaCl_2$, no combustion takes place hence separate experiments were also done for FWSF-1 under argon condition. It is interesting to see in Figure 6-1a that for both FWSFs, the PSD curves of PM_{10} collected under all conditions have unimodal distributions but with different mode diameters. For example, the mode diameters of PM_{10} from FWSF-1 with a spray SMD of ~40 μm under all conditions are ~1.6 μm while that of PM_{10} from FWSF-1 with spray SMD of ~60 μm in air is ~4.0 μm. For FWSF-2,

the mode diameter of PM_{10} is ~0.61 μm in air when it is spayed at a spray SMD of ~40 μm. As a result, as shown in Fig. 1b, the yields of PM_{10} from the combustion/pyrolysis of both FWSF-1 and FWSF-2 are dominantly distributed in $PM_{0.1\text{-}10}$, that accounts for ~98% of the total PM_{10} in all experiments. The elemental PSDs and yields of PM_{10} in Figure 6-2 further show that only Ca and Cl were found in PM_{10}.

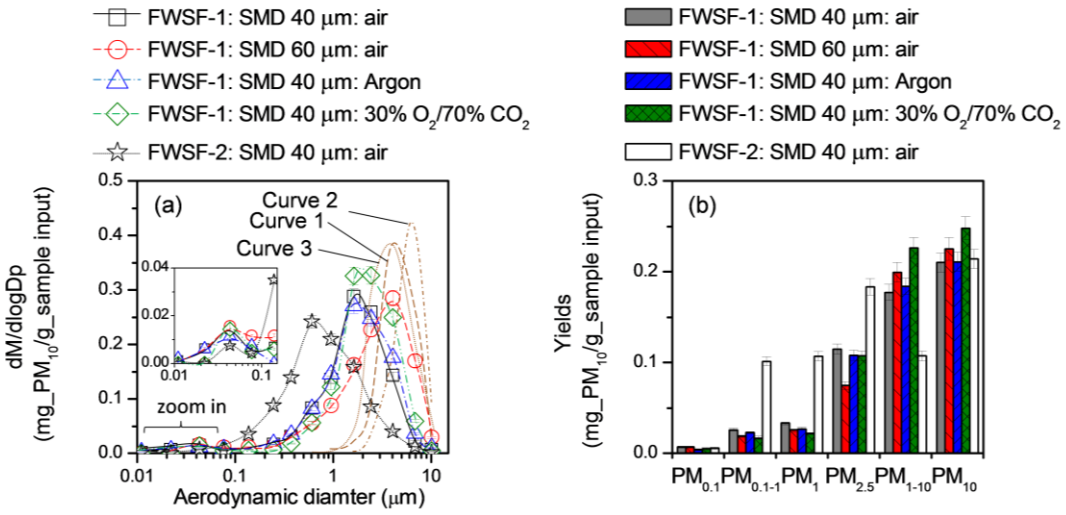

Figure 6-1 PSDs and yields of PM_{10} from the combustion/pyrolysis of FWSF-1 (formulated bio-oil water-soluble fraction of calcium chloride solution) in air, argon and 30% O_2/70% CO_2 with spray SMDs of ~40 and ~60 μm and FWSF-2 (formulated bio-oil water-soluble fraction of organics—calcium-chloride-solution mixture) in air with spray SMD of ~40 μm; Curves "1", "2" and "3" are the modelled PSD curves of PM_{10} from the combustion of FWSF-1 with SMD of ~40 and ~60 μm and FWSF-2 with SMD of ~40 μm in air, respectively, based on the assumption that one spray droplet produces one PM particle.

At least four important observations can be made from the results presented in Figures 6-1 and 6-2. First, the PSDs and yields of total PM_{10} and Ca in PM_{10} from the combustion of FWSFs are consistent with the previous report on PM_{10} emission from bio-oil combustion[285] that Ca would mainly contribute to $PM_{0.1\text{-}10}$. In addition, it is interesting to see that in absence of organic matter, the Ca in FWSF-1 would also contribute to $PM_{1\text{-}10}$ during combustion. It should be noted that the transformation mechanisms of catalysed sintering reactions and coagulation/formation of aluminosilicate species during bio-oil combustio[285] is not

applicable to the case of FWSF-1 in this study because no combustion of organics takes place. In this case, an FWSF-1 solution droplet experiences evaporation followed by crystallization and fusion to form PM.

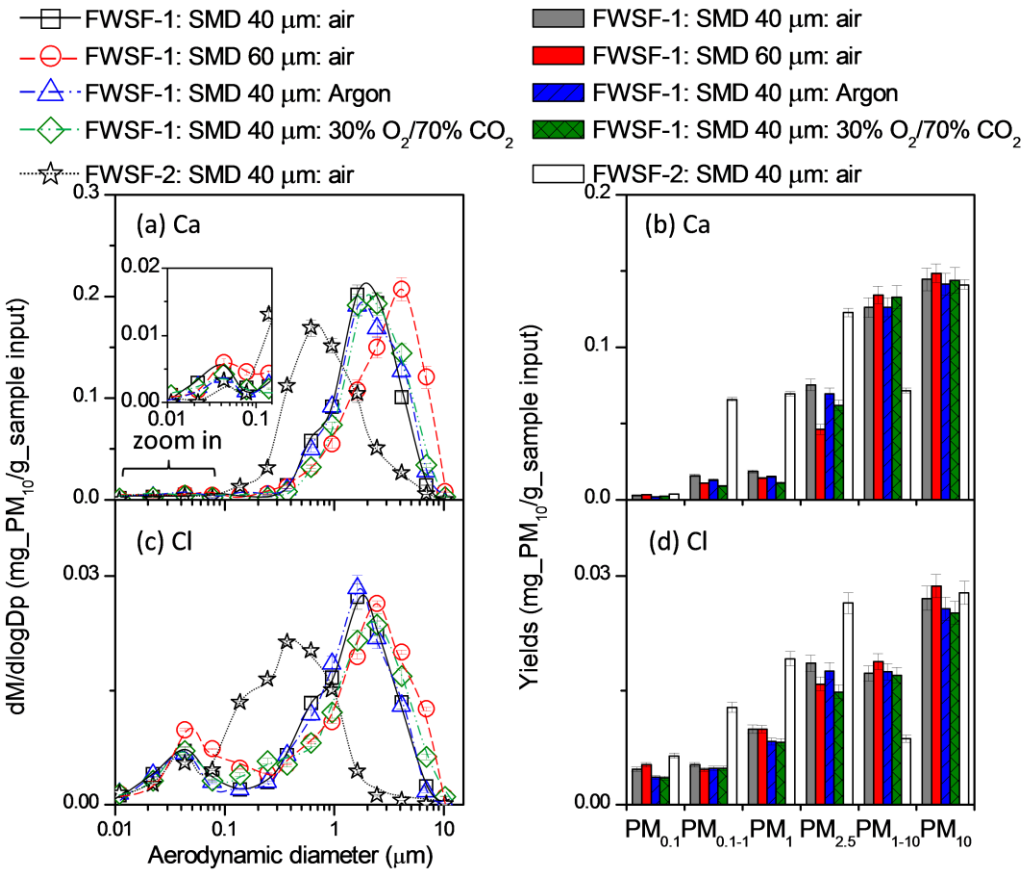

Figure 6-2 Elemental PSDs and yields of PM_{10} from the combustion/pyrolysis of FWSF-1 (formulated bio-oil water-soluble fraction of calcium chloride solution) in air, argon, and 30% O_2/70% CO_2 with spray SMDs of ~40 and ~60 μm and FWSF-2 (formulated bio-oil water-soluble fraction of organics—calcium-chloride-solution mixture) in air with spray SMD of ~40 μm, respectively.

Second, in the range of 0.01-0.1 μm (see the zoom-in insert figures in Figures 6-1a and 6-2a), a small fine mode at ~0.043 μm is actually present in each of the PSD curve of PM_{10}. Though the fine mode in $PM_{0.1}$ accounts only for ~2% of the total PM_{10}, its formation cannot be explained by the well-known gas-phase reaction mechanism since Ca is refractory and the combustion temperature (1400 ℃) is considerable lower than the boiling points of possible Ca compounds. A plausible explanation is that the spray of the FWSFs forms mist of fine droplets which

experience evaporation, crystallization and further nucleation/condensation to form fine Ca-containing particles and distributed in $PM_{0.1}$.

Third, Figure 6-1a shows that as the spray SMD increases from ~40 to ~60 μm, the mode diameter for the PSD curve of PM_{10} from FWSF-1 combustion shifts to a larger size (from ~1.6 to ~4.0 μm). This is not surprising because the mode position of the DSD curve for the FWSF-1 spray with an SMD of ~60 μm is considerably larger than that of ~40 μm, as shown in Figure 6-3. Spray with larger droplet sizes produces PM_{10} of larger sizes during combustion because a larger droplet conserves more inorganic species and thus produces a larger PM particle. This in turn support the formation of PM during FWSF-1 combustion is via droplet evaporation followed by crystallization and fusion.

Fourth, Figure 6-1a shows that the mode diameter for the PSD curve of PM_{10} from the combustion of the FWSF-2 (~0.61 μm) is considerably smaller than that of FWSF-1 (~1.6 μm) when the sprays have the same SMD of ~40 μm. This is also reflected in the PM yields presented in Figure 6-1b which shows PM_{1-10} contributes only ~50% of the total PM_{10} from FWSF-2 but ~83% of the total PM_{10} from FWSF-1. Figure 6-3 further shows that the mode positions of droplet size distribution curves for the FWSF-1 and FWSF-2 sprays with same SMD are very close. The results clearly indicate that when organic matter is present in the FWSF, the sizes of PM_{10} are considerably reduced. Therefore, there must be considerably more extensive breakup of droplets takes place during the combustion of FWSF-2 than that of FWSF-1. Such phenomenon is referred to as microexplosion, which is known to take place during the combustion of liquid hydrocarbon fuels.[286] Microexplosion becomes extensive when the fuel droplets contain multi-components of different boiling points because the components with relatively lower boiling points would build up vapours within the droplet, leading to droplet expansion thus fragmentation.[286] This is exactly the case for FWSF-2.

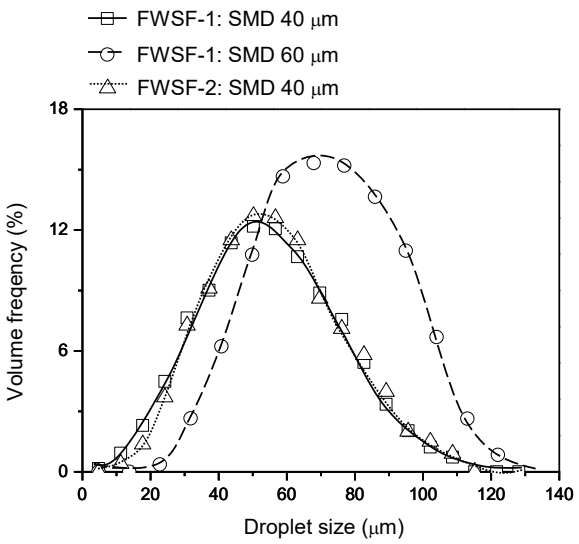

Figure 6-3 Spray droplet size distributions (by volume) of FWSF-1 (formulated bio-oil water-soluble fraction of calcium chloride solution) with SMDs of ~40 and ~60 μm and FWSF-2 formulated bio-oil water-soluble fraction of organics—calcium-chloride-solution mixture) with SMD of ~40 μm, respectively.

6.3 Chemical Reactions Responsible for PM_{10} Formation during the Combustion of FWSFs

Panels a and b of Figure 6-1 show that the $PM_{0.1\text{-}10}$ from FWSF-1 under air and argon conditions are very similar, which is not surprising because FWSF-1 contains no organics and no combustion takes place. However, the $PM_{0.1\text{-}10}$ under air (or argon) condition is lower than that under 30% O_2/70% CO_2 condition, indicating that there are different mechanisms responsible for $PM_{0.1\text{-}10}$ formation. As shown in panels a and b of Figure 6-2, the Ca in $PM_{0.1\text{-}10}$ from FWSF-1 under the three conditions is actually almost the same. Therefore, the Ca in $PM_{0.1\text{-}10}$ from air (or argon) and oxyfuel is in different chemical forms. The results in the panels c and d of Figure 6-2 further show that Cl is also present in $PM_{0.1\text{-}10}$, demonstrating the presence of $CaCl_2$ in $PM_{0.1\text{-}10}$. Further calculation shows that $CaCl_2$ only accounts for ~17% of the total $PM_{0.1\text{-}10}$, indicating that the majority of Ca in $PM_{0.1\text{-}10}$ is actually in chemical forms other than $CaCl_2$. Considering the presence of steam generated from water in FWSFs, those forms of Ca should be CaO or $Ca(OH)_2$ (under air or argon condition). The formation of CaO and $Ca(OH)_2$ could be

explained by hydrolysis reactions between $CaCl_2$ and H_2O (reported previously [287]) as listed below:

$$CaCl_2(l) + H_2O \leftrightharpoons CaO + 2HCl(g) \quad 6\text{-}1$$

$$CaCl_2(l) + 2H_2O \leftrightharpoons Ca(OH)_2 + 2HCl(g) \quad 6\text{-}2$$

It was demonstrated [287] that fused $CaCl_2$ could react with steam H_2O to form CaO at ~840 °C. $Ca(OH)_2$ could also be formed under such reaction conditions when the water content in the flue gas is higher than 24 % because $Ca(OH)_2$ could be stable in the fused $CaCl_2$ due to its lower activity coefficient in the melt form when it is equilibrated with the ambient water vapour [287]. However, in this study, the temperature is 1400 °C and the water content in the feed gas is only ~8% so that the formation of $Ca(OH)_2$ is less likely. This is further confirmed by the calculation based on the assumption that apart from Ca and Cl, the rest of $PM_{0.1\text{-}10}$ is O, showing that the molar ratio of Ca (in form of other than $CaCl_2$) to O is close to ~1.0, clearly indicating those Ca being in the form of CaO in $PM_{0.1\text{-}10}$.

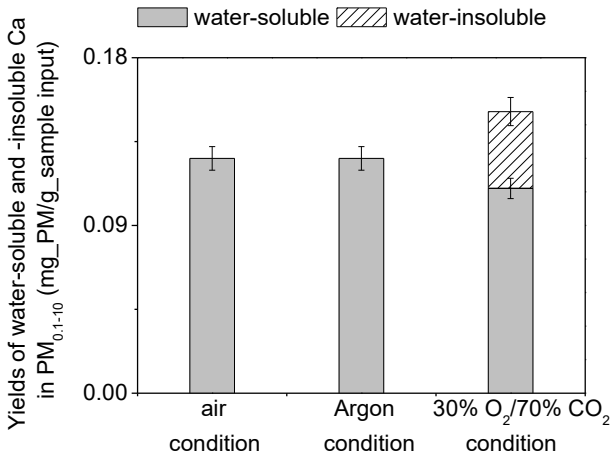

Figure 6-4 Yields of water-soluble and -insoluble Ca in $PM_{0.1\text{-}10}$ from the combustion/pyrolysis of FWSF-1 (formulated bio-oil water-soluble fraction of calcium chloride solution) under air, argon, and 30% O_2/70% CO_2 atmosphere conditions with spray SMD of ~40 µm, respectively.

However, under oxyfuel condition, CaO can be partially transformed into $CaCO_3$ in the presence of high concentration of CO_2 as the flue gas cools. The formation of $CaCO_3$ in $PM_{0.1\text{-}10}$ under 30% O_2/70% CO_2 condition is supported by the fact that all

Ca in $PM_{0.1\text{-}10}$ from air (or argon) condition is water soluble, ~27% of Ca in $PM_{0.1\text{-}10}$ from 30% O_2/70% CO_2 is water insoluble (see Figure 6-4). It is noted that given the large quantity of deionised water used, $Ca(OH)_2$ formed from CaO with water can all be dissolved in water in this study. Calculation based on the assumption that apart from Ca, Cl, and O, the rest of $PM_{0.1\text{-}10}$ is all CO_3, the molar ratio of Ca (which is not in forms of $CaCl_2$ and CaO) to CO_3 is close to ~1.0. This clearly indicates the presence of $CaCO_3$ in $PM_{0.1\text{-}10}$ under 30% O_2/70% CO_2. This in turn explains the difference in the yields of $PM_{0.1\text{-}10}$ between 30% O_2/70% CO_2 and air (or argon) conditions.

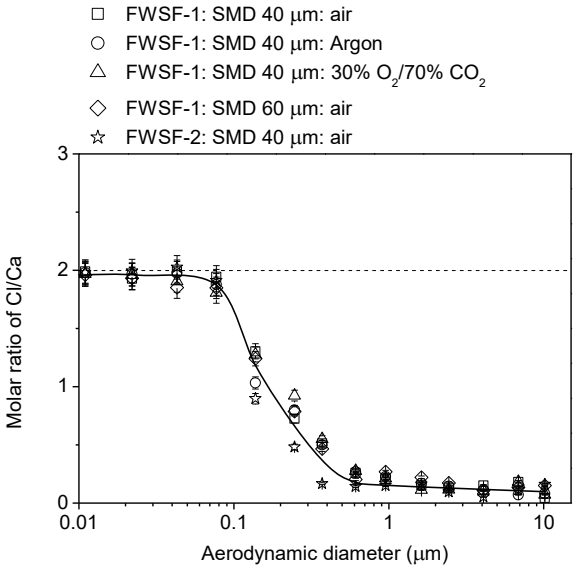

Figure 6-5 Molar ratios of Cl/Ca in the net PM_{10} from the combustion/pyrolysis of FWSF-1 (formulated bio-oil water-soluble fraction of calcium chloride solution) in air, argon, and 30% O_2/70% CO_2 with spray SMDs of ~40 and ~60 μm and FWSF-2 (formulated bio-oil water-soluble fraction of organics—calcium-chloride-solution mixture) in air with spray SMD of ~40 μm, respectively.

Further efforts were taken to estimate the molar ratios of Cl/Ca in PM_{10} based on the chemical analysis of PM samples collected in different stages of DLPI for all experiments. The results presented in Figure 6-5 show that the molar ratio of Cl/Ca is ~2.0 for $PM_{0.1}$, and decreases from ~2.0 to ~0.2 for $PM_{0.1\text{-}1}$ with increasing PM size then remains ~0.2 for $PM_{1\text{-}10}$. There are two possible pathways responsible for

the presence of $CaCl_2$ in PM_{10}, i.e. (1) unreacted $CaCl_2$ in larger PM particles due to insufficient hydrolysis reaction; and (2) re-chlorination of CaO under air/argon condition (or $CaCO_3$ under oxyfuel condition) by HCl. Thus, Figure 6-5 indicates the different extents of chlorination of PM particles with different sizes. For $PM_{0.1}$, the Cl/Ca molar ratio is close to ~2.0, indicating the complete chlorination occurred in $PM_{0.1}$. The bimodal distribution of PSD curves of Cl in PM_{10} in Fig. 2c could be explained by these two pathways that responsible for the existence of $CaCl_2$ in PM_1 and $PM_{1\text{-}10}$.

6.4 Modelling of the PSDs for PM_{10} during the Combustion of FWSFs

Further efforts were taken to predict the PSDs of PM_{10} during the combustion of FWSFs. The prediction is based on the assumption of one droplet forming one PM particle during combustion so that the PSDs of PM_{10} can be derived from the DSDs of FWSF spray. Briefly, as the FWSFs are solutions, it is plausible to consider the $CaCl_2$ being uniformly distributed in the droplets. Therefore, based the one droplet to one PM particle assumption, the diameter of the PM particle formed during combustion could be estimated via mass conservation of the inorganic species before and after the droplet evaporation according to Eq.6-3:

$$\rho_{PM} \cdot V_{PM} = \rho_{droplet} \cdot V_{droplet} \cdot C \qquad 6\text{-}1$$

where ρ_{PM} is the density of the PM particle (3.35 g/cm^3, density of CaO); $\rho_{droplet}$ is the density of the solution (1 and 1.08 g/mL for FWSF-1 and FWSF-2, respectively); V_{PM} and $V_{droplet}$ are the volumes of the PM particle and the droplet, respectively; C is the concentrations of the inorganic specie in the solution (0.02 wt% for Ca). With rearrangement, Eq. 6-3 can be further simplified as:

$$d_{PM} = d_{droplet} \cdot \sqrt[3]{\frac{\rho_{droplet} \cdot C}{\rho_{PM}}} \quad 6\text{-}2$$

where, $d_{droplet}$ is the droplet diameter. In this study, the limit of the calculated d_{PM} is $0.1\ \mu m$ constrained by the measurement resolution. It should also be noted that based on the aforementioned discussion, CaO is considered as the only inorganic species in PM, and the real diameter of the PM particle is converted to the equivalent aerodynamic diameter[39] for comparisons with experimental data on the PSDs of PM_{10}.

The predicted PSD curves of PM_{10} from the combustion of FWSF-1 with spray SMD of ~40 and ~60 μm and FWSF-2 with spray SMD of ~40 μm in air are plotted in Figure 6-1a. It can be seen that there are significant differences between experimental and predicted PSD curves. For the combustion of FWSF-1 with spray SMDs of ~40 and ~60 μm, the coarse mode positions (at ~4.0 and ~6.8 μm) of the PM_{10} PSD curves based on model predictions are larger than those (~1.6 and ~4.0 μm) based on experimental results, respectively. The results indicate that even for the organics-free FWSF-1, the droplets must experience breakup after spray into the furnace. Such breakup can be attributed to the high temperature ambient in the furnace that can suddenly increase gas velocity and its relative velocity against the liquid sheet of the droplets, resulting in droplet breakup.[288,289] Similar observation can also be found between the experimental and estimated PM_{10} from the combustion of FWSF-2 with spray SMD of ~40 μm, with the mode position being ~0.61 μm based on experimental result and ~4.0 μm based on model prediction. In this case, in addition to the same mechanism applied to FWSF-1 due to higher relative velocity between gas and droplets at high temperature, microexplosion of FWSF-2 is another key mechanism for droplet breakup, as discussed in Section 6.2.

6.5 Conclusion

This study reports a systemic study on PM_{10} emission from the combustion of FWSFs via a DTF system at 1400 °C in air and 30% O_2/70% CO_2 conditions. FWSF-1 was prepared via dissolving calcium chloride into deionized water and FWSF-2 was a mixture of the calcium chloride solution with a list of organic chemicals based on the composition of bio-oil WSF. The results show that the combustion of FWSFs produces mainly $PM_{0.1-10}$ emission (~98% of the total PM_{10}), similar to bio-oil combustion. Since there are no combustibles in FWSF-1, the PM_{10} was produced through mechanism of droplet evaporation followed by crystallization, fusion, and hydrolysis to form CaO fine particles in air (or argon) or partially $CaCO_3$ in 30% O_2/70% CO_2. The organics present in the FWSF-2 play an important role in PM_{10} formation as FWSF-2 combustion produces PM_{10} with PSD shifting to considerably smaller sizes, indicating extensive break up of droplets takes place. Combustion of sprays with larger droplet sizes produces PM_{10} with increased sizes. The results also show that upon cooling CaO produced during combustion in air can react with HCl (g) to form $CaCl_2$ in $PM_{0.1}$. On the assumption that one droplet produces one PM particle, the predicted PSDs of PM_{10} are much bigger than the experimentally-measured PSDs of PM_{10} from the combustion of FWSFs. This confirms that spray droplets experience breakup, which is extensive in the case of FWSF-2 due to the presence of organics in the fuel.

Chapter 7 Bioslurry for Stationary Applications: Particulate Matter Emission during Combustion under Air and Oxyfuel Conditions

7.1 Introduction

Bioslurry is a mixture of biochar and bio-oil from biomass pyrolysis and has the advantages of considerably higher energy density enabling transportation, in comparison with biomass.[32,137] Bioslurry produced from mallee biomass pyrolysis in Western Australia is proved to be economically feasible, of low life-cycle energy and carbon footprints.[31] It also meets essential requirements of slurry fuels for stationary combustion and gasification applications.[30]

Emission of particulate matter (PM), especially for PM_{10} (i.e. PM with aerodynamic diameter less than 10 μm), is an important consideration[45] in stationary power stations because of the difficulties in capturing these fine particulates and the adverse impacts to atmosphere and human health.[41,59,290] Combustion of solid fuels e.g. coal and biomass share similar ash-transformation mechanisms under conventional air combustion conditions.[41,55,202,291] Recent studies[54,55,285] extended such knowledge to fuel combustion under oxyfuel conditions[78,292-294] that facilitate carbon capture. While PM emission was investigated from the combustion of renewable solid fuels such as biomass and biochar,[61,66,67] there is no study on PM emission from bioslurry combustion under either air or step-change oxyfuel combustion conditions.

Therefore, the objective of this study is to investigate PM_{10} emission from bioslurry combustion in a lab-scaled drop-tube furnace at 1400 °C under air or oxyfuel conditions. Bioslurry samples with two biochar loading levels (5 and 10 wt%) were considered. The properties of the bio-oil, biochar, and the two bioslurry were given in Table 7-1. The PM_{10} emission intensity during bioslurry combustion is also

benchmarked against those from other solid fuels under similar combustion conditions.

Table 7-1 Properties of bio-oil, biochar, 5% bioslurry, 10% bioslurry

Samples	Bio-oil	Biochar	5 % Bioslurry	10 % Bioslurry
Proximate Analysis				
Water content (wt%, ar[a])	24.3	3.0	23.7	21.1
Ash (wt%, ar[a])	0.0	2.7	0.2	0.3
Volatile matter (wt%, ar[a])	74.1	17.0	63.6	55.2
Fixed carbon (wt%, ar[a])	1.6	77.3	12.5	23.4
Elemental Analysis (wt%)				
C[a, d]	41.54	89.28	43.47	45.50
H[a, d]	7.48	3.43	6.41	6.50
N[a, d]	0.11	0.13	0.10	0.12
O[e]	50.87	7.16	50.02	47.88
Viscosity (20 ^{o}C, mPa s)	102.3	na[b]	122.2	152.1
LHV[f] (MJ/kg)	17.7	29.1	17.6	18.3

[a] As-received basis for bio-oil and bioslurry. [b] Not applicable. [c] Dry basis. [d] Dry and ash-free basis for biochar. [e] By difference. [f] Lower heating value based on calculation.

7.2 Characterisation of PM_{10} from Bioslurry Combustion

Figure 7-1 further presents the contributions of major elements (Na, K, Cl, S, Mg, Ca, Al, Si and Fe) from the parent fuels (bio-oil and biochar) to those in the bioslurry fuels. It can be seen that Cl, Al, and Fe in bioslurry are mainly from bio-oil while Na, K, S, Mg, Ca, and Si are mainly from biochar. The loading of biochar into bio-oil significantly increases the concentrations of K, S, Mg, Ca and Si in bioslurry and K, Ca and Si are the major inorganic elements in bioslurry.

Figure 7-2 presents the particle size distributions (PSDs) and yields of PM_{10} emission from bio-oil and bioslurry combustion under both the air and two oxyfuel conditions. The PSDs of PM_{10} all follow bimodal distributions, with a fine mode at ~0.022 μm, and a coarse mode at ~2.4 μm. The shapes of PSD curves from bioslurry combustion are similar with that from bio-oil (i.e. bioslurry with zero biochar loading level) combustion, except for the shift of coarse mode position to the right side compared to that of bio-oil (~1.6 μm) indicating the enhanced formation of PM_{1-10} from bioslurry

combustion. On the basis of yield, PM_{1-10} contributes to the majority (~70%) of the total PM_{10} from bioslurry combustion. Furthermore, $PM_{2.5}$ accounts for about half of the total PM_{10} while PM_1 is dominantly $PM_{0.1}$ that contributes to ~50 wt% of the total PM_1.

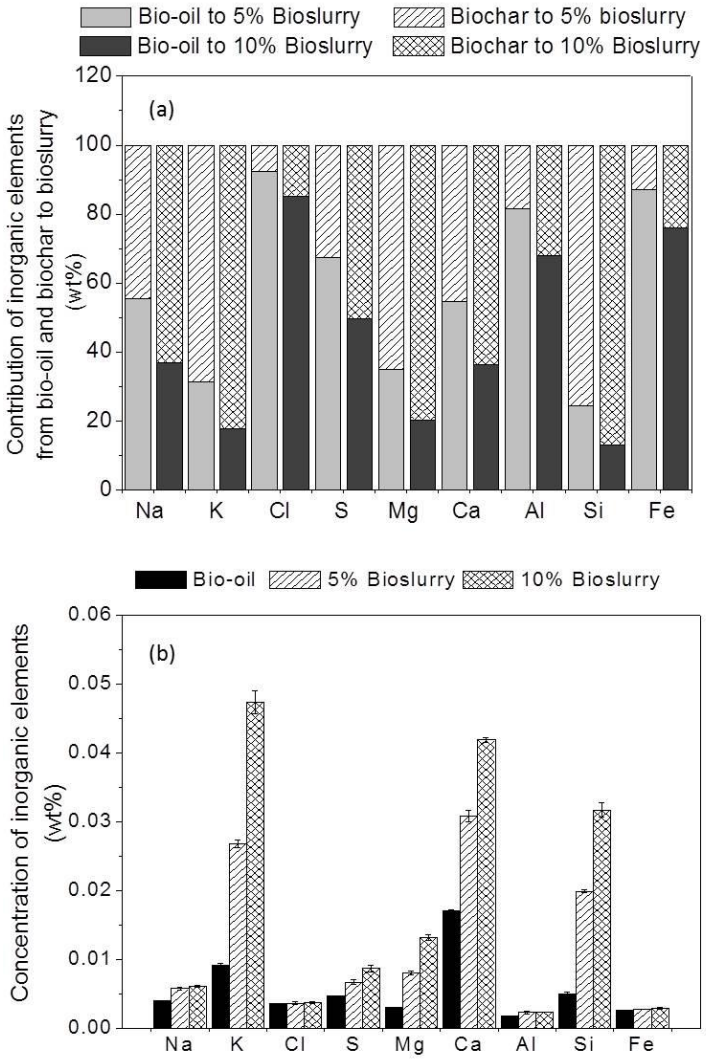

Figure 7-1 (a) Contributions of major inorganic elements (Na, K, Cl, S, Mg, Ca, Al, Si and Fe) from bio-oil and biochar to bioslurry; (b) Concentration of inorganic elements in bio-oil, 5% bioslurry and 10% bioslurry, respectively.

Figures 7-3 and 7-4 further present the elemental PSDs and yields of inorganic elements in PM_{10}. The PSD curves of almost all the elements follow a unimodal distribution. For volatile elements including Na, K, Cl, and S, the PSD have a fine mode at ~0.022 μm while for refractory elements including Mg, Ca, Al, Si, and Fe,

the PSDs have a coarse mode at ~2.4 μm. For the volatile elements, each is mainly emitted in PM_1, especially $PM_{0.1}$ that accounts for ~74-84 wt% of the total amount of the respective element in PM_1. For the refractory elements, each is dominantly presented in PM_{1-10} that accounts for ~74-87 wt% of the total amount of the respective element in PM_{10}. It is well known that the formation of $PM_{0.1}$ from volatile elements is due to gaseous-phase reactions, vaporization, homogeneous nucleation and/or heterogeneous condensation,[64,279] while the formation of PM_{1-10} from refractory elements is due to catalysed sintering reactions and coagulation and formation of aluminosilicates species.[50,178] The refractory elements only contribute ~10-22 wt% of the total amount of respective elements in PM_1, however, they account for ~40-60 wt% of the total amount of respective elements in $PM_{2.5}$, suggesting that these elements are of significant importance to the formation of $PM_{1-2.5}$ (i.e. PM with aerodynamic diameter between 1 μm to 2.5 μm). The possible mechanisms responsible for the occurrences of these refractory elements in $PM_{1-2.5}$ include agglomeration or coagulation of the oxide particles, or re-oxidation of the reduced species in burning char particles followed by nucleation and further coagulation.[197,202,275] It is also noted that the chemical characteristics and the shapes of the PSD curves of PM_{10} from bioslurry combustion are similar with those observed for combustion of bio-oil, biochar and biomass,[66,67,285] suggesting similar PM_{10} formation mechanisms. The shift of coarse mode for refractory elements in PM_{1-10} to the right side from the combustion of bioslurry compared to that of bio-oil could also be found similar to the obviation for total PM_{10} in Figure 7-2, which could be explained by the enhanced coalescence of refractory ash species due to the participation of biochar during combustion.

7.3 Effect of Biochar Loading Level on PM_{10} Emission from Bioslurry Combustion

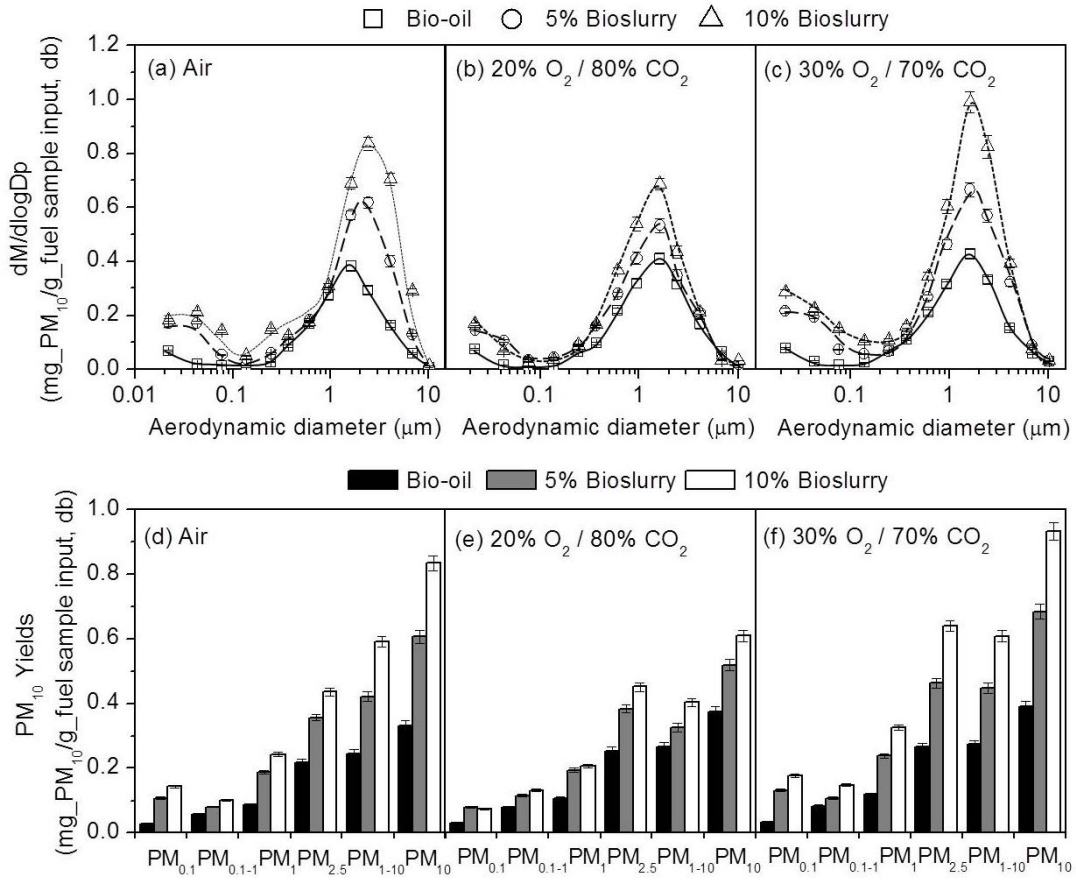

Figure 7-2 Particle size distributions (PSDs) and yields of PM_{10} from combustion of bio-oi, 5% bioslurry and 10% bioslurry under air, 20% O_2/ 80% CO_2 and 30% O_2/ 70% CO_2, respectively.

Loading of biochar into bio-oil for the production of bioslurry fuels increases the concentrations of the inorganic species in the fuels from ~0.05 wt% in bio-oil (with zero biochar loading), to ~0.105 wt% in 5% bioslurry and ~0.154 wt% in 10% bioslurry (see Figure 7-1b). The main inorganic elements include K, Ca and Si which are abundant in biochar. Therefore, an increase in biochar loading level leads to an increase in PM emission during bioslurry combustion. This is evident in Figure 7-2 (see panels a – c) which shows the heights of the peaks for both the fine mode (~0.04 μm) and the coarse mode (~2.4 μm) of PM_{10} during combustion being in the order of 10% bioslurry > 5% bioslurry > bio-oil. Consequently, the yields of PM_1 from the combustion of 5% bioslurry and 10% bioslurry under air increase to ~0.18 and ~0.24 (mg/g, i.e. mass of PM produced from per gram of fuel sample input, hereafter the same), respectively, from ~0.08 mg/g from the combustion of bio-oil while the yields

of PM_{1-10} increase to ~0.42 and ~0.59 mg/g from the combustion of 5% bioslurry and 10% bioslurry, respectively, from ~0.24 mg/g from the combustion of bio-oil.

The conclusion is further confirmed by the elemental PSDs and yields of PM in Figures 7-3 and 7-4. It is clearly shown that an increase in the biochar loading level in bioslurry leads to increases in the peak heights of both the fine and coarse models in the elemental PSDs modes and yields of all the elements in PM_{10}. Such increases are substantial for the groups of "Na+K", Mg, Ca and "Al+Si" because biochar contributes significantly to these elements in bioslurry (see data in Figure 7-1). Furthermore, Figure 7-2 also shows that the obvious increases in the yields of PM_1 from the combustion of bioslurry in comparison to that from the combustion of bio-oil cannot be simply explained by the direct contribution of biochar combustion to PM_1 emission. For example, the PM_1 only accounts for less than 10% of the total PM_{10} during biochar combustion,[67] but as shown in Figure 7-2 the additions of biochar into bioslurry fuels lead to considerably increases in the emission of PM_1, accounting for ~35% and ~30% of PM10 during the combustion of 5% bioslurry and 10% bioslurry, respectively. In Figures 7-3 and 7-4, it is clear that for the groups of "Na+K", the combustion of bioslurry produces significantly more "Na+K" in PM_1 (~0.031 and ~0.036 mg/g for 5% bioslurry and 10% bioslurry under air compared with ~0.008 mg/g for bio-oil under air). While the exact mechanisms are unknown, there are two mechanisms that may be responsible for such observations. One is that during bioslurry preparation and storage some volatile inorganic species in biochar can be leached into the liquid phase via the acidic bio-oil in bioslurry.[99] The other is that there may be potential interactions between the volatiles from bio-oil and biochar during bioslurry combustion (such volatile-char interactions are known to enhance PM_1 during combustion[69]).

7.4 Effect of Oxyfuel Combustion Conditions on PM_{10} Emission from Bioslurry Combustion

It was recently reported that during the complete combustion of bio-oil, PM emission is insensitive to combustion atmosphere (air or oxyfuel conditions) because bio-oil combustion is dominantly in the gaseous phase.[285] Such conclusions are consistent with the data on the PSDs and yields of PM_{10} from bio-oil combustion presented in Figure 7-2 under the three conditions (i.e. air, 20% O_2/ 80% CO_2 and 30% O_2 /70% CO_2). However, bioslurry is a two-phase fuel and has different behaviour in comparison to bio-oil during combustion. Figure 7-2 shows that the PM_{10} yields during the combustion of 5% bioslurry and 10% bioslurry in air are ~0.61 and ~0.83 mg/g, respectively. For these two bioslurry fuels, changing from air to 20% O_2/ 80% CO_2 condition leads to a decrease in the yields of PM_{10} to ~0.52 and ~0.61 mg/g, respectively. Such decreases are contributed by the reductions in both PM_1 (from ~0.19 and ~0.24 mg/g under air to ~0.18 and ~0.21 mg/g 20% O_2/ 80% CO_2 condition) and PM_{1-10} (from ~0.42 and ~0.59 mg/g under air to ~0.26 and ~0.32 mg/g 20% O_2/ 80% CO_2 condition) for 5% bioslurry and 10% bioslurry, respectively. However, changing from air to 30% O_2/ 70% CO_2 condition leads to increases in the difference in the yields of PM_{10} from ~0.61 and ~0.83 mg/g in air to ~0.68 and ~0.93 mg/g, respectively for both 5% bioslurry and 10% bioslurry during combustion. Such increases are mainly contributed by the increases in PM_1 (from ~0.19 and ~0.24 mg/g under air to ~0.24 and ~0.32 mg/g under 30% O_2/ 70% CO_2 condition) but the differences in the yields of PM_{1-10} are small (~0.42 and ~0.59 mg/g under air vs ~0.44 and ~0.61 under 30% O_2/ 70% CO_2 condition) for 5% bioslurry and 10% bioslurry, respectively.

The decreases in PM_1 and PM_{1-10} when switching from air conditions to 20% O_2/ 80% CO_2 condition can be attributed to the decrease in burning char particle temperature during combustion. Combustion of solid fuel particles are known to have lower char particle temperatures under 20% O_2/ 80% CO_2 conditions than that under air conditions.[293-296] A simplified single-particle model[54] was then used for estimating the temperatures of burning char particles under air and oxyfuel conditions in this

study. Two assumptions were made in the calculation, i.e. char oxidation producing only CO (i.e. CO being oxidised in the bulk gas phase) and the temperature gradient within char particle and reaction at boundary layer being negligible. The model predictions show that the temperatures of burning char particles are ~1420 and 1690 °C under 20% O_2/ 80% CO_2 condition and air conditions, respectively. It is well known that during combustion under 20% O_2/ 80% CO_2 condition, the lower O_2 diffusion rate in CO_2 and the higher heat capacity of CO_2[297] result in decreased flame temperature of burning char particles. A reduction in char burning temperature would

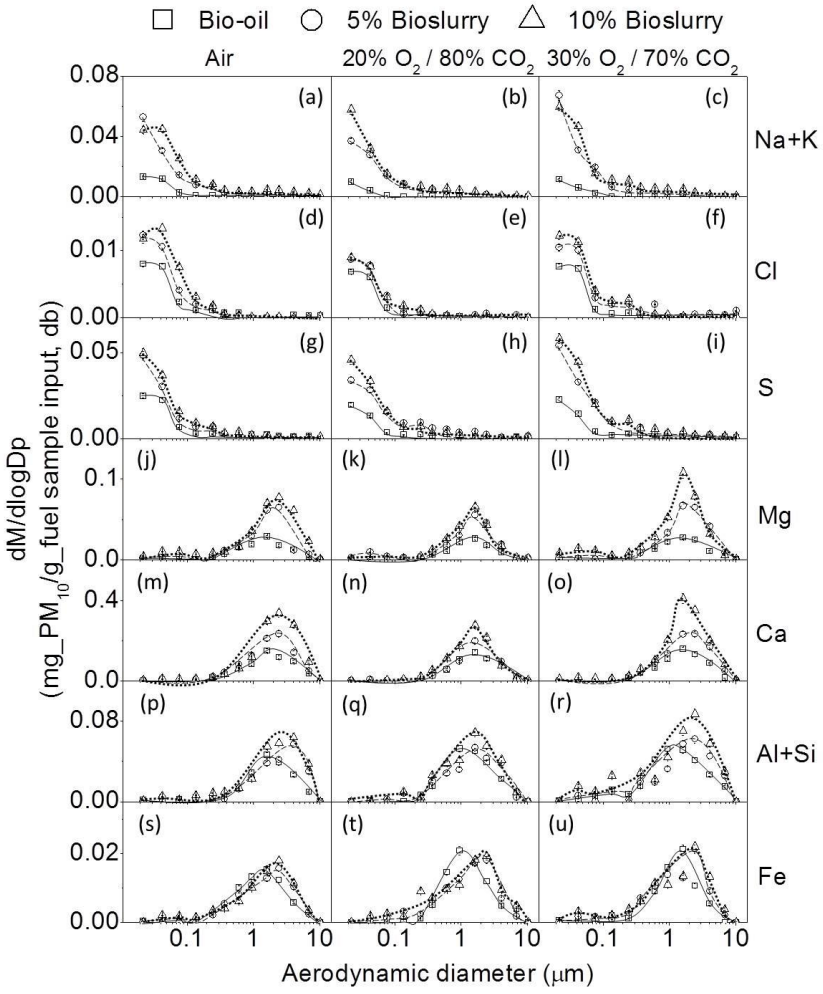

Figure 7-3 Elemental PSDs of PM_{10} from combustion of bio-oi, 5% bioslurry and 10% bioslurry under air, 20% O_2/ 80% CO_2 and 30% O_2/ 70% CO_2, respectively.

decrease the release of volatile metals hence PM_1 emission. Under 20% O_2/ 80% CO_2 condition, the fragmentation of burning char particles and ash particle

coagulation are also weakened, leading to a reduction in PM_{1-10} emission. However, under 30% O_2/ 70% CO_2 condition, the temperature of burning char particle is predicted to be ~1700 °C that is very close to that under air condition. The increases in the emission of PM_{10} (mainly PM_1) could be explained by enhanced sulfation of alkali species at a higher O_2 concentration which correlates well with the increase in the yield of S in PM_{10} under 30% O_2/ 70% CO_2 condition (see Figure 7-4).[298]

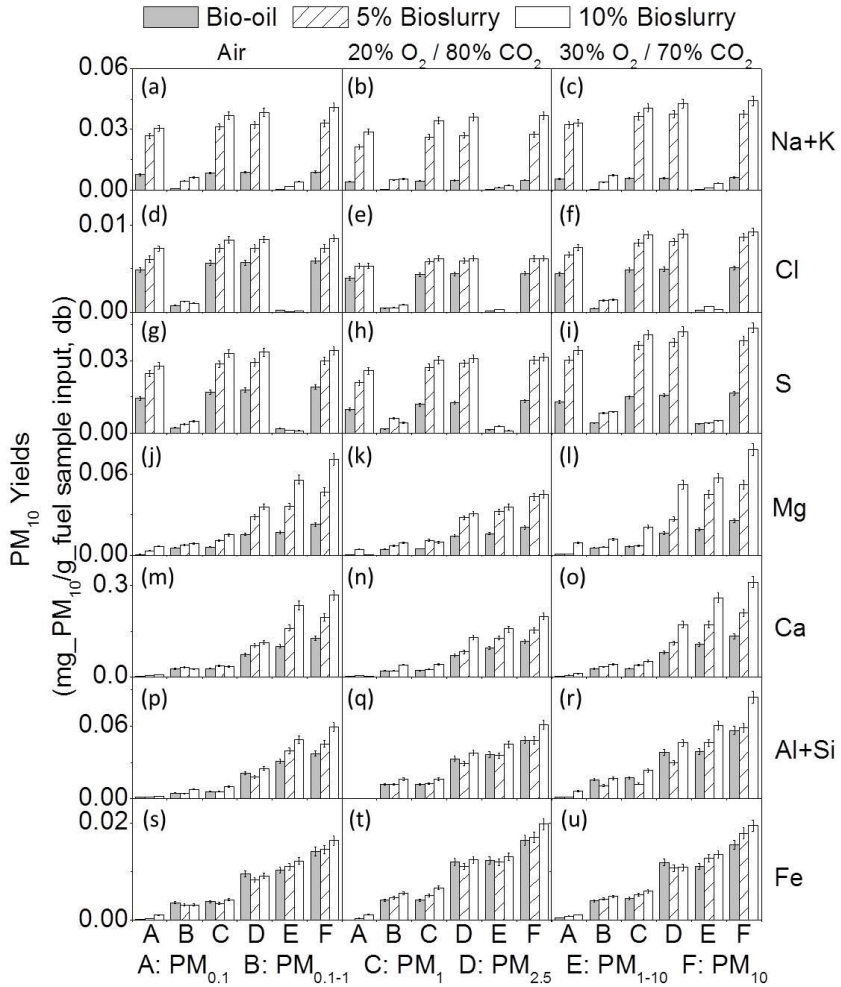

Figure 7-4 Elemental yields of PM_{10} from combustion of bio-oi, 5% bioslurry and 10% bioslurry under air, 20% O_2/ 80% CO_2 and 30% O_2/ 70% CO_2, respectively.

It is further noticed in Figure 7-2 that during the combustion of bioslurry, the coarse mode in PM_{1-10} shifts from ~2.4 μm under air condition to a smaller size of ~1.6 μm under the two oxyfuel conditions. The results in Figure 7-3 further show that such shift in the coarse mode is mainly for Mg and Ca. Therefore, it appears that catalysed

sintering process of carbonates[202] is weakened during bioslurry combustion under oxyfuel conditions. This is plausible because the excessively elevated CO_2 concentration under oxyfuel conditions would shift the equilibrium of the repeated formation and decomposition process of Mg/Ca carbonate during combustion. The results suggest that this hinders the growth of Mg/Ca-rich particles through this process, resulting in shifting the PM_{1-10} particles to smaller sizes.

7.5 Benchmarking PM_{10} Emission from the Combustion of Bioslurry against those of Other Solid Fuels

Bioslurry is considered as a promising substitution fuel for coal in stationary applications so that PM_{10} emission in such applications is an important consideration. For this reason, this study further benchmarked the PM_{10} emission intensity of bioslurry against some of literature data reported for coal, biomass, and biochar under the combustion conditions pertinent to stationary applications. Therefore, the literature data on PM_{10} emission from the combustion of brown coal[172], mallee biomass[66] and biochar[67] are used for such benchmarking as this data were obtained under similar combustion conditions, as shown in Figure 7-5.

As shown in Figure 7-5, the benchmarking on the yields of PM (including $PM_{0.1}$, $PM_{0.1-1}$, PM_1, $PM_{2.5}$, PM_{1-10}, and PM_{10}) are normalized to three different bases, i.e. fuel input, ash input and energy input basis. On a unit mass of fuel input basis (see Figure 7-5a), bioslurry produces the lowest amount of PM_{10} (~0.61 and ~0.83 mg/g_fuel_input for 5% bioslurry and 10% bioslurry, respectively) during combustion, in comparison to coal (~2.7 mg/g_fuel_input), biomass (~3.0 mg/g_fuel_input) and biochar (~4.0 mg/g_fuel_input). It should be noted that the data on a unit ash input basis is an indication of the ability of ash-forming species in the parent fuel in producing PM emission during combustion. As shown in Figure 7-5b, the ash-forming species in biochar has propensity in leading to the emission of PM_{10} (both PM_1 and PM_{1-10}). The ash-forming species in bioslurry have higher

tendencies to produce PM_{10} (both PM_1 and PM_{1-10}) than biochar but lower than that of coal. In practice, substitution of solid fuels by bioslurry fuels in stationary applications is generally expected to be on the basis of same energy input into the reactor.

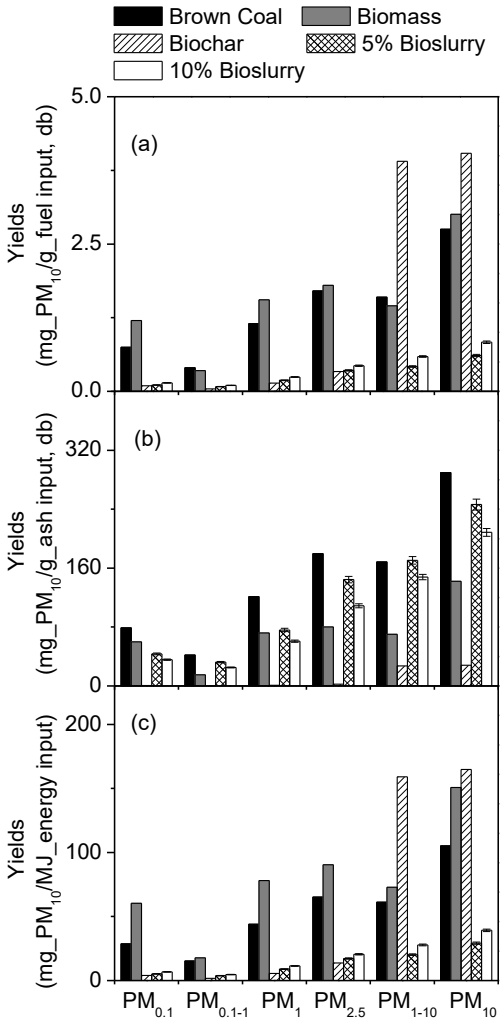

Figure 7-5 Yields of $PM_{0.1}$, $PM_{0.1-1}$, PM_1, $PM_{2.5}$, PM_{1-10}, and PM_{10} from combustion of coal, biomass, biochar, 5% bioslurry and 10% bioslurry based on fuel input, ash input, and energy input, respectively. The data for coal, biomass, and biochar are based on our previous studies[66,67,172] on PM emission under similar combustion conditions.

As shown in Figure 7-5c, when normalised on the basis of unit energy input, bioslurry leads to substantially lower emission of PM_{10} (~29.3 and ~39.2 mg/MJ_energy_input, for 5% bioslurry and 10% bioslurry respectively) than coal (~105.1 mg/MJ_energy_input), biomass (~150.8 mg/MJ_energy_input) and biochar (~164.8 mg/MJ_energy_input). It is expected that bioslurry performs better than

brown coal during combustion in terms of PM_{10} emission because coal has a high ash content and its ash-forming species have higher propensities of PM_{10} emission during combustion. It is interesting to see that in comparison to biomass and biochar, bioslurry fuels still leads to better performance in term of PM_{10} (both PM_1 and PM_{1-10}) emission during combustion although the ash-forming species in bioslurry has a higher propensities for producing PM_{10} (both PM_1 and PM_{1-10}) that those in biomass and biochar. This is due to the fact that the contents of ash-forming species in bioslurry fuels are extremely low (~0.19 and ~0.31 % for 5% bioslurry and 10% bioslurry, as shown in Table 7-1), which are considerably lower than those of biomass (~4.0 %) and biochar (~13.7 %).

7.6 Conclusion

This study focused on the PM_{10} emission from spray combustion of bioslurry fuels with 5% and 10% biochar loading levels in a lab-scale DTF system at 1400 °C under air and two oxyfuel conditions. PM_{10} from bioslurry combustion follows a bimodal distribution, with a fine mode at ~0.022 μm and a coarse mode at ~2.4 μm. PM_{1-10} accounts for ~70-73 wt% of the total PM_{10}. The chemical compositions of PM_{10} and the elemental PSDs and yields of PM_{10} from bioslurry combustion indicate that the mechanisms responsible for ash transformation during bioslurry combustion are similar to those for other biofuels such as biomass, bio-oil, and biochar. The PM_{10} emission increases with increasing biochar loading level in bioslurry because the concentrations of ash-forming species in biochar is substantially higher than those in bio-oil (hence bioslurry). Under 20% O_2/ 80% CO_2 condition, PM_1 and PM_{1-10} emissions from bioslurry combustion are lower than those under air conditions due to the lower combustion temperature of char particles. However, under 30% O_2/ 70% CO_2 conditions, the emission of PM_{10} is higher than that under air. Such an increase is mainly contributed by the increase in PM_1 emission, most likely as a result of increasing O_2 concentration leading to enhanced sulfation of alkali species. When

benchmarking against other solid fuels such as coal, biomass or biochar, the ash-forming species in bioslurry have a lower propensity than those in coal but a higher propensity than those in biomass and biochar in producing PM_{10} during combustion. In practice, as the substitution of bioslurry fuels for coal, biomass or biochar are typically on the same energy input, bioslurry fuels still leads to considerably better performance in term of PM_{10} emission than not only coal but also biomass and biochar during combustion because of the substantially low ash content of bioslurry fuels.

Chapter 8 Synergy on Particulate Matter Emission during the Combustion of Bio-oil/biochar Slurry (Bioslurry)

8.1 Introduction

Bio-oil/biochar slurry (i.e. bioslurry) is prepared by suspending fine biochar particles into fast pyrolysis bio-oil.[30-32,137] It offers a series of advantages including high energy density, low production cost, low energy and carbon footprints, suitable for transport, and adaptable to conventional combustion devices for stationary applications such as combustions in boilers.[30-32] Particulate matter (PM) emission especially those with aerodynamic diameter size less than 1, 2.5 and 10 μm (hereafter referred to as PM_1, $PM_{2.5}$ and PM_{10}, respectively) during fuel combustion, are important considerations for stationary power generation. These PMs are notorious due to high capture cost[299] and adverse impact to human health. Once emitted to the atmosphere, PM particles may easily pass through the human respiration system, deposit in the lung and cause related diseases.[41] While extensive investigations were carried out on PM emissions from the combustion of coal,[47,50,52,56,291] biomass,[58,65,241,300-302] bio-oil[285] and biochar,[67] the studies on PM emission during bioslurry combustion is scarce.[303]

The two-phase nature of bioslurry dictates that the combustion process of such a fuel and the related PM emission may be complicated. It is known that when biochar is mixed with bio-oil, inorganic species in biochar may be leached from biochar into bio-oil phase.[99,101] During combustion, reactions between bio-oil and biochar particles may potentially influence the transformation of inorganic species in bioslurry. For example, during bioslurry pyrolysis, the primary biochar may be deposited with coke produced from bio-oil cracking.[304] Both indirect and direct[68,69] evidences show that volatiles may react with char to enhance PM_1 emission during

biomass combustion. Clearly, synergy is likely to take place during bioslurry combustion to influence PM emission but little investigation has been undertaken to study such an important aspect that is largely unknown.

Consequently, the objectives of this study are to carry out a systematic set of experiments to investigate the synergy on PM_{10} emission during the combustion of bioslurry in a laboratory-scale drop-tube furnace (DTF) in air at 1400 °C. To investigate the potential synergy, a series of fuel samples are considered, including bio-oil, biochar, bioslurry prepared from the bio-oil and biochar, bio-oil and biochar fractions filtered from bioslurry after its preparation and storage. The properties of bio-oil, biochar, bioslurry samples with 5 and 10% biochar, slurry-oil and slurry-char are listed in Table 8-1. Direct experimental evidences are obtained to demonstrate the synergy, and key mechanisms responsible for such synergy are discussed.

8.2 Direct Evidence for the Presence of Synergy on PM Emission during Bioslurry Combustion

Figure 8-1 compares the experimentally-measured particle size distributions (PSDs) of PM_{10} from the combustions of the bioslurry with 5% biochar and bioslurry with 10% biochar with the predicted values via the addition of the PM_{10} emission from the separate combustion of bio-oil and biochar. Evidence can be clearly seen for synergy on PM_{10} emission during bioslurry combustion. The panels a and b show that the peaks of the fine modes (at ~0.043 μm) in the PSDs of both bioslurry with 5% biochar and bioslurry with 10% biochar are considerably higher than that of "5% biochar + 95% bio-oil" and "10% biochar + 90% bio-oil". The peaks for the coarse modes (at ~2.4 μm) exhibit opposite trends.

Further efforts were then taken to compare the experimentally-determined yields of PM_1, $PM_{2.5}$, $PM_{1\text{-}10}$ and PM_{10} from bioslurry combustion with the calculated values via the addition of the respective data from the separate combustion of bio-oil and

Table 8-1. Properties of bio-oil, biochar, bioslurry with 5% biochar, bioslurry with 10% biochar, slurry-oil, and slurry-char

samples	bio-oil	biochar	bioslurry with 5% biochar	bioslurry with 10% biochar	slurry-oil[a]	slurry-char[a]
proximate analysis (wt%, ar[b])						
water/moisture	24.7	2.4	23.2	20.2	22.3	2.0
ash	0.1	3.0[c]	0.2	0.3	0.1	1.8[c]
volatile matter	73.1	16.4[c]	65.4	61.6	75.9	14.3[c]
fixed carbon	2.1	80.6[c]	11.2	17.9	1.7	83.9[c]
elemental analysis (wt%, ar[b])						
C	41.47	86.83[d]	43.55	45.60	43.70	82.99[d]
H	6.37	3.34[d]	6.74	6.55	7.80	3.83[d]
N	0.11	0.13[d]	0.11	0.11	0.12	0.12[d]
O[e]	52.05	9.70[d]	49.60	47.73	48.38	13.06[d]
contents of major inorganic species (wt%, ar[b])						
Na	0.0040	0.0647[d]	0.0058	0.0096	0.0045	0.0584[d]
K	0.0091	0.3997[d]	0.0268	0.0463	0.0133	0.3538[d]
Cl	0.0036	0.0059[d]	0.0034	0.0035	0.0036	0.0052[d]
S	0.0048	0.0464[d]	0.0065	0.0086	0.0051	0.0428[d]
Mg	0.0031	0.1155[d]	0.0080	0.0132	0.0037	0.1081[d]
Ca	0.0171	0.2851[d]	0.0308	0.0429	0.0197	0.2552[d]
Al	0.0017	0.0080[d]	0.0023	0.0020	0.0017	0.0078[d]
Si	0.0040	0.3133[d]	0.0199	0.0327	0.0040	0.3086[d]
Fe	0.0022	0.0078[d]	0.0028	0.0027	0.0023	0.0076[d]
viscosity (20 °C, mPa s)	106.2	na[f]	120.5	148.4	121.1	na[f]
LHV[g] (MJ/kg)	16.9	28.3	17.9	18.3	18.4	27.6

[a] separated from bioslurry with 10% biochar; [b] as-received basis for bio-oil, slurry-oil, and bioslurry; [c] dry basis; [d] dry and ash-free basis; [e] by difference; [f] not applicable; [g] lower heating value

bio-char. If the experimental results are equal to the calculated values, the yields of PM should be all plotted on the diagonal line in Figure 8-2. This is clearly not the case. For PM_1 yields, the experimental results are 0.19 and 0.24 mg/g during the combustion of bioslurry with 5% biochar and bioslurry with 10% biochar, respectively, which are considerably higher than the calculated values of 0.07 and 0.09 mg/g for the respective "bio-oil + biochar" cases. For $PM_{2.5}$ yields, the experimental results are 0.35 and 0.43 mg/g that are also considerably higher than the calculated values of 0.21 and 0.30 mg/g, respectively. For $PM_{1\text{-}10}$ yields, the experimental results are 0.42 and 0.59 mg/g that are actually lower than the calculated values of 0.48 mg/g and 0.66 mg/g, respectively. Therefore, synergy on PM emission clearly takes place during bioslurry combustion, resulting in increases in PM_1 and $PM_{2.5}$ yields and a decrease in $PM_{1\text{-}10}$ yield. Such synergy leads to an overall increase in PM_{10} emissions from the calculated values of 0.56 and 0.75 mg/g to 0.61 and 0.83 mg/g during the combustion of bioslurry with 5% biochar and bioslurry with 10% biochar, respectively.

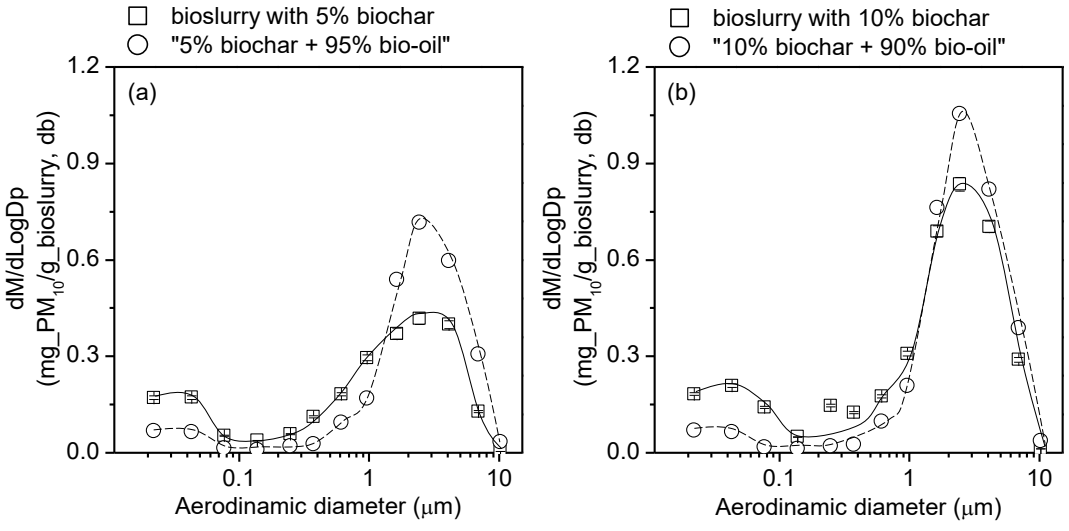

Figure 8-1 Comparisons between the experimental and predicted PSDs (a-b) of PM10 from the combustion of bioslurry with 5% biochar and bioslurry with 10% biochar in the DTF at 1400 °C, respectively.

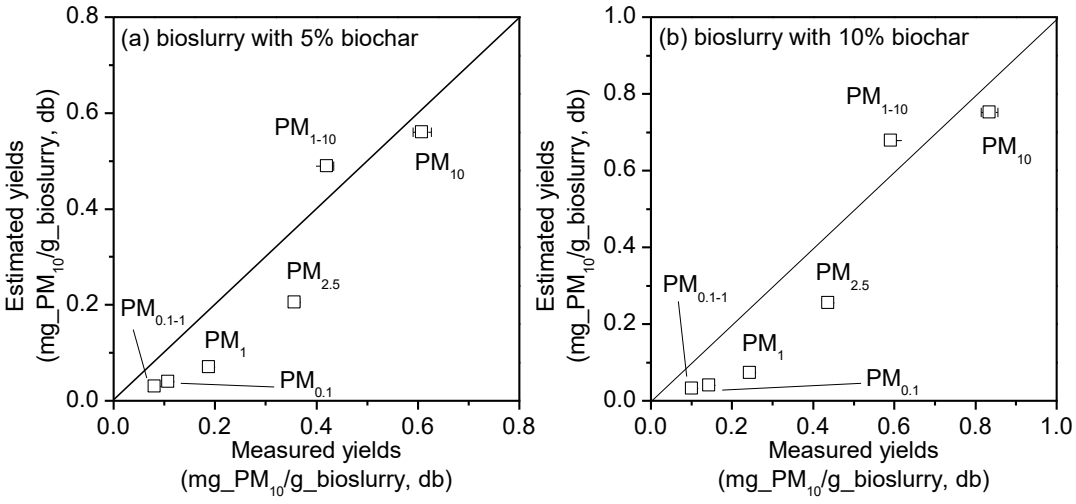

Figure 8-2 Comparisons between the experimental and predicted yields (a-b) of PM_{10} from the combustion of bioslurry with 5% biochar and bioslurry with 10% biochar in the DTF at 1400 °C, respectively.

8.3 Synergy on PM Emission from Bioslurry Combustion due to Biochar Leaching by Bio-oil

After preparation, bioslurry with 10% biochar was separated into slurry-oil and slurry-char via a series of separation process (see Figure 3-3 in Chapter 3). It is known that as biochar is mixed with bio-oil for preparing bioslurry, leaching of inorganic species in biochar by acidic bio-oil may take place to alter the forms of the inorganic species in bioslurry.[99,101] Figure 8-3 shows the comparisons in the distributions of some major inorganic elements in bio-oil and biochar fractions before and after mixing as bioslurry and stored for 1 week. The results in Figure 8-3 show that the proportions of Na, K, S, Mg, and Ca in slurry-oil fraction of bioslurry are higher than those in the original bio-oil. Clearly, there are redistributions of these inorganic species in the biochar and bio-oil phases due to the leaching of inorganic species from biochar by bio-oil. Such an effect of leaching may have synergistic effect on PM emission during bioslurry combustion.

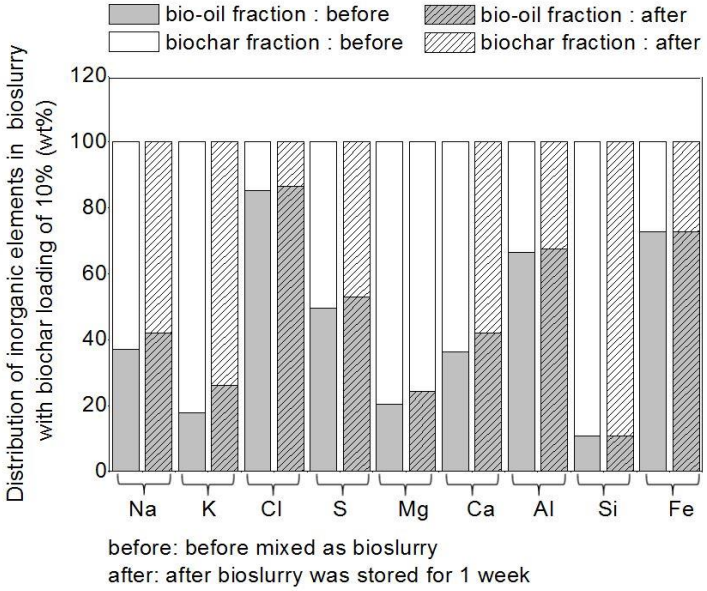

Figure 8-3 Comparison of the distributions of the major inorganic elements (Na, K, Cl, S, Mg, Ca, Al, Si and Fe) in bio-oil and biochar fractions of bioslurry (with biochar loading rate of 10%) before the bioslurry is prepared and after the bioslurry was stored for 1 week.

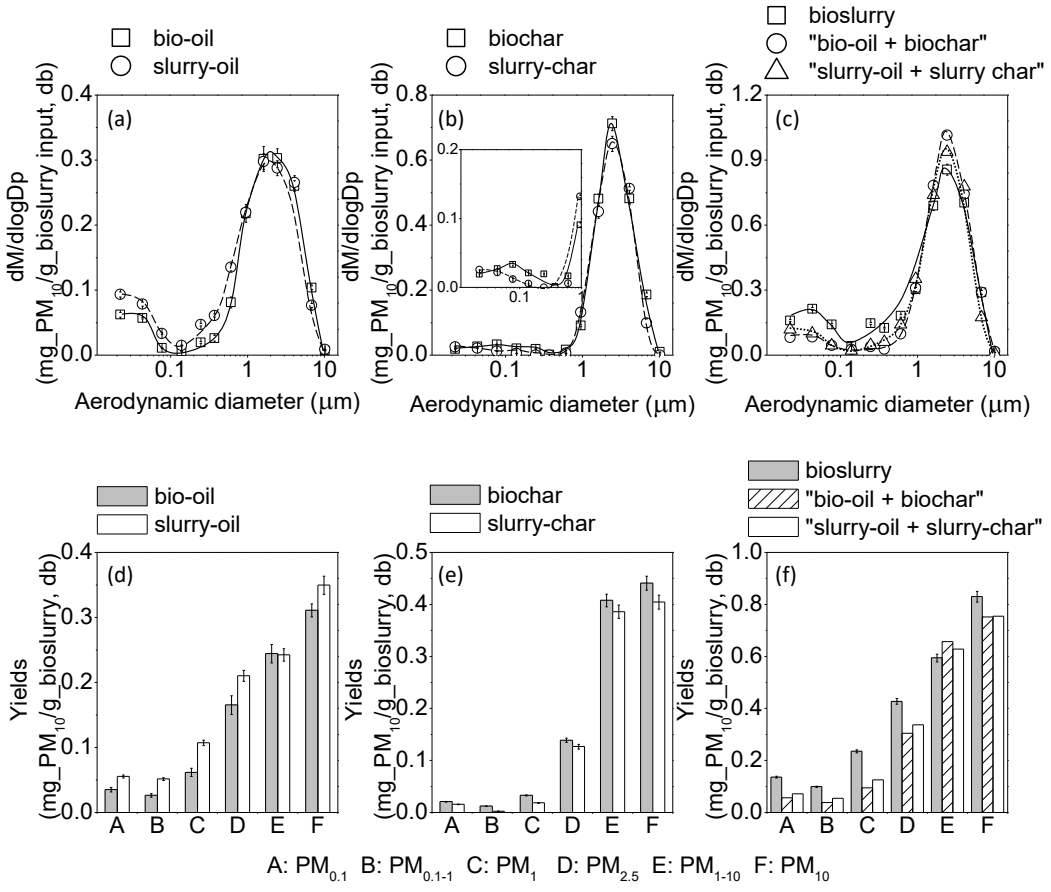

Figure 8-4 PSDs and yields of PM_{10} from the combustion of (a, d) bio-oil and slurry-oil, (b, e) biochar and slurry-char, (c, f) bioslurry (10% char loading rate), "bio-oil + biochar", and "slurry-oil + slurry-char" in the DTF at 1400 °C, respectively.

To obtain the direct evidence of leaching effect on PM_{10} emission during bioslurry combustion, both original bio-oil and biochar and the slurry-oil and slurry-char separated from bioslurry were combusted in the DTF system under the same conditions for PM_{10} collection. Figure 8-4 presents the PSDs and yields of PM_{10} from the combustion of the bio-oil, slurry-oil, biochar, slurry-char and bioslurry, respectively. The calculated PSDs and yields of PM_{10} based on the direct addition of those from individual fractions are also presented in Figure 8-4 for comparison, including those for "bio-oil + biochar", and "slurry-oil + slurry-char". All the data are normalized to unit mass of dry basis bioslurry input for comparison. Figure 8-4a clearly shows that the peak of the fine mode of slurry-oil is higher than that of bio-oil while the peak of the coarse mode shows remains almost the same. Therefore, as shown in Figure 8-4d, the combustion of slurry-oil leads to a higher PM_1 emission (0.10 mg/g) than that (0.06 mg/g) from the combustion of the original bio-oil while the PM_{1-10} emissions are similar. Figure 8-4d also shows that the increase in PM_1 is contributed by those in both $PM_{0.1}$ and $PM_{0.1-1}$ (accounting for ~44% and ~56% of the total PM_1 increment, respectively). Such a synergy is further elaborated in Figures 8-5 and 8-6 in terms of the elemental PSDs and yields of Na, K, Cl, S, Mg, Ca, Al, Si, and Fe in PM_{10} from the combustion of bio-oil and slurry-oil. It is clearly shown in Figures 8-5 and 8-6 that the increase in $PM_{0.1}$ from slurry-oil combustion is mainly due to the increases in the Na, K and S emission in $PM_{0.1}$, while the increase in $PM_{0.1-1}$ is mainly contributed by the increases in Mg and Ca in $PM_{0.1-1}$, when compared with those from the original bio-oil. As a result, the total increase in Na, K and S in $PM_{0.1}$ accounts for ~84% of the total increase in $PM_{0.1}$. Further calculation of the molar ratio of the increases in (Na+K) and 2S in $PM_{0.1}$ (with value of ~2.5) indicates that some of the alkali species in the increased $PM_{0.1}$ are in forms other than sulphates (such as in forms of NaOH or KOH[305]). For $PM_{0.1-1}$, on the basis that the total increase of inorganics in $PM_{0.1-1}$ are in forms of oxides, further calculations show that the Mg and Ca species account for ~97% of the total increase in $PM_{0.1-1}$.

Such increase in PM_1 and the elements in PM_1 correlates well with the aforementioned redistribution of these inorganic species in bio-oil and biochar fractions of bioslurry. Therefore, it is concluded that these inorganic elements are transformed from biochar into bio-oil fraction as results of leaching and contribute to the increase in PM_1 emission during the combustion of slurry-oil. It is well known that vaporization followed by homogeneous nucleation and/or heterogeneous condensation contribute to $PM_{0.1}$ emission[64,300] while agglomeration of oxide particles, and/or re-oxidation of the reduced species in burning char particles followed by nucleation and coagulation contribute to $PM_{0.1\text{-}1}$ emission.[202,275]

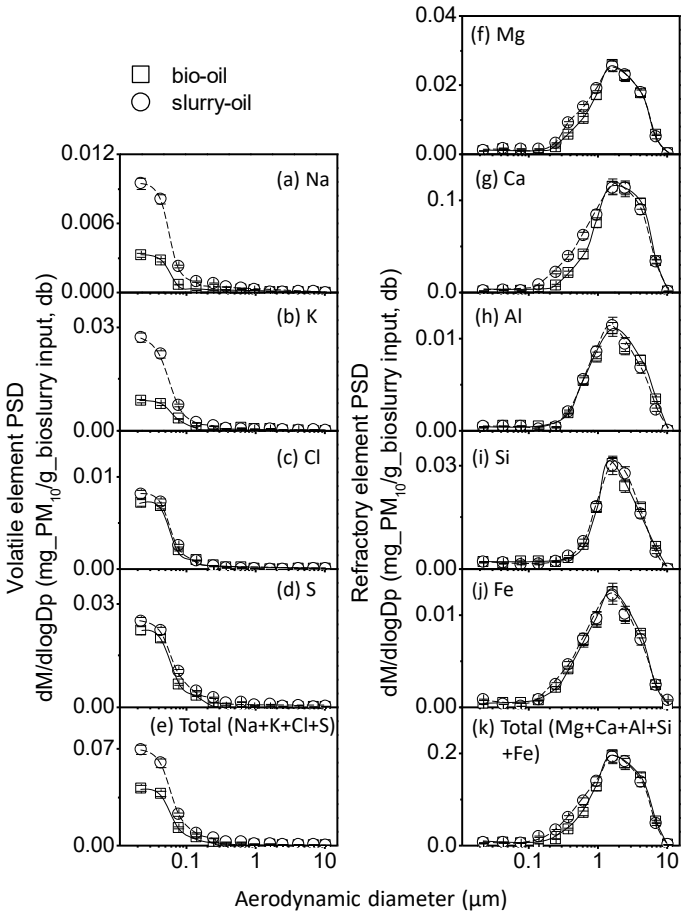

Figure 8-5 Elemental PSDs of Na, K, Cl, S, total volatile elements (i.e. Na+K+Cl+S), Mg, Ca, Al, Si and total refractory elements (i.e. Mg+Ca+Al+Si+Fe) in PM_{10} from the combustion of bio-oil and slurry-oil in the DTF at 1400 °C, respectively.

The panels b and c of Figure 8-4 present the PSDs and yields of PM_{10} from the combustion of the original biochar and slurry-char separated from the bioslurry. The

PSD curves show that the heights of both coarse and fine modes of PM_{10} from the combustion of slurry-char are reduced in comparison to those from the combustion of the original biochar. As a result, the yields PM_1 and PM_{1-10} (0.02 and 0.38 mg/g) from the combustion of slurry-char are lower than those (0.03 and 0.41 mg/g) from the combustion of the original biochar, respectively. As shown in Figures 8-7 and 8-8, such reductions are contributed by the reductions in the yields of volatile elements (Na, K, Cl and S) in PM_1 (especially in $PM_{0.1}$) and the yields of refractory elements (Mg and Ca) in PM_{1-10}. These correlate well with the removals of these elements in biochar due to the leaching of biochar by the acidic bio-oil (see Figure 8-3).

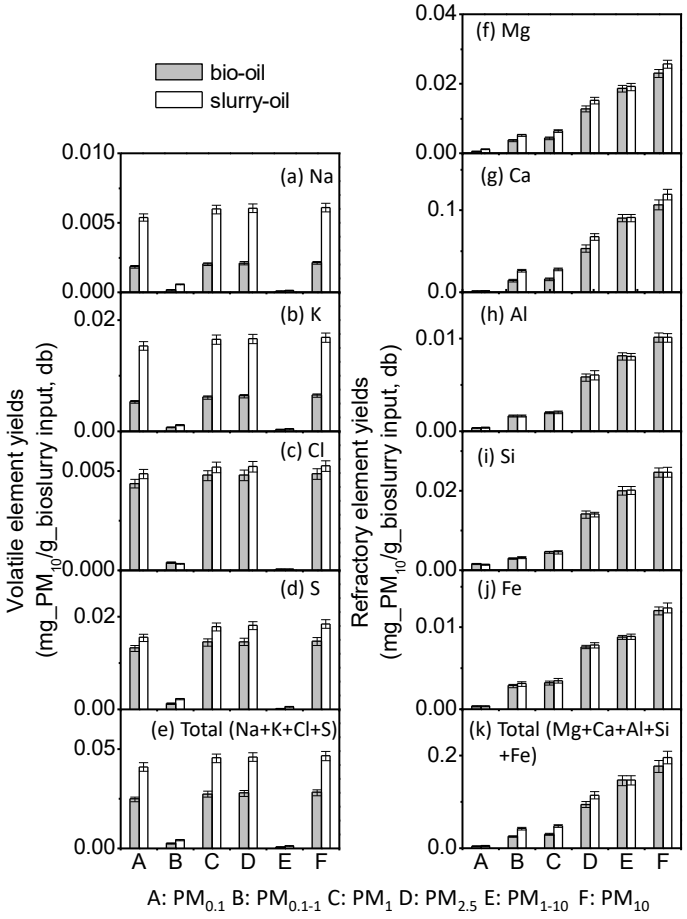

Figure 8-67. Elemental yields of Na, K, Cl, S, total volatile elements (i.e. Na+K+Cl+S), Mg, Ca, Al, Si and total refractory elements (i.e. Mg+Ca+Al+Si+Fe) in PM_{10} from the combustion of bio-oil and slurry-oil in the DTF at 1400 °C, respectively.

The panels c and f of Figure 8-4 present further evidence on the influence of biochar leaching by bio-oil on PM_{10} emission from bioslurry combustion, via the comparison

in the calculated values of PM_{10} emission from "bio-oil + biochar" and "slurry-oil + slurry-char". Obviously, the calculations indicate a higher PM_1 emission (0.12 mg/g) and a lower PM_{1-10}, emission (0.63 mg/g) for the case of "slurry-oil + slurry-char" in comparison to the respective calculated values (0.09 and 0.66 mg/g, respectively) for the case of "bio-oil + biochar". The higher PM_1 emission is contributed by both higher $PM_{0.1}$ and $PM_{0.1-1}$ emissions. It is also noted that the total PM_{10} between "bio-oil + biochar" and "slurry-oil + slurry-char" remains almost unchanged. Figures 8-9 and 8-10 further show that the increase in the calculated PM_1 emission for the case of "slurry-oil + slurry-char" is due to the higher emissions of Na and K in $PM_{0.1}$ and Ca in $PM_{0.1-1}$, which correlates well with the increasing contents of these elements in slurry-oil in comparison to bio-oil (see Figures 8-5 and 8-6). Figures 8-9 and 8-10 also show that the decrease in the calculated PM_{1-10} emission for the case of "slurry-oil + slurry-char" is due to the lower emissions of the refractory elements (i.e. Mg and Ca) in PM_{1-10}, which correlates well with the decreasing contents of these elements in slurry-char in comparison to biochar (see Figures 8-7 and 8-8). Clearly, these results prove that the leaching of biochar by bio-oil in bioslurry leads to the increase in PM_1 and decrease in PM_{1-10} emissions during combustion. It is also interesting to note that the mass ratio of the increase of Mg and Ca in $PM_{0.1-1}$ to the decrease of Mg and Ca in PM_{1-10} from "bio-oil + biochar" to "slurry-oil + slurry-char" is ~1.0. This suggests that in addition to the leaching of volatile elements (e.g. Na and K), the leaching of biochar by bio-oil has also transformed refractory elements (i.e. Mg and Ca) that would have formed PM_{1-10} into $PM_{0.1-1}$ and contributed to PM_1 emission during combustion.

8.4 Synergy on PM Emission during Bioslurry Combustion due to Interactions Between the Combustions of Bio-oil and Biochar Fractions

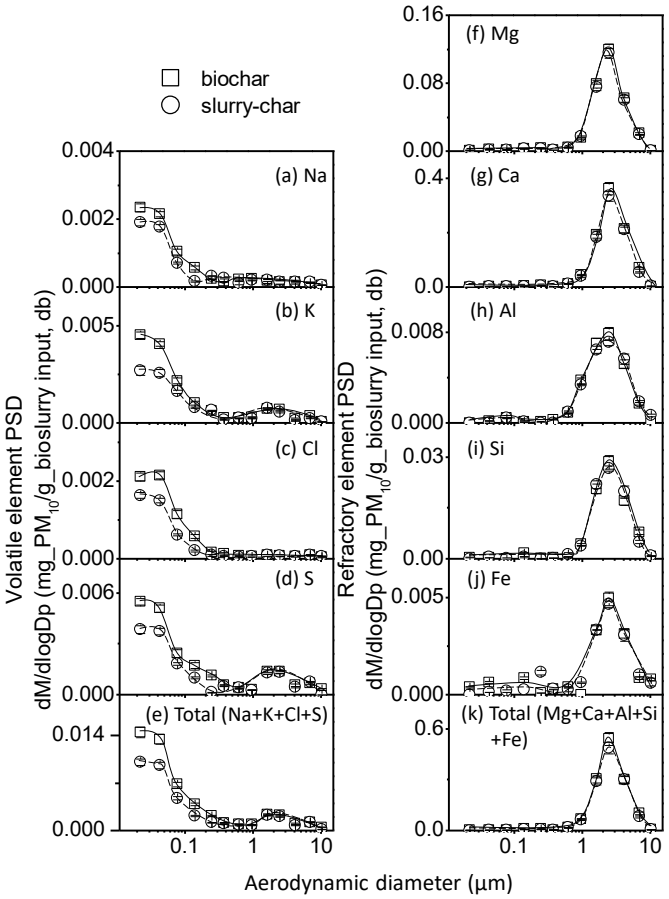

Figure 8-7 Elemental PSDs of Na, K, Cl, S, total volatile elements (i.e. Na+K+Cl+S), Mg, Ca, Al, Si and total refractory elements (i.e. Mg+Ca+Al+Si+Fe) in PM_{10} from the combustion of biochar and slurry-char in the DTF at 1400 °C, respectively.

Further efforts were then taken to compare the calculated PM_{10} emission for the case of "slurry-oil + slurry-char" with the experimental data from the direct combustion of bioslurry, as shown in the panels c and f of Figure 8-4. It is clear that the experimental yield of PM_1 from direct bioslurry combustion (0.24 mg/g) is higher than the calculated yield of PM_1 (0.12 mg/g) for the case of "slurry-oil + slurry-char", and that of the $PM_{1\text{-}10}$ (0.59 mg/g) from direct bioslurry combustion is slightly lower than the calculated case (0.63 mg/g). In fact, both the yields of $PM_{0.1}$ and $PM_{0.1\text{-}1}$ (0.14 and 0.10 mg/g) from direct bioslurry combustion are higher than the calculated values (0.07 and 0.05 mg/g) for the case of "slurry-oil + slurry-char", respectively. The results suggest that apart from the effect of biochar leaching by bio-oil during

bioslurry preparation, there is additional synergy that takes place during bioslurry combustion and is responsible for such observations.

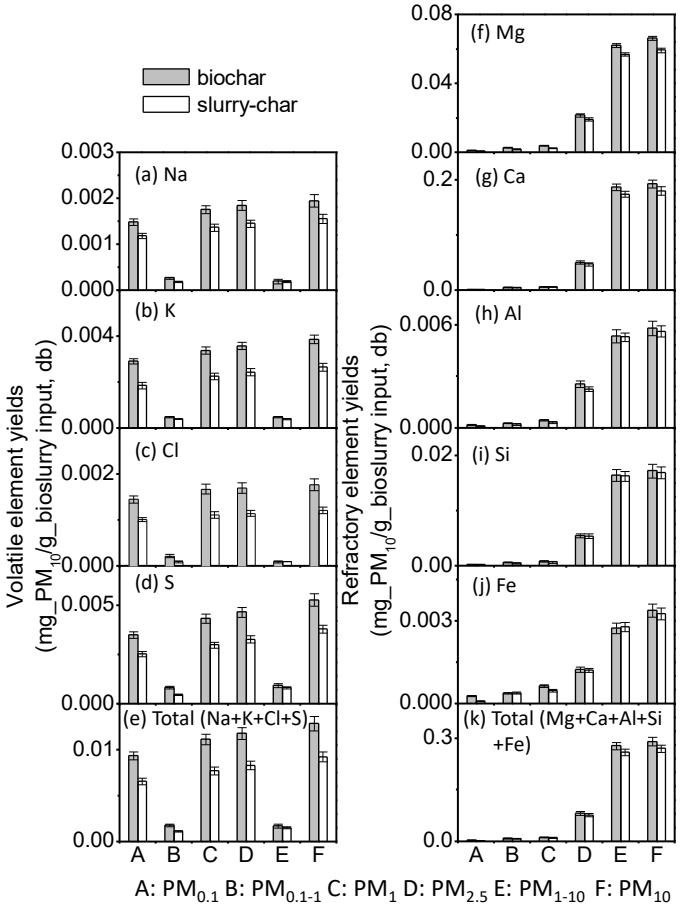

Figure 8-8 Elemental yields of Na, K, Cl, S, total volatile elements (i.e. Na+K+Cl+S), Mg, Ca, Al, Si and total refractory elements (i.e. Mg+Ca+Al+Si+Fe) in PM_{10} from the combustion of biochar and slurry-char in the DTF at 1400 °C, respectively.

Clearly, the results in the panels c and f of Figure 8-4 indicate that in comparison to the combustion of bioslurry individual fraction (bio-oil or biochar fraction), there are interactions between the combustion of the two fractions during bioslurry combustion and such interactions result in synergy in PM_{10} emission. While the details of such interactions are unknown, there are at least two possibilities. One possibility is the so-called "volatile-char interactions", i.e. the interactions between volatiles and char during combustion. It is known that bio-oil combustion is dominantly driven by gaseous-phase volatiles combustion[285] while the biochar combustion is dominated by solid-phase combustion.[67] Bioslurry is a two-phase fuel

mixture so that during bioslurry combustion both gaseous-phase combustion and solid-phase combustion would exist simultaneously. During rapid devolatilisation/combustion, it is expected that intensive volatile-char interactions can take place between the volatiles from bio-oil and biochar. A recent study[69] has provided direct experimental evidence on the volatile-char interactions enhancing the emission of PM_1 (dominantly $PM_{0.1}$). Such a mechanism is expected to play a similar role in the combustion of bioslurry, during which the pyrolysis of the bio-oil fraction generates volatiles containing reactive species for reacting with char particles to enhancing the release of inorganic species in char. It is also known that volatile-char interactions are more effective for the release of volatile elements than refractory elements.[69,306] This is consistent with the data presented in Figure 8-10 that the yields of volatile elements in $PM_{0.1}$ for the case of direct bioslurry combustion are higher than those from the calculated values for the case of "slurry-oil + slurry-char", while the yields of the refractory elements in $PM_{0.1}$ in both cases are similar.

Another important observation is that in Figure 8-4f there is an increase in the yield of $PM_{0.1\text{-}1}$ and a decrease in the yield of $PM_{1\text{-}10}$ from direct bioslurry combustion in comparison to the respective calculated values from the case of "slurry-oil + slurry-char". Figure 8-10 further shows that such differences are contributed by the differences in the yields of refractory elements in $PM_{0.1\text{-}1}$ and $PM_{1\text{-}10}$, respectively. However, such an observation in Figure 8-4f cannot be explained by the effect of "volatile-char interactions" because volatile-char interactions are ineffective in enhancing the release of refractory elements.[69,306] One possible reason is that during bioslurry combustion, compared to biochar alone, the biochar particles soaked with bio-oil[30] may have resulted in chars with elevated reactivity via rapid devolatilisation. This would in turn enhance char fragmentation and burning during combustion, leading to the transformation of those refractory elements in $PM_{1\text{-}10}$ into smaller particle sizes. This is further supported by the fact that the mass ratio of the total increase of refractory elements in $PM_{0.1\text{-}1}$ to the total decrease in $PM_{1\text{-}10}$ is around 1.0,

clearly indicating the shift of these refractory elements from PM_{1-10} to $PM_{0.1-1}$ during bioslurry combustion.

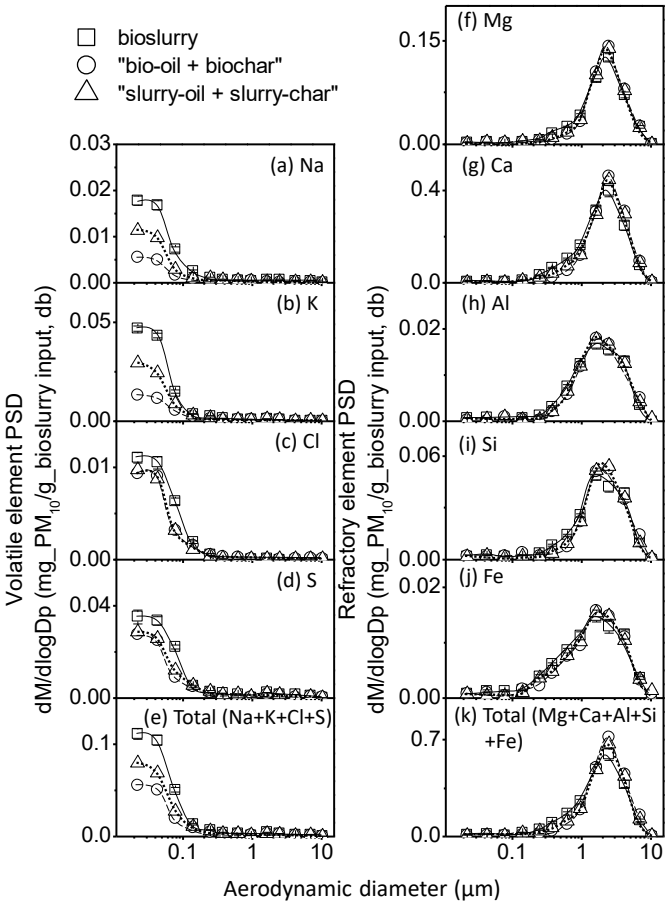

Figure 8-9 Elemental PSDs of Na, K, Cl, S, total volatile elements (i.e. Na+K+Cl+S), Mg, Ca, Al, Si and total refractory elements (i.e. Mg+Ca+Al+Si+Fe) in PM_{10} from the combustion of bioslurry, "bio-oil + biochar", and "slurry-oil + slurry-char" in the DTF at 1400 °C, respectively.

Based on the above discussion, during bioslurry combustion, there are two types of synergetic effects on PM_{10} emission during bioslurry combustion, i.e. the leaching effect and the interactions between the combustions of the bio-oil and biochar fractions. Both mechanisms lead to increase in PM_1 emission and decrease of PM_{1-10} during bioslurry combustion. Based on the experimental data for bioslurry with 10% biochar, the second mechanism (i.e. interactions between the combustions of bio-oil and biochar fractions) contributes to a net increase of 0.12 mg/g in (i.e. ~80% of) the

total increase of 0.15 mg/g in PM_1 and a net of 0.04 mg/g in (i.e. ~60% of) the total decrease of 0.07 mg/g in $PM_{1\text{-}10}$ during bioslurry combustion.

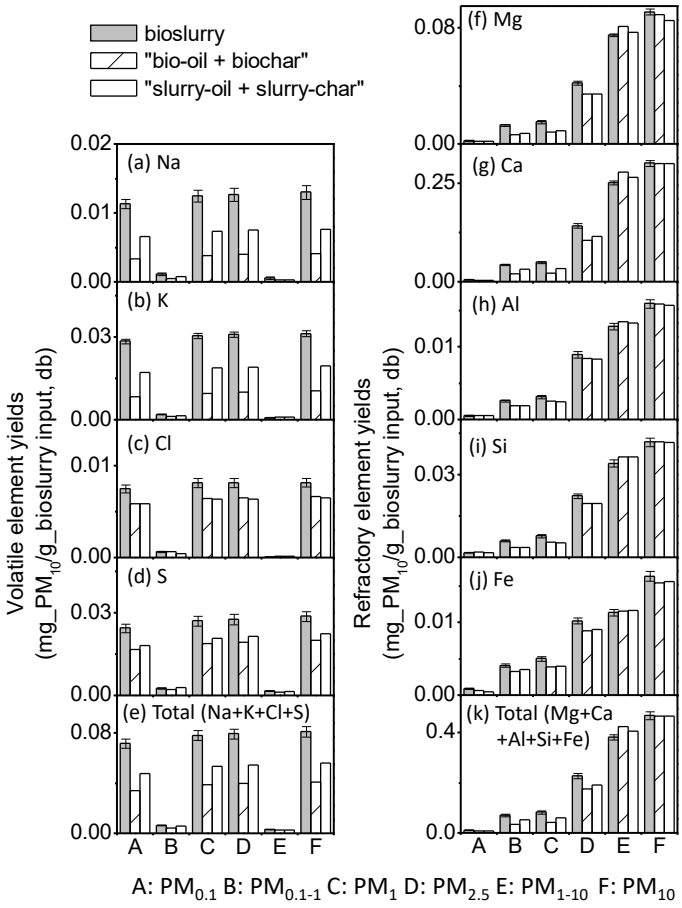

Figure 8-10 Elemental yields of Na, K, Cl, S, total volatile elements (i.e. Na+K+Cl+S), Mg, Ca, Al, Si and total refractory elements (i.e. Mg+Ca+Al+Si+Fe) in PM_{10} from the combustion of bioslurry, "bio-oil + biochar", and "slurry-oil + slurry-char" in the DTF at 1400 °C, respectively.

8.5 Conclusions

To investigate the influence of synergy during bioslurry combustion on PM_{10} emission, series combustion experiments were conducted via a drop-tube-furnace system at 1400 °C. The bioslurry, the bio-oil and biochar before and after prepared as bioslurry were all burned separately for PM_{10} collection. The PM_{10} emission from the direct combustion of bioslurry is higher than the sum of the PM_{10} emissions from separate bio-oil and biochar combustion, indicating the existence of synergy. Two mechanisms were found to be responsible for such synergy effects in PM_{10} emission.

One is the leaching effect, evidenced by comparison in the PM_{10} from the combustion of bio-oil and biochar before and after prepared as bioslurry. The leaching effect contributes to the increase in PM_1 and decrease in PM_{1-10} due to the transformation of the inorganic species from biochar fraction into bio-oil fraction. The other is the interactions between the combustions of bio-oil and biochar fractions, also leading to the increase in PM_1 and decrease in PM_{1-10}. The results show that the second mechanism contributes to ~80% of the total increase in PM_1 and ~60% of the total decrease in PM_{1-10}.

Chapter 9 Combustion of Biofuel Mixtures Containing Crude Glycerol (CG): Effect of Interactions between CG and Fuel Components on Particulate Matter Emission

9.1 Introduction

Crude glycerol (CG) is a waste by-product produced from biodiesel industry and its utilisation is of critical importance for both economic and environmental considerations.[141] CG has several undesired fuel properties (e.g. low energy contents, high viscosity and high ash content) that hinder its use for direct combustion in boilers or furnaces.[284] Recent study has tried to address these issues via mixing CG with bio-oil and/or biochar from biomass fast pyrolysis to produce CG-containing biofuel mixtures (including blends and most importantly slurries) for burning in stationary combustion applications.[35] Further investigation also verified that water-soluble fraction of bio-oil (WSF) instead of the whole bio-oil for preparing these mixtures can achieve higher CG uptake (over 50% in the fuel mixture).[36] These prepared CG-containing fuel mixtures have demonstrated improved fuel properties compared to CG or even bio-oil alone as a fuel.[35,36]

Combustion of coal,[52,291] biomass,[66,241] bio-oil,[285] biochar,[67] bioslurry[307] and CG[75] are known to produce emission of particulate matter with aerodynamic diameter less than 10 μm (i.e. PM_{10}), which is a notorious issue for power plants. PM_{10} is difficult to be captured [43] and has adverse impact on environment and human health.[41] Extensive studies were conducted on PM emission from the combustion of coal,[52,291] biomass,[66,241] heavy fuel oil[70] and bioslurry.[307] However, there has been no study on PM_{10} emission from the combustion of the aforementioned CG-containing fuel blends and slurries. Furthermore, it is reported that during the combustion of bioslurry, synergy would exist to influence the emission of PM_{10}.[307] Sodium chloride

is the main impurity in CG[75] which can provide Cl during the combustion of CG-including mixtures. Therefore, the multiple fuel components in these fuel mixtures may experience interactions during combustion which would lead to potential interactions on PM_{10} emission that warrants investigation.

Therefore, this study reports a systematic investigation into PM_{10} emission during the combustion of various biofuel-CG mixtures, including BMCG, WSFCG, BMCGB, and WSFCGB (see in Chapter 3) in a laboratory-scale drop-tube furnace (DTF) at 1400 ℃ in air, focusing on the effect of potential interactions between CG and fuel components in the fuel mixtures on PM_{10} emission. The combustion of fuel components like bio-oil, WSF, biochar, CG, and slurry of BB and WSFB were also carried out for supplementary support. The properties of these fuels were reported in Table 9-1.

9.2 Yields and Mass-based PSDs of PM_{10} from the Combustion of Various Fuel Mixtures

Figure 9-1 presents the PSDs and yields of PM_{10} emission from the combustion of the CG-containing fuel mixtures, i.e. the two blends (BMCG and WSFCG, see Figure 9-1 a and b) and the two slurries (BMCGB and WSFCGB, see Figure 9-1 c and d). Further information for the PM_{10} from the combustion of individual fuels and other fuel mixtures without CG in this study can be found in Figure 9-2. Figure 9-1a shows that the PSDs of PM_{10} emission from the combustion of the two blends show unimodal distribution with a fine mode at ~0.043 μm, with ~88.2 and ~99.3 % of PM_{10} is distributed in PM_1 (see Figure 9-1b). The dominant production of PM_1 from the combustion of the two blend fuels is reasonable as the combustion of liquid fuels favours PM_1 emission via the mechanism of vaporization of volatile element species, followed by gas-phase reaction, nucleation, and condensation.[75,285] This is also demonstrated in the PSDs and yields from the combustion of the individual liquid fuel components (see Figure 9-2), where CG, bio-oil, and WSF also produce unimod

Table 9-1 Properties of the four fuel components, i.e. biochar, bio-oil, bio-oil water-soluble fraction (WSF) and crude glycerol (CG), two fuel blends, i.e. bio-oil/methanol/CG blend (BMCG) and WSF/CG blend (WSFCG) and four slurry fuels, i.e. bio-oil/biochar slurry (BB), WSF/biochar slurry (WSFB), BMCG/biochar slurry (BMCGB) and WSFCG/biochar slurry (WSFCGB) used in this study.

samples	**fuel components**				**fuel blends**		**slurry fuels**			
	biochar	**bio-oil**	**WSF**	**CG**	**BMCG**	**WSFCG**	**BB**	**WSFB**	**BMCGB**	**WSFCGB**
proximate analysis (wt%, ar[a])										
water/moisture	2.4	25.1	64.1	16.0[c]	29.0	30.4	22.8	57.9	26.1	27.4
ash	1.9[b]	0.02	0.02	4.0[c]	0.2	2.8	0.3	0.3	0.4	2.7
volatile matter	25.1[b]	73.5	32.5	80.0[c]	53.9	65.6	53.7	29.8	51.4	62.8
fixed carbon	73.0[b]	1.4	3.4	0.0[c]	16.9	1.2	23.2	12.0	22.1	7.0
elemental analysis (wt%, ar[a])										
C	77.96[d]	42.39	18.81	31.30[c]	41.73	27.56	45.95	24.73	45.35	32.60
H	3.23[d]	7.14	9.03	8.73[c]	7.49	8.82	6.75	8.45	7.06	8.26
N	0.12[d]	0.05	0.02	0.00[c]	0.07	0.01	0.06	0.03	0.07	0.02
O[e]	18.69[d]	50.42	72.14	59.96[c]	50.71	63.61	47.24	66.79	47.52	59.12
concentrations of inorganic elements (ppm, ar[a])										
Na	137.50±3.60[d]	1.04±0.01	0.63±0.03	15734.36[c]	629.99±25.00	11011.19±17.00	14.54±0.30	14.32±0.36	580.74±2.64	9923.82±5.16
K	3468.38±75.50[d]	12.54±0.40	8.72±0.12	0.00[c]	11.29±1.20	2.62±0.12	358.12±7.80	354.68±1.08	357.00±8.25	349.19±7.12
Cl	nd[f]	22.17±0.88	18.02±0.72	24285.64[c]	990.75±29.62	16994.41±67.08	19.95±0.80	16.22±0.64	891.69±26.66	15294.96±60.37
S	2020.24±11.95[d]	150.83±6.03	69.11±2.76	0.00[c]	135.75±4.21	20.73±0.41	330.44±9.91	264.22±5.28	324.20±14.59	220.68±11.17
Mg	920.24±22.22[d]	1.69±0.35	1.51±0.07	0.00[c]	1.52±0.15	0.45±0.03	93.54±0.70	93.38±1.25	93.39±2.17	92.43±4.05
Ca	2302.45±45.30[d]	13.72±0.45	12.02±0.51	0.00[c]	12.35±0.65	3.61±0.20	242.59±4.51	241.06±5.56	241.36±4.56	233.49±9.25
Al	48.15±1.24[d]	12.67±2.13	11.13±0.78	0.00[c]	11.40±0.45	3.34±0.05	16.22±0.18	14.83±0.13	15.01±1.03	7.82±0.84
Si	343.92±29.29[d]	14.64±1.45	11.41±0.46	0.00[c]	13.18±0.76	3.42±0.10	47.57±1.41	44.65±0.16	46.25±2.01	37.47±1.23
Fe	49.02±0.33[d]	9.50±1.36	5.61±0.09	0.00[c]	8.55±0.15	1.68±0.03	13.45±0.29	9.95±0.05	12.60±0.19	6.42±0.82
P	214.83±7.63[d]	nd[f]	nd[f]	0.00[c]	nd[f]	nd[f]	21.48±1.20	21.60±1.08	21.48±0.80	21.52±0.94
density (g/ml, ar[a])	0.55±0.01[g]	1.19±0.01	1.07±0.01	1.23[c]	1.16±0.01	1.19±0.01	1.20±0.01	1.11±0.01	1.19±0.02	1.21±0.02
surface tension (20 °C, mN/m)	na[h]	31.9±0.7	42.3±0.2	52.0±0.5	24.8±0.2	46.8±0.6	35.2±0.4	44.7±0.5	33.7±0.2	49.4±0.2
viscosity (20 °C, mPa s)	na[h]	158.9±2.0	5.8±0.1	81.4±2.0	74.8±2.4	21.4±0.6	463.5±3.8	8.8±0.7	185.9±0.9	49.9±0.4
LHV[i] (MJ/kg)	25.2	16.4	9.5	14.2	29.7	12.8	17.3	11.1	29.2	14.0

[a] as-received basis for bio-oil, WSF, CG, BMCG, WSFCG, BB, WSFB, BMCGB and WSFCGB; [b] dry basis; [c] calculated based on compounds used for preparing the CG; [d] dry and ash-free basis; [e] by difference; [f] not detected; [g] g/cm^3; [h] not applicable; [i] lower heating value via calculation.

-al distributions of PM_{10} with a fine mode at ~0.043 μm with the yields of PM_1 accounting for ~98.1, ~59.4, and ~85.8 % respectively.

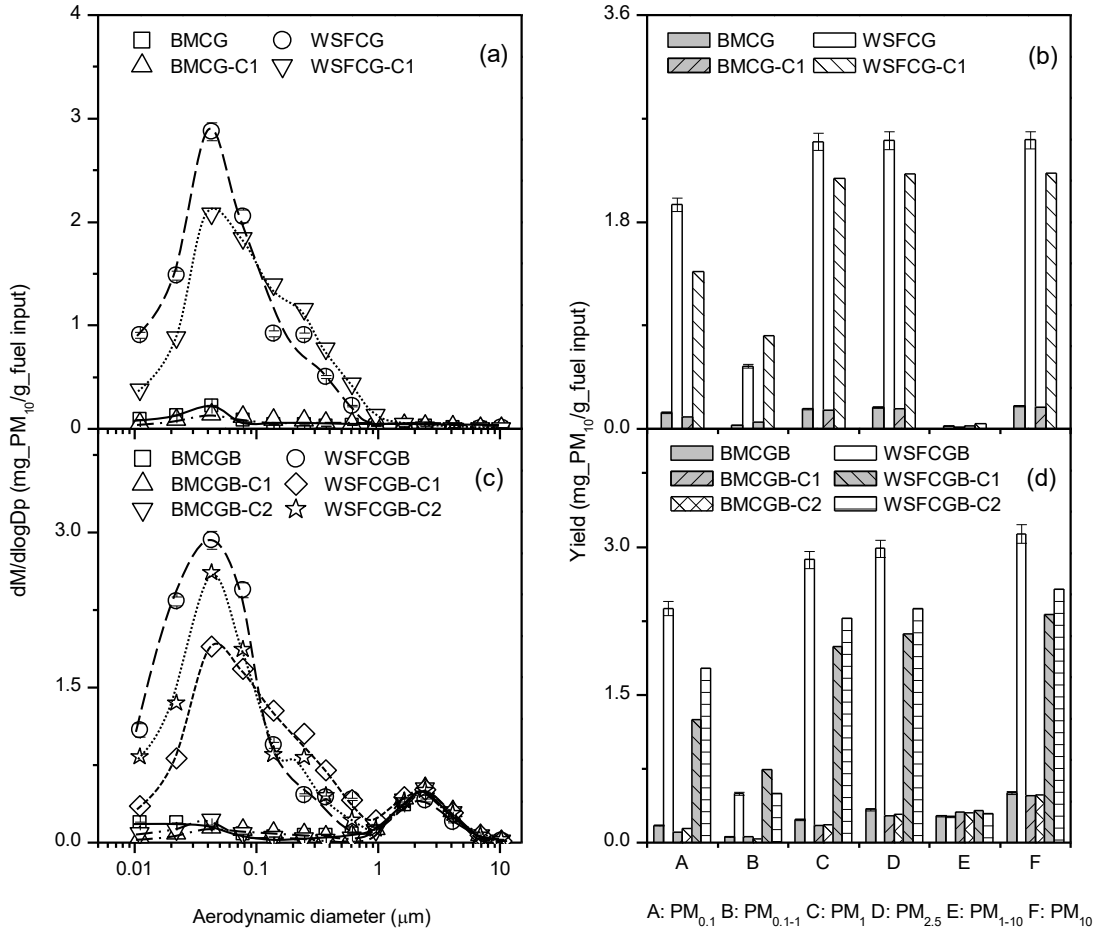

Figure 9-1 Mass-based PSDs (a and c) and yields (b and d) of PM_{10} produced from the combustion of (a and b) two fuel blends, i.e. bio-oil/methanol/CG blend (BMCG) and WSF/CG blend (WSFCG), and (c and d) two slurry fuels, i.e. BMCG/biochar slurry (BMCGB) and WSFCG/biochar slurry (WSFCGB).The respective cases suffixed with "-C1" represent the calculated results via direct addition of the experimental results for individual fuel components (bio-oil, WSF, CG and/or biochar) in the fuel mixtures. Those suffixed with "-C2" represent the calculated results via direct addition of the experimental results for biochar and the respective fuel blend (BMCG or WSFCG).

Comparatively, as shown in Figure 9-1c, the combustion of the two slurries produces bimodal distribution of PM_{10} with a fine mode at ~0.043 μm and a coarse mode at ~2.4 μm. The amounts of PM_1 account for ~48.0 and 91.7% of the total PM_{10} for BMCGB and WSFCGB (see Figure 9-1d), respectively, which are lower than those for the respective parent blend fuels (i.e., BMCG and WSFCG). Similar observation was also found for the PM_{10} emission of the other two slurries (i.e. BB and WSFB, see Figure 9-2). Such observations can be attributed to two reasons. One is that the increase in $PM_{1\text{-}10}$ emission as a result of the presence of biochar into the slurry fuels.[67] This is clearly supported by the results presented in Figure 9-2 that shows the

combustion of biochar producing PM_{10} with a unimodal distribution (dominantly PM_{1-10} that accounts for ~91.6 % of the total PM_{10}). The other is that the liquid phase is still the dominant fraction of the slurry fuels. Therefore, the combustion of the slurry fuels would generate extensive PM_1 emission.

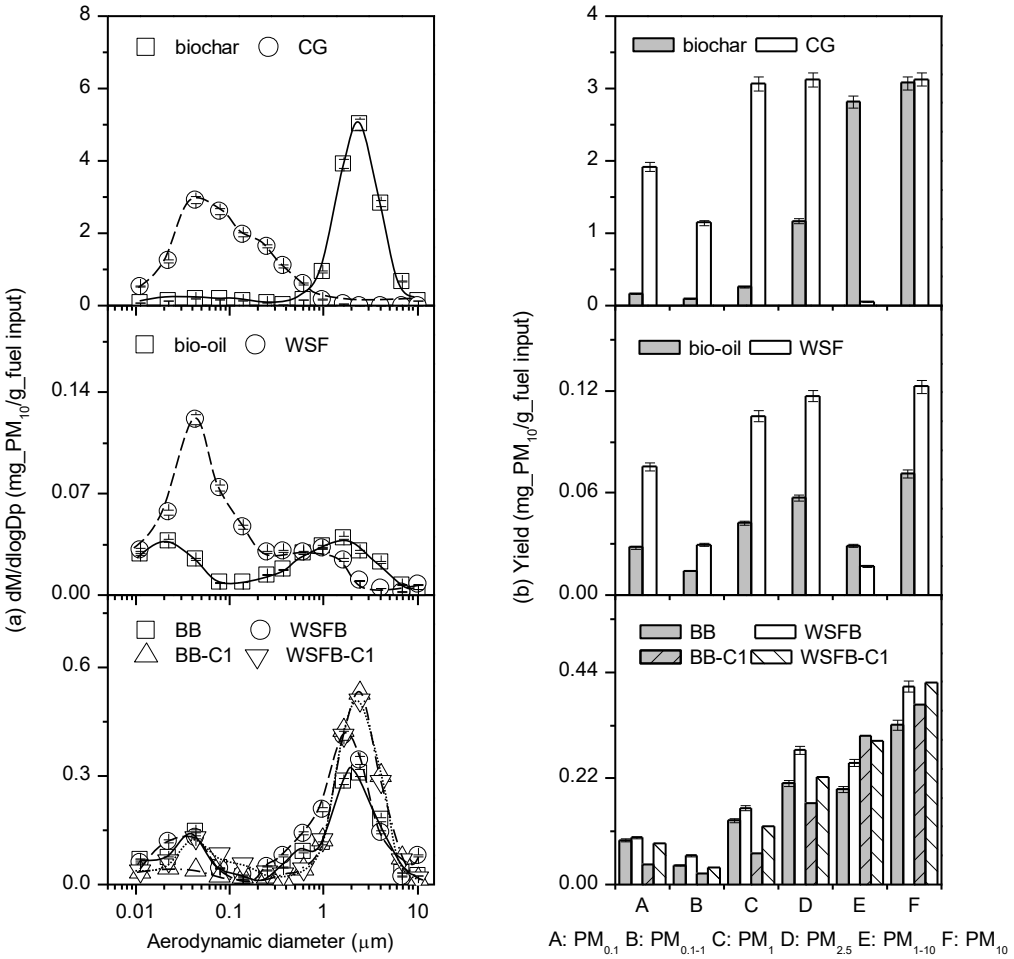

Figure 9-2 Mass-based PSDs (a) and yields (b) of PM_{10} emission from the combustion of biochar, bio-oil, water-soluble fraction of bio-oil (WSF), formulated crude glycerol (CG), bio-oil/biochar bioslurry (BB), and WSF/biochar bioslurry (WSFB). The calculated results are also presented for comparisons. All legends are same as those in Fiure 9-1.

Figures 9-3 and 9-4 present the elemental PSDs and yields of PM_{10} emission from the combustion of the two blends (BMCG and WSFCG) and two slurries (BMCGB and WSFCGB). It is not surprising to see that the volatile species (i.e. Na, K, Cl, and S) in PM_{10} produced from the combustion of both the blends and the slurries have unimodal distributions with a fine mode at ~0.022–0.043 μm, due to the well-known mechanism of vaporization and condensation.[52] Such observations are consistent with the PSDs of these volatile elements in the PM_{10} produced from the combustion of the bio-oil, WSF, CG, BB, and WSFB (see Figures 9-5−9-7). It is also not surprising that the refractory species (i.e. Mg, Ca, Al, Si, and Fe) in PM_{10} produced

during the combustion of the two slurries (BMCGB and WSFCGB) have unimodal distributions with a coarse mode at ~2.438 μm. Such observations are consistent with the PSDs of these elements in the PM_{10} produced from biochar combustion (see Figure 9-1). Clearly, the PSDs of refractory elements in PM_{10} from the combustion of the two

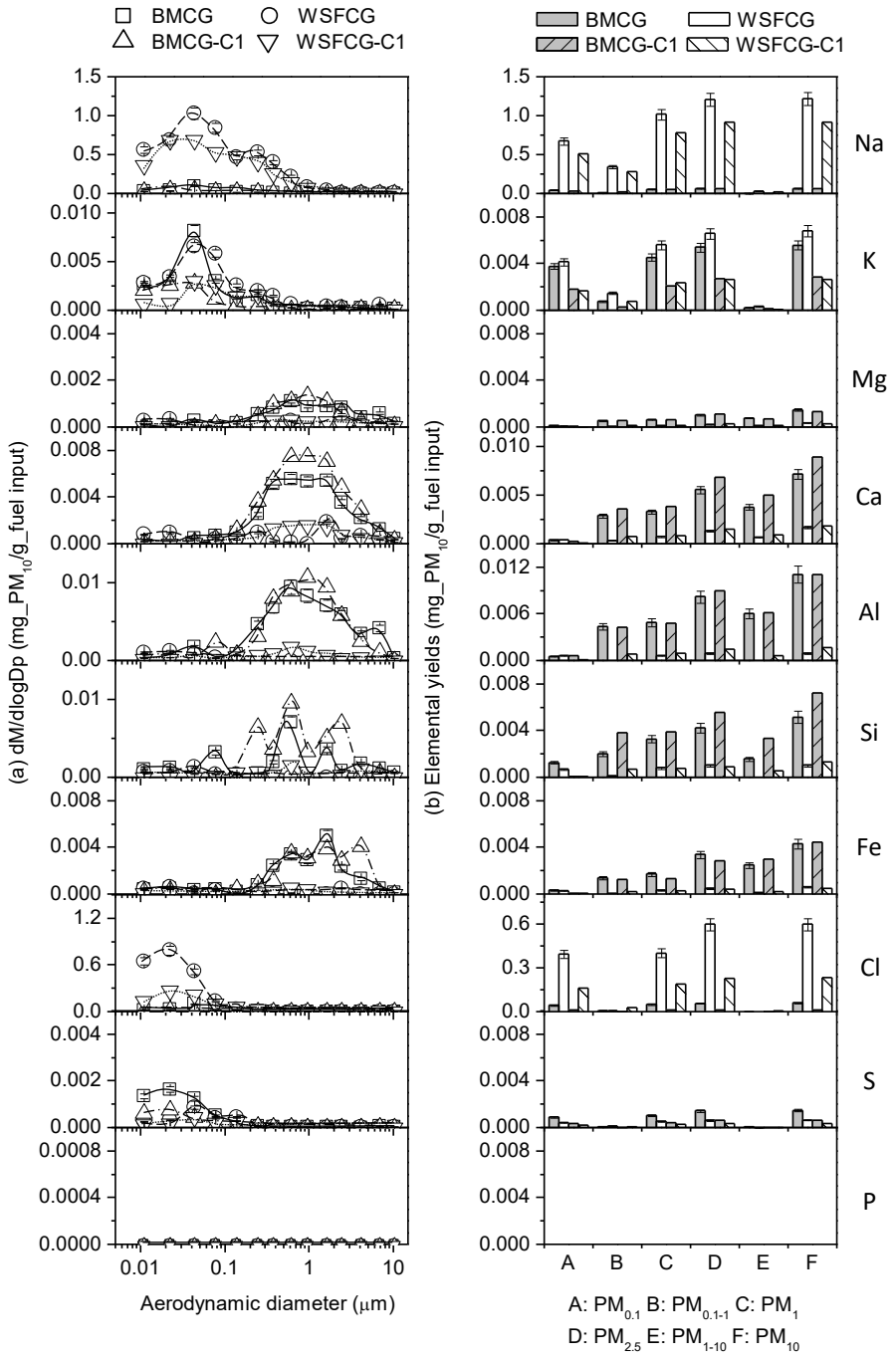

Figure 9-3 Mass-based PSDs (a) and yields (b) of major elements (Na, K, Mg, Ca, Si, Al, Fe, Cl, S, and P) in PM_{10} collected from the combustion of the two fuel blends. The calculated results are also presented for comparisons. All legends are same as those in Fiure 9-1.

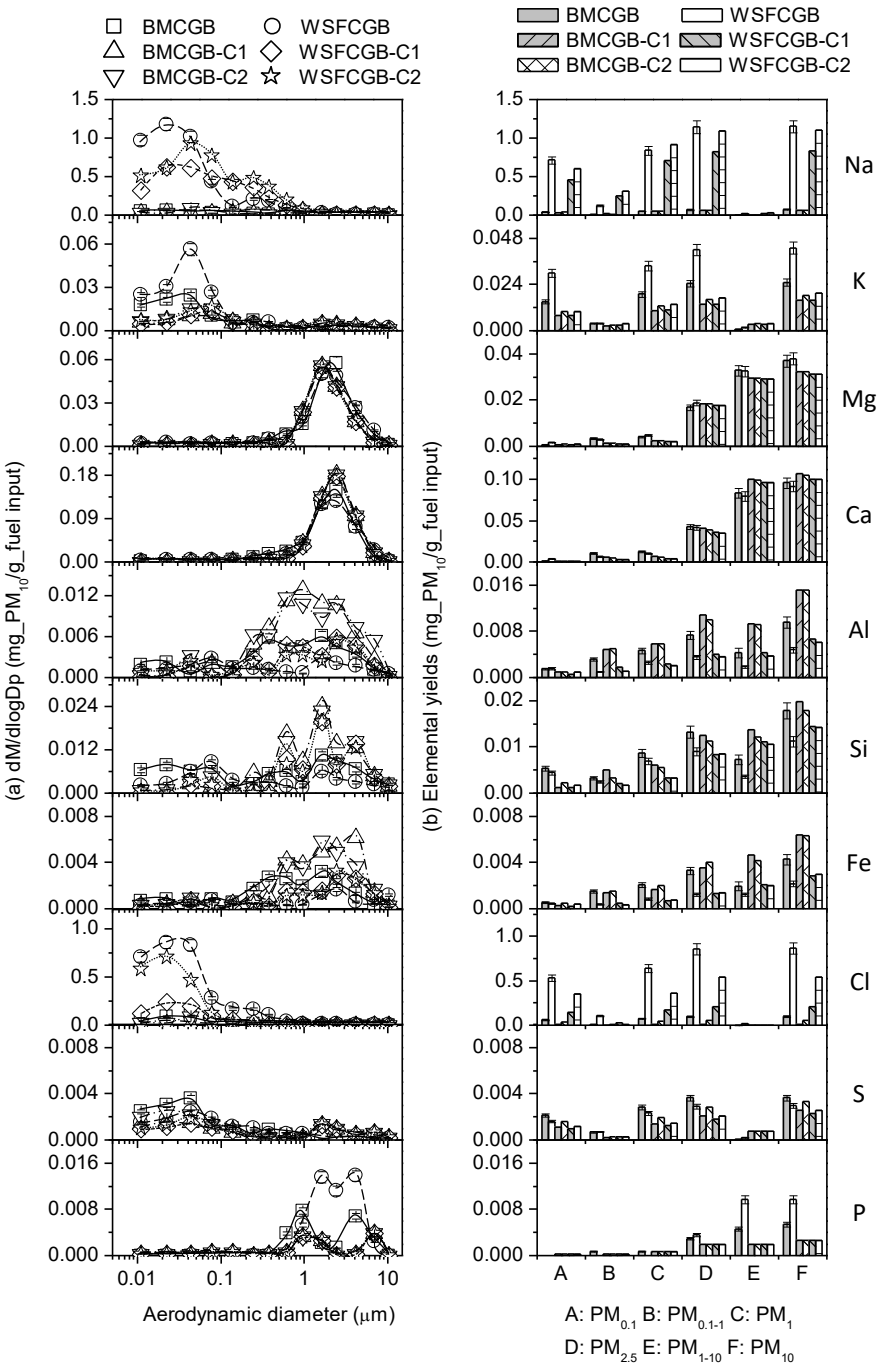

Figure 9-4 Mass-based PSDs (a) and yields (b) of major elements (Na, K, Mg, Ca, Si, Al, Fe, Cl, S, and P) in PM_{10} collected from the combustion of the two slurry fuels. The calculated results are also presented for comparisons. All legends are same as those in Figure 9-1.

slurries are predominantly contributed by the combustion of the biochar fraction so that the presence of these refractory elements in PM_{1-10} can be explained by the mechanisms of catalysed sintering and coalescence.[66] However, the PSDs of the refractory elements in PM_{10} produced from the combustion of the blend fuel BMCG exhibit unimodal distributions with a mode peak at ~1.0 μm, which is smaller than those ~2.438 μm for the cases of biochar and two slurries. Such differences indicate

the weakened ash particle growth of these refractory elements during the combustion of the BMCG in comparison to that of biochar and two slurries. Furthermore, it is noteworthy that the emission of these refractory elements in PM_{10} from the combustion of the WSFCG blend is negligible, apparently due to the fact that both the concentrations of the refractory elements in the fuel (see Table 9-1) are very low. Another interesting finding from Figures 9-3 and 9-4 is that the emissions of Cl in PM_1 produced from the combustion of the CG-containing fuel mixtures (i.e., the two blends of BMCG and WSFCG, and two slurries of BMCGB and WSFCGB) are considerably higher than those from the combustion of other biofuels including bio-oil, biochar, WSF, BB, and WSFB (see Figures 9-5−9-7). This can be attributed to the high Cl contents of the BMCG, WSFCG, BMCGB, and WSFCGB (see Table 9-1). CG has a high Cl content (see Table 9-1) and its combustion results in high Cl emission in PM_1 (see Figure 9-5).

9.3 Effect of Interactions between CG and Fuel Components on PM_{10} Emission during Combustion

A close examination on the experimental results presented in Figures 9-1, 9-3, and 9-4 suggests that there are synergies on PM_{10} emission during the combustion of the CG-containing fuel blends and slurry fuels. Further efforts were then taken to calculate PM_{10} emission from the combustion of each fuel mixture via direct addition of the experimental results on PM_{10} emission for individual fuel components in the fuel mixture. For BMCG, WSFCG, BMCGB and WSFCGB, the predicted values were calculated via direct additions of the PM_{10} emission from individual fuel components (i.e., biochar, bio-oil, WSF, and CG) in these fuel mixtures, presented as "BMCG-C1", "WSFCG-C1", "BMCGB-C1" and "WSFCGB-C1" in Figures 9-1, 9-3, and 9-4, respectively. Similar calculations were also done for BB and WSFB (presented as "BB-C1" and "WSFB-C1" in Figure 9-2 and 9-7) for understanding the synergy taking place during the combustion of BMCGB and WSFCGB. This study also considers one additional calculation method for BMCGB and WSFCGB, i.e. direct addition of PM_{10} emission from the fuel blend and biochar, with the calculated values presented as "BMCGB-C2" and "WSFCGB-C2" in Figures 9-1, 9-3, and 9-4. The comparisons between the experimental results and the calculated values for the

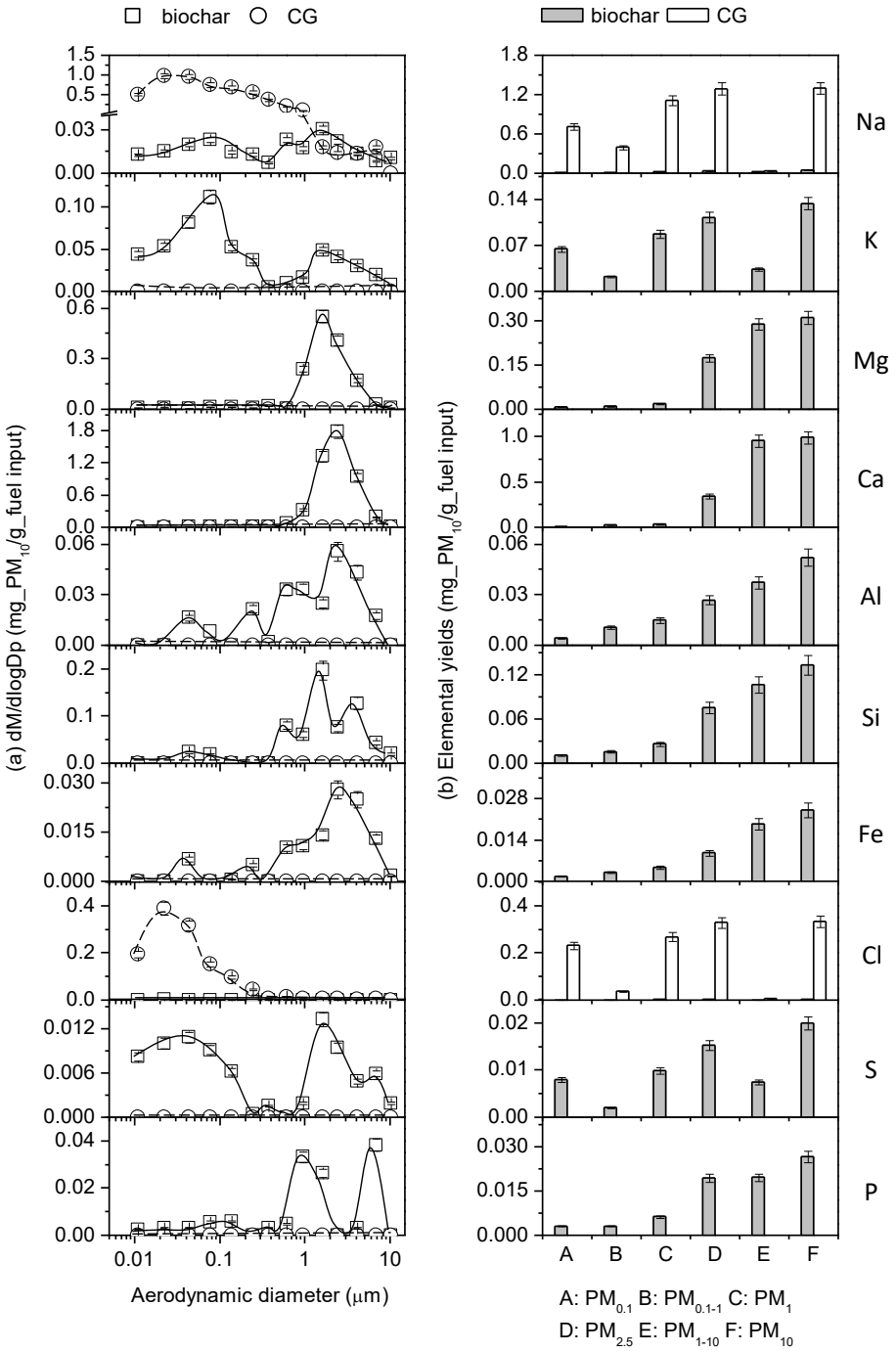

Figure 9-5 Mass-based PSDs (a) and yields (b) of major elements (Na, K, Mg, Ca, Si, Al, Fe, Cl, S, and P) in PM_{10} collected from the combustion of biochar and formulated crude glycerol (CG).

fuel mixtures lead to three important observations on PM_{10} emission during the combustion of fuel mixtures.

First, synergy is evident in Figure 9-1 that show the experimental results on PM_1 emission from the combustion of the CG-containing fuel blends (i.e. BMCG and WSFCG) are higher than the calculated values (i.e. BMCG-C1 and WSFCG-C1). Clearly, interactions take place between CG and bio-oil/WSF during fuel mixture

combustion, leading to increased PM_1. Figure 9-3 further shows that these are results of increases in volatile elements including Na, K and Cl in PM_1. As shown in Figure 9-3, the increase in Cl is dominantly contributed by CG combustion. The results could be explained by that the abundant Cl released from CG enhances chlorination of these volatile elements during the combustion of the CG-containing mixtures and then increases the PM_1 emission.[154,165]

Second, the influence of synergy between the liquid phase and solid phase of slurry fuels on PM_{10} emission during combustion is also demonstrated by the experimental results presented in Figure 9-2. It can be seen in Figure 9-2 that the emissions of PM_1 from the combustion of BB and WSFB are higher than the respective calculated values (i.e. BB-C1 and WSFB-C1), while, those of PM_{1-10} show the opposite. The results presented in Figure 9-7 further show that these are results of increases in both volatile and refractory elements in PM_1 and decreases in these elements in PM_{1-10}. Conclusion in Chapter 8 has revealed that two key mechanisms, i.e. leaching effect and interactions between bio-oil and biochar during combustion, are responsible for such synergistic effects. Both mechanisms result in increased PM_1 emission and decreased PM_{1-10} emission. The leaching effect refers to the leaching of both volatile and refractory inorganic species from biochar into bio-oil or WSF due to the acidic nature of bio-oil.[35] The interactions between bio-oil and biochar during combustion refer to volatile-char interactions that enhances PM_1 emission[69] and enhanced char fragmentation that shifts some of refractory inorganic species in PM_{1-10} into PM_1.[307]

Third, Figure 9-1 also shows that the results on PM_1 emission from the combustion of the CG-containing fuel slurries (i.e. BMCGB and WSFCGB) are higher than the calculated values (i.e. BMCGB-C2 and WSFCGB-C2). Figure 9-4 further shows that such increases are results of increases in both volatile and refractory inorganic elements in PM_1. These can be at least partially attributed to the same mechanisms for the interactions between biochar and bio-oil (or WSF), as discussed for the second observation. Moreover, such interactions between biochar and CG-containing fuel blend (BMCG or WSFCG) are intensified due to the enhanced chlorination of both volatile and refractory inorganic species in biochar during the combustion of CG-containing fuel slurries due to the abundant presence of Cl in CG. This is evident by the increases in Al, Si and Fe in $PM_{0.1}$ and the decreases these elements in PM_{1-10}

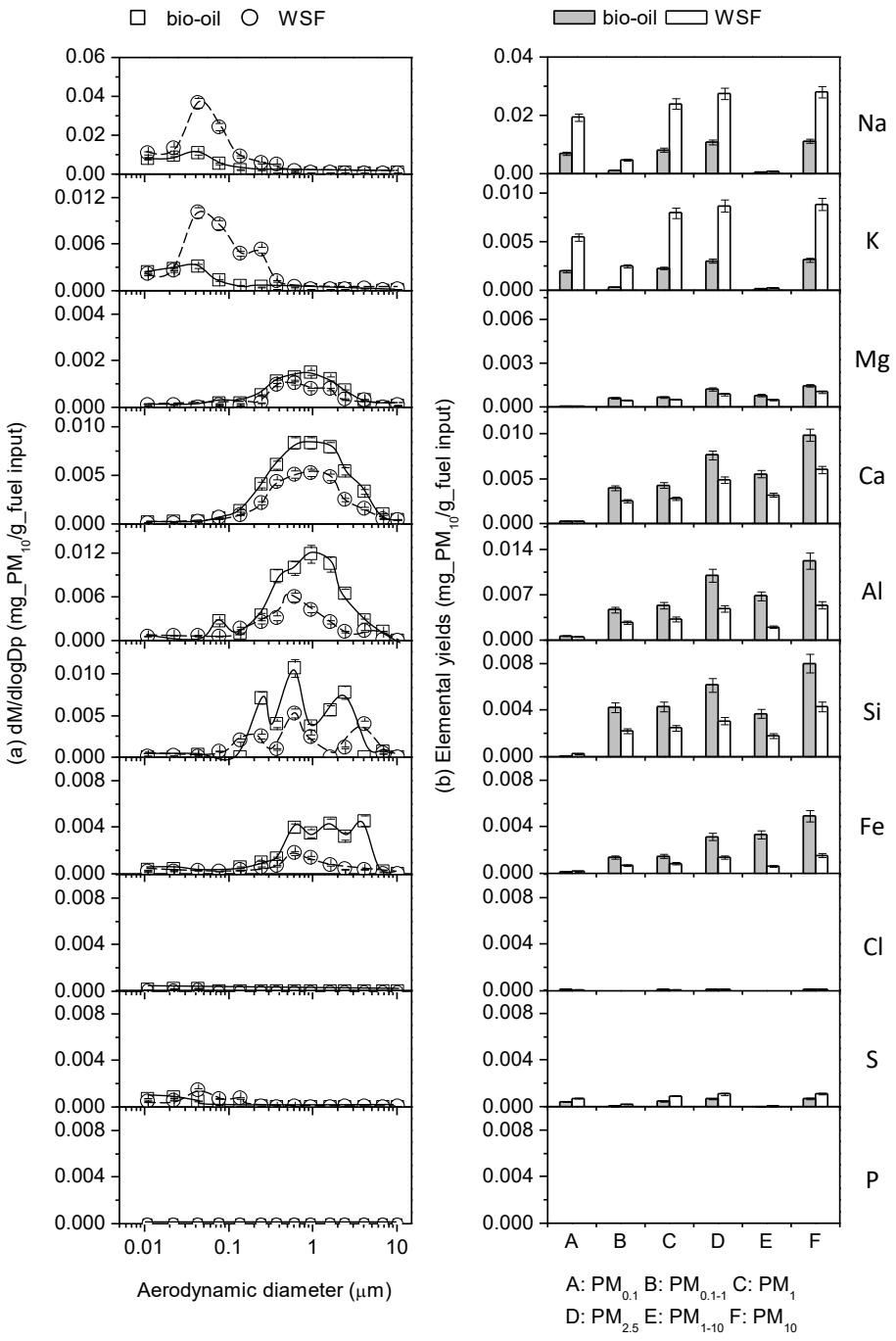

Figure 9-6 Mass-based PSDs (a) and yields (b) of major elements (Na, K, Mg, Ca, Si, Al, Fe, Cl, S, and P) in PM_{10} collected from the combustion of the bio-oil and water-soluble fraction of bio-oil (WSF).

(see Figure 9-4). Chlorination of oxides of Al, Si and Fe is known to take place under local reducing conditions.[308-310] Figure 9-4 also shows that volatile inorganic species for BMCGB-C1 (or WSFCGB-C1) are lower than that for BMCGB-C2 (or WSFCGB-C2). The results indicate that chlorination of volatile inorganic species originated from the liquid phase (i.e. BMCG and WSFCG) also take place during the combustion of CG-containing slurry fuels.

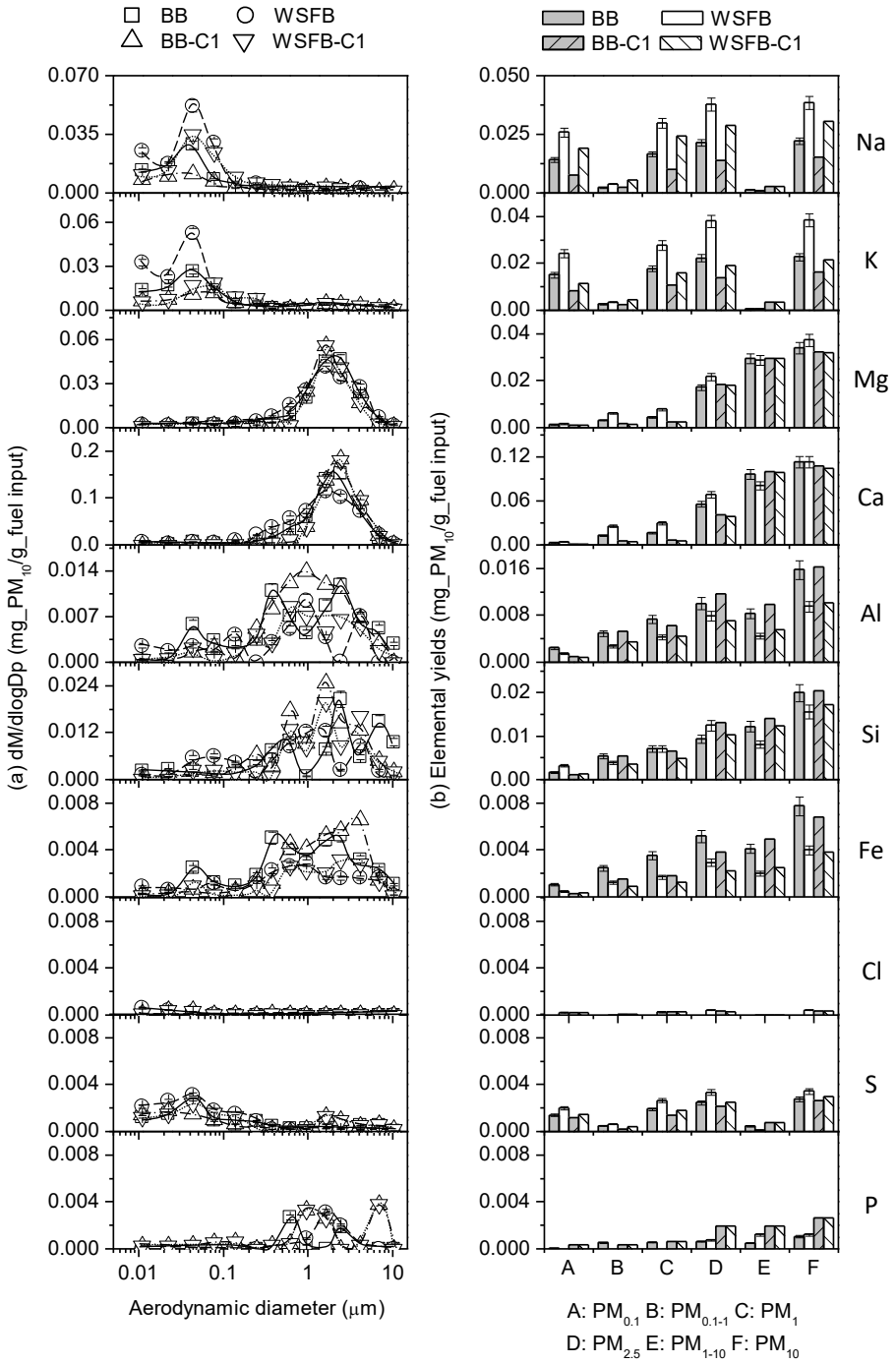

Figure 9-7 Mass-based PSDs (a) and yields (b) of major elements (Na, K, Mg, Ca, Si, Al, Fe, Cl, S, and P) in PM_{10} collected from the combustion of the bio-oil/biochar slurry and WSF/biochar slurry. WSF means water-soluble fraction of bio-oil. The calculated results are also presented for comparisons. All legends are same as those in Fiure 9-1.

9.4 Conclusions

A systematic investigation was carried out for PM_{10} emission from the combustion of various CG-containing fuel mixtures. The results show that the combustion of CG-containing slurry fuels (i.e. BMCGB or WSFCGB) produce PM_{10} having bimodal distributions of PM_{10} with a fine mode at ~0.022 μm and a coarse mode at

~2.438 μm. However, the combustion of CG-containing fuel blends (i.e. BMCG or WSFCG) produce PM_{10} having unimodal distributions with a fine mode at ~0.043 μm. During the combustion of BMCG and WSFCG, ~88.2% and ~99.3% of the total PM_{10} is distributed in PM_1, respectively. The introduction of biochar increases the PM_{1-10} to ~53.1% and ~8.4% of the total PM_{10}, respectively, during the combustion of BMCGB and WSFCGB. Synergistic effect takes place on PM_{10} emission during the combustion of CG-containing biofuel mixtures. For CG-containing fuel blends, the Cl originated from CG enhances chlorination of volatile inorganic species in the fuel blends and increases the emissions of these species in PM_1. For CG-containing slurry fuels, chlorination is also enhanced for both volatile and refractory inorganic species in biochar, resulting in increases of both volatile and refractory inorganic species in PM_1 and decreases of refractory inorganic species in PM_{1-10}.

Chapter 10 Trace Elements in Various Individual and Mixed Biofuels: Abundance and Release in Particulate Matter during Combustion

10.1 Introduction

Biofuels derived from biomass fast pyrolysis including bio-oil, biochar, and bio-oil/biochar mixture (i.e. bioslurry), are promising substitutions for coal in stationary combustion applications because of the renewable nature and small carbon footprint of these fuels.[11,20,32] Mixing bio-oil (or its water-soluble fraction i.e. WSF) with crude glycerol (CG) that is a waste by-product of biodiesel production, with or without biochar addition, has been demonstrated to produce mixed biofuels that overcome at least some of undesired fuel properties (e,g. high viscosity) of CG and meet specifications for combustion in stationary power stations.[35,36] One important consideration for any fuel combustion in stationary power stations is emission of particulate matter (PM). On the one hand, PM emitted into atmosphere has adverse impacts on human health.[41] Trace elements in the emitted PM are of particular concerns because of the toxicological effect of these elements.[311] On the other hand, current cleaning devices such as electrostatic precipitators have low efficiency and high cost to capture PM.[312,313]

Trace elements in coal and the release of trace element during coal combustion have been extensively studied.[51,79,84,151] Trace elements can be grouped into three groups (Group I: non–vaporisation; Group II: vaporisation–condensation; and Group III: vaporization–non-condensation) based on respective volatilities during coal combustion.[51,84,151] Correlated to this classification, some trace elements can be partitioned in both bottom ash and fly ash (e.g. Mn, Ti, Ni, V, Cr, Cu, Co, Zn, Pb, Cd, and As) while others can be completely released in the vapor phase (e.g. Hg, Cl, and Br). There have been various reports on the abundance of major elements (e.g. Na, K, Mg, Ca, Al, Si, and Fe) in biofuels and the emission of these major elements in PM during the combustion of these biofuels (including bio-oil,[285] biochar,[67] bioslurry,[303] crude glycerol[75] and mixed biofuels[314]). There have also been reports on the emission of trace elements during the combustion of solid fuels such as coal, biomass and

solid wastes.[84,89,315,316] However, the abundance of trace elements in the mixed biofuels (liquid or slurry) based on bio-oil and/or biochar and the emission of trace elements during the combustion of these mixed fuels have been seldom reported. In addition, the substitution of these biofuels for conventional fuels (e.g. coal) in stationary combustion applications is on an energy basis.[7] Therefore, benchmarking of trace element emission on a unit energy basis for these individual and mixed biofuels against conventional fuels is essential and of practical importance. Furthermore, for mixed biofuels which consists of various fuel components, synergy may also take place during the combustion and such synergy may affect PM_{10} emission. This was demonstrated in a recent study that studied the release of major elements in PM with aerodynamic diameter of less than 10 μm (PM_{10}) during the combustion of bio-oil/biochar slurry (bioslurry).[307] It was also reported that chlorine (Cl) can strongly influence the transformation of inorganic species during combustion.[60,63,64,154,186] Therefore, as the major impurity in CG,[34] Cl in CG may play an important role in the transformation of trace elements during the combustion of these mixed biofuels. However, there have been little reports on these important aspects concerning the abundance of trace element in these individual and mixed biofuels and the emission of trace elements during the combustion of these biofuels.

Therefore, the objective of this study is to investigate trace element emission in PM_{10} from the combustion of various individual and mixed biofuels based on bio-oil and biochar in a laboratory-scale drop-tube-furnace (DTF) at 1400 °C in air. In this study, eleven trace elements are considered and analysed, including Ti, V, Cr, Mn, Ni, Co, Cu, Zn, As, Cd, and Pb. The emission of these trace elements in PM_{10} is also benchmarked and compared on the bases of both mass and energy input.

10.2 Trace Elements in Individual and Mixed Biofuels

Table 10-1 and Table 10-2 lists the general properties and concentrations of trace elements (including Ti, V, Cr, Mn, Ni, Co, Cu, Zn, As, Cd, and Pb) based on both mass and energy input basis of the individual and mixed biofuels (biochar, bio-oil, WSF, CG, blend-1, blend-2, slurry-1, slurry-2, slurry-3, and slurry-4). It can be seen from Table 10-2 that there is little trace element in the CG that was formulated from analytical-grade glycerol, sodium chloride and deionised water based on the compositions of CG in practice.[36] This is important because CG product contains

little trace elements[117] and the formulated CG provides a simple system for studying the synergy of Cl in CG on the emission of trace elements from other fuel components during mixed biofuels combustion. Practically, benchmarking of trace elements in these biofuels based on energy input (in addition to mass) is of great important because substitutions of these biofuels for coal in the boiler are on the same basis of energy input.

There are two important observations from the results in Table 10-2. One is that biochar has the highest concentrations of trace elements, on both mass and energy input bases, in comparison to the other biofuels. The concentration of total trace elements from biochar on mass and energy bases are ~110.838 mg/kg and ~4.398 mg/MJ, respectively. This is reasonable as after pyrolysis under the conditions for bio-oil production, the majorities of the inorganic species in biomass would be retained in biochar.[26,121,317] The retentions of these trace elements are clearly seen in the bio-oil and WSF samples, indicating that these trace element species were released into volatiles during pyrolysis.[121] As results of the high concentrations of trace elements in biochar, the concentrations of trace elements in slurry fuels are higher than the respective liquid fuel components in the slurry fuels. These are clearly evident on both mass and energy bases for slurry-1 (~21.664 mg/kg and ~1.252 mg/MJ), slurry-2 (~16.725 mg/kg and ~1.506 mg/MJ), slurry-3 (~20.558 mg/kg and ~1.209 mg/MJ), and slurry-4 (~12.543 mg/kg and ~0.896 mg/MJ), in comparison to bio-oil (~12.212 mg/kg and ~0.744 mg/MJ), WSF (~9.875 mg/kg and ~1.039 mg/MJ), blend-1 (~10.990 mg/kg and ~0.682 mg/MJ), and blend-2 (~2.756 mg/kg and ~0.215 mg/MJ), respectively.

The other is that Zn and Mn are the most abundant trace elements in these biofuels. For example, for biochar, Mn accounts for ~43.1% of the total trace elements, followed by Ni (~17.8%), Zn (~16.3%), Cr (~10.8%), Ti (~6.3%), Cu (~4.7%), and the rest ~1.0% shared by V, Co, As, Cd, and Pb. For bio-oil, WSF, the two blend fuels, and the four slurry fuels, Zn accounts for ~23.2−57.4% of the total trace elements, followed by Mn (~15.5−37.9%), Ni (~7.7−16.1%), Cr (~4.8−10.4%), Cu (~5.0−7.4%), Ti (~0.7−5.9%), Pb (~0.9−3.4%), Cd (~0.6−2.6%), and the rest shared by As, Co, and V. Figure 10-1 further presents the distribution of these trace elements in the liquid fuel and biochar fractions of various slurry fuels. It can be seen

that Ti, V, Cr, Mn, Ni, and Co in slurry fuels are mainly contributed by the biochar fraction (accounting for ~52.9−97.6%), while, elements of Cu, Zn, As, Cd, and Pb in slurry fuels (except Cu, Zn, and As for slurry-4) are mainly from the liquid fuel fraction (accounting for ~51.7−91.3%). In the case of slurry-4, Cu, Zn, and As are dominantly contributed from biochar (accounting for ~55.0−72.9%). In fact, for all the eleven elements in slurry-4, the contributions from the liquid fuel fraction are lower compared to the rest slurry fuels. Such low contributions of the liquid fuel fractions can be attributed to the high proportion of CG which has diluted these trace elements in the liquid fraction (i.e. WSF/CG) of slurry-4.

10.3 Release of Trace Elements in PM_{10} from the Combustion of Individual and Mixed Biofuels

Figures 10-2−10-4 and Tables 10-3−10-5 present the PSDs and yields of trace elements (i.e., Ti, V, Cr, Mn, Ni, Co, Cu, Zn, As, Cd, and Pb) in PM_{10} emission from the combustion of the individual biofuels (i.e., biochar, bio-oil, WSF, and CG) and mixtures (i.e., blend-1, blend-2, slurry-1, slurry-2, slurry-3, and slurry-4) based on fuel mass input, respectively. Indeed, there is little emission of trace elements in PM_{10} during CG combustion (seen Table 10-3). In this study, the results on the eleven trace elements are discussed based on the classic categorisation of trace elements[151] into Group I (non-vaporisation), Group II (vaporisation-condensation) and Group 3 (volatile) trace elements based on the volatilities of these trace elements.

Group 1 includes Ti, Mn, Ni, and Co. Figures 10-2−10-4 show that the PSDs of Ti, Mn, Ni, and Co in PM_{10} from combustion of most biofuels have unimodal distributions with a coarse mode at ~2.4 μm. The exceptions are PSDs of Ti from the combustion of the WSF and blend-2, and PSDs of Mn and Ni from the combustion of blend-2, for which the concentrations of Ti, Mn and Ni in WSF (see Table 10-3) and blend-2 (see Table 10-4) are low hence almost no modes are observed in the elemental PSDs of these trace elements in PM_{10} for these two biofuels (see Figure 10-3). For other biofuels, ~58.5−89.8% of Ti, Mn, Ni, and Co in PM_{10} is distributed in $PM_{1\text{-}10}$, indicating that these elements favour transfer into $PM_{1\text{-}10}$ during the combustion of those biofuels. This is reasonable because Ti, Mn, Ni, and Co are

commonly grouped as non-vaporisation elements because of non-volatile nature (high melting/boiling points).[79,311] During the combustion process, the oxide crystals of these elements would retain in the burning char particles and/or undergo coalescence to form PM_{1-10}.

Group 2 consists of V, Cr, Cu, Zn, As, and Cd. During the combustion of liquid fuels (i.e., bio-oil, WSF and the two blends), these trace elements are presented in PM_1 and the respective elemental PSDs have unimodal distributions. For example, in Figure 10-3 the PSDs of Cu, Zn, As, and Cd in PM_{10} show unimodal distributions with a fine mode at ~0.043 μm and V and Cr in PM_{10} have unimodal distributions with a fine mode at ~0.077 μm. It is noted that the concentrations of V and Cr in blend-2 are very low so that the emission of V and Cr from blend-2 combustion is negligible. However, during the combustion of biochar (for all the Group 2 elements) or slurry fuels that contain biochar (for V and Cr), these elements contribute to both PM_1 and PM_{1-10}. As shown in Figures 10-2 and 10-4, the PSDs of these trace elements in PM_{10} have bimodal distributions including a fine mode at ~0.043μm and a coarse mode at ~1.6 μm. The presence of these Group 2 trace elements in PM_1 during biofuel combustion can be attributed to the formation of volatile species (oxides or chlorides[68]) that subsequently undergo homogeneous nucleation, and/or heterogeneous condensation during combustion.[64] However, the presence of these trace elements in PM_{1-10} requires the presence of biochar particles so that agglomeration of fine ash particles (with high melting/boiling points, formed between these trace elements and refractory elements such as Mg, Ca, Al, Si, and Fe) is possible to form PM_{1-10} during combustion.[83,248] It is also noted that ~44.9−85.8% of these trace elements in PM_{10} is distributed in PM_1 during biochar combustion while ~51.1−98.5% of these trace elements in PM_{10} is distributed in PM_1 during the combustion of liquid and slurry fuels. The results indicate that the presence of liquid or blend fuels enhances the release of these trace elements in biochar as part of PM_1.

Table 10-1 Fuel properties of individual and mixed biofuels.

samples	proximate analysis (wt%, ar[a])				elemental analysis (wt%, ar[a])					density (g/ml, ar[a])	surface tension (20 °C, mN/m)	viscosity (20 °C, mPa s)	LHV[c] (MJ/kg)
	moisture/ water	ash	volatile matter	fixed carbon	C	H	N	S	O[b]				
biochar	2.4±0.1	1.30±0.2[d]	25.0±0.7[d]	73.7±0.7[d]	77.93±0.03[d]	3.20±0.02[d]	0.11±0.01[d]	0.20±0.01[d]	18.56	0.55±0.01	na[e]	na[e]	25.2
bio-oil	24.8±0.5	≤0.01	73.1±1.0	2.1±1.0	42.46±0.05	7.17±0.10	0.07±0.01	≤0.01	50.29	1.19±0.01	31.9±0.7	158.9±2.0	16.4
WSF[f]	64.1±1.0	≤0.01	32.3±1.0	3.6±0.3	18.94±0.08	8.77±0.05	≤0.01	≤0.01	72.27	1.07±0.01	42.3±0.2	5.8±0.1	9.5
CG[f]	16.0[g]	4.00[g]	80.0[g]	0.0[g]	31.30[g]	8.73[g]	0.00[g]	0.00[g]	59.97	1.23±0.01	52.0±0.5	81.4±2.0	14.2
blend-1[f]	29.0±0.3	0.17±0.1	53.9±1.0	16.9±1.1	41.24±0.05	7.44±0.02	0.05±0.01	≤0.01	51.26	1.16±0.01	24.8±0.2	74.8±2.4	16.1
blend-2[f]	30.4±0.3	2.80±0.1	65.6±1.2	1.2±0.1	27.58±0.02	8.74±0.05	<0.01	<0.01	63.68	1.19±0.10	46.8±0.6	21.4±0.6	12.8
slurry-1[f]	22.9±0.5	0.14±0.1	53.7±1.1	23.2±1.2	46.01±0.02	6.77±0.01	0.06±0.01	0.03±0.01	47.13	1.20±0.01	35.2±0.4	463.5±3.8	17.3
slurry-2[f]	58.0±0.9	0.14±0.1	29.8±0.9	12.0±0.9	24.81±0.07	8.22±1.60	0.02±0.01	0.03±0.01	66.92	1.11±0.01	44.7±0.5	8.8±0.7	11.1
slurry-3[f]	26.2±0.2	0.28±0.1	51.4±1.2	22.1±1.2	46.70±0.04	6.02±0.01	0.06±0.01	0.03±0.01	47.19	1.19±0.02	33.7±0.2	185.9±0.9	17.0
slurry-4[f]	27.5±0.8	2.65±0.1	62.8±1.8	7.0±0.6	32.62±0.02	8.19±0.05	≤0.01	0.02±0.01	59.16	1.21±0.02	49.4±0.2	49.9±0.4	14.0

[a] as-received basis for bio-oil, WSF, CG, blend-1, blend-2, slurry-1, slurry-2, slurry-3 and slurry-4; [b] by difference; [c] lower heating value based on calculation; [d] dry basis; [e] not applicable; [f] WSF stands for water-soluble fraction of bio-oil, CG stands for crude glycerol, blend-1 stands for bio-oil/methanol/CG blend, blend-2 stands for WSF/CG blend, slurry-1 stands for bio-oil/biochar slurry, slurry-2 stands for WSF/biochar slurry, slurry-3 stands for bio-oil/methanol/CG/biochar slurry, slurry-4 stands for WSF/CG/biochar slurry; [g] calculated values based on formula.

Table 10-2 Concentrations of trace elements (Ti, V, Cr, Mn, Ni, Co, Cu, Zn, As, Cd, and Pb) and Cl in various individual and mixed biofuels

concentration		biochar	bio-oil	WSF[a]	CG[a]	blend-1[a]	blend-2[a]	slurry-1[a]	slurry-2[a]	slurry-3[a]	slurry-4[a]
Ti	(mg/kg[b])	7.007±0.695	0.666±0.052	0.007±0.001	0.007±0.001	0.599±0.057	0.002±0.001	1.274±0.092	0.681±0.041	1.214±0.053	0.676±0.314
	(mg/MJ[c])	0.278±0.027	0.040±0.003	≤0.001	<0.001	0.037±0.004	<0.001	0.074±0.006	0.061±0.004	0.071±0.004	0.048±0.022
V	(mg/kg[b])	0.780±0.038	0.041±0.005	0.046±0.006	≤0.001	0.036±0.003	0.016±0.002	0.112±0.002	0.130±0.015	0.101±0.001	0.089±0.002
	(mg/MJ[c])	0.031±0.002	0.002±0.001	0.005±0.001	<0.001	0.002±0.001	≤0.001	0.006±0.001	0.012±0.002	0.006±0.001	0.006±0.001
Cr	(mg/kg[b])	11.956±0.587	0.591±0.039	0.673±0.032	0.005±0.001	0.532±0.024	0.232±0.008	1.683±0.097	1.847±0.094	1.630±0.081	1.360±0.397
	(mg/MJ[c])	0.474±0.023	0.036±0.002	0.071±0.003	<0.001	0.033±0.002	0.018±0.001	0.097±0.006	0.166±0.009	0.096±0.005	0.097±0.029
Mn	(mg/kg[b])	47.463±1.373	1.893±0.087	1.464±0.035	0.002±0.001	1.704±0.011	0.439±0.018	6.274±0.224	4.583±0.063	6.104±0.174	4.574±0.114
	(mg/MJ[c])	1.883±0.054	0.115±0.005	0.154±0.004	<0.001	0.106±0.001	0.034±0.002	0.362±0.013	0.413±0.006	0.359±0.011	0.327±0.011
Ni	(mg/kg[b])	19.667±0.778	0.935±0.034	0.705±0.028	0.044±0.007	0.841±0.027	0.243±0.009	2.735±0.063	1.903±0.038	2.651±0.034	1.897±0.134
	(mg/MJ[c])	0.780±0.031	0.057±0.002	0.074±0.003	0.003±0.001	0.052±0.002	0.019±0.001	0.158±0.004	0.171±0.004	0.156±0.002	0.135±0.010
Co	(mg/kg[b])	0.266±0.015	0.016±0.001	0.013±0.001	<0.001	0.014±0.001	0.004±0.001	0.040±0.001	0.039±0.003	0.038±0.001	0.026±0.003
	(mg/MJ[c])	0.010±0.001	≤0.001	≤0.001	<0.001	≤0.001	<0.001	0.002±0.001	0.003±0.001	0.002±0.001	0.002±0.001
Cu	(mg/kg[b])	5.169±0.148	0.657±0.020	0.645±0.025	0.024±0.004	0.591±0.006	0.163±0.006	1.089±0.003	0.988±0.025	1.030±0.027	0.645±0.013
	(mg/MJ[c])	0.205±0.006	0.040±0.001	0.068±0.003	0.002±0.001	0.036±0.001	0.013±0.001	0.063±0.001	0.089±0.003	0.061±0.002	0.046±0.001
Zn	(mg/kg[b])	17.926±0.314	6.985±0.362	5.861±0.285	0.044±0.001	6.287±0.188	1.458±0.060	8.013±0.148	6.102±0.085	7.384±0.274	3.039±0.033
	(mg/MJ[c])	0.711±0.012	0.426±0.013	0.617±0.030	0.003±0.001	0.390±0.012	0.114±0.005	0.463±0.009	0.549±0.008	0.434±0.016	0.217±0.003
As	(mg/kg[b])	0.015±0.004	0.010±0.002	0.004±0.001	0.002±0.001	0.009±0.001	≤0.001	0.010±0.001	0.005±0.001	0.009±0.001	0.002±0.001
	(mg/MJ[c])	≤0.001	≤0.001	<0.001	<0.001	<0.001	<0.001	≤0.001	<0.001	≤0.001	<0.001
Cd	(mg/kg[b])	0.154±0.022	0.172±0.010	0.144±0.004	<0.001	0.155±0.001	0.103±0.005	0.170±0.003	0.124±0.002	0.154±0.016	0.108±0.008
	(mg/MJ[c])	0.006±0.001	0.010±0.006	0.015±0.001	<0.001	0.010±0.001	0.008±0.001	0.010±0.001	0.011±0.001	0.009±0.001	0.007±0.001
Pb	(mg/kg[b])	0.434±0.018	0.245±0.020	0.311±0.011	<0.001	0.220±0.004	0.093±0.002	0.262±0.005	0.322±0.001	0.240±0.010	0.126±0.004
	(mg/MJ[c])	0.017±0.001	0.015±0.001	0.033±0.001	<0.001	0.013±0.001	0.007±0.001	0.015±0.001	0.029±0.001	0.014±0.001	0.009±0.001
total	(mg/kg[b])	110.838±3.938	12.212±0.632	9.875±0.428	0.129±0.015	10.990±0.321	2.756±0.108	21.664±0.636	16.725±0.366	20.558±0.670	12.543±1.022
	(mg/MJ[c])	4.398±0.156	0.744±0.038	1.039±0.045	0.009±0.001	0.682±0.020	0.215±0.008	1.252±0.037	1.506±0.033	1.209±0.039	0.896±0.073
Cl	(mg/kg[b])	nd[d]	22.2±1.1	18.0±0.7	24285.6[e]	990.7±41.6	16994.4±723.1	19.9±2.1	16.2±1.0	891.6±35.5	15294.9±640.8
	(mg/MJ[c])	nd[d]	1.3±0.1	1.9±0.1	1711.4[e]	61.5±2.6	1327.7±56.5	1.1±0.1	1.5±0.1	52.4±2.1	1092.5±45.8

[a] WSF stands for water-soluble fraction of bio-oil, CG stands for crude glycerol, blend-1 stands for bio-oil/methanol/CG blend, blend-2 stands for WSF/CG blend; slurry-1 stands for bio-oil/biochar slurry, slurry-2 stands for WSF/biochar slurry, slurry-3 stands for bio-oil/methanol/CG/biochar slurry, slurry-4 stands for WSF/CG/biochar slurry; [b] as-received basis for bio-oil, WSF, CG, blend-1, blend-2, slurry-1, slurry-2, slurry-3 and slurry-4, dry and ash free basis for biochar; [c] obtained via calculation; [d] not detected; [e] calculated values based on formula.

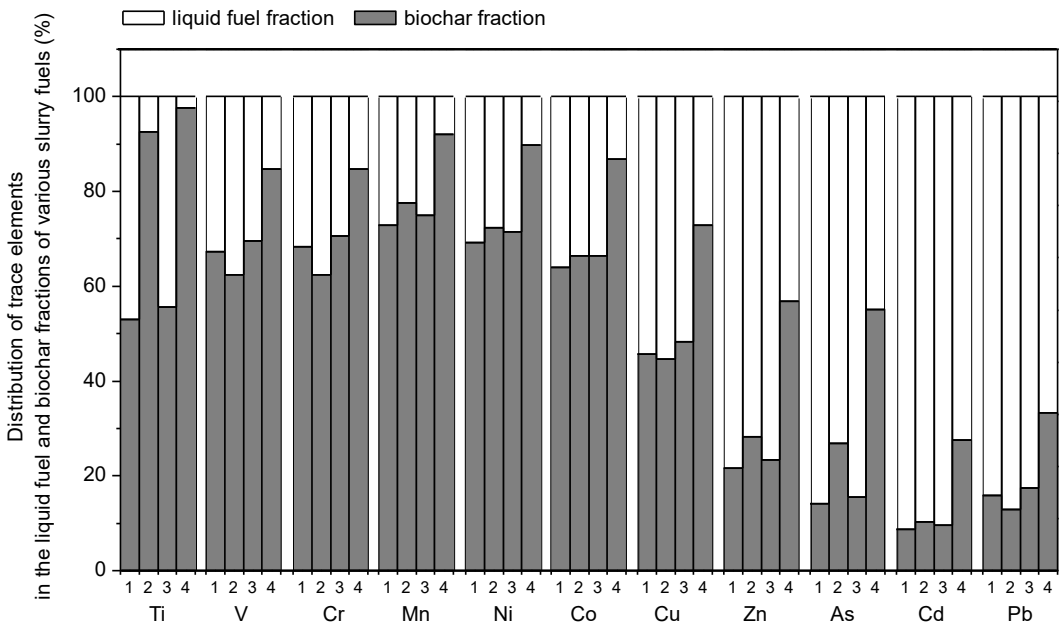

Figure 10-1 Distribution of trace elements (including Ti, V, Cr, Mn, Ni, Co, Cu, Zn, As, Cd, and Pb) in the liquid fuel and biochar fractions of various slurry fuels. The numbers of 1, 2, 3, and 4 in the X-axis stand for slurry-1 (bio-oil/biochar slurry), slurry-2 (WSF/biochar slurry), slurry-3 (bio-oil/methanol/CG/biochar slurry), and slurry-4 (WSF/CG/biochar slurry), respectively. WSF stands for water-soluble fraction of bio-oil. CG stands for crude glycerol.

Group 3 trace element of concern in these biofuels is only Pb. Figures 10-2−10-4 show that the PSDs of Pb in PM_{10} have unimodal distributions with a fine mode at ~0.043 μm from the combustion of all biofuels. These result in ~76.7−98.7% of Pb being distributed in PM_1. This correlates well with Pb being classified as a Group 3 trace element.[80,151] This is also consistent with the report on Pb being released dominantly in PM_1 during biosolid combustion, in the forms of oxides and chlorides.[68]

In practice, substitutions of biofuels for coal in stationary combustion applications would be on the basis of sample energy input into the furnace. Therefore, it is of critical importance to benchmark the emission of trace elements in PM_{10} from the combustion of these biofuels based on energy input. Table 10-6 shows the yields of various trace elements (Ti, V, Cr, Mn, Ni, Co, Cu, Zn, As, Cd, and Pb) and all eleven

elements together as "Total" in PM_1, $PM_{2.5}$, and PM_{10} based on energy input of the fuels. Four important observations can be made from the results presented in Table 10-6. First, biochar has the highest total trace element emission (~0.699 mg/MJ) among the biofuels in this study, followed by slurry fuels (~0.167−0.353 mg/MJ), and then liquid fuels (≤ ~0.132 mg/MJ). Second, emission of trace elements on unit energy basis from biochar mainly contributes to PM_{1-10} (accounting for ~71.0 %), while, that liquid fuels favour in PM_1 (accounting for ~55.8−72.8 %) and for the slurry fuels, trace element emission is almost equally distributed in PM_1 and PM_{1-10}. Third, different biofuels show different capabilities of emission for each trace element. In details, for Ti, Mn, and Ni (Group 1 elements) and V and Cr (Group 2 elements), biochar has substantially higher emissions based on energy input than the rest of biofuels, with Ti, Mn, and Ni mainly contributed to PM_{1-10}, and V and Cr to both PM_1 and PM_{1-10}. For example, the energy based yields of Ti, Mn, Ni, V, and Cr in PM_{10} from biochar combustion are ~0.108, ~0.265, ~0.124, ~0.019, and ~0.120 mg/MJ, which are considerably higher than those from the liquid and slurry fuels with values of less than ~0.031, ~0.111, ~0.068, ~0.006, and ~0.037 mg/MJ, respectively. This correlates well with the concentrations of these trace elements in the biofuels on an energy input basis (see Table 3). While, different to Ti, Mn, Ni, V and Cr, the energy-based emissions of Cu and Zn (Group 2 elements) in PM_{10} (presented mainly in PM_1) from biochar combustion are similar to those of the rest biofuels. In fact, the energy-based emission of Cu (~0.028 mg/MJ) and Zn (~0.031 mg/MJ) from biochar are slightly lower than that of slurry-2 (~0.044 and ~0.039 mg/MJ for Cu and Zn, respectively), but higher than that of the rest of biofuels. For Pb (Group 3 element), the liquid and slurry fuels have relatively higher emission in PM_{10} (especially in PM_1) than biochar based on the same energy input. The energy-based yield of Pb in PM_{10} is ≤ 0.001mg/MJ from biochar, which is lower than ~0.003−0.014 mg/MJ from the liquid and slurry fuels. Lastly, on an energy input

basis, the yields of trace elements in PM_{10} during combustion of these biofuels roughly follow a decreasing order of Mn, Ni, Cr, Ti, Cu (Zn), V, Pb, Cd, Co (As).

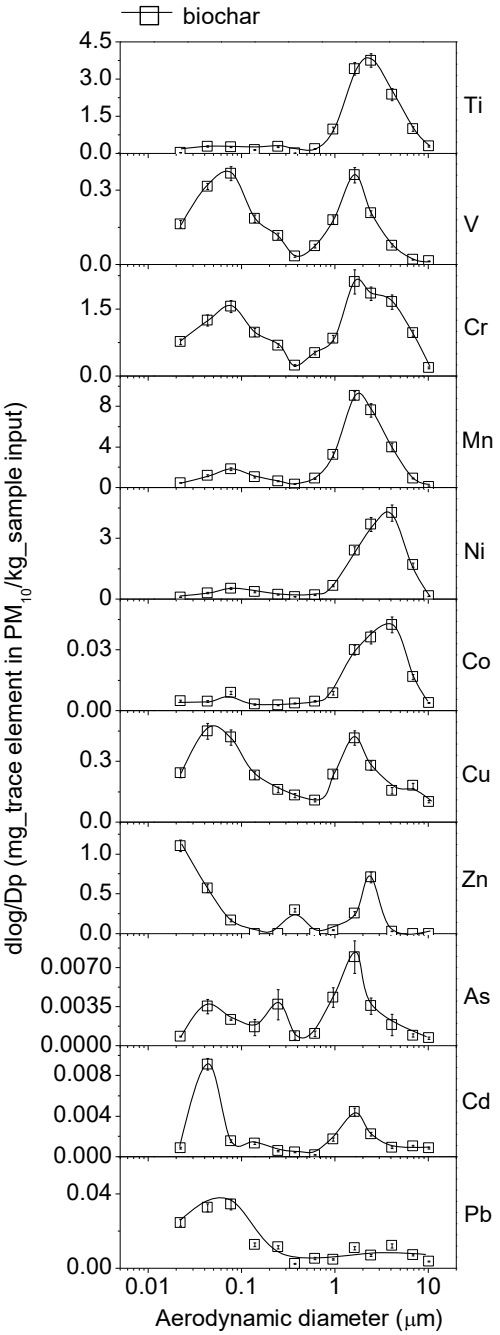

Figure 10-2 Mass-based particle size distributions (PSDs) of Ti, V, Cr, Mn, Ni, Co, Cu, Zn, As, Cd, and Pb in PM_{10} collected from the combustion of biochar.

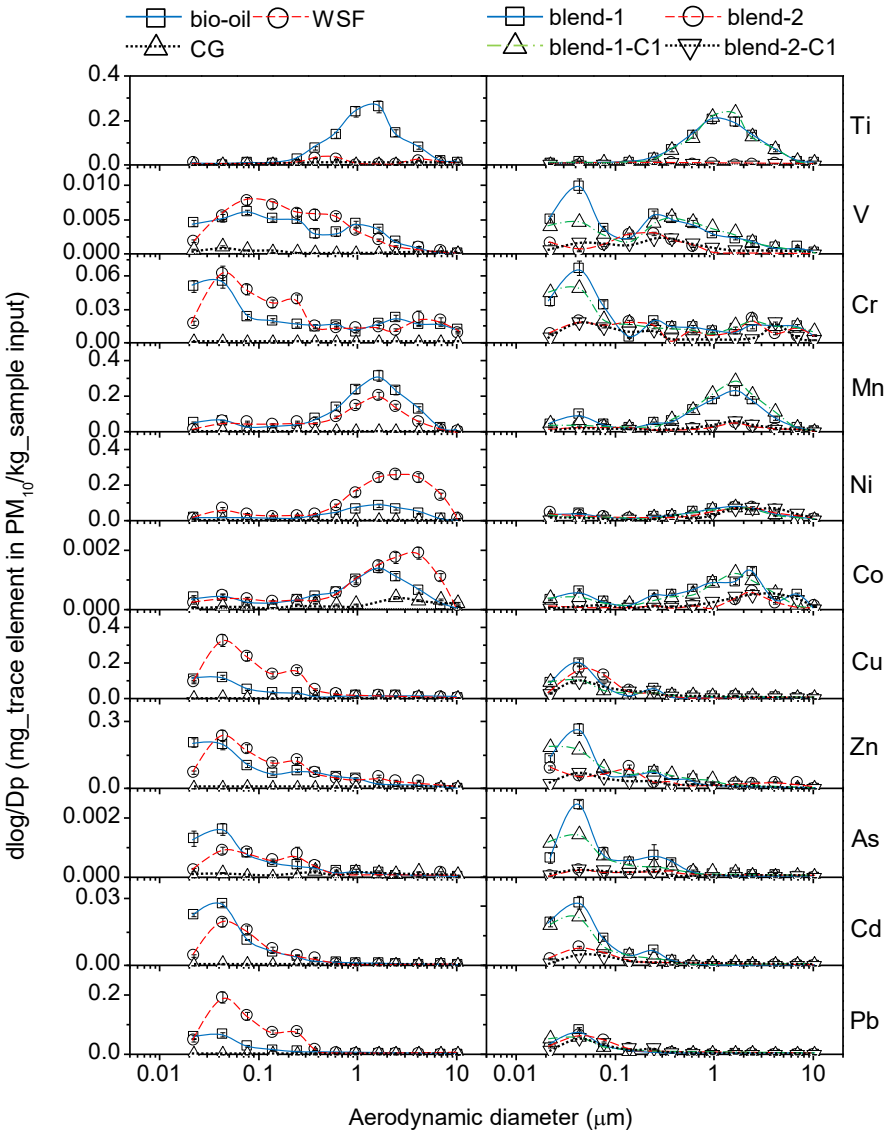

Figure 10-3 Mass-based particle size distributions (PSDs) of Ti, V, Cr, Mn, Ni, Co, Cu, Zn, As, Cd, and Pb in PM_{10} collected from the combustion of bio-oil, WSF (water-soluble fraction of bio-oil), CG (crude glycerol), and two fuel blends, i.e., blend-1 (bio-oil/methanol/CG blend) and blend-2 (WSF/CG blend), respectively. The respective cases suffixed with "-C1" represent the calculated results via direct addition of the experimental results for individual parent fuels (bio-oil, WSF and CG)..

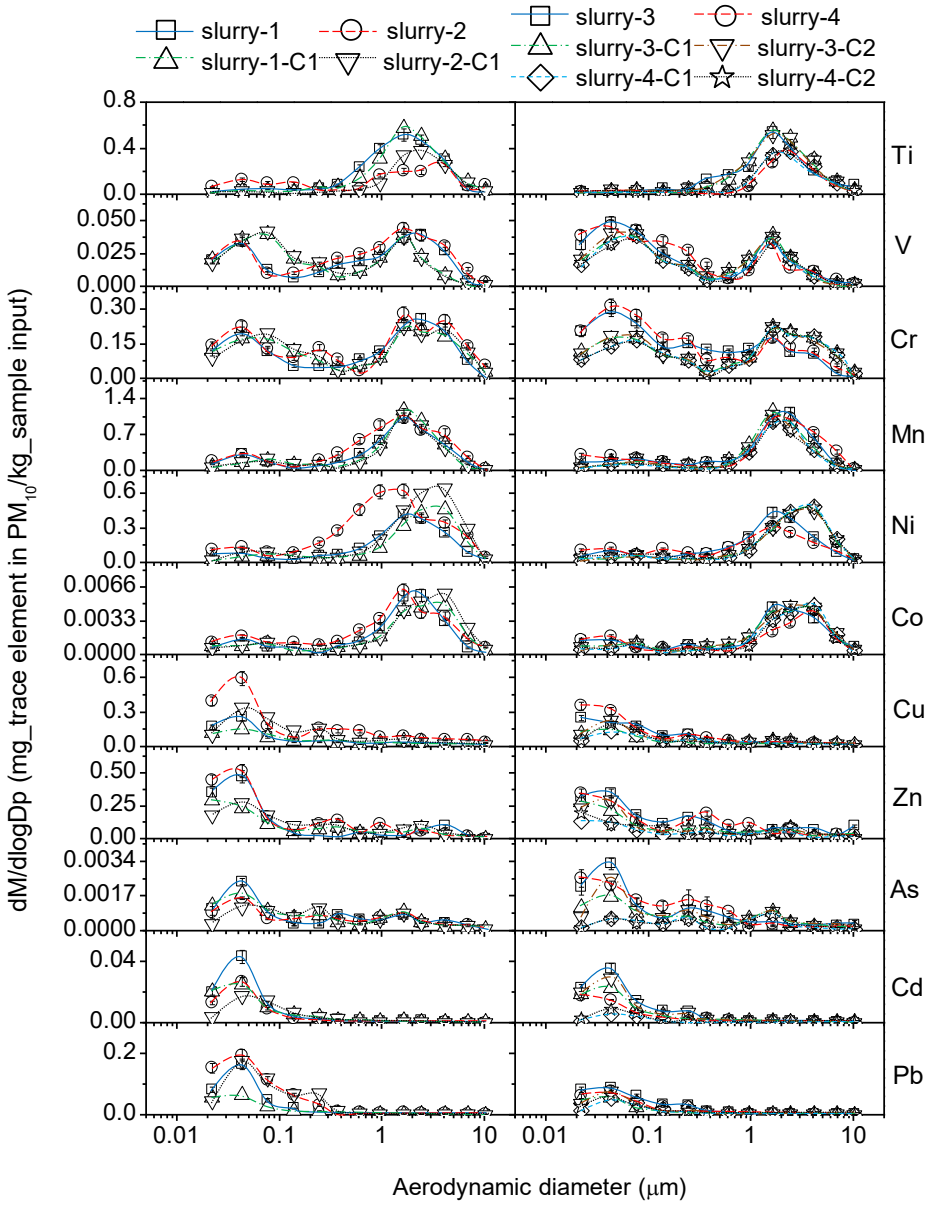

Figure 10-4 Mass-based particle size distributions (PSDs) of Ti, V, Cr, Mn, Ni, Co, Cu, Zn, As, Cd, and Pb in PM_{10} collected from the combustion of the four slurry fuels, i.e., slurry-1 (bio-oil/biochar slurry), slurry-2 (WSF/biochar slurry), slurry-3 (bio-oil/methanol/CG/biochar slurry), and slurry-4 (WSF/CG/biochar slurry), respectively. WSF stands for water-soluble fraction of bio-oil. CG stands for crude glycerol. The respective cases suffixed with "-C1" represent the calculated results via direct addition of the experimental results for individual parent fuels (bio-oil, WSF, CG and/or biochar). Those suffixed with "-C2" represent the calculated results via direct addition of the experimental results for biochar and the respective fuel blend, i.e. blend-1 (bio-oil/methanol/CG blend) for slurry-3 and blend-2 (WSF/CG blend) for slurry-4.

Table 10-3 Yields of trace elements in PM_{10} from the combustion of individual fuels

yields (mg_PM/kg_fuel input)		biochar	bio-oil	WSF[a]	CG[a]
Ti	PM_1	0.277±0.030	0.052±0.003	0.017±0.001	<0.001
	PM_{1-10}	2.444±0.101	0.159±0.009	0.007±0.001	<0.001
	PM_{10}	2.722±0.131	0.211±0.013	0.024±0.002	≤0.001
V	PM_1	0.310±0.011	0.007±0.001	0.009±0.001	≤0.001
	PM_{1-10}	0.176±0.011	0.002±0.001	0.002±0.001	<0.001
	PM_{10}	0.486±0.021	0.009±0.001	0.011±0.001	≤0.001
Cr	PM_1	1.459±0.059	0.049±0.001	0.055±0.002	<0.001
	PM_{1-10}	1.563±0.094	0.020±0.002	0.028±0.002	<0.001
	PM_{10}	3.023±0.153	0.069±0.003	0.083±0.004	<0.001
Mn	PM_1	1.537±0.074	0.096±0.004	0.082±0.003	0.002±0.001
	PM_{1-10}	5.139±0.205	0.196±0.010	0.118±0.005	<0.001
	PM_{10}	6.677±0.279	0.292±0.014	0.200±0.008	0.002±0.001
Ni	PM_1	0.444±0.033	0.034±0.002	0.068±0.003	0.002±0.001
	PM_{1-10}	2.686±0.126	0.059±0.003	0.219±0.007	≤0.001
	PM_{10}	3.130±0.159	0.093±0.005	0.287±0.010	0.003±0.001
Co	PM_1	0.008±0.001	≤0.001	≤0.001	<0.001
	PM_{1-10}	0.028±0.002	≤0.001	≤0.001	<0.001
	PM_{10}	0.036±0.003	0.002±0.001	0.002±0.001	<0.001
Cu	PM_1	0.426±0.023	0.097±0.004	0.250±0.007	0.003±0.001
	PM_{1-10}	0.279±0.017	0.014±0.002	0.015±0.004	0.002±0.001
	PM_{10}	0.705±0.040	0.111±0.006	0.265±0.011	0.005±0.001
Zn	PM_1	0.573±0.030	0.194±0.006	0.204±0.007	0.002±0.001
	PM_{1-10}	0.222±0.014	0.020±0.003	0.034±0.004	0.002±0.001
	PM_{10}	0.794±0.044	0.214±0.010	0.237±0.011	0.004±0.001
As	PM_1	0.003±0.001	≤0.001	≤0.001	<0.001
	PM_{1-10}	0.004±0.001	<0.001	<0.001	<0.001
	PM_{10}	0.007±0.002	≤0.001	≤0.001	<0.001
Cd	PM_1	0.004±0.001	0.019±0.001	0.014±0.001	<0.001
	PM_{1-10}	0.002±0.001	≤0.001	<0.001	<0.001
	PM_{10}	0.006±0.001	0.020±0.001	0.014±0.001	<0.001
Pb	PM_1	0.031±0.002	0.048±0.002	0.133±0.003	<0.001
	PM_{1-10}	0.009±0.001	0.002±0.001	0.002±0.002	<0.001
	PM_{10}	0.040±0.003	0.050±0.003	0.135±0.005	≤0.001

[a] WSF stands for water-soluble fraction of bio-oil, CG stands for crude glycerol.

Table 10-4 Yields of trace elements in PM_{10} from the combustion of two fuel blends

yields (mg_PM/kg_fuel input)		blend-1[a]	blend-1-C1[b]	blend-2[a]	blend-2-C1[b]
Ti	PM_1	0.056±0.005	0.047±0.003	0.005±0.001	0.005±0.001
	PM_{1-10}	0.132±0.009	0.143±0.009	0.005±0.001	0.002±0.001
	PM_{10}	0.188±0.014	0.190±0.011	0.010±0.001	0.007±0.001
V	PM_1	0.008±0.001	0.007±0.001	0.003±0.001	0.003±0.001
	PM_{1-10}	0.002±0.001	0.002±0.001	<0.001	<0.001
	PM_{10}	0.010±0.001	0.009±0.001	0.003±0.001	0.004±0.001
Cr	PM_1	0.047±0.004	0.044±0.002	0.021±0.001	0.017±0.001
	PM_{1-10}	0.016±0.001	0.018±0.002	0.012±0.002	0.008±0.001
	PM_{10}	0.063±0.005	0.062±0.004	0.033±0.002	0.025±0.001
Mn	PM_1	0.102±0.008	0.086±0.004	0.035±0.002	0.026±0.001
	PM_{1-10}	0.145±0.009	0.176±0.009	0.027±0.002	0.036±0.002
	PM_{10}	0.247±0.017	0.263±0.013	0.062±0.004	0.062±0.003
Ni	PM_1	0.046±0.003	0.031±0.002	0.043±0.002	0.022±0.001
	PM_{1-10}	0.056±0.004	0.053±0.003	0.060±0.004	0.067±0.002
	PM_{10}	0.102±0.007	0.084±0.005	0.103±0.006	0.089±0.003
Co	PM_1	<0.001	<0.001	<0.001	<0.001
	PM_{1-10}	≤0.001	≤0.001	<0.001	<0.001
	PM_{10}	≤0.001	≤0.001	<0.001	≤0.001
Cu	PM_1	0.118±0.009	0.088±0.004	0.107±0.004	0.077±0.003
	PM_{1-10}	0.011±0.002	0.013±0.002	0.003±0.002	0.006±0.001
	PM_{10}	0.129±0.011	0.101±0.006	0.110±0.006	0.083±0.004
Zn	PM_1	0.182±0.012	0.174±0.006	0.094±0.003	0.063±0.002
	PM_{1-10}	0.009±0.002	0.018±0.003	0.024±0.003	0.011±0.001
	PM_{10}	0.191±0.014	0.192±0.009	0.118±0.006	0.074±0.003
As	PM_1	≤0.001	≤0.001	<0.001	<0.001
	PM_{1-10}	<0.001	<0.001	<0.001	<0.001
	PM_{10}	≤0.001	≤0.001	<0.001	<0.001
Cd	PM_1	0.021±0.002	0.017±0.001	0.006±0.001	0.004±0.001
	PM_{1-10}	<0.001	≤0.001	<0.001	<0.001
	PM_{10}	0.021±0.002	0.018±0.001	0.006±0.001	0.004±0.001
Pb	PM_1	0.048±0.004	0.043±0.002	0.045±0.002	0.040±0.001
	PM_{1-10}	0.002±0.001	0.002±0.001	≤0.001	≤0.001
	PM_{10}	0.049±0.005	0.045±0.003	0.046±0.002	0.041±0.002

[a] blend-1 stands for bio-oil/methanol/CG blend (CG refers to crude glycerol), blend-2 stands for WSF/CG blend (WSF refers to water-soluble fraction of bio-oil); [b] "-C1" represent the calculated results via direct addition of the experimental results for individual fuels (bio-oil, WSF and CG).

Table 10-5 Yields of trace elements in PM_{10} from the combustion of various slurry fuels

	yields (mg_PM/kg_fuel input)	slurry-1[a]	slurry-1-C1[b]	slurry-2[a]	slurry-2-C1[b]	slurry-3[a]	slurry-3-C1[b]	slurry-3-C2[c]	slurry-4[a]	slurry-4-C1[b]	slurry-4-C2[c]
Ti	PM_1	0.109±0.011	0.074±0.006	0.133±0.010	0.043±0.004	0.102±0.008	0.070±0.006	0.078±0.008	0.035±0.004	0.033±0.003	0.032±0.003
	PM_{1-10}	0.370±0.022	0.388±0.019	0.211±0.015	0.251±0.011	0.333±0.020	0.373±0.017	0.363±0.018	0.240±0.013	0.247±0.010	0.249±0.011
	PM_{10}	0.479±0.033	0.462±0.025	0.344±0.025	0.089±0.015	0.435±0.028	0.443±0.023	0.441±0.026	0.275±0.017	0.279±0.013	0.281±0.014
V	PM_1	0.028±0.002	0.038±0.002	0.032±0.002	0.039±0.001	0.044±0.003	0.037±0.001	0.039±0.002	0.052±0.003	0.034±0.001	0.033±0.001
	PM_{1-10}	0.026±0.002	0.020±0.001	0.033±0.002	0.019±0.001	0.018±0.001	0.019±0.001	0.019±0.001	0.015±0.001	0.018±0.001	0.018±0.001
	PM_{10}	0.054±0.004	0.057±0.003	0.065±0.004	0.058±0.002	0.062±0.004	0.056±0.002	0.058±0.003	0.067±0.004	0.052±0.002	0.051±0.002
Cr	PM_1	0.165±0.012	0.190±0.007	0.204±0.011	0.195±0.007	0.311±0.014	0.186±0.007	0.188±0.009	0.319±0.018	0.161±0.006	0.165±0.007
	PM_{1-10}	0.188±0.009	0.174±0.011	0.213±0.014	0.181±0.011	0.121±0.007	0.172±0.011	0.171±0.011	0.121±0.009	0.164±0.010	0.167±0.011
	PM_{10}	0.353±0.021	0.364±0.018	0.418±0.025	0.377±0.018	0.433±0.021	0.358±0.018	0.359±0.020	0.441±0.027	0.325±0.016	0.332±0.018
Mn	PM_1	0.308±0.019	0.240±0.011	0.432±0.021	0.227±0.010	0.305±0.013	0.232±0.011	0.246±0.014	0.349±0.021	0.177±0.008	0.185±0.009
	PM_{1-10}	0.644±0.026	0.690±0.029	0.798±0.035	0.620±0.024	0.701±0.022	0.673±0.028	0.644±0.029	0.717±0.037	0.546±0.022	0.538±0.022
	PM_{10}	0.952±0.045	0.930±0.040	1.231±0.056	0.847±0.034	1.006±0.035	0.904±0.039	0.890±0.043	1.067±0.058	0.723±0.030	0.723±0.031
Ni	PM_1	0.114±0.008	0.075±0.005	0.290±0.014	0.105±0.006	0.111±0.006	0.072±0.005	0.086±0.006	0.167±0.007	0.064±0.004	0.083±0.005
	PM_{1-10}	0.288±0.011	0.322±0.015	0.468±0.028	0.466±0.019	0.287±0.008	0.316±0.015	0.319±0.016	0.231±0.010	0.329±0.014	0.323±0.016
	PM_{10}	0.402±0.019	0.397±0.020	0.759±0.041	0.571±0.025	0.398±0.014	0.389±0.020	0.404±0.022	0.397±0.017	0.393±0.018	0.406±0.021
Co	PM_1	≤0.001	≤0.001	0.002±0.001	≤0.001	≤0.001	≤0.001	≤0.001	0.002±0.001	≤0.001	≤0.001
	PM_{1-10}	0.004±0.001	0.004±0.001	0.004±0.001	0.004±0.001	0.003±0.001	0.004±0.001	0.004±0.001	0.003±0.001	0.003±0.001	0.003±0.001
	PM_{10}	0.005±0.002	0.005±0.001	0.006±0.001	0.005±0.001	0.005±0.001	0.005±0.001	0.005±0.001	0.004±0.001	0.004±0.001	0.004±0.001
Cu	PM_1	0.168±0.013	0.130±0.006	0.413±0.020	0.268±0.009	0.229±0.007	0.121±0.006	0.149±0.010	0.282±0.011	0.112±0.004	0.139±0.006
	PM_{1-10}	0.027±0.003	0.041±0.003	0.080±0.007	0.041±0.005	0.031±0.003	0.039±0.003	0.038±0.004	0.029±0.004	0.033±0.003	0.031±0.003
	PM_{10}	0.195±0.016	0.171±0.009	0.493±0.027	0.309±0.014	0.260±0.010	0.161±0.009	0.187±0.014	0.312±0.015	0.145±0.007	0.170±0.009
Zn	PM_1	0.280±0.021	0.232±0.009	0.377±0.019	0.241±0.009	0.321±0.013	0.214±0.008	0.212±0.014	0.301±0.014	0.114±0.005	0.142±0.006
	PM_{1-10}	0.046±0.005	0.040±0.004	0.055±0.07	0.052±0.005	0.079±0.005	0.038±0.004	0.030±0.003	0.054±0.07	0.032±0.002	0.043±0.003
	PM_{10}	0.326±0.026	0.271±0.013	0.433±0.026	0.293±0.014	0.400±0.018	0.252±0.012	0.242±0.017	0.355±0.021	0.146±0.007	0.185±0.009
As	PM_1	≤0.001	≤0.001	≤0.001	≤0.001	0.002±0.001	≤0.001	0.002±0.001	0.003±0.001	<0.001	<0.001
	PM_{1-10}	<0.001	≤0.001	<0.001	<0.001	<0.001	<0.001	<0.001	<0.001	<0.001	<0.001
	PM_{10}	0.002±0.001	0.002±0.001	0.002±0.001	≤0.001	0.003±0.001	≤0.001	0.002±0.001	0.003±0.001	≤0.001	≤0.001
Cd	PM_1	0.023±0.002	0.018±0.001	0.014±0.001	0.013±0.001	0.023±0.001	0.016±0.001	0.019±0.001	0.013±0.001	0.004±0.001	0.005±0.001
	PM_{1-10}	≤0.001	≤0.001	≤0.001	<0.001	≤0.001	≤0.001	<0.001	<0.001	<0.001	<0.001
	PM_{10}	0.024±0.002	0.019±0.001	0.015±0.001	0.013±0.001	0.025±0.002	0.017±0.001	0.020±0.002	0.013±0.001	0.005±0.001	0.006±0.001
Pb	PM_1	0.089±0.007	0.046±0.002	0.149±0.007	0.123±0.003	0.081±0.003	0.042±0.002	0.046±0.004	0.062±0.003	0.039±0.001	0.044±0.002
	PM_{1-10}	0.003±0.001	0.003±0.001	0.006±0.002	0.003±0.001	0.005±0.001	0.002±0.001	0.002±0.001	≤0.001	0.002±0.001	≤0.001
	PM_{10}	0.091±0.008	0.049±0.003	0.155±0.009	0.126±0.004	0.086±0.004	0.044±0.003	0.049±0.005	0.063±0.003	0.041±0.002	0.045±0.002

[a] slurry-1 stands for bio-oil/biochar slurry, slurry-2 stands for WSF/biochar slurry (WSF refers to water-soluble fraction of bio-oil), slurry-3 stands for bio-oil/methanol/CG/biochar slurry (CG refers to crude glycerol), slurry-4 stands for WSF/CG/biochar slurry; [b] "-C1" represents the calculated result via direct addition of the experimental results for individual fuels (bio-oil, WSF, CG and/or biochar); [c] "-C2" represents the calculated result via direct addition of the experimental results for biochar and the respective fuel blend, i.e. blend-1 (bio-oil/methanol/CG blend) for slurry-3 and blend-2 (WSF/CG blend) for slurry-4.

Table 10-6 Yields of trace elements in PM_{10} based on unit energy input during the combustion of various individual and mixed biofuels

	yields (mg/MJ[a])	biochar	bio-oil	WSF[b]	CG[b]	blend-1[b]	blend-2[b]	slurry-1[b]	slurry-2[b]	slurry-3[b]	slurry-4[b]
Ti	PM_1	0.011±0.001	0.003±0.001	0.002±0.001	<0.001	0.003±0.001	<0.001	0.006±0.001	0.012±0.001	0.006±0.001	0.002±0.001
	$PM_{2.5}$	0.044±0.002	0.009±0.001	0.002±0.001	<0.001	0.008±0.001	<0.001	0.017±0.001	0.019±0.001	0.015±0.001	0.007±0.001
	PM_{10}	0.108±0.005	0.013±0.001	0.003±0.001	<0.001	0.012±0.001	≤0.001	0.028±0.002	0.031±0.002	0.026±0.002	0.019±0.001
V	PM_1	0.012±0.001	<0.001	≤0.001	<0.001	<0.001	<0.001	≤0.001	0.003±0.001	0.002±0.001	0.004±0.001
	$PM_{2.5}$	0.016±0.001	<0.001	≤0.001	<0.001	<0.001	<0.001	0.002±0.001	0.004±0.001	0.003±0.001	0.004±0.001
	PM_{10}	0.019±0.001	<0.001	≤0.001	<0.001	<0.001	<0.001	0.003±0.001	0.006±0.001	0.003±0.001	0.005±0.001
Cr	PM_1	0.058±0.002	0.003±0.001	0.006±0.001	<0.001	0.003±0.001	≤0.001	0.009±0.001	0.018±0.001	0.018±0.001	0.023±0.002
	$PM_{2.5}$	0.080±0.004	0.003±0.001	0.006±0.001	<0.001	0.003±0.001	0.002±0.001	0.013±0.001	0.025±0.001	0.022±0.001	0.026±0.002
	PM_{10}	0.120±0.006	0.004±0.001	0.009±0.001	<0.001	0.004±0.001	0.003±0.001	0.020±0.001	0.037±0.002	0.025±0.001	0.031±0.002
Mn	PM_1	0.061±0.003	0.005±0.001	0.008±0.001	<0.001	0.006±0.001	0.003±0.001	0.018±0.001	0.039±0.002	0.018±0.001	0.025±0.002
	$PM_{2.5}$	0.154±0.006	0.012±0.001	0.016±0.001	<0.001	0.011±0.001	0.004±0.001	0.036±0.001	0.075±0.003	0.034±0.001	0.043±0.002
	PM_{10}	0.265±0.011	0.018±0.001	0.021±0.001	<0.001	0.015±0.001	0.005±0.001	0.055±0.003	0.111±0.005	0.059±0.002	0.076±0.004
Ni	PM_1	0.017±0.001	0.002±0.001	0.007±0.001	<0.001	0.003±0.001	0.003±0.001	0.006±0.001	0.026±0.001	0.006±0.001	0.012±0.001
	$PM_{2.5}$	0.040±0.002	0.004±0.001	0.015±0.001	<0.001	0.004±0.001	0.005±0.001	0.014±0.001	0.049±0.002	0.014±0.001	0.019±0.001
	PM_{10}	0.124±0.006	0.006±0.001	0.030±0.001	<0.001	0.006±0.001	0.008±0.001	0.023±0.001	0.068±0.004	0.023±0.001	0.028±0.001
Co	PM_1	<0.001	<0.001	<0.001	<0.001	<0.001	<0.001	<0.001	<0.001	<0.001	<0.001
	$PM_{2.5}$	<0.001	<0.001	<0.001	<0.001	<0.001	<0.001	<0.001	<0.001	<0.001	<0.001
	PM_{10}	≤0.001	<0.001	<0.001	<0.001	<0.001	<0.001	<0.001	<0.001	<0.001	<0.001
Cu	PM_1	0.017±0.001	0.006±0.001	0.026±0.001	<0.001	0.007±0.001	0.008±0.001	0.010±0.001	0.037±0.002	0.013±0.001	0.020±0.001
	$PM_{2.5}$	0.022±0.001	0.006±0.001	0.027±0.001	<0.001	0.008±0.001	0.008±0.001	0.010±0.001	0.040±0.002	0.014±0.001	0.021±0.001
	PM_{10}	0.028±0.002	0.007±0.001	0.028±0.001	<0.001	0.008±0.001	0.008±0.001	0.011±0.001	0.044±0.003	0.015±0.001	0.022±0.001
Zn	PM_1	0.023±0.001	0.012±0.001	0.021±0.001	<0.001	0.011±0.001	0.007±0.001	0.016±0.001	0.034±0.002	0.019±0.001	0.021±0.001
	$PM_{2.5}$	0.025±0.001	0.013±0.001	0.023±0.001	<0.001	0.011±0.001	0.008±0.001	0.016±0.001	0.036±0.002	0.020±0.001	0.024±0.001
	PM_{10}	0.031±0.002	0.013±0.001	0.025±0.001	<0.001	0.011±0.001	0.009±0.001	0.019±0.001	0.039±0.003	0.023±0.001	0.025±0.002
As	PM_1	<0.001	<0.001	<0.001	<0.001	<0.001	<0.001	<0.001	<0.001	<0.001	<0.001
	$PM_{2.5}$	<0.001	<0.001	<0.001	<0.001	<0.001	<0.001	<0.001	<0.001	<0.001	<0.001
	PM_{10}	<0.001	<0.001	<0.001	<0.001	<0.001	<0.001	<0.001	<0.001	<0.001	<0.001
Cd	PM_1	<0.001	≤0.001	≤0.001	<0.001	≤0.001	<0.001	≤0.001	≤0.001	≤0.001	≤0.001
	$PM_{2.5}$	<0.001	≤0.001	≤0.001	<0.001	≤0.001	<0.001	≤0.001	≤0.001	≤0.001	≤0.001
	PM_{10}	<0.001	≤0.001	≤0.001	<0.001	≤0.001	<0.001	≤0.001	≤0.001	≤0.001	≤0.001
Pb	PM_1	≤0.001	0.003±0.001	0.014±0.001	<0.001	0.003±0.001	0.003±0.001	0.005±0.001	0.013±0.001	0.005±0.001	0.004±0.001
	$PM_{2.5}$	≤0.001	0.003±0.001	0.014±0.001	<0.001	0.003±0.001	0.003±0.001	0.005±0.001	0.014±0.001	0.005±0.001	0.004±0.001
	PM_{10}	≤0.001	0.003±0.001	0.014±0.001	<0.001	0.003±0.001	0.003±0.001	0.005±0.001	0.014±0.001	0.005±0.001	0.004±0.001
total	PM_1	0.201±0.010	0.036±0.001	0.087±0.003	≤0.001	0.038±0.003	0.028±0.001	0.074±0.005	0.184±0.009	0.090±0.004	0.113±0.006
	$PM_{2.5}$	0.385±0.017	0.053±0.002	0.107±0.003	≤0.001	0.052±0.004	0.032±0.001	0.116±0.007	0.264±0.013	0.129±0.005	0.151±0.007
	PM_{10}	0.699±0.033	0.065±0.003	0.132±0.005	≤0.001	0.062±0.005	0.038±0.002	0.167±0.010	0.353±0.019	0.183±0.008	0.214±0.012

[a] calculated based on mass-based yields and LHV in Table 2; [b] WSF stands for water-soluble fraction of bio-oil, CG stands for crude glycerol, blend-1 stands for bio-oil/methanol/CG blend, blend-2 stands for WSF/CG blend, slurry-1 stands for bio-oil/biochar slurry, slurry-2 stands for WSF/biochar slurry, slurry-3 stands for bio-oil/methanol/CG/biochar slurry, slurry-4 stands for WSF/CG/biochar slurry; [b] as-received basis for bio-oil, WSF, CG, blend-1, blend-2, slurry-1, slurry-2, slurry-3 and slurry-4, dry and ash free basis for biochar.

10.4 Synergy on Trace Element Emission in PM_{10} during the Combustion of Mixed Biofuels

To explore the influence of synergy on trace element emission in PM_{10} during the combustion of mixed biofuels, further efforts were then made to compare the experimental values from the combustion of each mixed biofuel with the calculated values via direct addition of the experimental results from the combustion of individual biofuel components in the mixed biofuels. For blend-1, blend-2, slurry-1, slurry-2, slurry-3, and slurry-4, the predicted values were calculated via direct addition of the trace element emission data from individual parent fuels (i.e., biochar, bio-oil, WSF, and CG) in these mixed biofuels, presented in Figures 10-3 and 10-4 and Tables 10-4 and 10-5 as "blend-1-C1", "blend-2-C1", "slurry-1-C1", "slurry-2-C1", "slurry-3-C1" and "slurry-4-C1", respectively. For slurry-3 and slurry-4, one additional calculation method was also considered, i.e. direct addition of the trace element emission results from the combustion of the fuel blends and biochar, with the calculated values presented as "slurry-3-C2" and "slurry-4-C2" in Figure 10-4 and Table 10-5. Comparison between the calculated values and the experimental results leads to three important findings.

First, Figure 10-3 and Table 10-4 show that combustion of blend-1 and blend-2 leads to higher emissions of some trace elements (Ni, Cu and Zn) in PM_1 in comparison to the corresponding calculations (i.e., blend-1-C1 and blend-2-C1). The enhanced release of these trace elements in PM_1 during combustion of the fuel blends can be attributed to increased release of Cl. The combustion of CG is known to release substantial HCl[75] due to the abundant inherent Cl in CG (see Table 10-2). Increasing presence of HCl in the combustion system is known to enhance the chlorination of these trace elements hence lead to increasing emission of these trace elements in PM_1.[165,247,248]

Second, in Figure 10-4 and Table 10-5, combustion of slurry-1 and slurry-2 leads to increased emission of Ti, Mn, Ni, Cu, Zn, and Pb in PM_1 in comparison to the calculated estimations of slurry-1-C1 and slurry-2-C1, respectively. This indicates that interactions during the combustion of different biofuel components increase the emission of these trace elements in PM_1 during the combustion of slurry fuels, possibly due to three possible mechanisms. The first mechanism is the "leaching effect",[307] i.e. during the storage of slurry the liquid fraction (bio-oil or WSF) of the slurry may leach some of the trace element species from biochar into the liquid phase, increasing the emission of these trace elements in PM_1.[99,307] The second mechanism is "volatile-char interactions" which can enhance the emission of PM_1 as a result of the reactions between char and volatiles produced from the slurry fuels during combustion.[69] The last mechanism is the potentially enhanced gasification of biochar by steam from the liquid fraction of the slurry fuels, leading to increased volatilization/vaporization of trace elements from biochar fraction via enhanced fragmentation of biochar particle during combustion.[318]

Lastly, the results in Figure 10-4 and Table 10-5 show that the emissions of Cr, Mn, Ni, Cu, Zn, Cd, and Pb in PM_1 during the combustion of slurry-3 and slurry-4 are higher than the respective estimations (i.e., slurry-3-C1/-C2 and slurry-4-C1/C2), respectively. Such increases can also be attributed to the aforementioned synergies in blend-1, blend-2, slurry-1 and slurry-2, i.e., the enhanced chlorination, "leaching effect", "volatile-char interaction", and steam gasification. In addition, the comparison between the experimental results with the estimated values of slurry-3-C2 and slurry-4-C2 further indicates that the chlorination of trace elements took place not only as gas phase reactions but also as heterogeneous reactions between Cl and trace elements in biochar particles during combustion of slurry-3 and slurry-4.

10.5 Conclusion

A series of systematic experiments were conducted in a DTF system in air at 1400 °C to investigate the emission of trace elements (including Ti, V, Cr, Mn, Ni, Co, Cu, Zn, As, Cd, and Pb) in PM_{10} during the combustion of various individual and mixed biofuels, including bio-oil, WSF, CG, biochar, bio-oil/methanol/CG blend, WSF/CG blend, bio-oil/biochar slurry, WSF/biochar slurry, bio-oil/methanol/CG/biochar slurry, and WSF/CG/biochar slurry. The abundance of these trace elements in these biofuels indicates that: (1) the concentrations of these trace elements in biochar are considerably higher than those in other biofuels; and (2) Zn and Mn are the most abundant trace elements in these biofuels, followed by Ni, Cr, Cu, Ti, Pb, Cd, As, Co, and V. For slurry biofuels, Ti, V, Cr, Mn, Ni and Co are mainly contributed by the biochar fraction while Cu, Zn, As, Cd and Pb are mainly contributed by the liquid fraction. During the combustion of all biofuels, the PSDs of both Group I trace elements (Ti, Mn, Ni, and Co) and Group III trace element (Pb) show unimodal distribution, with the former mainly presented in $PM_{1\text{-}10}$ and the latter in PM_1. For Group II trace elements (V, Cr, As, Cu, Zn and Cd), the PSDs of these trace elements have unimodal distributions (presented in PM_1) during the combustion of liquid biofuels but have bimodal distributions during the combustion of biochar. During the combustion of slurry fuels, the PSDs of V and Cr have bimodal distributions but those of other Group II trace elements (As, Cu, Zn and Cd) show unimodal distributions (presented in PM_1). Based on unit energy input, biochar produces the highest total trace element emission in PM_{10} (dominantly in $PM_{1\text{-}10}$) among the ten biofuels, followed by slurry fuels (in PM_1 and $PM_{1\text{-}10}$), and then liquid fuels (dominantly in PM_1). For each trace element on the basis of same energy input, biochar combustion produces highest emission of Ti, Mn, Ni, V, and Cr in PM_{10}, while combustion of liquid and slurry fuels produces highest emission of Pb, and combustion of all ten biofuels produces similar Cu and Zn emission. Comparisons between the experimental and calculated results of trace element emission in PM_{10} from the combustion of individual and mixed biofuels indicate that direct combustion

of the mixed biofuels leads to synergy among biofuel components in the mixed biofuels, resulting in enhanced trace elements emission in PM_1.

Chapter 11 Conclusions and Recommendations

11.1 Introduction

This thesis has reported a series of systematic investigation into PM_{10} emission during the combustion of bio-oil and various bio-oil based biofuels in a laboratory-scale drop-tube furnace at 1400 °C under various atmosphere conditions. The range of biofuels considered in the experimental program include bio-oil, bio-oil fractions, bio-oil/biochar fuel slurry (bioslurry, referred to as BB), and CG-containing biofuel mixtures, i.e. bio-oil/methanol/CG blend fuel (BMCG), WSF/CG blend fuel (WSFCG, WSF refers to water-soluble fraction of bio-oil), bio-oil/methanol/CG/biochar fuel slurry (BMCGB), and WSF/CG/biochar fuel slurry (WSFCGB). Detailed findings from this PhD study and some recommendations for future work are listed below.

11.2 Conclusions

Conclusions are summarised and listed below according to the four objectives of this thesis study.

11.2.1 Particulate matter emission from bio-oil incomplete combustion under conditions relevant to stationary applications

- The particle size distributions (PSDs) of the PM_{10} and water-soluble PO_4^{3-} in PM_{10} all exhibit a bimodal distribution. On the other hand, whereas the PSDs of volatile elements (i.e., Na, K, Cl, and S in form of water-soluble SO_4^{2-}) demonstrate a unimodal distribution, those of Mg and Ca are dependent on combustion atmosphere (i.e., unimodal distribution for air combustion and bimodal distribution for O_2 combustion).

- Fine char particles (>0.45 μm) in the raw bio-oil play significant roles in the emission of PM_{10} and its key forming elements (Mg and Ca). The combustion of the filtrated bio-oil in air results in considerable reductions in the mass of PM with aerodynamic diameters of 0.1−10 μm as well as that of Mg and Ca in the PM with a size range of 0.372−10 μm, in comparison with their raw bio-oil combustion counterparts.
- Combustion atmospheres also have significant effects on the emission of PM_{10} and its key inorganic elements. Switching combustion atmosphere from air to O_2 leads to an increase of ~74.2% in PM_1 yield but a decrease of ~27.2% in $PM_{1\text{-}10}$ yield. Whereas the increased PM_1 yield can be attributed to the increased yields of Na, K, Mg, Ca, SO_4^{2-} and PO_4^{3-} in PM_1, the reduction of $PM_{1\text{-}10}$ yield is most likely due to the decreased amount of unburned carbonaceous material in $PM_{1\text{-}10}$, as a result of the improved burnout under O_2.

11.2.2 Emission of particulate matter during the combustion of bio-oil and its fractions under air and oxyfuel conditions

- The PSDs of PM_{10} from the combustion of bio-oil have a bimodal distribution (i.e. a fine mode at ~0.03μm and a coarse mode at ~2.0 μm).
- The water-insoluble fraction and the fine char particles in the raw bio-oil have insignificant contributions to PM_{10} emission during the combustion of the raw bio-oil. The results suggest that water-soluble fraction plays a key role in PM_{10} emission during the combustion of the raw bio-oil.
- As gaseous phase reactions play a dominant role during bio-oil combustion, switching combustion atmosphere from air to oxy-fuel conditions leads to insignificant differences in PM_{10} emission, expect that more Fe appears to be emitted as $PM_{0.1\text{-}1}$ as influenced by the excessive CO_2 under oxyfuel conditions.

11.2.3 Mechanistic investigation into particulate matter formation during air and oxyfuel combustion of formulated water-soluble fractions of bio-oil

- The combustion of FWSFs produces mainly $PM_{0.1-10}$ emission (~98% of the total PM_{10}), similar to bio-oil combustion.
- Since there is no combustibles in FWSF-1, the PM_{10} was produced through mechanism of droplet evaporation followed by crystallization, fusion, and hydrolysis to form CaO fine particles in air (or argon) or partially $CaCO_3$ in 30% O_2/70% CO_2.
- The organics present in the FWSF-2 play an important role in PM_{10} formation as FWSF-2 combustion produces PM_{10} with PSD shifting to considerably smaller sizes, indicating extensive break up of droplets takes place.
- Combustion of sprays with larger droplet sizes produces PM_{10} with increased sizes.
- The results also show that upon cooling CaO produced during combustion in air can react with HCl (g) to form $CaCl_2$ in $PM_{0.1}$.
- On the assumption that one droplet produces one PM particle, the predicted PSDs of PM_{10} are much bigger than the experimentally-measured PSDs of PM_{10} from the combustion of FWSFs. This confirms that spray droplets experience breakup, which is extensive in the case of FWSF-2 due to the presence of organics in the fuel.

11.2.4 Bioslurry for stationary applications: particulate matter emission during combustion under air and oxyfuel conditions

- PM_{10} from bioslurry combustion follows a bimodal distribution, with a fine mode at ~0.022 μm and a coarse mode at ~2.4 μm. PM_{1-10} accounts for ~70-73 wt% of the total PM_{10}.
- The chemical compositions of PM_{10} and the elemental PSDs and yields of PM_{10} from bioslurry combustion indicate that the mechanisms responsible for

ash transformation during bioslurry combustion are similar to those for other biofuels such as biomass, bio-oil, and biochar.

- The PM_{10} emission increases with increasing biochar loading level in bioslurry because the concentrations of ash-forming species in biochar is substantially higher than those in bio-oil (hence bioslurry).
- Under 20% O_2/ 80% CO_2 condition, PM_1 and PM_{1-10} emissions from bioslurry combustion are lower than those under air conditions due to the lower combustion temperature of char particles. However, under 30% O_2/ 70% CO_2 conditions, the emission of PM_{10} is higher than that under air. Such an increase is mainly contributed by the increase in PM_1 emission, most likely as a result of increasing O_2 concentration leading to enhanced sulfation of alkali species.
- When benchmarking against other solid fuels such as coal, biomass or biochar, the ash-forming species in bioslurry have a lower propensity than those in coal but a higher propensity than those in biomass and biochar in producing PM_{10} during combustion. In practice, as the substitution of bioslurry fuels for coal, biomass or biochar are typically on the same energy input, bioslurry fuels still leads to considerably better performance in term of PM_{10} emission than not only coal but also biomass and biochar during combustion because of the substantially low ash content of bioslurry fuels.

11.2.5 Synergy on particulate matter emission during the combustion of bio-oil/biochar slurry (bioslurry)

- The PM_{10} emission from the direct combustion of bioslurry is higher than the sum of the PM_{10} emissions from separate bio-oil and biochar combustion, indicating the existence of synergy.
- Two mechanisms were found to be responsible for such synergy effects in PM_{10} emission. One is the leaching effect, evidenced by comparison in the PM_{10} from the combustion of bio-oil and biochar before and after prepared as

bioslurry. The leaching effect contributes to the increase in PM_1 and decrease in PM_{1-10} due to the transformation of the inorganic species from biochar fraction into bio-oil fraction. The other is the interactions between the combustions of bio-oil and biochar fractions, also leading to the increase in PM_1 and decrease in PM_{1-10}. The results show that the second mechanism contributes to ~80% of the total increase in PM_1 and ~60% of the total decrease in PM_{1-10}.

11.2.6 Combustion of biofuel mixtures containing crude glycerol (CG): effect of interactions between CG and fuel components on particulate matter emission

- The combustion of CG-containing slurry fuels (i.e. BMCGB or WSFCGB) produce PM_{10} having bimodal distributions of PM_{10} with a fine mode at ~0.022 μm and a coarse mode at ~1.624−2.438 μm. However, the combustion of CG-containing fuel blends (i.e. BMCG or WSFCG) produce PM_{10} having unimodal distributions with a fine mode at ~0.043 μm.
- During the combustion of BMCG and WSFCG, ~88.2% and ~99.3% of the total PM_{10} is distributed in PM_1, respectively. The introduction of biochar increases the PM_{1-10} to ~53.1% and ~8.4% of the total PM_{10}, respectively, during the combustion of BMCGB and WSFCGB.
- Synergistic effect takes place on PM_{10} emission during the combustion of CG-containing biofuel mixtures. For CG-containing fuel blends, the Cl originated from CG enhances chlorination of volatile inorganic species in the fuel blends and increases the emissions of these species in PM_1. For CG-containing slurry fuels, chlorination is also enhanced for both volatile and refractory inorganic species in biochar, resulting in increases of both volatile and refractory inorganic species in PM_1 and decreases of refractory inorganic species in PM_{1-10}.

11.2.7 Trace elements in various individual and mixed biofuels: abundance and release in particulate matter during combustion

- The abundance of these trace elements in these biofuels indicates that: (1) the concentrations of these trace elements in biochar are considerably higher than those in other biofuels; and (2) Zn and Mn are the most abundant trace elements in these biofuels, followed by Ni, Cr, Cu, Ti, Pb, Cd, As, Co, and V.
- For slurry biofuels, Ti, V, Cr, Mn, Ni and Co are mainly contributed by the biochar fraction while Cu, Zn, As, Cd and Pb are mainly contributed by the liquid fraction.
- During the combustion of all biofuels, the PSDs of both Group I trace elements (Ti, Mn, Ni, and Co) and Group III trace element (Pb) show unimodal distribution, with the former mainly presented in PM_{1-10} and the latter in PM_1. For Group II trace elements (V, Cr, As, Cu, Zn and Cd), the PSDs of these trace elements have unimodal distributions (presented in PM_1) during the combustion of liquid biofuels but have bimodal distributions during the combustion of biochar. During the combustion of slurry fuels, the PSDs of V and Cr have bimodal distributions but those of other Group II trace elements (As, Cu, Zn and Cd) show unimodal distributions (presented in PM_1).
- Based on unit energy input, biochar produces the highest total trace element emission in PM_{10} (dominantly in PM_{1-10}) among the ten biofuels, followed by slurry fuels (in PM_1 and PM_{1-10}), and then liquid fuels (dominantly in PM_1). For each trace element on the basis of same energy input, biochar combustion produces highest emission of Ti, Mn, Ni, V, and Cr in PM_{10}, while combustion of liquid and slurry fuels produces highest emission of Pb, and combustion of all ten biofuels produces similar Cu and Zn emission.
- Comparisons between the experimental and calculated results of trace element emission in PM_{10} from the combustion of individual and mixed

biofuels indicate that direct combustion of the mixed biofuels leads to synergy among biofuel components in the mixed biofuels, resulting in enhanced trace elements emission in PM_1.

11.3 Recommendations

- Incomplete combustion was carried out for bio-oil combustion and unburned carbon PM samples were collected. However, the focus in this thesis is on inorganic ash specie. The knowledge on the formation/emission of the carbonaceous PM should also be explored in future study.
- Due to the time constraints, this PhD study has not been able to complete the investigation into the effect of combustion atmosphere (e.g. oxyfuel combustion conditions) on the emission of trace element in PM during the combustion of bio-oil based biofuels. This warrants further investigation.
- Limited by the current experiment rigs, visual observations of the combustion of the bio-oil based biofuels has not been impossible. Future work will be needed to update the experimental facilities so that visual observations of the combustion of these liquid or slurry fuels can be made. This will provide powerful insights into the combustion of these bio-oil based biofuels.
- Considering the importance of co-firing with coal in existing coal-fired power plants, the synergy on PM emission during co-firing of these bio-oil based biofuels with coal should be investigated in future research program.
- Bio-oil is reactive and unstable and updating is often needed for further use. Future work should also be conducted on PM emission during the combustion of the upraded biofuels.

References

(1) *World Energy Outlook 2016*; Washington, D.C., 16th November, 2016.

(2) *The Retirement of Coal-Fired Power Stations*; Australian Energy Council: Canberra 10th November, 2016.

(3) *Australia's Emissions Projections 2014-15*; Clean Energy Council 2015.

(4) *Solid Biofuels for Energy: A Lower Greenhouse Gas Alternative*. Springer: London, 2011.

(5) Klass, D. L., *Biomass for Renewable Energy, Fuels, and Chemicals*. Elsevier: 1998.

(6) Wu, H.; Fu, Q.; Giles, R.; Bartle, J., *Energy & Fuels* **2008,** 22, 190-198, doi:https://doi.org/10.1021/ef7002969.

(7) McKendry, P., *Bioresource Technology* **2002,** 83, 37-46, doi:https://doi.org/10.1016/S0960-8524(01)00118-3.

(8) Arasto, A.; Tsupari, E.; Kärki, J.; Sormunen, R.; Korpinen, T.; Hujanen, S., *Energy Procedia* **2014,** 63, 6745-6755, doi:https://doi.org/10.1016/j.egypro.2014.11.710.

(9) Cellura, M.; La Rocca, V.; Longo, S.; Mistretta, M., *Journal of Cleaner Production* **2014,** 85, 359-370, doi:https://doi.org/10.1016/j.jclepro.2013.12.059.

(10) Demirbas, A., *Energy Sources, Part A: Recovery, Utilization, and Environmental Effects* **2007,** 29, 549-561, doi:https://doi.org/10.1080/009083190957694.

(11) Abdullah, H.; Wu, H., *Energy & Fuels* **2009,** 23, 4174-4181, doi:https://doi.org/10.1021/ef900494t.

(12) Huber, G. W.; Iborra, S.; Corma, A., *Chemical Reviews* **2006,** 106, 4044-4098, doi:https://doi.org/10.1021/cr068360d.

(13) Prins, M. J.; Ptasinski, K. J.; Janssen, F. J. J. G., *Journal of Analytical and Applied Pyrolysis* **2006,** 77, 28-34, doi:https://doi.org/10.1016/j.jaap.2006.01.002.

(14) Demirbas, A., *Progress in Energy and Combustion Science* **2007,** 33, 1-18, doi:https://doi.org/10.1016/j.pecs.2006.06.001.

(15) Naik, S. N.; Goud, V. V.; Rout, P. K.; Dalai, A. K., *Renewable and Sustainable Energy Reviews* **2010,** 14, 578-597, doi:https://doi.org/10.1016/j.rser.2009.10.003.

(16) Sims, R. E. H.; Mabee, W.; Saddler, J. N.; Taylor, M., *Bioresource Technology* **2010,** 101, 1570-1580, doi:https://doi.org/10.1016/j.biortech.2009.11.046.

(17) Maschio, G.; Koufopanos, C.; Lucchesi, A., *Bioresource Technology* **1992,** 42, 219-231, doi:https://doi.org/10.1016/0960-8524(92)90025-S.

(18) Bridgwater, A. V.; Peacocke, G. V. C., *Renewable and Sustainable Energy Reviews* **2000,** 4, 1-73, doi:https://doi.org/10.1016/S1364-0321(99)00007-6.

(19) Bridgewater, A., *Thermal Science* **2004,** 8, 21-50, doi:https://doi.org/10.2298/tsci0402021b.

(20) Czernik, S.; Bridgwater, A. V., *Energy & Fuels* **2004,** 18, 590-598, doi:https://doi.org/10.1021/ef034067u.

(21) Mohan, D.; Pittman, C. U.; Steele, P. H., *Energy & Fuels* **2006,** 20, 848-889, doi:https://doi.org/10.1021/ef0502397.

(22) Oasmaa, A.; Solantausta, Y.; Arpiainen, V.; Kuoppala, E.; Sipilä, K., *Energy & Fuels* **2010,** 24, 1380-1388, doi:https://doi.org/10.1021/ef901107f.

(23) Nigam, P. S.; Singh, A., *Progress in Energy and Combustion Science* **2011,** 37, 52-68, doi:https://doi.org/10.1016/j.pecs.2010.01.003.

(24) Bridgwater, A. V., *Biomass and Bioenergy* **2012,** 38, 68-94, doi:https://doi.org/10.1016/j.biombioe.2011.01.048.

(25) Xiu, S.; Shahbazi, A., *Renewable and Sustainable Energy Reviews* **2012,** 16, 4406-4414, doi:https://doi.org/10.1016/j.rser.2012.04.028.

(26) Abdullah, H.; Mediaswanti, K. A.; Wu, H., *Energy & Fuels* **2010,** 24, 1972-1979, doi:https://doi.org/10.1021/ef901435f.

(27) Bridgwater, A. V.; Cottam, M. L., *Energy & Fuels* **1992,** 6, 113-120, doi:https://doi.org/10.1021/ef00032a001.

(28) No, S.-Y., *Renewable and Sustainable Energy Reviews* **2014,** 40, 1108-1125, doi:http://dx.doi.org/10.1016/j.rser.2014.07.127.

(29) Chiaramonti, D.; Oasmaa, A.; Solantausta, Y., *Renewable and Sustainable Energy Reviews* **2007,** 11, 1056-1086, doi:https://doi.org/10.1016/j.rser.2005.07.008.

(30) Abdullah, H.; Mourant, D.; Li, C.-Z.; Wu, H., *Energy & Fuels* **2010,** 24, 5669-5676, doi:https://doi.org/10.1021/ef1008117.

(31) Yu, Y.; Wu, H., *Energy & Fuels* **2010,** 24, 5660-5668, doi:https://doi.org/10.1021/ef100957a.

(32) Wu, H.; Yu, Y.; Yip, K., *Energy & Fuels* **2010,** 24, 5652-5659, doi:https://doi.org/10.1021/ef1008105.

(33) Zhang, M.; Wu, H., *Energy & Fuels* **2014,** 28, 4650-4656, doi:https://doi.org/10.1021/ef501176z.

(34) Zhang, M.; Wu, H., *Fuel* **2015,** 159, 118-127, doi:https://doi.org/10.1016/j.fuel.2015.06.062.

(35) Gao, W.; Zhang, M.; Wu, H., *Fuel* **2016,** 176, 72-77, doi:https://doi.org/10.1016/j.fuel.2016.02.056.

(36) Zhang, M.; Wu, H., *Energy & Fuels* **2016,** 30, 8419-8424, doi:https://doi.org/10.1021/acs.energyfuels.6b01964.

(37) Gao, W.; Zhang, M.; Wu, H., *Fuel* **2017,** 207, 240-243, doi:https://doi.org/10.1016/j.fuel.2017.06.090.

(38) Gao, W.; Zhang, M.; Wu, H., *Energy & Fuels* **2017,** 31, 8348-8355, doi:https://doi.org/10.1021/acs.energyfuels.7b01475.

(39) Hinds, W. C., *Aerosol Technology: Properties, Behavior, and Measurement of Airborne Particles*. Second ed.; John Willey & Sons, Inc.: New York, 1999.

(40) Finkelman, R. B.; Orem, W.; Castranova, V.; Tatu, C. A.; Belkin, H. E.; Zheng, B.; Lerch, H. E.; Maharaj, S. V.; Bates, A. L., *International Journal of Coal Geology* **2002,** 50, 425-443, doi:https://doi.org/10.1016/S0166-5162(02)00125-8.

(41) Lighty, J. S.; Veranth, J. M.; Sarofim, A. F., *Journal of the Air & Waste Management Association* **2000,** 50, 1565-1618, doi:https://doi.org/10.1080/10473289.2000.10464197.

(42) Linak, W. P.; Wendt, J. O. L., *Fuel Processing Technology* **1994,** 39, 173-198, doi:https://doi.org/10.1016/0378-3820(94)90179-1.

(43) Jaworek, A.; Krupa, A.; Czech, T., *Journal of Electrostatics* **2007,** 65, 133-155, doi:https://doi.org/10.1016/j.elstat.2006.07.012.

(44) Desrosiers, R. E.; Riehl, J. W.; Ulrich, G. D.; Chiu, A. S., *Symposium (International) on Combustion* **1979,** 17, 1395-1403, doi:https://doi.org/10.1016/S0082-0784(79)80131-9.

(45) Flagan, R. C., *Symposium (International) on Combustion* **1979,** 17, 97-104, doi:https://doi.org/10.1016/S0082-0784(79)80013-2.

(46) Wendt, J. O. L., *Progress in Energy and Combustion Science* **1980,** 6, 201-222, doi:https://doi.org/10.1016/0360-1285(80)90007-6.

(47) Neville, M.; Quann, R. J.; Haynes, B. S.; Sarofim, A. F., *Symposium (International) on Combustion* **1981,** 18, 1267-1274, doi:https://doi.org/10.1016/S0082-0784(81)80130-0.

(48) Quann, R. J.; Neville, M.; Janghorbani, M.; Mims, C. A.; Sarofim, A. F., *Environmental Science & Technology* **1982,** 16, 776-781, doi:https://doi.org/10.1021/es00105a009.

(49) Quann, R. J.; Sarofim, A. F., *Symposium (International) on Combustion* **1982,** 19, 1429-1440, doi:https://doi.org/10.1016/S0082-0784(82)80320-2.

(50) Helble, J. J.; Sarofim, A. F., *Combustion and Flame* **1989,** 76, 183-196, doi:https://doi.org/10.1016/0010-2180(89)90066-7.

(51) Clarke, L. B., *Fuel* **1993,** 72, 731-736, doi:https://doi.org/10.1016/0016-2361(93)90072-A.

(52) Xu, M.; Yu, D.; Yao, H.; Liu, X.; Qiao, Y., *Proceedings of the Combustion Institute* **2011,** 33, 1681-1697, doi:http://dx.doi.org/10.1016/j.proci.2010.09.014.

(53) Gao, X.; Li, Y.; Garcia-Perez, M.; Wu, H., *Energy & Fuels* **2012,** 26, 6783-6791, doi:https://doi.org/10.1021/ef300211u.

(54) Jia, Y.; Lighty, J. S., *Environmental Science & Technology* **2012,** 46, 5214-5221, doi:https://doi.org/10.1021/es204196s.

(55) Kazanc, F.; Levendis, Y. A., *Energy & Fuels* **2012,** 26, 7127-7139, doi:https://doi.org/10.1021/ef301087r.

(56) Kazanc, F.; Levendis, Y. A.; Maffei, T., *Energy & Fuels* **2013,** 27, 4984-4998, doi:https://doi.org/10.1021/ef400814q.

(57) Li, G.; Li, S.; Dong, M.; Yao, Q.; Guo, C. Y.; Axelbaum, R. L., *Fuel* **2013,** 106, 544-551, doi:https://doi.org/10.1016/j.fuel.2012.10.035.

(58) Valmari, T.; Kauppinen, E. I.; Kurkela, J.; Jokiniemi, J. K.; Sfiris, G.; Revitzer, H., *Journal of Aerosol Science* **1998,** 29, 445-459, doi:https://doi.org/10.1016/S0021-8502(97)10021-0.

(59) Lind, T.; Valmari, T.; Kauppinen, E. I.; Sfiris, G.; Nilsson, K.; Maenhaut, W., *Environmental Science & Technology* **1999,** 33, 496-502, doi:https://doi.org/10.1021/es9802596.

(60) Knudsen, J. N.; Jensen, P. A.; Dam-Johansen, K., *Energy & Fuels* **2004,** 18, 1385-1399, doi:https://doi.org/10.1021/ef049944q.

(61) Jiménez, S.; Ballester, J., *Combustion and Flame* **2005,** 140, 346-358, doi:http://dx.doi.org/10.1016/j.combustflame.2004.12.004.

(62) Jiménez, S.; Ballester, J., *Proceedings of the Combustion Institute* **2005,** 30, 2965-2972, doi:https://doi.org/10.1016/j.proci.2004.08.099.

(63) Davidsson, K. O.; Åmand, L.-E.; Leckner, B.; Kovacevik, B.; Svane, M.; Hagström, M.; Pettersson, J. B. C.; Pettersson, J.; Asteman, H.; Svensson, J.-E.; Johansson, L.-G., *Energy & Fuels* **2007,** 21, 71-81, doi:https://doi.org/10.1021/ef060306c.

(64) van Lith, S. C.; Jensen, P. A.; Frandsen, F. J.; Glarborg, P., *Energy & Fuels* **2008,** 22, 1598-1609, doi:https://doi.org/10.1021/ef060613i.

(65) Gao, X.; Wu, H., *Energy & Fuels* **2010,** 24, 4571-4580, doi:https://doi.org/10.1021/ef100701r.

(66) Gao, X.; Rahim, M. U.; Chen, X.; Wu, H., *Proceedings of the Combustion Institute* **2017,** 36, 3313-3319, doi:https://doi.org/10.1016/j.proci.2016.08.072.

(67) Gao, X.; Wu, H., *Energy & Fuels* **2011,** 25, 2702-2710, doi:https://doi.org/10.1021/ef200296u.

(68) Liaw, S. B.; Rahim, M. U.; Wu, H., *Energy & Fuels* **2016,** 30, 5766-5771, doi:https://doi.org/10.1021/acs.energyfuels.6b00776.

(69) Chen, X.; Liaw, S. B.; Wu, H., *Combustion and Flame* **2017,** 182, 90-101, doi:https://doi.org/10.1016/j.combustflame.2017.04.005.

(70) Sippula, O.; Hokkinen, J.; Puustinen, H.; Yli-Pirilä, P.; Jokiniemi, J., *Atmospheric Environment* **2009,** 43, 4855-4864, doi:https://doi.org/10.1016/j.atmosenv.2009.07.022.

(71) Miller, C. A.; Linak, W. P.; King, C.; Wendt, J. O. L., *Combustion Science and Technology* **1998,** 134, 477-502, doi:https://doi.org/10.1080/00102209808924146.

(72) Linak, W. P.; Andrew Miller, C.; Wendt, J. O. L., *Proceedings of the Combustion Institute* **2000,** 28, 2651-2658, doi:http://dx.doi.org/10.1016/S0082-0784(00)80684-0.

(73) Linak, W. P.; Miller, C. A.; Wendt, J. O. L., *Journal of the Air & Waste Management Association* **2000,** 50, 1532-1544, doi:https://doi.org/10.1080/10473289.2000.10464171.

(74) Bohon, M. D.; Metzger, B. A.; Linak, W. P.; King, C. J.; Roberts, W. L., *Proceedings of the Combustion Institute* **2011,** 33, 2717-2724, doi:https://doi.org/10.1016/j.proci.2010.06.154.

(75) Steinmetz, S. A.; Herrington, J. S.; Winterrowd, C. K.; Roberts, W. L.; Wendt, J. O. L.; Linak, W. P., *Proceedings of the Combustion Institute* **2013,** 34, 2749-2757, doi:https://doi.org/10.1016/j.proci.2012.07.050.

(76) Oasmaa, A.; Czernik, S., *Energy & Fuels* **1999,** 13, 914-921, doi:https://doi.org/10.1021/ef980272b.

(77) Lu, Q.; Li, W.-Z.; Zhu, X.-F., *Energy Conversion and Management* **2009,** 50, 1376-1383, doi:https://doi.org/10.1016/j.enconman.2009.01.001.

(78) Toftegaard, M. B.; Brix, J.; Jensen, P. A.; Glarborg, P.; Jensen, A. D., *Progress in Energy and Combustion Science* **2010,** 36, 581-625, doi:https://doi.org/10.1016/j.pecs.2010.02.001.

(79) Smith, R. D., *Progress in Energy and Combustion Science* **1980,** 6, 53-119, doi:https://doi.org/10.1016/0360-1285(80)90015-5.

(80) Clarke, L. B.; Sloss, L. L., *Trace elements-emissions from coal combustion and gasification*. IEA Coal Research: London, 1992.

(81) Martinez-Tarazona, M. R.; Spears, D. A., *Fuel Processing Technology* **1996,** 47, 79-92, doi:https://doi.org/10.1016/0378-3820(96)01001-6.

(82) Senior, C. L.; Bool, L. E.; Morency, J. R., *Fuel Processing Technology* **2000,** 63, 109-124, doi:https://doi.org/10.1016/S0378-3820(99)00092-2.

(83) Miller, B. B.; Kandiyoti, R.; Dugwell, D. R., *Energy & Fuels* **2002,** 16, 956-963, doi:https://doi.org/10.1021/ef0200065.

(84) Xu, M.; Yan, R.; Zheng, C.; Qiao, Y.; Han, J.; Sheng, C., *Fuel Processing Technology* **2004,** 85, 215-237, doi:https://doi.org/10.1016/S0378-3820(03)00174-7.

(85) James, D. W.; Krishnamoorthy, G.; Benson, S. A.; Seames, W. S., *Fuel Processing Technology* **2014,** 126, 284-297, doi:https://doi.org/10.1016/j.fuproc.2014.05.002.

(86) Wang, C.; Liu, X.; Li, D.; Si, J.; Zhao, B.; Xu, M., *Proceedings of the Combustion Institute* **2015,** 35, 2793-2800, doi:https://doi.org/10.1016/j.proci.2014.07.004.

(87) Boman, C.; Öhman, M.; Nordin, A., *Energy & Fuels* **2006,** 20, 993-1000, doi:https://doi.org/10.1021/ef050375b.

(88) Chalot, M.; Blaudez, D.; Rogaume, Y.; Provent, A.-S.; Pascual, C., *Environmental Science & Technology* **2012,** 46, 13361-13369, doi:https://doi.org/10.1021/es3017478.

(89) Nzihou, A.; Stanmore, B., *Journal of Hazardous Materials* **2013,** 256-257, 56-66, doi:https://doi.org/10.1016/j.jhazmat.2013.02.050.

(90) Jerzak, W., *Energy & Fuels* **2017,** 31, 1969-1979, doi:https://doi.org/10.1021/acs.energyfuels.6b02814.

(91) Lind, T.; Hokkinen, J.; Jokiniemi, J. K., *Fuel Processing Technology* **2007,** 88, 737-746, doi:https://doi.org/10.1016/j.fuproc.2007.03.004.

(92) Miller, B.; Dugwell, D.; Kandiyoti, R., *Energy & Fuels* **2006,** 20, 520-531, doi:https://doi.org/10.1021/ef058013r.

(93) Reddy, M. S.; Basha, S.; Joshi, H. V.; Jha, B., *Journal of Hazardous Materials* **2005,** 123, 242-249, doi:https://doi.org/10.1016/j.jhazmat.2005.04.008.

(94) Kaivosoja, T.; Jalava, P. I.; Lamberg, H.; Virén, A.; Tapanainen, M.; Torvela, T.; Tapper, U.; Sippula, O.; Tissari, J.; Hillamo, R.; Hirvonen, M. R.; Jokiniemi, J., *Atmospheric Environment* **2013,** 77, 193-201, doi:https://doi.org/10.1016/j.atmosenv.2013.05.014.

(95) Vaughan, A., Global Coal Consumption Forecast to Slow. *The Guardian; London (UK)* Dec 18, 2017, 2017, p 22.

(96) Carrasco, J. L.; Gunukula, S.; Boateng, A. A.; Mullen, C. A.; DeSisto, W. J.; Wheeler, M. C., *Fuel* **2017,** 193, 477-484, doi:https://doi.org/10.1016/j.fuel.2016.12.063.

(97) Vienescu, D. N.; Wang, J.; Le Gresley, A.; Nixon, J. D., *Bioresource Technology* **2018,** 249, 626-634, doi:https://doi.org/10.1016/j.biortech.2017.10.069.

(98) Abdullah, H.; Wu, H., *Energy & Fuels* **2011,** 25, 1759-1771, doi:https://doi.org/10.1021/ef101535e.

(99) Zhang, M.; Liaw, S. B.; Wu, H., *Energy & Fuels* **2013,** 27, 7560-7568, doi:https://doi.org/10.1021/ef401888j.

(100) Ghezelchi, M. H.; Garcia-Perez, M.; Wu, H., *Energy & Fuels* **2015,** 29, 8058-8065, doi:https://doi.org/10.1021/acs.energyfuels.5b02089.

(101) Zhang, M.; Wu, H., *Energy & Fuels* **2015,** 29, 2535-2541, doi:https://doi.org/10.1021/acs.energyfuels.5b00274.

(102) Setyawan, H. Y.; Zhu, M.; Zhang, Z.; Zhang, D., *Energy* **2016,** 113, 153-159, doi:https://doi.org/10.1016/j.energy.2016.07.032.

(103) Zhang, M.; Wu, H., *Fuel* **2017,** 206, 230-238, doi:http://dx.doi.org/10.1016/j.fuel.2017.06.010.

(104) Dahmen, N.; Henrich, E.; Dinjus, E.; Weirich, F., *Energy, Sustainability and Society* **2012,** 2, 3, doi:https://doi.org/10.1186/2192-0567-2-3.

(105) Lehto, J.; Oasmaa, A.; Solantausta, Y.; Kytö, M.; Chiaramonti, D., *Applied Energy* **2014,** 116, 178-190, doi:https://doi.org/10.1016/j.apenergy.2013.11.040.

(106) Oasmaa, A.; Peacocke, C.; Gust, S.; Meier, D.; McLellan, R., *Energy & Fuels* **2005,** 19, 2155-2163, doi:https://doi.org/10.1021/ef040094o.

(107) Elliott, D. C., *Biomass Bioenergy* **1994,** 7, 179-185, doi:https://doi.org/10.1016/0961-9534(94)00057-Z.

(108) Zheng, J.-L.; Kong, Y.-P., *Energy Conversion and Management* **2010,** 51, 182-188, doi:https://doi.org/10.1016/j.enconman.2009.09.010.

(109) Hou, S.-S.; Huang, W.-C.; Rizal, F.; Lin, T.-H., *Applied Sciences* **2016,** 6, 326, doi:https://doi.org/10.3390/app6110326.

(110) Sipilä, K.; Kuoppala, E.; Fagernäs, L.; Oasmaa, A., *Biomass and Bioenergy* **1998,** 14, 103-113, doi:https://doi.org/10.1016/S0961-9534(97)10024-1.

(111) Wall, T.; Liu, Y.; Spero, C.; Elliott, L.; Khare, S.; Rathnam, R.; Zeenathal, F.; Moghtaderi, B.; Buhre, B.; Sheng, C.; Gupta, R.; Yamada, T.; Makino, K.; Yu, J., *Chemical Engineering Research and Design* **2009,** 87, 1003-1016, doi:https://doi.org/10.1016/j.cherd.2009.02.005.

(112) Dunnigan, L.; Ashman, P. J.; Zhang, X.; Kwong, C. W., *Journal of Cleaner Production* **2018,** 172, 1639-1645, doi:https://doi.org/10.1016/j.jclepro.2016.11.107.

(113) Mohan, D.; Pittman, C. U.; Bricka, M.; Smith, F.; Yancey, B.; Mohammad, J.; Steele, P. H.; Alexandre-Franco, M. F.; Gómez-Serrano, V.; Gong, H., *Journal of Colloid and Interface Science* **2007,** 310, 57-73, doi:https://doi.org/10.1016/j.jcis.2007.01.020.

(114) Wornat, M. J.; Porter, B. G.; Yang, N. Y. C., *Energy & Fuels* **1994,** 8, 1131-1142, doi:https://doi.org/10.1021/ef00047a018.

(115) Oasmaa, A.; Leppämäki, E.; Koponen, P.; Levander, J.; Tapola, E., *Physical Characterisation of Biomass-based Pyrolysis Liquids. Application of Standard Fuel Oil Analysis.* VTT Technical Research Center of Finland: Espoo, 1997.

(116) Elbaz, A. M.; Gani, A.; Hourani, N.; Emwas, A.-H.; Sarathy, S. M.; Roberts, W. L., *Energy & Fuels* **2015,** 29, 7825-7835, doi:https://doi.org/10.1021/acs.energyfuels.5b01739.

(117) Pyle, D. J.; Garcia, R. A.; Wen, Z., *Journal of Agricultural and Food Chemistry* **2008,** 56, 3933-3939, doi:https://doi.org/10.1021/jf800602s.

(118) Thompson, J. C.; He, B. B., *Applied Engineering in Agriculture* **2006,** 22, 261-265, doi:https://doi.org/10.13031/2013.20272.

(119) Jiang, L.; Agrawal, A. K., *Fuel* **2014,** 136, 177-184, doi:https://doi.org/10.1016/j.fuel.2014.07.027.

(120) Gupta, M.; Kumar, N., *Renewable and Sustainable Energy Reviews* **2012,** 16, 4551-4556, doi:https://doi.org/10.1016/j.rser.2012.04.001.

(121) Leijenhorst, E. J.; Wolters, W.; van de Beld, L.; Prins, W., *Fuel Processing Technology* **2016,** 149, 96-111, doi:https://doi.org/10.1016/j.fuproc.2016.03.026.

(122) Oasmaa, A.; Elliott, D. C.; Korhonen, J., *Energy & Fuels* **2010,** 24, 6548-6554, doi:https://doi.org/10.1021/ef100935r.

(123) Zhang, Q.; Chang, J.; Wang, T.; Xu, Y., *Energy Conversion and Management* **2007,** 48, 87-92, doi:https://doi.org/10.1016/j.enconman.2006.05.010.

(124) Yoosuk, B.; Boonpo, J.; Udomsap, P.; Sukkasi, S., *Korean Journal of Chemical Engineering* **2014,** 31, 2229-2236, doi:https://doi.org/10.1007/s11814-014-0190-4.

(125) Kim, T.-S.; Kim, J.-Y.; Kim, K.-H.; Lee, S.; Choi, D.; Choi, I.-G.; Choi, J. W., *Journal of Analytical and Applied Pyrolysis* **2012,** 95, 118-125, doi:https://doi.org/10.1016/j.jaap.2012.01.015.

(126) Li, H.; Xia, S.; Li, Y.; Ma, P.; Zhao, C., *Chemical Engineering Science* **2015,** 135, 258-265, doi:https://doi.org/10.1016/j.ces.2015.03.065.

(127) Scholze, B.; Meier, D., *Journal of Analytical and Applied Pyrolysis* **2001,** 60, 41-54, doi:http://dx.doi.org/10.1016/S0165-2370(00)00110-8.

(128) Garcia-Perez, M.; Chaala, A.; Pakdel, H.; Kretschmer, D.; Roy, C., *Biomass and Bioenergy* **2007,** 31, 222-242, doi:https://doi.org/10.1016/j.biombioe.2006.02.006.

(129) Oasmaa, A.; Kuoppala, E.; Gust, S.; Solantausta, Y., *Energy & Fuels* **2003,** 17, 1-12, doi:https://doi.org/10.1021/ef020088x.

(130) Oasmaa, A.; Kuoppala, E.; Solantausta, Y., *Energy & Fuels* **2003,** 17, 433-443, doi:https://doi.org/10.1021/ef020206g.

(131) Vitasari, C. R.; Meindersma, G. W.; de Haan, A. B., *Bioresource Technology* **2011,** 102, 7204-7210, doi:https://doi.org/10.1016/j.biortech.2011.04.079.

(132) Stankovikj, F.; McDonald, A. G.; Helms, G. L.; Olarte, M. V.; Garcia-Perez, M., *Energy & Fuels* **2017,** 31, 1650-1664, doi:https://doi.org/10.1021/acs.energyfuels.6b02950.

(133) Bayerbach, R.; Meier, D., *Journal of Analytical and Applied Pyrolysis* **2009,** 85, 98-107, doi:https://doi.org/10.1016/j.jaap.2008.10.021.

(134) Mullen, C. A.; Boateng, A. A., *Journal of Analytical and Applied Pyrolysis* **2011,** 90, 197-203, doi:https://doi.org/10.1016/j.jaap.2010.12.004.

(135) D'Alessio, J.; Lazzaro, M.; Massoli, P.; Moccia, V., *Symposium (International) on Combustion* **1998,** 27, 1915-1922, doi:https://doi.org/10.1016/S0082-0784(98)80035-0.

(136) Oasmaa, A.; van de Beld, B.; Saari, P.; Elliott, D. C.; Solantausta, Y., *Energy & Fuels* **2015,** 29, 2471-2484, doi:https://doi.org/10.1021/acs.energyfuels.5b00026.

(137) Henrich, E.; Weirich, F., *Environmental Engineering Science* **2004,** 21, 53-64, doi:https://doi.org/10.1089/109287504322746758.

(138) Trinh, T. N.; Jensen, P. A.; Dam-Johansen, K.; Knudsen, N. O.; Sørensen, H. R.; Szabo, P., *Biomass and Bioenergy* **2014,** 61, 227-235, doi:https://doi.org/10.1016/j.biombioe.2013.12.018.

(139) Agarwal, A. K., *Progress in Energy and Combustion Science* **2007,** 33, 233-271, doi:https://doi.org/10.1016/j.pecs.2006.08.003.

(140) Angeloni, M.; Remacha, P.; Martínez, A.; Ballester, J., *Fuel* **2016,** 184, 889-895, doi:https://doi.org/10.1016/j.fuel.2016.06.045.

(141) Quispe, C. A. G.; Coronado, C. J. R.; Carvalho Jr, J. A., *Renewable and Sustainable Energy Reviews* **2013,** 27, 475-493, doi:https://doi.org/10.1016/j.rser.2013.06.017.

(142) Service, C. R., Air Quality: EPA's 2013 Changes to the Particulate Matter (PM) Standard. In Congressional Research Service: 2015.

(143) Kim, K.-H.; Kabir, E.; Kabir, S., *Environment International* **2015,** 74, 136-143, doi:https://doi.org/10.1016/j.envint.2014.10.005.

(144) Dockery, D. W.; Pope, C. A., *Annual Review of Public Health* **1994,** 15, 107-132, doi:https://doi.org/10.1146/annurev.pu.15.050194.000543.

(145) Gauderman, W. J.; Avol, E.; Gilliland, F.; Vora, H.; Thomas, D.; Berhane, K.; McConnell, R.; Kuenzli, N.; Lurmann, F.; Rappaport, E.; Margolis, H.; Bates, D.; Peters, J., *New England Journal of Medicine* **2004,** 351, 1057-1067, doi:https://doi.org/10.1056/NEJMoa040610.

(146) Pope, C. A.; Dockery, D. W., *Journal of the Air & Waste Management Association* **2006,** 56, 709-742, doi:https://doi.org/10.1080/10473289.2006.10464485.

(147) Brook, R. D.; Rajagopalan, S.; Pope, C. A.; Brook, J. R.; Bhatnagar, A.; Diez-Roux, A. V.; Holguin, F.; Hong, Y.; Luepker, R. V.; Mittleman, M. A.; Peters,

A.; Siscovick, D.; Smith, S. C.; Whitsel, L.; Kaufman, J. D., *Circulation* **2010,** 121, 2331-2378, doi:https://doi.org/10.1161/CIR.0b013e3181dbece1.

(148) Hellén, H.; Hakola, H.; Haaparanta, S.; Pietarila, H.; Kauhaniemi, M., *Science of The Total Environment* **2008,** 393, 283-290, doi:https://doi.org/10.1016/j.scitotenv.2008.01.019.

(149) Straif, K.; Baan, R.; Grosse, Y.; Secretan, B.; El Ghissassi, F.; Cogliano, V., *The Lancet Oncology* **2006,** 7, 977-978, doi:https://doi.org/10.1016/S1470-2045(06)70969-X.

(150) Naeher, L. P.; Brauer, M.; Lipsett, M.; Zelikoff, J. T.; Simpson, C. D.; Koenig, J. Q.; Smith, K. R., *Inhalation Toxicology* **2007,** 19, 67-106, doi:https://doi.org/10.1080/08958370600985875.

(151) Smith, I. M., *Trace Elements from Coal Combustion: Emissions*. IEA Coal Research: London, 1987.

(152) Baxter, L. L., *Biomass and Bioenergy* **1993,** 4, 85-102, doi:https://doi.org/10.1016/0961-9534(93)90031-X.

(153) Hupa, M., *Energy & Fuels* **2012,** 26, 4-14, doi:https://doi.org/10.1021/ef201169k.

(154) Johansen, J. M.; Jakobsen, J. G.; Frandsen, F. J.; Glarborg, P., *Energy & Fuels* **2011,** 25, 4961-4971, doi:https://doi.org/10.1021/ef201098n.

(155) Mycock, J. C., *Handbook of Air Pollution Control Engineering and Technology*. Lewis Pub: 1995.

(156) Liu, X.; Xu, M.; Yao, H.; Yu, D.; Zhang, Z.; Lü, D., *Science in China Series E: Technological Sciences* **2009,** 52, 1521-1526, doi:https://doi.org/10.1007/s11431-009-0174-5.

(157) Ylätalo, S. I.; Hautanen, J., *Aerosol Science and Technology* **1998,** 29, 17-30, doi:https://doi.org/10.1080/02786829808965547.

(158) Qi, L.; Yuan, Y., *Powder Technology* **2013,** 245, 163-167, doi:https://doi.org/10.1016/j.powtec.2013.04.027.

(159) Barranco, R.; Gong, M.; Thompson, A.; Cloke, M.; Hanson, S.; Gibb, W.; Lester, E., *Fuel* **2007,** 86, 2521-2527, doi:https://doi.org/10.1016/j.fuel.2007.02.022.

(160) Tsai, R.; Mills, A. F., *Journal of Aerosol Science* **1995,** 26, 227-239, doi:https://doi.org/10.1016/0021-8502(94)00102-5.

(161) Lim, M. T.; Phan, A.; Roddy, D.; Harvey, A., *Renewable and Sustainable Energy Reviews* **2015,** 49, 574-584, doi:https://doi.org/10.1016/j.rser.2015.04.090.

(162) Coda, B.; Aho, M.; Berger, R.; Hein, K. R. G., *Energy & Fuels* **2001,** 15, 680-690, doi:https://doi.org/10.1021/ef000213+.

(163) Tran, Q. K.; Steenari, B.-M.; Iisa, K.; Lindqvist, O., *Energy & Fuels* **2004,** 18, 1870-1876, doi:https://doi.org/10.1021/ef049881b.

(164) Bäfver, L. S.; Rönnbäck, M.; Leckner, B.; Claesson, F.; Tullin, C., *Fuel Processing Technology* **2009,** 90, 353-359, doi:https://doi.org/10.1016/j.fuproc.2008.10.006.

(165) Sippula, O.; Lind, T.; Jokiniemi, J., *Fuel* **2008,** 87, 2425-2436, doi:https://doi.org/10.1016/j.fuel.2008.02.004.

(166) Al-Naiema, I.; Estillore, A. D.; Mudunkotuwa, I. A.; Grassian, V. H.; Stone, E. A., *Fuel* **2015,** 162, 111-120, doi:https://doi.org/10.1016/j.fuel.2015.08.054.

(167) Damle, A. S.; Ensor, D. S.; Ranade, M. B., *Aerosol Science and Technology* **1981,** 1, 119-133, doi:https://doi.org/10.1080/02786828208958582.

(168) McElroy, M. W.; Carr, R. C.; Ensor, D. S.; Markowski, G. R., *Science* **1982,** 215, 13-19.

(169) Kang, S.-G. Fundamental Studies of Mineral Matter Transformation during Pulverized Coal Combustion: Residual Ash Formation. Massachusetts Institute of Technology, 1991.

(170) Seames, W. S., *Fuel Processing Technology* **2003,** 81, 109-125, doi:https://doi.org/10.1016/S0378-3820(03)00006-7.

(171) Yu, D.; Xu, M.; Yao, H.; Liu, X.; Zhou, K.; Li, L.; Wen, C., *Proceedings of the Combustion Institute* **2009,** 32, 2075-2082, doi:https://doi.org/10.1016/j.proci.2008.07.037.

(172) Gao, X.; Rahim, M. U.; Chen, X.; Wu, H., *Fuel* **2014,** 117, 825-832, doi:https://doi.org/10.1016/j.fuel.2013.09.056.

(173) Linak, W. P.; Miller, C. A.; Seames, W. S.; Wendt, J. O. L.; Ishinomori, T.; Endo, Y.; Miyamae, S., *Proceedings of the Combustion Institute* **2002,** 29, 441-447, doi:https://doi.org/10.1016/S1540-7489(02)80058-X.

(174) Linak, W. P.; Peterson, T. W., *Aerosol Science and Technology* **1984,** 3, 77-96, doi:https://doi.org/10.1080/02786828408958996.

(175) Holve, D. J., *Combustion Science and Technology* **1986,** 44, 269-288, doi:https://doi.org/10.1080/00102208608960308.

(176) Zhang, L.; Ninomiya, Y., *Fuel* **2006,** 85, 194-203, doi:https://doi.org/10.1016/j.fuel.2005.03.034.

(177) Smith, R. D.; Campbell, J. A.; Nielson, K. K., *Atmospheric Environment (1967)* **1979,** 13, 607-617, doi:https://doi.org/10.1016/0004-6981(79)90189-6.

(178) Xiong, Y.; Akhtar, M. K.; Pratsinis, S. E., *Journal of Aerosol Science* **1993,** 24, 301-313, doi:https://doi.org/10.1016/0021-8502(93)90004-S.

(179) Marban, G.; Pis, J. J.; Fuertes, A. B., *Powder Technology* **1996,** 89, 71-78, doi:https://doi.org/10.1016/S0032-5910(96)03157-9.

(180) Mitchell, R. E.; Akanetuk, A. E. J., *Symposium (International) on Combustion* **1996,** 26, 3137-3144, doi:https://doi.org/10.1016/S0082-0784(96)80158-5.

(181) Yoshiie, R.; Tsuzuki, T.; Ueki, Y.; Nunome, Y.; Naruse, I.; Sato, N.; Ito, T.; Matsuzawa, Y.; Suda, T., *Proceedings of the Combustion Institute* **2013,** 34, 2895-2902, doi:https://doi.org/10.1016/j.proci.2012.08.009.

(182) Taylor, S. R., *Solar system evolution: a new perspective : an inquiry into the chemical composition, origin, and evolution of the solar system*. Cambridge University Press: 2001.

(183) Shah, K. V.; Cieplik, M. K.; Betrand, C. I.; van de Kamp, W. L.; Vuthaluru, H. B., *Fuel Processing Technology* **2010,** 91, 531-545, doi:https://doi.org/10.1016/j.fuproc.2009.12.016.

(184) Wen, C.; Yu, D.; Wang, J.; Wu, J.; Yao, H.; Xu, M., *Energy & Fuels* **2014,** 28, 5682-5689, doi:https://doi.org/10.1021/ef501264v.

(185) Wen, C.; Xu, M.; Yu, D.; Sheng, C.; Wu, H.; Zhang, P. a.; Qiao, Y.; Yao, H., *Proceedings of the Combustion Institute* **2013,** 34, 2383-2392, doi:https://doi.org/10.1016/j.proci.2012.07.080.

(186) Xu, Y.; Liu, X.; Zhang, P.; Guo, J.; Han, J.; Zhou, Z.; Xu, M., *Fuel* **2016,** 184, 185-191, doi:https://doi.org/10.1016/j.fuel.2016.07.015.

(187) Helble, J.; Neville, M.; Sarofim, A. F., *Symposium (International) on Combustion* **1988,** 21, 411-417, doi:https://doi.org/10.1016/S0082-0784(88)80268-6.

(188) Baxter, L. L.; Mitchell, R. E.; Fletcher, T. H., *Combustion and Flame* **1997,** 108, 494-502, doi:https://doi.org/10.1016/0010-2180(95)00120-4.

(189) Yan, L.; Gupta, R. P.; Wall, T. F., *Fuel* **2001,** 80, 1333-1340, doi:https://doi.org/10.1016/S0016-2361(00)00194-0.

(190) Wu, H.; Wall, T.; Liu, G.; Bryant, G., *Energy & Fuels* **1999,** 13, 1197-1202, doi:https://doi.org/10.1021/ef990081o.

(191) Helble, J. J.; Srinivasachar, S.; Boni, A. A., *Progress in Energy and Combustion Science* **1990,** 16, 267-279, doi:https://doi.org/10.1016/0360-1285(90)90036-3.

(192) Korbee, R.; Shah, K. V.; Cieplik, M. K.; Betrand, C. I.; Vuthaluru, H. B.; van de Kamp, W. L., *Energy & Fuels* **2010,** 24, 897-909, doi:https://doi.org/10.1021/ef9010737.

(193) Kang, S. G.; Sarofim, A. F.; Beér, J. M., *Symposium (International) on Combustion* **1992,** 24, 1153-1159, doi:https://doi.org/10.1016/S0082-0784(06)80136-0.

(194) Sasongko, D.; Stubington, J. F., *Chemical Engineering Science* **1996,** 51, 3909-3918, doi:https://doi.org/10.1016/0009-2509(96)00242-4.

(195) Baxter, L. L., *Combustion and Flame* **1992,** 90, 174-184, doi:https://doi.org/10.1016/0010-2180(92)90118-9.

(196) Raask, E., *Mineral Impurities in Coal Combustion: Behavior, Problems, and Remedial Measures*. Taylor & Francis: 1985.

(197) McLennan, A. R.; Bryant, G. W.; Stanmore, B. R.; Wall, T. F., *Energy & Fuels* **2000,** 14, 150-159, doi:https://doi.org/10.1021/ef990095u.

(198) Zevenhoven-Onderwater, M. Ash-Forming Matter in Biomass Fuels. Åbo Akademi Åbo/Turku, Finland, Finland, 2001.

(199) JimÉNez, S.; Ballester, J., *Combustion Science and Technology* **2006,** 178, 655-683, doi:https://doi.org/10.1080/00102200500241248.

(200) Gao, X.; Yani, S.; Wu, H., *Energy & Fuels* **2015,** 29, 5171-5175, doi:https://doi.org/10.1021/acs.energyfuels.5b01240.

(201) Yani, S.; Gao, X.; Wu, H., *Energy & Fuels* **2015,** 29, 800-807, doi:https://doi.org/10.1021/ef5023237.

(202) Chenevert, B. C.; Kramlich, J. C.; Nichols, K. M., *Symposium (International) on Combustion* **1998,** 27, 1719-1725, doi:https://doi.org/10.1016/S0082-0784(98)80012-X.

(203) Zellagui, S.; Trouvé, G.; Schönnenbeck, C.; Zouaoui-Mahzoul, N.; Brilhac, J.-F., *Fuel* **2017,** 189, 358-368, doi:https://doi.org/10.1016/j.fuel.2016.10.104.

(204) Costa, F. F.; Costa, M., *Fuel* **2015,** 159, 530-537, doi:https://doi.org/10.1016/j.fuel.2015.07.006.

(205) Gao, X. Emission of inorganic particulate matter during the combustion of biomass, biochar and Collie coal. 2011.

(206) Gao, X.; Wu, H., *Energy & Fuels* **2011,** 25, 4172-4181, doi:https://doi.org/10.1021/ef2008216.

(207) Öhman, M.; Nordin, A., *Energy & Fuels* **2000,** 14, 618-624, doi:https://doi.org/10.1021/ef990198c.

(208) Schmitt, V. E. M.; Kaltschmitt, M., *Fuel* **2013,** 109, 551-558, doi:https://doi.org/10.1016/j.fuel.2013.02.064.

(209) Silcox, G. D.; Kramlich, J. C.; Pershing, D. W., *Industrial & Engineering Chemistry Research* **1989,** 28, 155-160, doi:https://doi.org/10.1021/ie00086a005.

(210) Borgwardt, R. H.; Roache, N. F.; Bruce, K. R., *Industrial & Engineering Chemistry Fundamentals* **1986,** 25, 165-169, doi:https://doi.org/10.1021/i100021a026.

(211) Hu, Z.; Wang, X.; Adeosun, A.; Ruan, R.; Tan, H., *Fuel Processing Technology* **2018,** 171, 1-9, doi:https://doi.org/10.1016/j.fuproc.2017.11.002.

(212) Lahijani, P.; Zainal, Z. A.; Mohamed, A. R.; Mohammadi, M., *Bioresource Technology* **2013,** 144, 288-295, doi:https://doi.org/10.1016/j.biortech.2013.06.059.

(213) Tokarski, S.; Głód, K.; Ściążko, M.; Zuwała, J., *Energy* **2015,** 92, 24-32, doi:https://doi.org/10.1016/j.energy.2015.06.044.

(214) Nussbaumer, T., *Energy & Fuels* **2003,** 17, 1510-1521, doi:https://doi.org/10.1021/ef030031q.

(215) Wang, Q.; Yao, H.; Yu, D.; Dai, L.; Xu, M., *Energy & Fuels* **2007,** 21, 513-516, doi:https://doi.org/10.1021/ef060410u.

(216) Gani, A.; Morishita, K.; Nishikawa, K.; Naruse, I., *Energy & Fuels* **2005,** 19, 1652-1659, doi:https://doi.org/10.1021/ef049728h.

(217) Nordgren, D.; Hedman, H.; Padban, N.; Boström, D.; Öhman, M., *Fuel Processing Technology* **2013,** 105, 52-58, doi:https://doi.org/10.1016/j.fuproc.2011.05.027.

(218) Chao, C. Y. H.; Kwong, P. C. W.; Wang, J. H.; Cheung, C. W.; Kendall, G., *Bioresource Technology* **2008,** 99, 83-93, doi:https://doi.org/10.1016/j.biortech.2006.11.051.

(219) Lopes, H.; Gulyurtlu, I.; Abelha, P.; Crujeira, T.; Salema, D.; Freire, M.; Pereira, R.; Cabrita, I., *Fuel* **2009,** 88, 2373-2384, doi:https://doi.org/10.1016/j.fuel.2009.02.024.

(220) Wu, D.; Wang, Y.; Wang, Y.; Li, S.; Wei, X., *Renewable Energy* **2016,** 96, 91-97, doi:https://doi.org/10.1016/j.renene.2016.04.047.

(221) Jurado, N.; Simms, N. J.; Anthony, E. J.; Oakey, J. E., *Fuel* **2017,** 197, 145-158, doi:https://doi.org/10.1016/j.fuel.2017.01.111.

(222) Zheng, Y.; Jensen, P. A.; Jensen, A. D., *Fuel* **2008,** 87, 3304-3312, doi:https://doi.org/10.1016/j.fuel.2008.05.003.

(223) Henry, W. M.; Knapp, K. T., *Environmental Science & Technology* **1980,** 14, 450-456, doi:https://doi.org/10.1021/es60164a010.

(224) Goldstein, H. L.; Siegmund, C. W., *Environmental Science & Technology* **1976,** 10, 1109-1114, doi:https://doi.org/10.1021/es60122a006.

(225) Witzel, L.; Moszkowicz, P.; Claus, G., *Fuel* **1995,** 74, 1881-1886, doi:https://doi.org/10.1016/0016-2361(95)80023-B.

(226) Huffman, G. P.; Huggins, F. E.; Shah, N.; Huggins, R.; Linak, W. P.; Miller, C. A.; Pugmire, R. J.; Meuzelaar, H. L. C.; Seehra, M. S.; Manivannan, A., *Journal of the Air & Waste Management Association* **2000,** 50, 1106-1114, doi:https://doi.org/10.1080/10473289.2000.10464157.

(227) Happonen, M.; Mylläri, F.; Karjalainen, P.; Frey, A.; Saarikoski, S.; Carbone, S.; Hillamo, R.; Pirjola, L.; Häyrinen, A.; Kytömäki, J.; Niemi, J. V.; Keskinen, J.; Rönkkö, T., *Environmental Science & Technology* **2013,** 47, 14468-14475, doi:https://doi.org/10.1021/es4028056.

(228) Shibaoka, M., *Fuel* **1986,** 65, 449-450, doi:https://doi.org/10.1016/0016-2361(86)90314-5.

(229) Hurt, R. H.; Gibbins, J. R., *Fuel* **1995,** 74, 471-480, doi:https://doi.org/10.1016/0016-2361(95)98348-I.

(230) Hueglin, C.; Gaegauf, C.; Künzel, S.; Burtscher, H., *Environmental Science & Technology* **1997,** 31, 3439-3447, doi:https://doi.org/10.1021/es970139i.

(231) Johansson, L. S.; Tullin, C.; Leckner, B.; Sjövall, P., *Biomass and Bioenergy* **2003,** 25, 435-446, doi:https://doi.org/10.1016/S0961-9534(03)00036-9.

(232) Shibaoka, M., *Fuel* **1985,** 64, 263-269, doi:https://doi.org/10.1016/0016-2361(85)90227-3.

(233) Sarkar, A.; Rano, R.; Udaybhanu, G.; Basu, A. K., *Fuel Processing Technology* **2006,** 87, 259-277, doi:https://doi.org/10.1016/j.fuproc.2005.09.005.

(234) Wang, X.; Cotter, E.; Iyer, K. N.; Fang, J.; Williams, B. J.; Biswas, P., *Proceedings of the Combustion Institute* **2015,** 35, 2347-2354, doi:https://doi.org/10.1016/j.proci.2014.07.073.

(235) Andersen, M. E.; Modak, N.; Winterrowd, C. K.; Lee, C. W.; Roberts, W. L.; Wendt, J. O. L.; Linak, W. P., *Proceedings of the Combustion Institute* **2017,** 36, 4029-4037, doi:https://doi.org/10.1016/j.proci.2016.08.073.

(236) Lamberg, H.; Nuutinen, K.; Tissari, J.; Ruusunen, J.; Yli-Pirilä, P.; Sippula, O.; Tapanainen, M.; Jalava, P.; Makkonen, U.; Teinilä, K.; Saarnio, K.; Hillamo, R.; Hirvonen, M.-R.; Jokiniemi, J., *Atmospheric Environment* **2011,** 45, 7635-7643, doi:https://doi.org/10.1016/j.atmosenv.2011.02.072.

(237) Tissari, J.; Lyyränen, J.; Hytönen, K.; Sippula, O.; Tapper, U.; Frey, A.; Saarnio, K.; Pennanen, A. S.; Hillamo, R.; Salonen, R. O.; Hirvonen, M. R.; Jokiniemi, J., *Atmospheric Environment* **2008,** 42, 7862-7873, doi:https://doi.org/10.1016/j.atmosenv.2008.07.019.

(238) Torvela, T.; Tissari, J.; Sippula, O.; Kaivosoja, T.; Leskinen, J.; Virén, A.; Lähde, A.; Jokiniemi, J., *Atmospheric Environment* **2014,** 87, 65-76, doi:https://doi.org/10.1016/j.atmosenv.2014.01.028.

(239) Zhang, L.; Jiao, F.; Binner, E.; Bhattacharya, S.; Ninomiya, Y.; Li, C.-Z., *Fuel* **2011,** 90, 1361-1369, doi:https://doi.org/10.1016/j.fuel.2011.01.012.

(240) Sheng, C.; Lu, Y.; Gao, X.; Yao, H., *Energy & Fuels* **2007,** 21, 435-440, doi:https://doi.org/10.1021/ef060420v.

(241) Ruscio, A.; Kazanc, F.; Levendis, Y. A., *Energy & Fuels* **2014,** 28, 685-696, doi:https://doi.org/10.1021/ef401796w.

(242) Zhan, Z.; Fry, A.; Zhang, Y.; Wendt, J. O. L., *Proceedings of the Combustion Institute* **2015,** 35, 2373-2380, doi:https://doi.org/10.1016/j.proci.2014.07.001.

(243) Scheffknecht, G.; Al-Makhadmeh, L.; Schnell, U.; Maier, J., *International Journal of Greenhouse Gas Control* **2011,** 5, S16-S35, doi:https://doi.org/10.1016/j.ijggc.2011.05.020.

(244) Zhan, Z.; Fry, A.; Yu, D.; Xu, M.; Wendt, J. O. L., *Fuel Processing Technology* **2016,** 141, 249-257, doi:https://doi.org/10.1016/j.fuproc.2015.10.004.

(245) Zhan, Z.; Fry, A. R.; Wendt, J. O. L., *Fuel* **2016,** 181, 1214-1223, doi:https://doi.org/10.1016/j.fuel.2016.02.074.

(246) Davison, R. L.; Natusch, D. F. S.; Wallace, J. R.; Evans, C. A., *Environmental Science & Technology* **1974,** 8, 1107-1113, doi:https://doi.org/10.1021/es60098a003.

(247) Miller, B.; Dugwell, D. R.; Kandiyoti, R., *Energy & Fuels* **2003,** 17, 1382-1391, doi:https://doi.org/10.1021/ef030020x.

(248) Díaz-Somoano, M.; Unterberger, S.; Hein, K. R. G., *Fuel* **2006,** 85, 1087-1093, doi:https://doi.org/10.1016/j.fuel.2005.10.013.

(249) Clemens, A. H.; Damiano, L. F.; Gong, D.; Matheson, T. W., *Fuel* **1999,** 78, 1379-1385, doi:https://doi.org/10.1016/S0016-2361(99)00066-6.

(250) Ba, T.; Chaala, A.; Garcia-Perez, M.; Rodrigue, D.; Roy, C., *Energy & Fuels* **2004,** 18, 704-712, doi:https://doi.org/10.1021/ef030118b.

(251) Standard, A., AS 1038.4-2006 (2016). Coal and Coke—Analysis and Testing. Part 4: Coke—Proximate analysis. In Standards Australia: Sydney, Australia, 2016.

(252) Zhang, M.; Gao, X.; Wu, H., *Energy & Fuels* **2013,** 27, 6823-6830, doi:https://doi.org/10.1021/ef401632h.

(253) Standard, A., AS 1038.6.1—1997 (2013). Coal and Coke—Analysis and Testing. Part 6.1: Higher Rank Coal and Coke—Ultimate Analysis—Carbon and Hydrogen. In Standard Australia: Sydney, Australia, 2013.

(254) Sheng, C.; Azevedo, J. L. T., *Biomass and Bioenergy* **2005,** 28, 499-507, doi:http://dx.doi.org/10.1016/j.biombioe.2004.11.008.

(255) Yip, K.; Tian, F.; Hayashi, J.-i.; Wu, H., *Energy & Fuels* **2010,** 24, 173-181, doi:https://doi.org/10.1021/ef900534n.

(256) Rahim, M. U.; Gao, X.; Wu, H., *Fuel* **2014,** 129, 314-317, doi:https://doi.org/10.1016/j.fuel.2014.03.070.

(257) Standard, A., AS 1038.8. 1—1999 (2013). Coal and Coke—Analysis and Testing. Part 8.1: Coal and Coke—Chlorine—Eschka Method. In 2002.

(258) Standard, A., AS 1038.6.3.1—1997 (2013). Coal and Coke—Analysis and Testing. Part 6.3.1: Higher rank coal and coke—Utimate analysis—Total sulfur—Eschka method. In 2013.

(259) *Plant Analysis Procedures*. 2nd ed.; Springer, Dordrecht: Dordrecht, Netherlands, 2004.

(260) Vitolo, S.; Ghetti, P., *Fuel* **1994,** 73, 1810-1812, doi:https://doi.org/10.1016/0016-2361(94)90175-9.

(261) Shaddix, C. R.; Tennison, P. J., *Symposium (International) on Combustion* **1998,** 27, 1907-1914, doi:https://doi.org/10.1016/S0082-0784(98)80034-9.

(262) Martin, J. A.; Boateng, A. A., *Fuel* **2014,** 133, 34-44, doi:http://dx.doi.org/10.1016/j.fuel.2014.05.005.

(263) Khodier, A.; Kilgallon, P.; Legrave, N.; Simms, N.; Oakey, J.; Bridgwater, T., *Environmental Progress & Sustainable Energy* **2009,** 28, 397-403, doi:https://doi.org/10.1002/ep.10379.

(264) Tzanetakis, T.; Moloodi, S.; Farra, N.; Nguyen, B.; Thomson, M. J., *Energy & Fuels* **2011,** 25, 1405-1422, doi:https://doi.org/10.1021/ef101500f.

(265) Tzanetakis, T.; Moloodi, S.; Farra, N.; Nguyen, B.; McGrath, A.; Thomson, M. J., *Energy & Fuels* **2011,** 25, 4305-4321, doi:https://doi.org/10.1021/ef200904w.

(266) Moloodi, S.; Tzanetakis, T.; Nguyen, B.; Zarghami-Tehran, M.; Khan, U.; Thomson, M. J., *Energy & Fuels* **2012,** 26, 5452-5461, doi:https://doi.org/10.1021/ef300657d.

(267) Morris, W. J.; Yu, D.; Wendt, J. O. L., *Proceedings of the Combustion Institute* **2011,** 33, 3415-3421, doi:http://dx.doi.org/10.1016/j.proci.2010.05.059.

(268) Bragato, M.; Joshi, K.; Carlson, J. B.; Tenório, J. A. S.; Levendis, Y. A., *Fuel* **2012,** 96, 43-50, doi:http://dx.doi.org/10.1016/j.fuel.2011.12.072.

(269) Carbone, F.; Barone, A.; Pagliara, R.; Beretta, F.; D'Anna, A.; D'Alessio, A., *Environ. Eng. Sci.* **2008,** 25, 1379-1388, doi:https://doi.org/10.1089/ees.2007.0190.

(270) Nelson, P. F.; Shah, P.; Strezov, V.; Halliburton, B.; Carras, J. N., *Fuel* **2010,** 89, 810-816, doi:http://dx.doi.org/10.1016/j.fuel.2009.03.002.

(271) Lehto, J.; Oasmaa, A.; Solantausta, Y.; Kyto, M.; Chiaramonti, D., *Applied Energy* **2014,** 116, 178-190, doi:https://doi.org/10.1016/j.apenergy.2013.11.040.

(272) Tzanetakis, T.; Farra, N.; Moloodi, S.; Lamont, W.; McGrath, A.; Thomson, M. J., *Energy & Fuels* **2010,** 24, 5331-5348, doi:https://doi.org/10.1021/ef100670z.

(273) Shaddix, C.; Hardesty, D. *Combustion properties of biomass flash pyrolysis oils: final project report*; Sandia National Labs., Albuquerque, NM (US); Sandia National Labs., Livermore, CA (US): 1999.

(274) Gao, X.; Wu, H., *Environmental Science & Technology Letters* **2014,** 1, 60-64, doi:https://doi.org/10.1021/ez400165g.

(275) Huffman, G. P.; Huggins, F. E.; Shah, N.; Shah, A., *Progress in Energy and Combustion Science* **1990,** 16, 243-251, doi:https://doi.org/10.1016/0360-1285(90)90033-Y.

(276) Shah, A. D.; Huffman, G. P.; Huggins, F. E.; Shah, N.; Helble, J. J., *Fuel Processing Technology* **1995,** 44, 105-120, doi:https://doi.org/10.1016/0378-3820(95)00015-Y.

(277) Glarborg, P.; Marshall, P., *Combustion and Flame* **2005,** 141, 22-39, doi:https://doi.org/10.1016/j.combustflame.2004.08.014.

(278) Hindiyarti, L.; Frandsen, F.; Livbjerg, H.; Glarborg, P.; Marshall, P., *Fuel* **2008,** 87, 1591-1600, doi:https://doi.org/10.1016/j.fuel.2007.09.001.

(279) Christensen, K. A.; Livbjerg, H., *Journal of Aerosol Science* **1995,** 26, 691, doi:https://doi.org/10.1016/0021-8502(95)90180-9.

(280) Yu, D.; Morris, W. J.; Erickson, R.; Wendt, J. O. L.; Fry, A.; Senior, C. L., *International Journal of Greenhouse Gas Control* **2011,** 5, S159-S167, doi:https://doi.org/10.1016/j.ijggc.2011.04.003.

(281) Stanger, R.; Wall, T., *Progress in Energy and Combustion Science* **2011,** 37, 69-88, doi:https://doi.org/10.1016/j.pecs.2010.04.001.

(282) Lehmann, J., and Joseph, S., *Biochar for environmental management: science and technology*. Earthscan: Sterling, VA, 2009.

(283) Linak, W. P.; Yoo, J.-I.; Wasson, S. J.; Zhu, W.; Wendt, J. O. L.; Huggins, F. E.; Chen, Y.; Shah, N.; Huffman, G. P.; Gilmour, M. I., *Proceedings of the Combustion Institute* **2007,** 31, 1929-1937, doi:https://doi.org/10.1016/j.proci.2006.08.086.

(284) Queirós, P.; Costa, M.; Carvalho, R. H., *Proceedings of the Combustion Institute* **2013,** 34, 2759-2767, doi:https://doi.org/10.1016/j.proci.2012.07.058.

(285) Feng, C.; Gao, X.; Wu, H., *Proceedings of the Combustion Institute* **2017,** 36, 4061–4068, doi:https://doi.org/10.1016/j.proci.2016.08.053.

(286) Law, C. K., *Prog. Energy Combust. Sci.* **1982,** 8, 171-201, doi:https://doi.org/10.1016/0360-1285(82)90011-9.

(287) Kondo, H.; Asaki, Z.; Kondo, Y., *Metallurgical Transactions B* **1978,** 9, 477-483, doi:https://doi.org/10.1007/bf02654424.

(288) Walton, D.; Spence, M. K.; Reynolds, B. T., *Proceedings of the Institution of Mechanical Engineers* **2000,** 214, 531-537.

(289) Joseph, D. D.; Belanger, J.; Beavers, G. S., *International Journal of Multiphase Flow* **1999,** 25, 1263-1303, doi:https://doi.org/10.1016/S0301-9322(99)00043-9.

(290) Maynard, A. D.; Maynard, R. L., *Atmospheric Environment* **2002,** 36, 5561-5567.

(291) Carbone, F.; Beretta, F.; D'Anna, A., *Energy & Fuels* **2010,** 24, 6248-6256, doi:https://doi.org/10.1021/ef100780c.

(292) Buhre, B. J. P.; Elliott, L. K.; Sheng, C. D.; Gupta, R. P.; Wall, T. F., *Progress in energy and combustion science* **2005,** 31, 283-307, doi:https://doi.org/10.1016/j.pecs.2005.07.001.

(293) Bejarano, P. A.; Levendis, Y. A., *Combustion and Flame* **2008,** 153, 270-287, doi:https://doi.org/10.1016/j.combustflame.2007.10.022.

(294) Khatami, R.; Stivers, C.; Joshi, K.; Levendis, Y. A.; Sarofim, A. F., *Combustion and Flame* **2012,** 159, 1253-1271, doi:https://doi.org/10.1016/j.combustflame.2011.09.009.

(295) Fryda, L.; Sobrino, C.; Glazer, M.; Bertrand, C.; Cieplik, M., *Fuel* **2012,** 92, 308-317, doi:https://doi.org/10.1016/j.fuel.2011.08.013.

(296) Suriyawong, A.; Gamble, M.; Lee, M.-H.; Axelbaum, R.; Biswas, P., *Energy & Fuels* **2006,** 20, 2357-2363, doi:https://doi.org/10.1021/ef060178s.

(297) Hecht, E. S.; Shaddix, C. R.; Molina, A.; Haynes, B. S., *Proceedings of the Combustion Institute* **2011,** 33, 1699-1706, doi:https://doi.org/10.1016/j.proci.2010.07.087.

(298) Liaw, S. B.; Wu, H., *Energy & Fuels* **2017,** 31, 2317−2323, doi:https://doi.org/10.1021/acs.energyfuels.6b02337.

(299) Franco, A.; Diaz, A. R., *Energy* **2009,** 34, 348-354, doi:https://doi.org/10.1016/j.energy.2008.09.012.

(300) Christensen, K. A.; Livbjerg, H., *Aerosol Science and Technology* **1996,** 25, 185-199, doi:https://doi.org/10.1080/02786829608965390.

(301) Fernandes, U.; Costa, M., *Energy & Fuels* **2013,** 27, 1081-1092, doi:https://doi.org/10.1021/ef301428m.

(302) Fernandes, U.; Costa, M., *Fuel Processing Technology* **2012,** 103, 51-56, doi:https://doi.org/10.1016/j.fuproc.2011.08.020.

(303) Feng, C.; Wu, H., *Energy & Fuels* **2017,** 31, 7241-7246, doi:https://doi.org/10.1021/acs.energyfuels.7b01212.

(304) Stoesser, P.; Ruf, J.; Gupta, R.; Djordjevic, N.; Kolb, T., *Energy & Fuels* **2016,** 30, 6448-6457, doi:https://doi.org/10.1021/acs.energyfuels.6b00935.

(305) Fryda, L.; Sobrino, C.; Cieplik, M.; van de Kamp, W. L., *Fuel* **2010,** 89, 1889-1902, doi:http://dx.doi.org/10.1016/j.fuel.2009.11.022.

(306) Wu, H.; Quyn, D. M.; Li, C.-Z., *Fuel* **2002,** 81, 1033-1039, doi:https://doi.org/10.1016/S0016-2361(02)00011-X.

(307) Feng, C.; Wu, H., *Fuel* **2018,** 214, 546-553, doi:https://doi.org/10.1016/j.fuel.2017.11.057.

(308) Bailey, R. R.; Wightman, J. P., *Interaction of Hydrogen Chloride With Alumina*. Washington: National Aeronautics and Space Administration, Scientific and Technical Information Office ; Springfield, Va.: National Aeronautics and Space Administration, Scientific and Technical Information Office: Washington, 1978.

(309) Hupa, M.; Backnan, P.; Backman, R.; Tran, H., *Reactions between Iron and HCl-bearing Gases*. 1989.

(310) Chen, J. M.; Chang, F. W.; Chang, C. Y., *Industrial & Engineering Chemistry Research* **1990,** 29, 778-783, doi:https://doi.org/10.1021/ie00101a011.

(311) Schroeder, W. H.; Dobson, M.; Kane, D. M.; Johnson, N. D., *JAPCA* **1987,** 37, 1267-1285, doi:https://doi.org/10.1080/08940630.1987.10466321.

(312) Xu, Y.; Liu, X.; Zhang, Y.; Sun, W.; Zhou, Z.; Xu, M.; Pan, S.; Gao, X., *Energy & Fuels* **2016,** 30, 5930-5936, doi:https://doi.org/10.1021/acs.energyfuels.6b00425.

(313) Xu, Y.; Liu, X.; Cui, J.; Chen, D.; Xu, M.; Pan, S.; Zhang, K.; Gao, X., *Energy & Fuels* **2016,** 30, 7465-7473, doi:https://doi.org/10.1021/acs.energyfuels.6b00426.

(314) Feng, C.; Zhang, M.; Wu, H., *Industrial & Engineering Chemistry Research* **2018,** 57, 4132-4138, doi:https://doi.org/10.1021/acs.iecr.8b00441.

(315) Bläsing, M.; Chiavaroli, G.; Müller, M., *Fuel* **2013,** 111, 791-796, doi:https://doi.org/10.1016/j.fuel.2013.03.073.

(316) Wu, H.; Glarborg, P.; Frandsen, F. J.; Dam-Johansen, K.; Jensen, P. A.; Sander, B., *Fuel Processing Technology* **2013,** 105, 212-221, doi:https://doi.org/10.1016/j.fuproc.2011.05.007.

(317) Agblevor, F. A.; Besler, S., *Energy & Fuels* **1996,** 10, 293-298, doi:https://doi.org/10.1021/ef950202u.

(318) Xu, Y.; Liu, X.; Zhou, Z.; Sheng, L.; Wang, C.; Xu, M., *Applied Energy* **2014,** 133, 144-151, doi:https://doi.org/10.1016/j.apenergy.2014.07.051.

APPENDIX COPYRIGHT PERMISSION STATEMENTS

A. Figure 2-1, reprinted with permission from "Kim, K.-H.; Kabir, E.; Kabir, S., A review on the human health impact of airborne particulate matter. Environment International 2015, 74, 136-143."

B. Figure 2-2, reprinted with permission from "Xu, M.; Yu, D.; Yao, H.; Liu, X.; Qiao, Y., Coal Combustion-generated Aerosols: Formation and Properties. Proceedings of the Combustion Institute 2011, 33, (1), 1681-1697."

C. Figure 2-4, reprinted with permission from "Sippula, O.; Hokkinen, J.; Puustinen, H.; Yli-Pirilä, P.; Jokiniemi, J., Comparison of particle emissions from small heavy fuel oil and wood-fired boilers. Atmospheric Environment 2009, 43, 4855-4864."

D. Chapter 4, reprinted with permission from "Feng, C.; Gao, X.; Wu, H., Particulate matter emission from bio-oil incomplete combustion under conditions relevant to stationary applications. Fuel 2016, 171, 143-150."

E. Chapter 5, reprinted with permission from “Feng, C.; Gao, X.; Wu, H., Emission of Particulate Matter during the Combustion of Bio-oil and its Fractions under Air and Oxyfuel Conditions. Proceedings of the Combustion Institute 2017, 36, (3), 4061–4068.”

F. Chapter 7, reprinted with permission from "Feng, C.; Wu, H., Bioslurry for Stationary Applications: Particulate Matter Emission during Combustion under Air and Oxyfuel Conditions. Energy & Fuels 2017, 31, (7), 7241-7246."

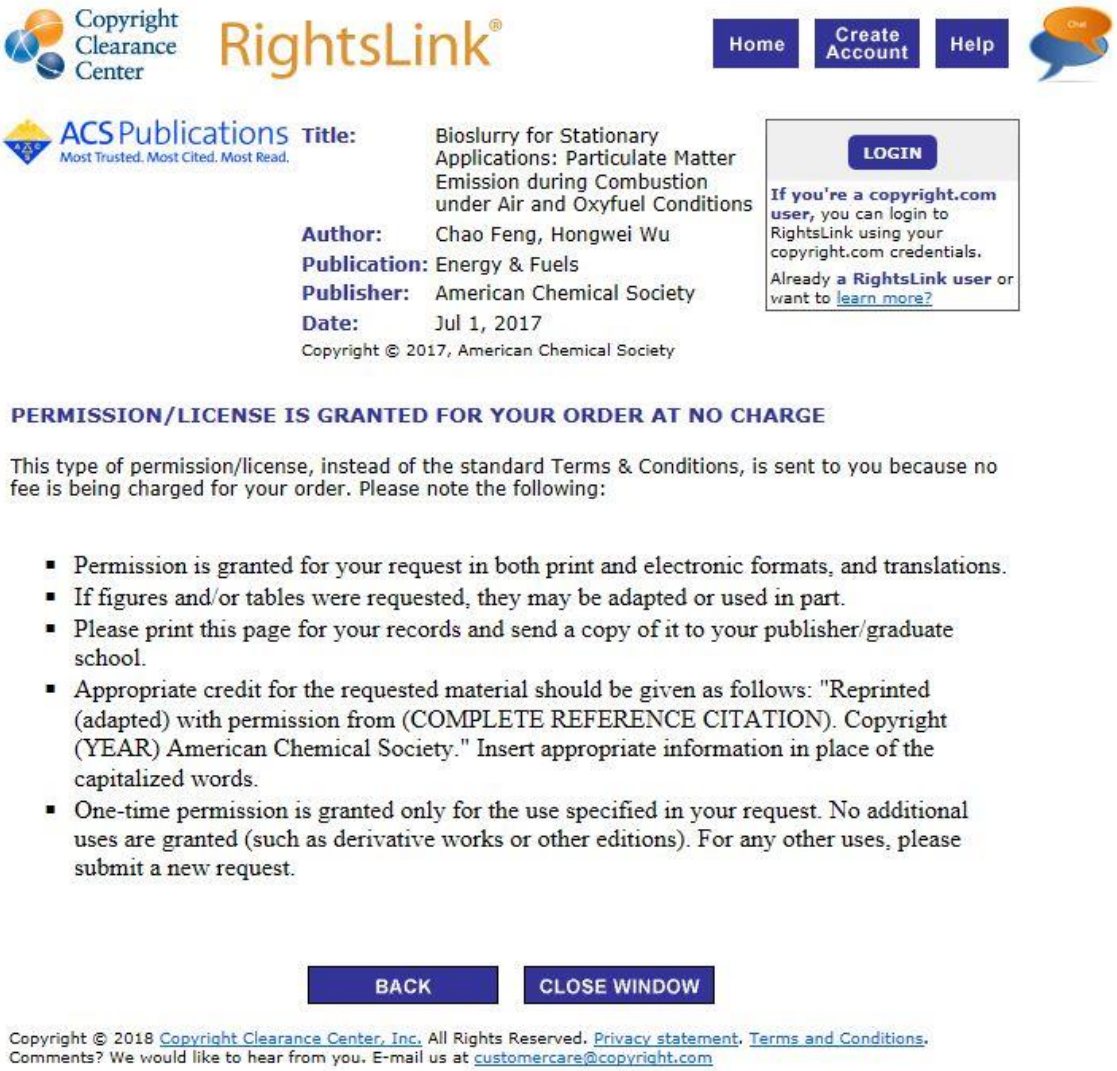

Copyright Clearance Center RightsLink®

Home | Create Account | Help

ACS Publications
Most Trusted. Most Cited. Most Read.

Title: Bioslurry for Stationary Applications: Particulate Matter Emission during Combustion under Air and Oxyfuel Conditions
Author: Chao Feng, Hongwei Wu
Publication: Energy & Fuels
Publisher: American Chemical Society
Date: Jul 1, 2017
Copyright © 2017, American Chemical Society

LOGIN

If you're a copyright.com user, you can login to RightsLink using your copyright.com credentials.
Already a RightsLink user or want to learn more?

PERMISSION/LICENSE IS GRANTED FOR YOUR ORDER AT NO CHARGE

This type of permission/license, instead of the standard Terms & Conditions, is sent to you because no fee is being charged for your order. Please note the following:

- Permission is granted for your request in both print and electronic formats, and translations.
- If figures and/or tables were requested, they may be adapted or used in part.
- Please print this page for your records and send a copy of it to your publisher/graduate school.
- Appropriate credit for the requested material should be given as follows: "Reprinted (adapted) with permission from (COMPLETE REFERENCE CITATION). Copyright (YEAR) American Chemical Society." Insert appropriate information in place of the capitalized words.
- One-time permission is granted only for the use specified in your request. No additional uses are granted (such as derivative works or other editions). For any other uses, please submit a new request.

BACK | CLOSE WINDOW

Copyright © 2018 Copyright Clearance Center, Inc. All Rights Reserved. Privacy statement. Terms and Conditions.
Comments? We would like to hear from you. E-mail us at customercare@copyright.com

G. Chapter 8, reprinted with permission from "Feng, C.; Wu, H., Synergy on particulate matter emission during the combustion of bio-oil/biochar slurry (bioslurry). Fuel 2018, 214, (Supplement C), 546-553."

H. Chapter 9, reprinted with permission from "Feng, C.; Zhang, M.; Wu, H., Combustion of Fuel Mixtures Containing Crude Glycerol (CG): Important Role of Interactions between CG and Fuel Components in Particulate Matter Emission. Industrial & Engineering Chemistry Research 2018, 57, (11), 4132-4138."

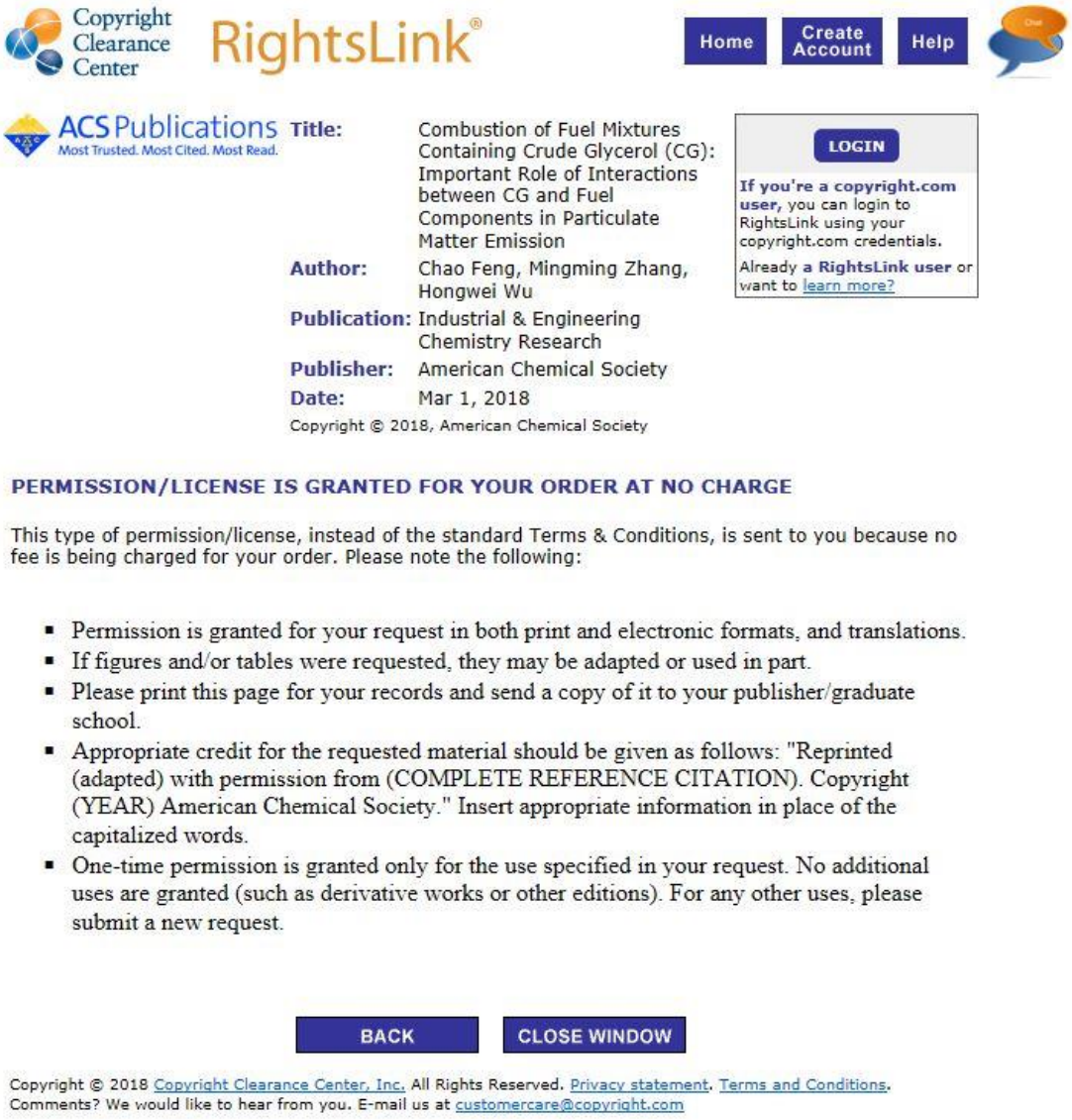

Copyright Clearance Center RightsLink®

Home | Create Account | Help

ACS Publications Most Trusted. Most Cited. Most Read.

Title: Combustion of Fuel Mixtures Containing Crude Glycerol (CG): Important Role of Interactions between CG and Fuel Components in Particulate Matter Emission

Author: Chao Feng, Mingming Zhang, Hongwei Wu

Publication: Industrial & Engineering Chemistry Research

Publisher: American Chemical Society

Date: Mar 1, 2018

Copyright © 2018, American Chemical Society

LOGIN

If you're a copyright.com user, you can login to RightsLink using your copyright.com credentials.

Already a RightsLink user or want to learn more?

PERMISSION/LICENSE IS GRANTED FOR YOUR ORDER AT NO CHARGE

This type of permission/license, instead of the standard Terms & Conditions, is sent to you because no fee is being charged for your order. Please note the following:

- Permission is granted for your request in both print and electronic formats, and translations.
- If figures and/or tables were requested, they may be adapted or used in part.
- Please print this page for your records and send a copy of it to your publisher/graduate school.
- Appropriate credit for the requested material should be given as follows: "Reprinted (adapted) with permission from (COMPLETE REFERENCE CITATION). Copyright (YEAR) American Chemical Society." Insert appropriate information in place of the capitalized words.
- One-time permission is granted only for the use specified in your request. No additional uses are granted (such as derivative works or other editions). For any other uses, please submit a new request.

BACK | CLOSE WINDOW

Copyright © 2018 Copyright Clearance Center, Inc. All Rights Reserved. Privacy statement. Terms and Conditions.
Comments? We would like to hear from you. E-mail us at customercare@copyright.com

I. Chapter 10, reprinted with permission from "Feng, C.; Zhang, M.; Wu, H., Trace Elements in Various Individual and Mixed Biofuels: Abundance and Release in Particulate Matter during Combustion. Energy & Fuels, 2018. 32(5): p. 5978-5989."

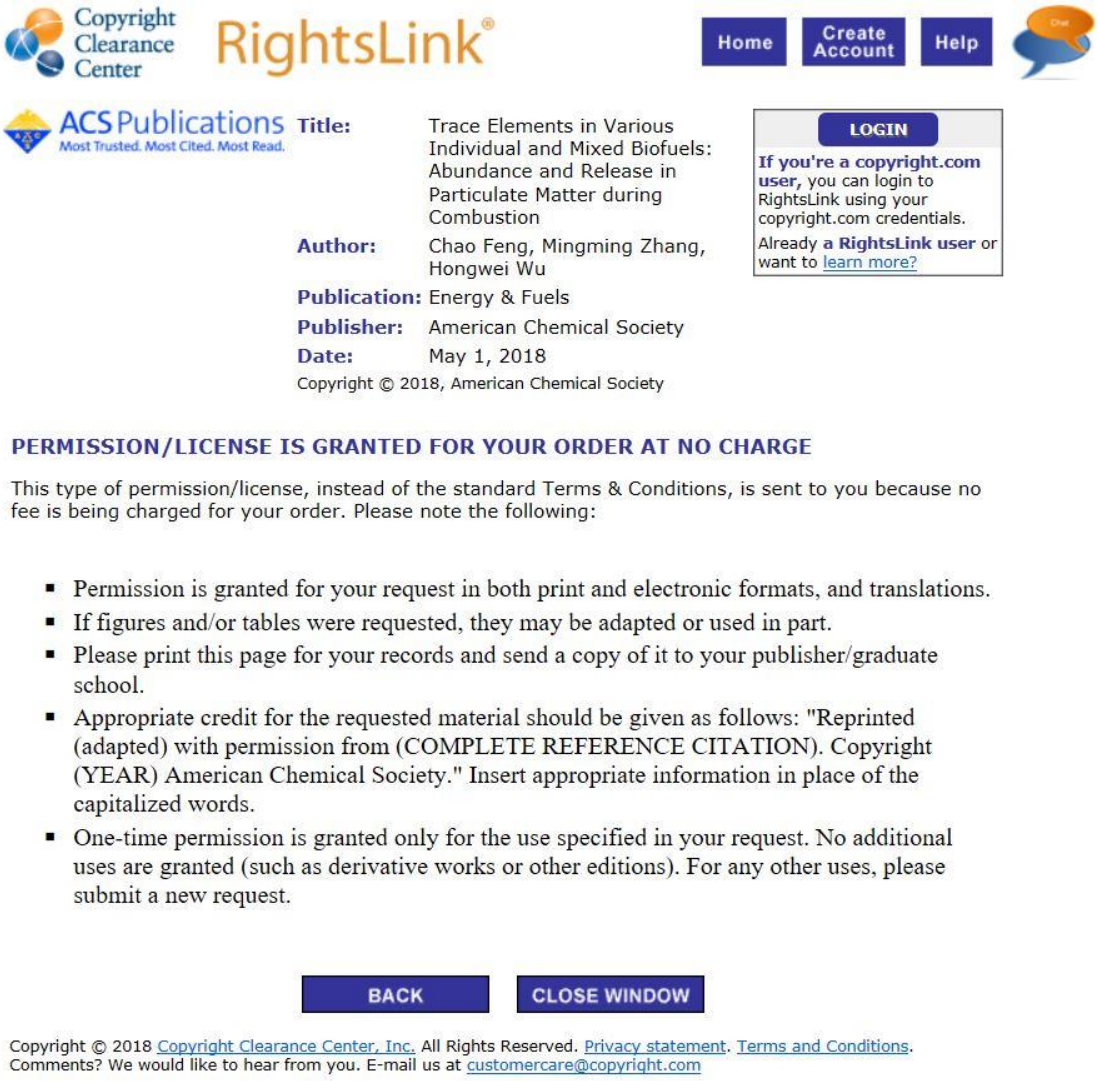

Copyright Clearance Center RightsLink®

Home | Create Account | Help

ACS Publications
Most Trusted. Most Cited. Most Read.

Title: Trace Elements in Various Individual and Mixed Biofuels: Abundance and Release in Particulate Matter during Combustion

Author: Chao Feng, Mingming Zhang, Hongwei Wu

Publication: Energy & Fuels

Publisher: American Chemical Society

Date: May 1, 2018

Copyright © 2018, American Chemical Society

LOGIN

If you're a copyright.com user, you can login to RightsLink using your copyright.com credentials.

Already a RightsLink user or want to learn more?

PERMISSION/LICENSE IS GRANTED FOR YOUR ORDER AT NO CHARGE

This type of permission/license, instead of the standard Terms & Conditions, is sent to you because no fee is being charged for your order. Please note the following:

- Permission is granted for your request in both print and electronic formats, and translations.
- If figures and/or tables were requested, they may be adapted or used in part.
- Please print this page for your records and send a copy of it to your publisher/graduate school.
- Appropriate credit for the requested material should be given as follows: "Reprinted (adapted) with permission from (COMPLETE REFERENCE CITATION). Copyright (YEAR) American Chemical Society." Insert appropriate information in place of the capitalized words.
- One-time permission is granted only for the use specified in your request. No additional uses are granted (such as derivative works or other editions). For any other uses, please submit a new request.

BACK | CLOSE WINDOW

Copyright © 2018 Copyright Clearance Center, Inc. All Rights Reserved. Privacy statement. Terms and Conditions.
Comments? We would like to hear from you. E-mail us at customercare@copyright.com